

**BEHAVIOR OF STRUCTURAL CONCRETE CANTILEVER PIERS USING T-HEADED
REINFORCING BARS AND VARIED PRESTRESSING DESIGN CRITERIA**

by

RUBEN MARIO SALAS PEREIRA, Lic.

THESIS

Presented to the Faculty of the Graduate School of

The University of Texas at Austin

in Partial Fulfillment

of the Requirements

for the Degree of

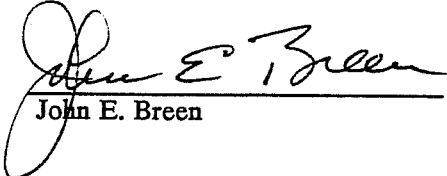
MASTER OF SCIENCE IN ENGINEERING

THE UNIVERSITY OF TEXAS AT AUSTIN

AUGUST 1994

**BEHAVIOR OF STRUCTURAL CONCRETE CANTILEVER PIERS USING T-HEADED
REINFORCING BARS AND VARIED PRESTRESSING DESIGN CRITERIA**

APPROVED:



John E. Breen



Michael E. Kreger

To my parents

ACKNOWLEDGEMENTS

The research program presented herein was conducted as part of CTR project No.1364, at the Phil M. Ferguson Structural Engineering Laboratory at the University of Texas at Austin. Funding for this project was provided by the Texas Department of Transportation. The support of this institution is greatly appreciated.

The author would like to especially thank Dr. John E. Breen, supervisor of this thesis, for his valuable advice and support. It was a privilege to have him as a professor and advisor. Dr. Breen's extraordinary way of transmitting technical and scientific knowledge is always inspirational.

The contribution of Dr. Michael E. Kreger, second reader for this thesis, is gratefully acknowledged.

The author also wishes to thank Scott Armstrong, Bradley Wood and Sarah Billington, with whom he formed the student team for the development of the overall research program. Scott began working with Series 1364-1A, which served as a basis for this thesis. His work was extensive and his contributions are gratefully acknowledged. Brad carried out the finite element analyses and developed programs for the calculation of ultimate capacities and reinforcement stress ranges. His assistance and always helpful suggestions are greatly appreciated. Special thanks go to Sarah, for her assistance, cooperation and friendship throughout the entire program.

The author is very thankful for the help he received during the construction and testing phases of the project. Especially, thanks go to James T. Doran and Mohamed Najah. Thanks are also extended to the technicians at the Ferguson Lab. The author would also like to acknowledge the assistance and friendship of his colleagues at the Laboratory.

The author would like to express his sincere thanks to the Universidad de Costa Rica and the International Road Federation for their financial support which allowed him to pursue his graduate studies. Special thanks go to Mr. Mario Arce, Director of the Civil Engineering Department of the Universidad de Costa Rica. His constant support was essential.

Additionally, thanks go to the Pan American Institute of Highways, Federal Highway Administration. Especially, to Mr. Enrique Ordoñez, Mr. George Shrieves and Mr. William Williams, for their invaluable support when starting the graduate program.

Many thanks go to Robert, Erich, Carolina, Bernardo and Sylvia for their friendship while in Austin.

In addition the author wishes to thank his parents and all of his family for their always inspiring example, unconditional love and constant support.

Finally, there are no words the author could use to thank God, who made all of this possible.

Rubén Salas Pereira
Austin, Texas, U.S.A.
August, 1994

ABSTRACT

BEHAVIOR OF STRUCTURAL CONCRETE CANTILEVER PIERS USING T-HEADED REINFORCING BARS AND VARIED PRESTRESSING DESIGN CRITERIA

by

RUBEN MARIO SALAS PEREIRA, M.S.E.

THE UNIVERSITY OF TEXAS AT AUSTIN, 1994

SUPERVISOR: JOHN E. BREEN

Six model concrete overhang structures with a mixture of prestressed and non-prestressed reinforcement, and using T-headed reinforcing bars as flexural reinforcement, were tested under static loading. These included two overhangs with 54 percent of the main flexural reinforcement prestressed, two with 74 percent of the main flexural reinforcement prestressed, and two with approximately 100 percent of the main flexural reinforcement prestressed.

The responses of the structures in terms of deflections, cracking and ultimate capacities and behavior are compared with theoretical predictions. Performance of T-headed reinforcement and different amounts of skin reinforcement are evaluated.

Test results from a previous investigation, which is closely related to the present investigation, are also compared. The structures of that investigation were similarly designed with varying mixtures of prestressed and non-prestressed reinforcement, including no prestressing and 100 percent prestressing. The combined results document the nature of the transition between conventionally reinforced and fully prestressed structures.

Constructability and economics are discussed for each overhang.

Design recommendations are made for the design of this type of structure.

TABLE OF CONTENTS

LIST OF TABLES	x
LIST OF FIGURES	xii
CHAPTER 1 INTRODUCTION.....	1
1.1 GENERAL	1
1.2 DESCRIPTION OF EXPERIMENTAL RESEARCH PROGRAM.....	3
1.3 OBJECTIVES	4
1.4 SCOPE	5
CHAPTER 2 RESEARCH PROGRAM	7
2.1 TYPICAL TxDOT PIER CAP DESIGN	7
2.2 MODEL SELECTION	8
2.3 SCALE FACTOR SELECTION/SCALE RELATIONS	8
2.3.1 Materials	9
2.3.2 Loads	9
2.4 MODEL DESIGN	10
2.4.1 Flexural design	12
2.4.2 Shear design/ Strut and tie models	20
2.4.3 Skin Reinforcement	28
2.4.4 Post-tensioning anchorage zone reinforcement.....	28
2.4.5 Column design	29
2.4.6 Fatigue considerations	29
2.5 MATERIALS	31
2.5.1 Concrete	31
2.5.2 Passive Reinforcement	33
2.5.3 Active Reinforcement	33
2.5.4 Ducts and Prestressing Hardware	38
2.5.5 Grout	38

2.5.6 T-heads	39
2.6 FABRICATION	41
2.6.1 Formwork	41
2.6.2 Reinforcing Cage	41
2.6.3 Casting of Concrete	43
2.6.4 Prestressing procedure	43
2.6.4.1 Models CO-PU-54S-TH	46
2.6.4.2 Models CO-PU-74S-TH	46
2.6.4.3 Models CO-PU-100S-TH	47
2.7 INSTRUMENTATION	48
2.7.1 Deflections	48
2.7.2 Strains	48
2.8 TEST SET-UP	52
2.9 TESTING PROCEDURE	52
2.9.1 Loading	52
2.9.2 Crack readings and deflections	58
CHAPTER 3 TEST RESULTS	59
3.1 LOAD VERSUS DEFLECTION RESPONSE	60
3.2 CRACKING	67
3.2.1 Models CO-PU-54S-TH	70
3.2.2 Models CO-PU-74S-TH	77
3.2.3 Models CO-PU-100S-TH	77
3.2.4 Nature of Cracking and Comparison of Models	84
3.3 FAILURE MODES	93
3.4 REINFORCEMENT STRAINS	95
CHAPTER 4 ANALYSIS OF RESULTS	112
4.1 DEFLECTIONS.....	112
4.2 MOMENT VERSUS DEFLECTION RESPONSE.....	115
4.3 CRACKING LOAD PREDICTIONS	116

4.4 CRACK WIDTHS.....	117
4.4.1 Allowable versus Test	117
4.4.2 Predictions versus Test	135
4.4.3 Brief Discussion on Crack Width Limits	140
4.5 PERFORMANCE OF SKIN REINFORCEMENT	145
4.6 PERFORMANCE OF T-HEADED REINFORCEMENT.....	148
4.7 STRESS RANGES	152
4.8 ULTIMATE FLEXURAL CAPACITY.....	152
CHAPTER 5 CONSTRUCTABILITY AND ECONOMICS	155
5.1 CONSTRUCTABILITY	155
5.2 ECONOMICS	156
CHAPTER 6 SUMMARY, CONCLUSIONS AND DESIGN RECOMMENDATIONS	163
6.1 SUMMARY	163
6.2 CONCLUSIONS	165
6.3 DESIGN RECOMMENDATIONS	167
REFERENCES	170
VITA	172

LIST OF TABLES

Table 2.1	Prototype and model design loads	10
Table 2.2	Summary of model design	11
Table 2.3	Model identification code	12
Table 2.4	Quantities of prestressed and non-prestressed reinforcement in specimens	13
Table 2.5	Strut and tie forces for overhang CO-PU-54S-TH-V	25
Table 2.6	Strut and tie forces for overhang CO-PU-54S-TH-I	25
Table 2.7	Strut and tie forces for overhang CO-PU-74S-TH-V	26
Table 2.8	Strut and tie forces for overhang CO-PU-74S-TH-I	26
Table 2.9	Strut and tie forces for overhang CO-PU-100S-TH-V	27
Table 2.10	Strut and tie forces for overhang CO-PU-100S-TH-I	27
Table 2.11	Stress ranges at service loads and strand Stresses at full service loads	30
Table 2.12	Concrete mix proportions	31
Table 2.13	Concrete mix properties at time of casting	32
Table 2.14	Concrete Cylinder Compressive Strengths	33
Table 2.15	Average Grout Compressive Strengths	39
Table 2.16	Results from tests of T-headed bars	40
Table 2.17	Load steps	54
Table 2.17	Load steps (continuation...)	54
Table 2.17	Load steps (continuation...)	54
Table 2.18	Age of concrete	57
Table 3.1	Cracking and failure loads	69
Table 3.2	Maximum crack width for overhang CO-PU-54S-TH-V (East side)	73
Table 3.3	Maximum crack width for overhang CO-PU-54S-TH-V (West side)	74
Table 3.4	Maximum crack width for overhang CO-PU-54S-TH-I (East side)	75
Table 3.5	Maximum crack width for overhang CO-PU-54S-TH-I (West side)	76
Table 3.6	Maximum crack width for overhang CO-PU-74S-TH-V (East side)	80
Table 3.7	Maximum crack width for overhang CO-PU-74S-TH-V (West side)	81
Table 3.8	Maximum crack width for overhang CO-PU-74S-TH-I (East side)	82
Table 3.9	Maximum crack width for overhang CO-PU-74S-TH-I (West side)	83

Table 3.10	Maximum crack width for overhang CO-PU-100S-TH-V (East side)	87
Table 3.11	Maximum crack width for overhang CO-PU-100S-TH-V (West side)	88
Table 3.12	Maximum crack width for overhang CO-PU-100S-TH-I (East side)	89
Table 3.13	Maximum crack width for overhang CO-PU-100S-TH-I (West side)	90
Table 3.14	Comparison of cracking	92
Table 4.1	Comparison of tip deflections at major load levels.....	113
Table 4.2	Cracking moments, predicted versus test.....	117
Table 4.3	Values of test vs. predicted maximum crack widths based on three options to account for prestressed and non-prestressed reinforcement	137
Table 4.4	Predicted crack widths versus test results.....	139
Table 4.5	Summary of CEB-FIP 90 crack width limits for post-tensioned structures under frequent load combination	142
Table 4.6	Summary of CEB-FIP 78 crack width limits for post-tensioned structures under frequent load combination.....	143
Table 4.7	Maximum crack width at each grid level in models CO-PU-54S-TH-V and CO-PU-54S-TH-I.....	147
Table 4.8	Model flexural capacities, predicted versus test	153
Table 5.1	Non-prestressed reinforcement quantities in prototype overhangs	157
Table 5.2	Prestressed reinforcement quantities in prototype overhangs	158
Table 5.3	Summary of reinforcement quantities in prototype overhangs	158

LIST OF FIGURES

Figure 1.1	Typical TxDOT bent cap design	2
Figure 2.1	Prototype structure and superstructure	7
Figure 2.2	Geometry of the scale specimens	8
Figure 2.3	Reinforcing cage for model CO-PU-54S-TH-V	14
Figure 2.4	Reinforcing cage for model CO-PU-54S-TH-I	15
Figure 2.5	Reinforcing cage for model CO-PU-74S-TH-V	16
Figure 2.6	Reinforcing cage for model CO-PU-74S-TH-I	17
Figure 2.7	Reinforcing cage for model CO-PU-100S-TH-V	18
Figure 2.8	Reinforcing cage for model CO-PU-100S-TH-I	19
Figure 2.9	Principal tensile stresses for specimen CO-PU-54S-TH under flexure service loads	21
Figure 2.10	Principal compressive stresses for specimen CO-PU-54S-TH under flexure service loads	22
Figure 2.11	Strut and tie model for overhang CO-PU-54S-TH-V	23
Figure 2.12	Strut and tie model for overhang CO-PU-54S-TH-I	23
Figure 2.13	Strut and tie model for overhangs CO-PU-74S-TH-V and CO-PU-100S-TH-V	24
Figure 2.14	Strut and tie model for overhangs CO-PU-74S-TH-I and CO-PU-100S-TH-I	24
Figure 2.15	Detail of confinement reinforcement in bearing area of post-tensioning anchorage	29
Figure 2.16	Column cage	29
Figure 2.17	Stress-strain curve for #2 reinforcing bar	34
Figure 2.18	Stress-strain curve for 7 gauge wire	35
Figure 2.19	Stress-strain curve for 3/8 in. (9.5 mm) diameter strand	36
Figure 2.20	Stress-strain curve for 1/2 in. (12.7 mm) diameter strand	37
Figure 2.21	Prestressing hardware for models CO-PU-74S-TH (V&I)	38
Figure 2.22	T-head dimensions	40
Figure 2.23	T-headed reinforcement in model CO-PU-74S-TH-V	42

Figure 2.24	Formwork	42
Figure 2.25	Reinforcement cage for model CO-PU-54S-TH-I	44
Figure 2.26	Casting of Specimen CO-PU-54S-TH	44
Figure 2.27	Example of plot obtained in a lift-off operation of a typical strand	45
Figure 2.28	Location of linear potentiometers, digital gages and dial gages	48
Figure 2.29	Location of strain gages for models CO-PU-54S-TH (V&I)	49
Figure 2.30	Location of strain gages for models CO-PU-74S-TH (V&I)	50
Figure 2.31	Location of strain gages for models CO-PU-100S-TH (V&I)	51
Figure 2.32	Test set-up	53
Figure 3.1	Moment-deflection response for models CO-PU-54S-TH (V&I)	61
Figure 3.2	Moment-deflection response for models CO-PU-74S-TH (V&I)	62
Figure 3.3	Moment-deflection response for models CO-PU-100S-TH (V&I)	63
Figure 3.4	Use of elastomeric pads in model CO-PU-100S-TH-V	64
Figure 3.5	Comparison of data from linear potentiometers and digital gages for the moment-deflection response of models CO-PU-54S-TH (V&I)	65
Figure 3.6	Comparison of moment-deflection curves	68
Figure 3.7	Crack number and location on East and West sides of CO-PU-54S-TH-V overhang	71
Figure 3.8	Crack number and location on East and West sides of CO-PU-54S-TH-I overhang	72
Figure 3.9	Crack number and location on East and West sides of CO-PU-74S-TH-V overhang	78
Figure 3.10	Crack number and location on East and West sides of CO-PU-74S-TH-I overhang	79
Figure 3.11	Crack number and location on East and West sides of CO-PU-100S-TH-V overhang	85
Figure 3.12	Crack number and location on East and West sides of CO-PU-100S-TH-I overhang	86
Figure 3.13	"Major" cracks at service flexure loads	91
Figure 3.14	Crack distribution in models CO-PU-54S-TH-V (East) after failure	94
Figure 3.15	Crushing in model CO-PU-54S-TH-V (East)	94
Figure 3.16	Crack distribution in model CO-PU-74S-TH-V (East) after failure	96
Figure 3.17	Crushing in model CO-PU-74S-TH-V (East)	96

Figure 3.18	Crack distribution in model CO-PU-100S-TH-I (East) after failure	97
Figure 3.19	Crushing in model CO-PU-100S-TH-I (East)	97
Figure 3.20	Effective strain gages for models CO-PU-54S-TH (V&I)	98
Figure 3.21	Effective strain gages for models CO-PU-74S-TH (V&I)	99
Figure 3.22	Effective strain gages for models CO-PU-100S-TH (V&I)	100
Figure 3.23	Resultant moment vs. strain in effective strain gages in flexural bars for model CO-PU-54S-TH-V	101
Figure 3.24	Resultant moment vs. strain in effective strain gages in skin reinforcement for model CO-PU-54S-TH-V	102
Figure 3.25	Resultant load vs. strain in effective strain gages in shear reinforcement for model CO-PU-54S-TH-V	102
Figure 3.26	Resultant load vs. strain in effective strain gages in shear reinforcement for model CO-PU-54S-TH-V (continuation...)	103
Figure 3.27	Resultant moment vs. strain in effective strain gages in flexural bars for model CO-PU-54S-TH-I	103
Figure 3.28	Resultant moment vs. strain in effective strain gages in skin reinforcement for model CO-PU-54S-TH-I	104
Figure 3.29	Resultant load vs. strain in effective strain gages in shear reinforcement for model CO-PU-54S-TH-I	104
Figure 3.30	Resultant load vs. strain in effective strain gages in shear reinforcement for model CO-PU-54S-TH-I (continuation...)	105
Figure 3.31	Resultant moment vs. strain in effective strain gages in flexural bars for model CO-PU-74S-TH-V	105
Figure 3.32	Resultant moment vs. strain in effective strain gages in skin reinforcement for model CO-PU-74S-TH-V	106
Figure 3.33	Resultant load vs. strain in effective strain gages in shear reinforcement for model CO-PU-74S-TH-V	106
Figure 3.34	Resultant moment vs. strain in effective strain gages in flexural bars for model CO-PU-74S-TH-I	107
Figure 3.35	Resultant moment vs. strain in effective strain gages in skin reinforcement for model CO-PU-74S-TH-I	107
Figure 3.36	Resultant load vs. strain in effective strain gages in shear reinforcement for model CO-PU-74S-TH-I	108
Figure 3.37	Resultant load vs. strain in effective strain gages in shear reinforcement for model CO-PU-74S-TH-I (continuation...)	108

Figure 3.38	Resultant moment vs. strain in effective strain gages in flexural bars for model CO-PU-100S-TH-V	109
Figure 3.39	Resultant moment vs. strain in effective strain gages in skin reinforcement for model CO-PU-100S-TH-V	109
Figure 3.40	Resultant load vs. strain in effective strain gages in shear reinforcement for model CO-PU-100S-TH-V	110
Figure 3.41	Resultant moment vs. strain in effective strain gages in flexural bars for model CO-PU-100S-TH-I	110
Figure 3.42	Resultant moment vs. strain in effective strain gages in skin reinforcement for model CO-PU-100S-TH-I	111
Figure 3.43	Resultant load vs. strain in effective strain gages in shear reinforcement for model CO-PU-100S-TH-I	111
Figure 4.1	Tip deflections at service flexure load level	114
Figure 4.2	Crack plots for CO-PU-54S-TH-V overhang with "virgin" loading curves	119
Figure 4.3	Crack plots for CO-PU-54S-TH-I overhang with "virgin" loading curves	120
Figure 4.4	Crack plots for CO-PU-74S-TH-V overhang with "virgin" loading curves	121
Figure 4.5	Crack plots for CO-PU-74S-TH-I overhang with "virgin" loading curves	121
Figure 4.6	Crack plots for CO-PU-100S-TH-V overhang with "virgin" loading curves	123
Figure 4.7	Crack plots for CO-PU-100S-TH-I overhang with "virgin" loading curves	124
Figure 4.8	Comparison of overhang crack width envelopes based on virgin loading curves	125
Figure 4.9	Crack plots for CO-PU-54S-TH-V overhang with "complete" loading curves ..	128
Figure 4.10	Crack plots for CO-PU-54S-TH-I overhang with "complete" loading curves ...	129
Figure 4.11	Crack plots for CO-PU-74S-TH-V overhang with "complete" loading curves ..	130
Figure 4.12	Crack plots for CO-PU-74S-TH-I overhang with "complete" loading curves ...	131
Figure 4.13	Crack plots for CO-PU-100S-TH-V overhang with "complete" loading curves	132
Figure 4.14	Crack plots for CO-PU-100S-TH-I overhang with "complete" loading curves	133
Figure 4.15	Comparison of overhang crack width envelopes based on complete loading curves.....	134
Figure 4.16	Performance of overhangs in terms of maximum crack widths when compared to allowable values in different codes of practice	144
Figure 4.17	Comparison of crack patterns in models CO-PU-100S-TH-V and CO-PU-100S-TH-I at failure	149

Figure 4.18	Comparison of moment-deflection responses of models CO-PU-74S-TH (V&I) using T-heads, versus models CO-PU-74S (V&I) using standard hooks	151
Figure 5.1	Comparison of total weight of reinforcement for prototype overhangs	159
Figure 5.2	Comparison of total estimated cost for the reinforcement in prototype overhangs.....	160

CHAPTER 1 INTRODUCTION

1.1 GENERAL

Design of elevated urban structures above existing highways often requires the use of large cantilever bent caps. During the design phase of the San Antonio "Y" project the Texas Department of Transportation (TxDOT) found a number of difficulties and inconsistencies while applying AASHTO Standard Specifications for Highway Bridges (1983) [1]. The problems arose as designers attempted to satisfy both serviceability and strength requirements for the large cantilever pier structures. Due to the compartmentalization of the AASHTO design specifications the very large prestressed structures of unusual geometry had to be designed utilizing both the reinforced concrete and prestressed concrete specifications, found in completely separate chapters. Additionally, problems were also found when designing overhangs with concentrated loads having span-to-depth (a/d) ratios near one. In these cases it was not clear whether corbel design or deep beam design should govern. Designers conservatively tried to satisfy both approaches. This resulted in highly congested reinforcing cages resulting in poor constructability and somewhat uneconomical designs. Figure 1.1 shows an example of a typical TxDOT bent cap design.

In order to find improved solutions, it is necessary to look at relatively new philosophies of design that have been developed and investigated during recent years. The general structural concrete approach presented by Schlaich et.al. [2] and endorsed by the IABSE Colloquium on Structural Concrete [3] is a logical way of providing a smooth transition between conventionally reinforced and fully prestressed structures. With the use of this concept, prestressed structures are designed for a mix of active (prestressed) and passive (non-prestressed) reinforcement without arbitrary requirements for limiting service level tensile stresses. The structures may be cracked under service loads but cracks are controlled. This results in a reduced consumption of prestressing steel and avoids unnecessarily high factors of safety against failure. With regard to the design of discontinuity regions such as those in corbel, bracket or deep beam structures, previous research conducted at the University of Texas at Austin [4], TxDOT Project 1127, highly recommended the use of strut-and-tie-models as useful and rational detailing tools. As expressed in that report, the use of the method enables the designer to have a better understanding of the

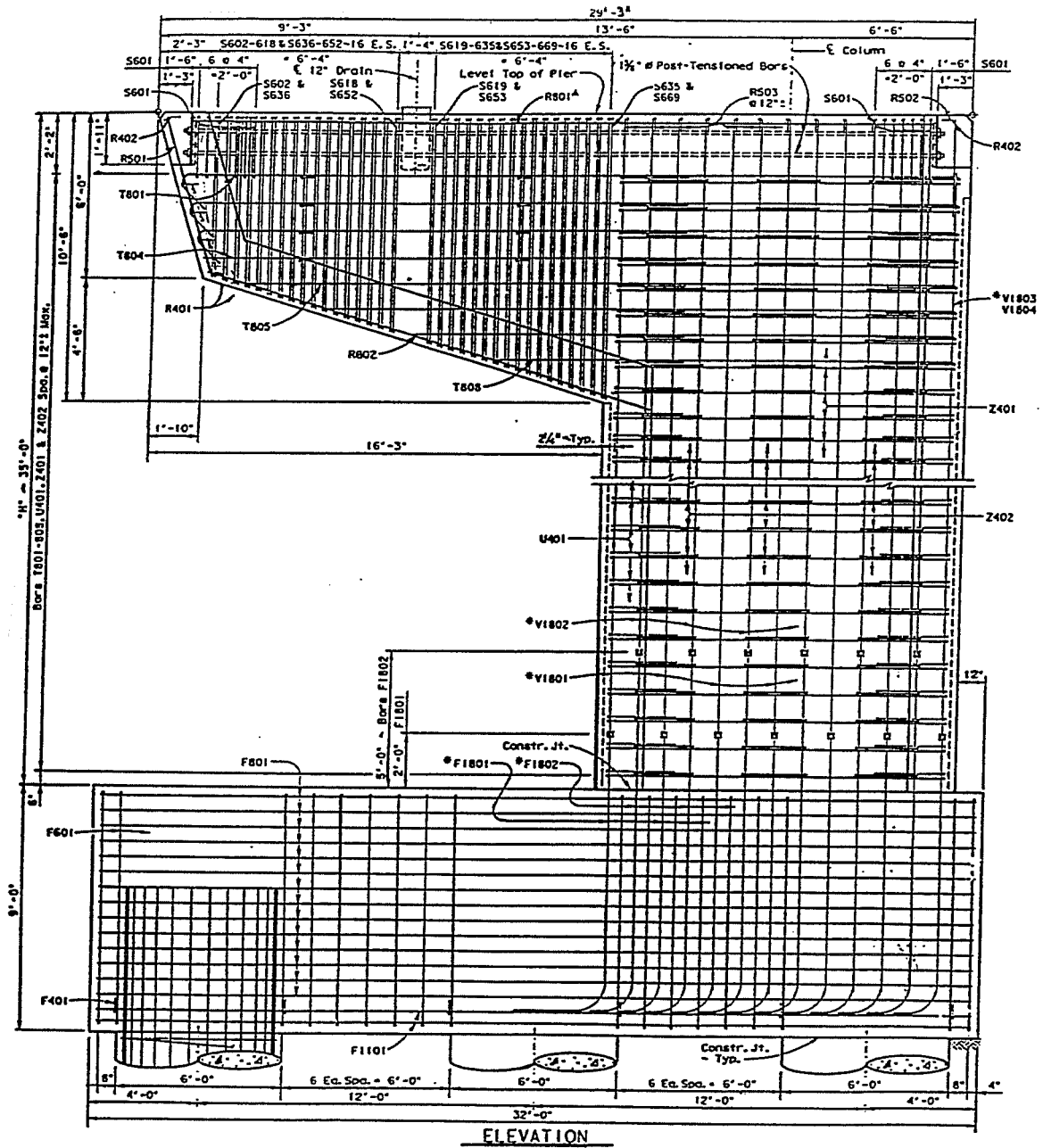


Figure 1.1 Typical TxDOT Bent Cap Design

distribution of internal forces in the structure. In particular, it is of great assistance in proportioning reinforcement.

Concerning congestion in reinforcement development areas, the use of T-headed reinforcing bars has also been studied as a new technique that has been used with success in offshore structures, especially for shear reinforcement. This practice, which replaces hooked bars, not only reduces the congestion in problem regions, allowing for an adequate placement of the concrete mix, but also makes construction of the reinforcing cages much easier.

1.2 DESCRIPTION OF EXPERIMENTAL RESEARCH PROGRAM

The overall research program, "Design of Large Structural Members Utilizing Partial Prestressing", CTR Project No. 1364, currently being carried out at the University of Texas at Austin is divided into three major series of tests.

The first series "Behavior of Structural Concrete Cantilever Piers" was divided into two parts, Series 1364-1A and Series 1364-1B. Series 1364-1A, where the author participated in the construction and testing phases, is being reported by Armstrong [5]. That series consisted of the design, construction and testing of 6 different overhang designs using models at a 1/5.5 scale with straight strands as active reinforcement. They included:

- a) Reinforced concrete design (current AASHTO provisions), with minimum skin reinforcement suggested by Frantz and Breen [6],
- b) Prestressed concrete design with allowable stresses governing (current AASHTO provisions),
- c) Prestressed concrete design with the strength design approach governing for flexure, strut-and-tie modelling using vertical ties for shear, and minimum skin reinforcement,
- d) Prestressed concrete design with the strength design approach governing for flexure, strut-and-tie modelling using inclined ties for shear, and minimum skin reinforcement,
- e) Mixed reinforcement design (74 percent prestressed reinforcement, 26 percent non-prestressed reinforcement) with the strength design approach governing for flexure, strut-and-tie modelling using vertical ties for shear, and minimum skin reinforcement, and

- f) Mixed reinforcement design (74 percent prestressed reinforcement, 26 percent non-prestressed reinforcement) with the strength design approach governing for flexure, strut-and-tie modelling using inclined ties for shear, and minimum skin reinforcement.

Series 1364-1B, which is the subject of this thesis, involved the design, construction, and testing of 6 additional overhang structures similar to those tested in Series 1364-1A, using models at a 1/5.5 scale. The specimens in this series vary the amount of prestressing, use T-headed reinforcing bars for flexure, and vary the skin reinforcement. The complete description of models in Series 1364-1B is presented in Section 2.4.

The second series "Behavior of Two-Span Continuous Pier Caps with Varying Levels of Prestress" is currently being documented by Billington [7]. This series involved the design, construction and testing of four-two span continuous beams constructed at a 1/4 scale, including:

- a) Reinforced concrete design (current AASHTO provisions),
- b) Prestressed concrete design with allowable stresses governing (AASHTO provisions),
- c) Prestressed concrete design with strength design approach governing for flexure, strut-and-tie modelling for shear, and minimum skin reinforcement according to Frantz and Breen [6], and
- d) Mixed reinforcement design (71 percent prestressed reinforcement, 29 percent non-prestressed reinforcement), strut and tie modelling for shear, and minimum skin reinforcement according to Frantz and Breen [6].

The last series of the experimental research program will test overall specimens similar to Figure 1.1 and is currently under development. It is envisioned to last approximately two years.

This series is intended to unify test results and conclusions from the first and second series. It will test more details including several larger size complete specimens including the overhang, column and footing.

1.3 OBJECTIVES

The overall objectives of this research program are:

- a) to develop a better understanding of the influence of post-tensioning on the requirements for non-prestressed reinforcement in large structural concrete members,

- b) to develop a rational, unified design methodology for structural concrete that is envisioned to include applications of strut-and-tie models and to facilitate the efficient use of mixed prestressed and non-prestressed reinforcement,
- c) to make the findings of this study available for consideration by code and specification-writing bodies as soon as results of the research program are approved by TxDOT.

The specific objectives of this portion of the research program, Series 1364-1B, are:

- a) to design, build, and test under static loading six 1/5.5 scale post-tensioned cantilever bents with varying mixtures of prestressed and non-prestressed reinforcement using strut-and-tie models for shear design, and to compare results with allowable and analytical performance,
- b) to test T-headed reinforcing bars for flexure in all models to evaluate their performance in crack control, in reducing congestion in anchorage areas, and in improving constructability of the reinforcing cages when compared to the results from Series 1364-1A,
- c) to evaluate the use of different areas of skin reinforcement in controlling crack widths at service loads (minimum face steel and skin reinforcement suggested by Frantz and Breen [6]).

1.4 SCOPE

The scope of the experimental program includes comparison of moment-deflection responses of the six overhang structures tested with different mixtures of prestressed and non-prestressed reinforcement, comparison of crack width data, and stress ranges. The results are compared to earlier tests to evaluate any benefit due to the use of T-headed reinforcing bars, as well as conclusions from the use of different amounts of skin reinforcement.

Since this research study is part of a more comprehensive research program, this thesis is limited to drawing preliminary conclusions and recommendations from the six-overhang models tested and analyzed. Major conclusions from Research Project No. 1364 based on results of all test series will be presented in a future document.

This thesis is organized into six chapters. Chapter 2 deals with the research program, including model selection criteria, scale factor relations, materials, fabrication, instrumentation and

testing procedures. Chapter 3 provides test results including moment-deflection response, cracking loads and patterns and ultimate behavior. Chapter 4 discusses test results, including comparison with data from previous research and from theoretical analyses. Chapter 5 discusses material quantities, constructability, costs and economic benefits. Chapter 6 includes a summary, conclusions and preliminary design recommendations.

CHAPTER 2 RESEARCH PROGRAM

The purpose of this experimental program was to study the behavior of varied mixtures of prestressed and non-prestressed reinforcement in design of large bridge support structures using an ultimate design approach, including the state of the art in strut-and-tie modelling for shear, the state of the art in T-headed reinforcement for all non-prestressed flexural reinforcing steel, and varying amounts of skin reinforcement. All three specimens (six-overhangs) were designed, fabricated, post-tensioned and tested at the Ferguson Structural Engineering Laboratory at the University of Texas at Austin.

2.1 TYPICAL TxDOT PIER CAP DESIGN

Pier cap designs that presented design challenges in the San Antonio "Y" Project were studied by Armstrong in the first series (Series 1364-1A [5]) in order to determine a typical prototype structure shown in Figure 2.1. Typical reinforcing bars used in those designs included #11 and #8 bars for flexural reinforcement, and #6 and #4 bars for shear reinforcement in the overhang structure. For the column section typical bars included #18 bars for the vertical (main) steel and #4 bars for the horizontal (stirrup) steel.

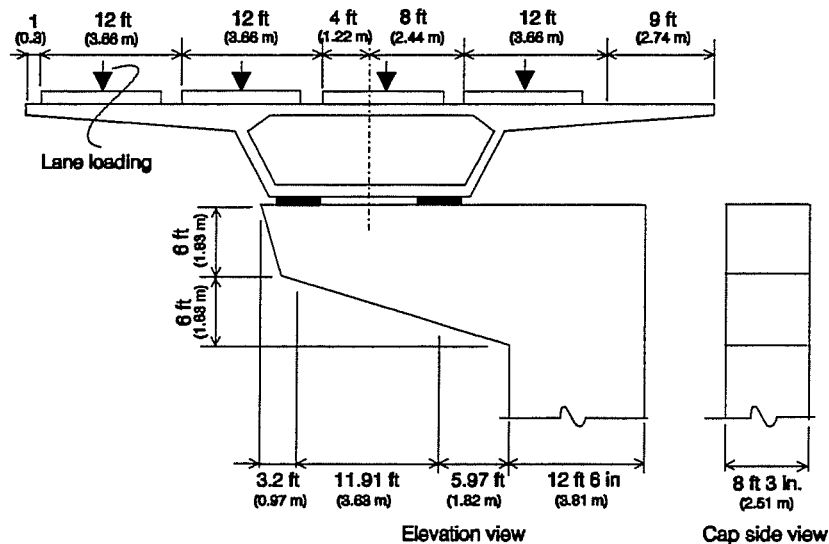


Figure 2.1 Prototype Structure and Superstructure

2.2 MODEL SELECTION

The model geometry used for construction of test specimens is shown in Figure 2.2. This geometry was selected to allow testing of two cantilever overhangs simultaneously, providing a balanced moment at the column section. At ultimate load levels it was recognized that only one overhang would fail. This was accepted since the focus of the experimental program was the performance of the models at service loads and full information at service load levels as well as factored load levels could be obtained for both overhangs.

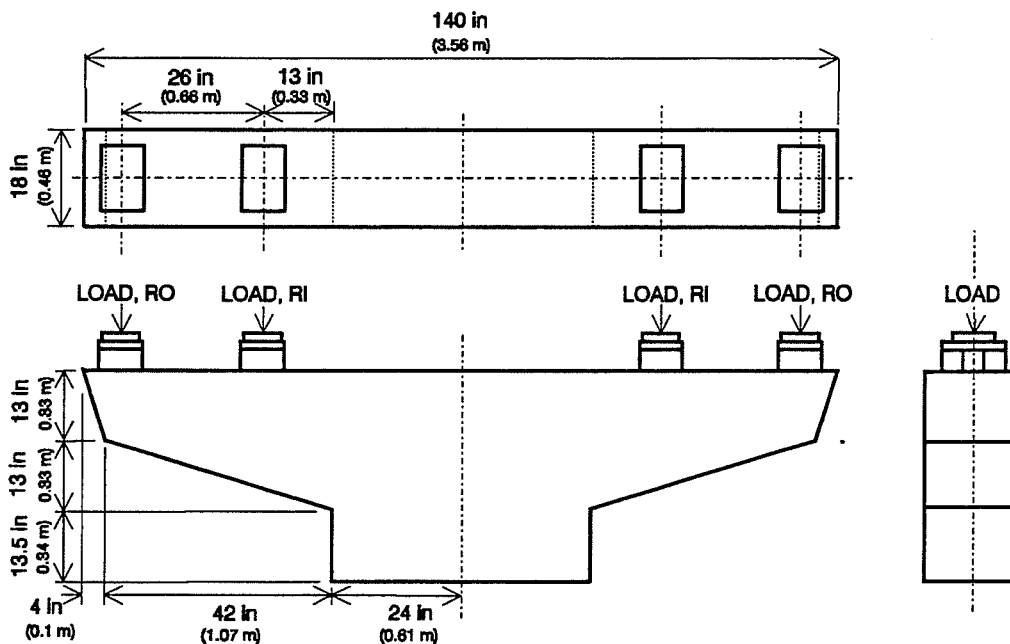


Figure 2.2 Geometry of the Scale Specimens

2.3 SCALE FACTOR SELECTION/SCALE RELATIONS

Various geometric scale factors were studied based on economics, available materials, fabrication methods, and testing procedures. After this review, a scale factor of 5.5 was chosen. One of the major considerations was the ability to scale down the commonly used #11 and #8 reinforcing bars to available deformed #2 bars and 7 gage wire, respectively. In addition, this scale factor allowed for a modest size test set-up without exceeding the capacity of the available testing equipment.

2.3.1 Materials

The concrete mix design was carried out to provide a concrete strength at 28 days of 5000 psi (34.5 MPa), as commonly used by TxDOT (see details in Section 2.5.1). The maximum aggregate size was limited to 3/8 in. (9.5 mm) to allow for adequate placement of the mix. With this design the stress-strain behavior of the concrete was assumed to be equal to that of the prototype, allowing for use of stress and strain scale factors equal to unity.

2.3.2 Loads

Load relations between prototype and model were calculated, based on scale factors as [8]:

1. Loads distributed over an area:

$$\textit{Model load per unit area} = \textit{prototype load per unit area} \quad [2.1]$$

2. Loads distributed over a length

$$\textit{Model load per unit length} = \frac{1}{5.5} \times \textit{prototype load per unit length} \quad [2.2]$$

3. Concentrated loads

$$\textit{Model load} = \frac{1}{5.5^2} \times \textit{prototype load} \quad [2.3]$$

4. Gravity loads

$$\textit{Model density} = 5.5 \times \textit{prototype density} \quad [2.4]$$

Using these relations the measured strain in the model was assumed equal to the prototype strain, and the model deflections were 1/5.5 times the prototype deflections.

The requirement for increased model density was overcome with the application of external loads from the loading rams as discussed in Section 2.9.

2.4 MODEL DESIGN

Models were designed based on controlling loads in typical TxDOT designs, as in Pier D36 of the San Antonio "Y" - Project III- C&D. Group I loading based on AASHTO provisions with three outside lanes loaded controlled the required moment capacity, while Group I loading with four lanes loaded controlled the required shear capacity. Design loads for prototype and model structures are summarized in Table 2.1.

Table 2.1 Prototype and Model Design Loads

Description		Prototype Load		Model Load	
		kips	(kN)	kips	(kN)
Flexure Design Loads					
Service Loads	Ro *	1680	(7473)	55.5	(247)
	Ri *	1031	(4586)	34.1	(152)
	Dead load cap ***	220	(979)	1.32 model 5.94 additional ****	(5.87 model) (26.42 additional)
Factored Loads **	Ro	2621	(11658)	86.6	(385)
	Ri	1212	(5391)	40.1	(178)
	Dead Load cap	286	(1272)	1.7 model 7.7 additional	(7.56 model) (34.25 additional)
Shear Design Loads					
Service Loads	Ro	1376	(6120)	45.5	(202)
	Ri	1376	(6120)	45.5	(202)
	Dead Load cap	220	(979)	1.32 model 5.94 additional	(5.87 model) (26.42 additional)
Factored Loads	Ro	1959	(8714)	64.8	(288)
	Ri	1959	(8714)	64.8	(288)
	Dead Load cap	286	(1272)	1.7 model 7.7 additional	(7.56 model) (34.25 additional)

* Ri and Ro (see Figure 2.2) include dead loads from superstructure, live load and impact.

** Load factors are based on Group I loading (AASHTO provisions).

*** Overhang dead load refers to the resultant dead load applied at the centroid of the structure.

**** Additional dead loads (simulated dead loads) were applied to the models through the same loading rams used to apply the Ri and Ro loads. 75.4 percent of the additional dead load was applied in combination with Ri load (at 13 inches from the face of the column), while 24.6 percent was applied in combination with the Ro load (at 39 inches from the face of the column).

All models were designed using the strength design approach for flexure and strut and tie modelling for shear-diagonal tension. T-heads were used with all flexural #2 bars as described in Section 2.5.6, and standard hooks were used with all 7 gage wire. Table 2.2 shows a summary of the design characteristics per model. Model identification codes are explained in Table 2.3. The overall dimensions and reinforcing steel layouts are shown in Figures 2.3 to 2.8 for each of the six overhang models. Table 2.4 summarizes steel quantities for each model.

Table 2.2 Summary of model design

Model	Prestressed Reinforcement Percentage (ultimate design for flexure)	Strut and Tie model (Shear)	Skin Reinforcement
CO-PU-54S-TH-V	54	vertical tie	as per Frantz [6]
CO-PU-54S-TH-I	54	inclined tie	minimum
CO-PU-74S-TH-V	74	vertical tie	minimum
CO-PU-74S-TH-I	74	inclined tie	minimum
CO-PU-100S-TH-V	100	vertical tie	as per Frantz [6]
CO-PU-100S-TH-I	100	inclined tie	minimum

T-Headed reinforcement for all non-prestressed flexural reinforcement (#2 reinforcing bars).

Table 2.3 Model identification code

Model ID	Description
CO	Type of structure: Cantilever overhang
PU	Design Philosophy: Prestress design with ultimate strength method governing
54S-74S-100S	Percentage of reinforcement which is prestressed and type of steel: X % prestressing, with strands
TH	Type of anchorage for non-prestressed flexural reinforcement: T-heads
V - I	Type of strut and tie model used for shear: Vertical tie or Inclined tie
Example	CO-PU-54S-TH-V

2.4.1 Flexural design

AASHTO standard provisions for ultimate strength, including a strength reduction (ϕ) factor of 0.9, were used to determine the quantity of post-tensioning steel needed to achieve 100 percent of the required ultimate capacity of the structure. Mixed reinforcement structures were designed for flexure by taking the desired percentage of that quantity of prestressing steel needed to achieve 100 percent of the required ultimate capacity (for prestressing steel at its calculated ultimate stress) to provide the amount of ultimate tensile force contributed by the prestressed reinforcement. Then the proper number of #2 bars, $f_y=75.1$ ksi ($f_y=518$ MPa), was added as non-prestressed reinforcement to provide the required balance of the moment capacity. Finally the service level post-tensioning force was determined based on the area of prestressing steel times the effective post-tensioning stress.

Table 2.4 Quantities of prestressed and non-prestressed reinforcement in specimens

Model	10 gage wire*		7 gage wire		#2 reforc. bar		1/2" (13 mm) strand		3/8" (9.5mm) strand		Total non-prestr. reinforcement		Total prestressed reinforcement	
	lb	(kg)	lb	(kg)	lb	(kg)	lb	(kg)	lb	(kg)	lb	(kg)	lb	(kg)
CO-PU-54S-TH-V	19.78	(8.90)	3.73	(1.68)	19.71	(8.87)	10.88	(4.89)	0.00	(0.00)	43.22	(19.45)	10.88	(4.89)
CO-PU-54S-TH-I	19.55	(8.80)	10.92	(4.91)	16.13	(7.26)	10.88	(4.89)	0.00	(0.00)	46.60	(20.97)	10.88	(4.89)
CO-PU-74S-TH-V	17.35	(7.81)	3.13	(1.41)	8.96	(4.03)	10.88	(4.89)	7.25	(3.26)	29.44	(13.25)	18.13	(8.16)
CO-PU-74S-TH-I	17.56	(7.90)	7.62	(3.43)	8.96	(4.03)	10.88	(4.89)	7.25	(3.26)	34.14	(15.36)	18.13	(8.16)
CO-PU-100S-TH-V	17.35	(7.81)	4.63	(2.08)	7.17	(3.23)	18.13	(8.16)	3.63	(1.63)	29.15	(13.12)	21.75	(9.79)
CO-PU-100S-TH-I	17.56	(7.90)	6.13	(2.76)	3.58	(1.61)	18.13	(8.16)	3.63	(1.63)	27.27	(12.27)	21.75	(9.79)

* Includes post-tensioning anchorage zone reinforcement.

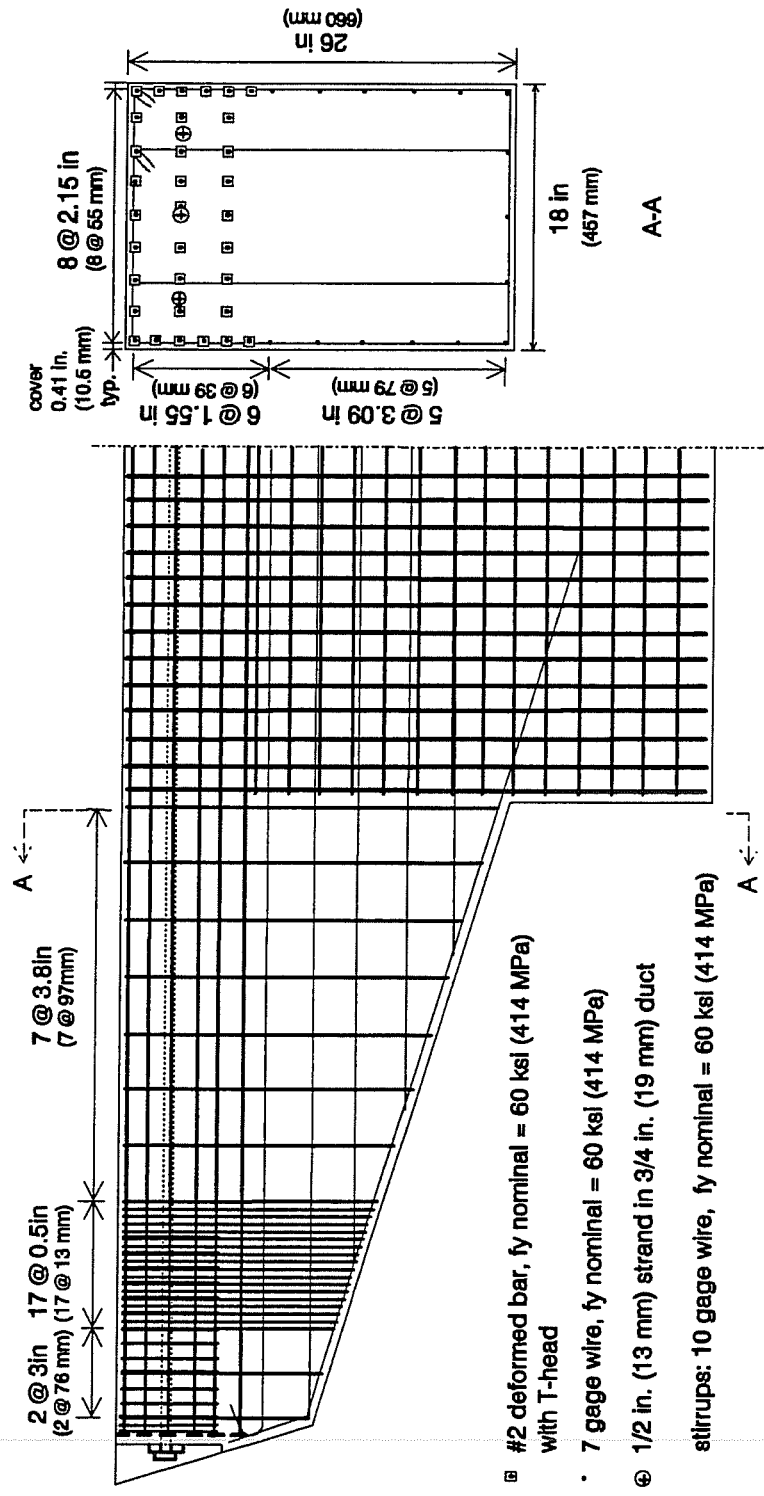


Figure 2.3 Reinforcing Cage for Model CO-PU-54S-TH-V

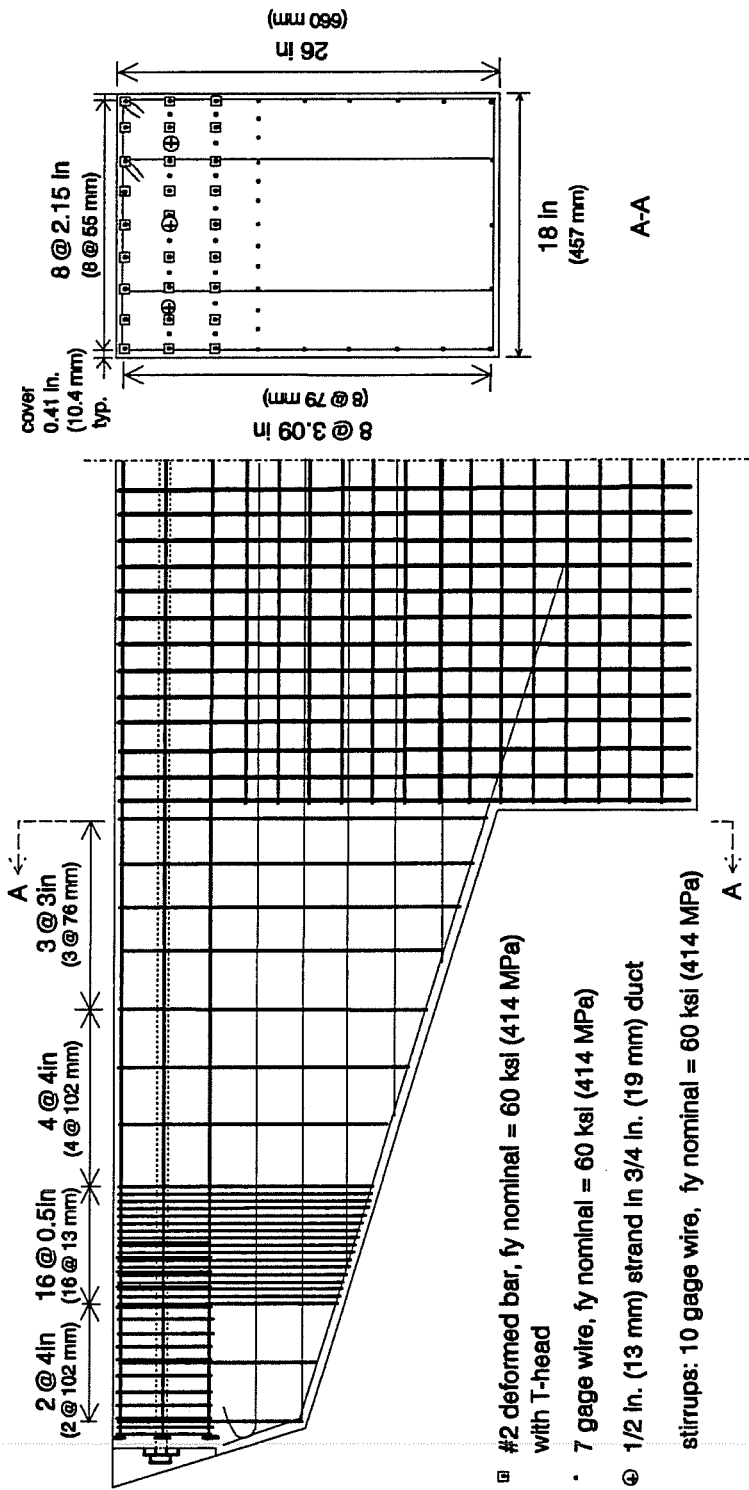


Figure 2.4 Reinforcing Cage for Model CO-PU-54S-TH-I

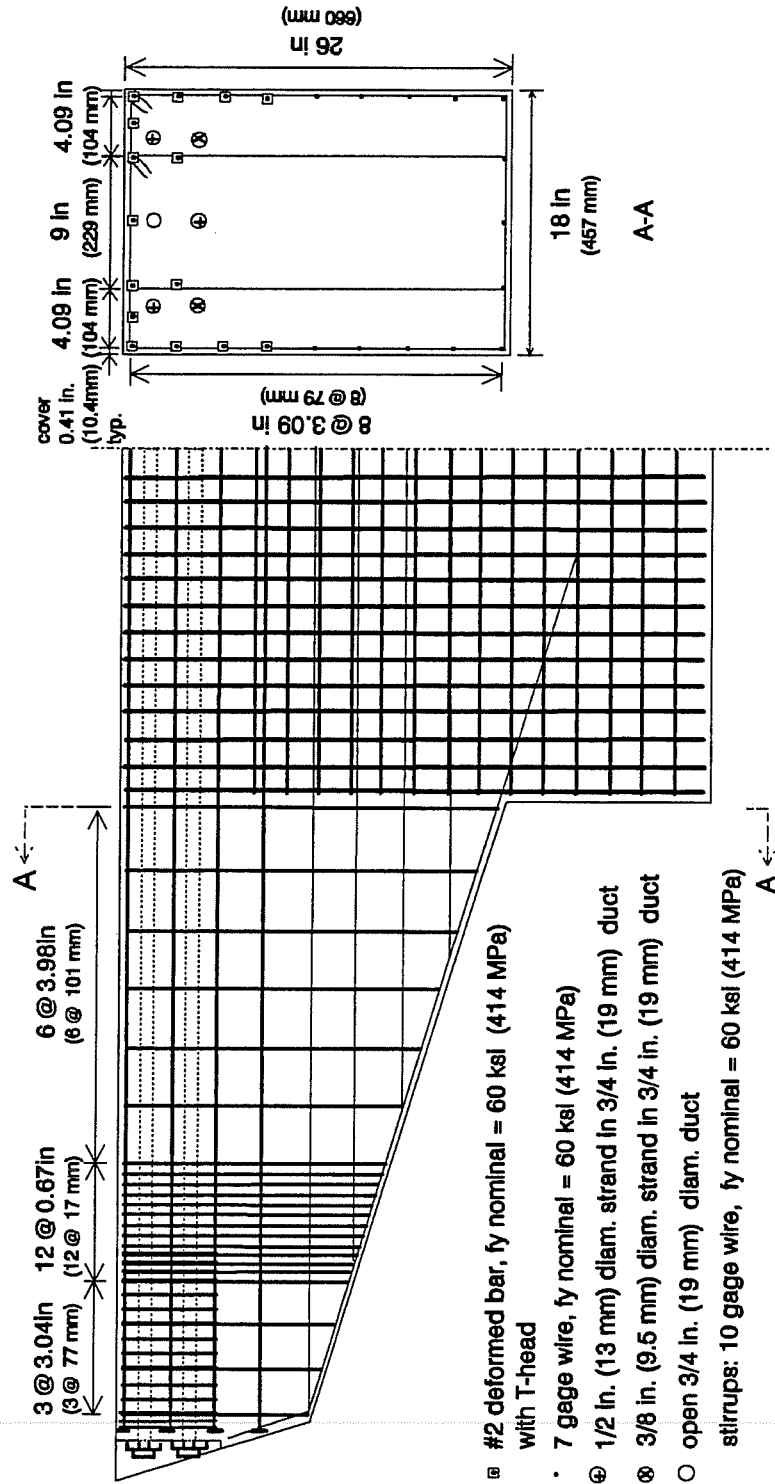


Figure 2.5 Reinforcing Cage for Model CO-PU-74S-TH-V

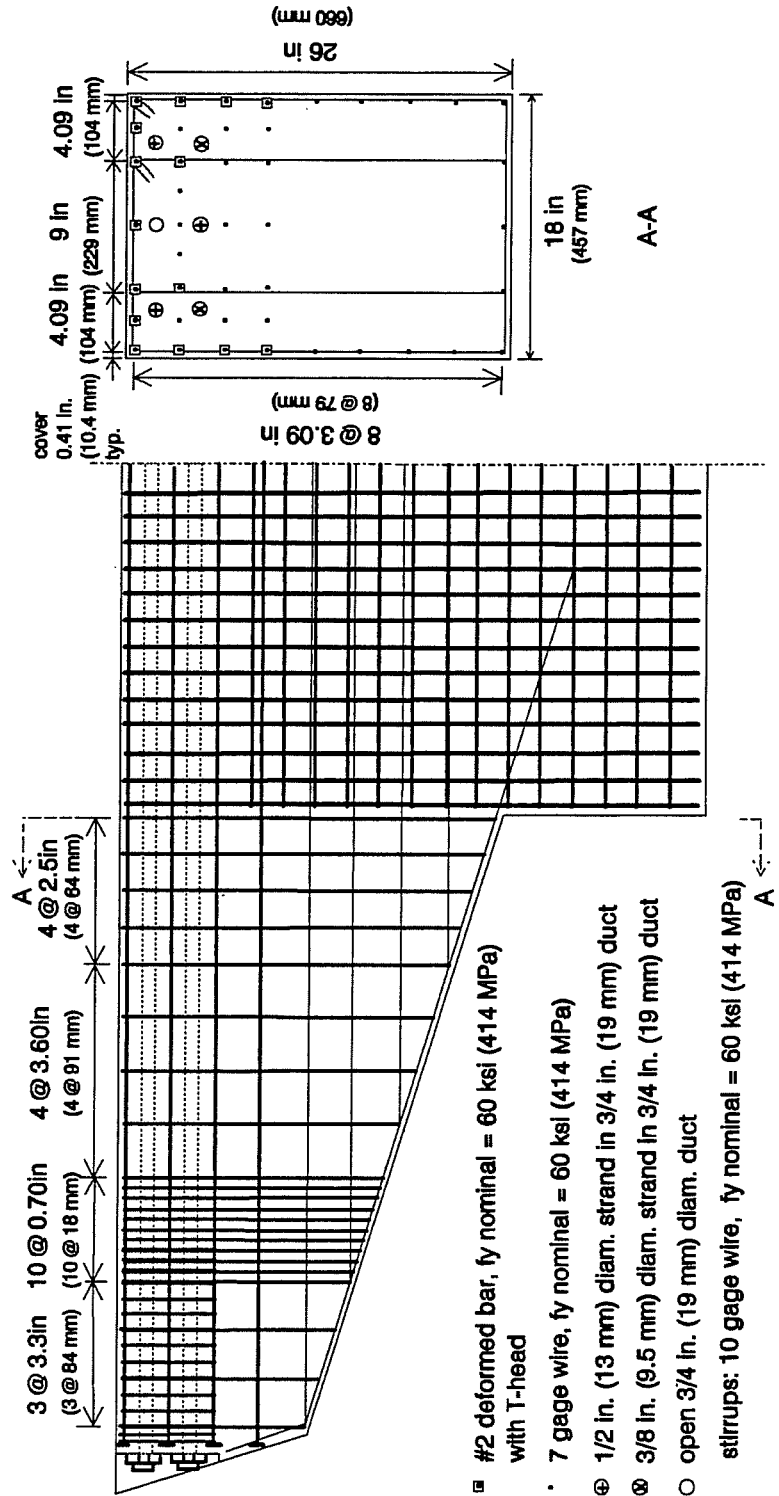


Figure 2.6 Reinforcing Cage for Model CO-PU-74S-TH-I

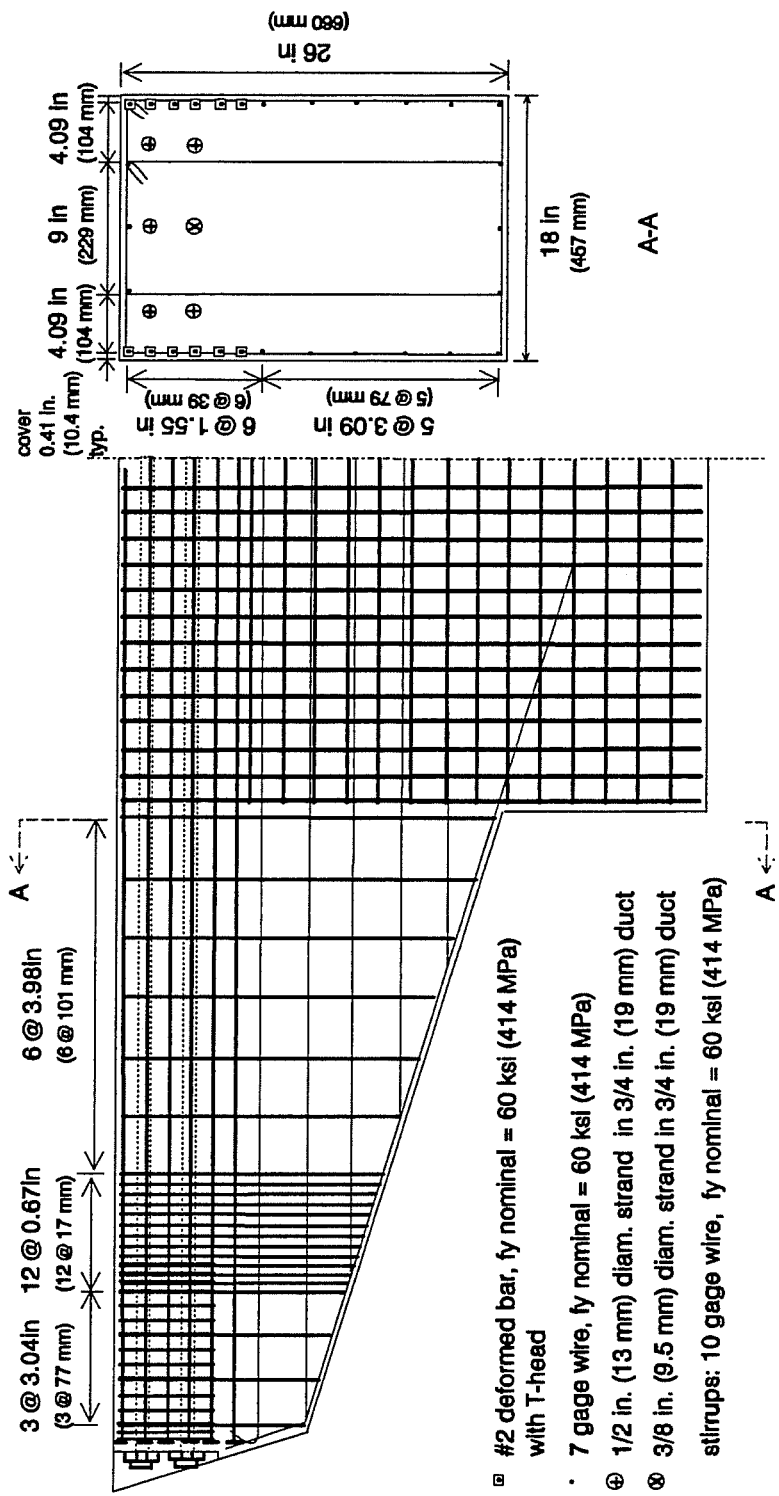


Figure 2.7 Reinforcing Cage for Model CO-PU-100S-IH-V

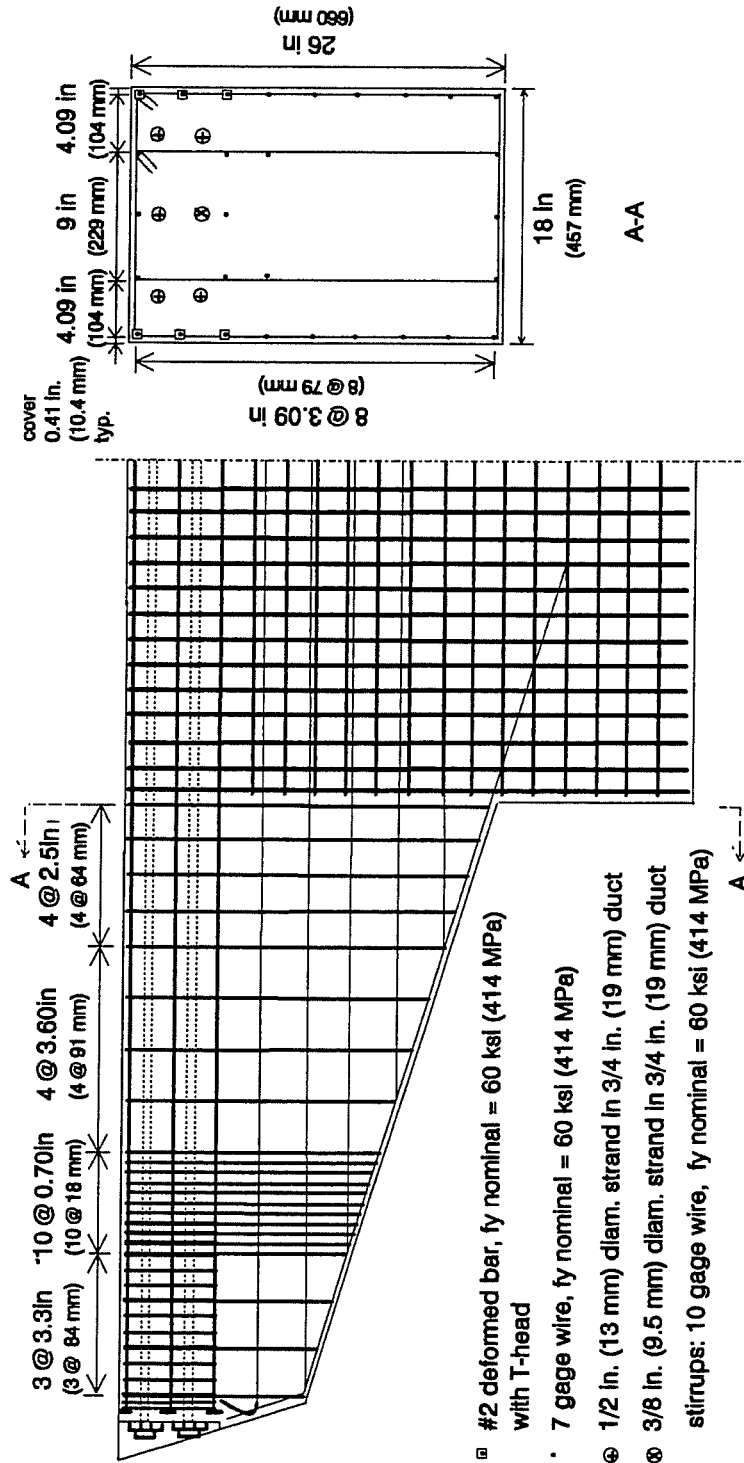


Figure 2.8 Reinforcing Cage for Model CO-PU-100S-TH-I

Prestressing steel was designed with an eccentricity of 9.4 in (239 mm). For models CO-PU-54S-TH (V&I) the post-tensioning steel consisted of a single row of three 1/2 in. (13 mm) diameter, grade 270 (1860 MPa), low relaxation strands, located as indicated in Figures 2.3 and 2.4. Model CO-PU-74S-TH (V&I) post-tensioning steel consisted of two rows. There were two 1/2 in. (13 mm) diameter strands in the top row. The bottom row had one 1/2 in. (13 mm) strand in the middle, and two 3/8 in. (9.5 mm) diameter strands on the outside as indicated in Figures 2.5 and 2.6. Models CO-PU-100S-TH (V&I) were post-tensioned with the use of two rows of strands. The top row had three 1/2 in. (13 mm) strands. The bottom row had two 1/2 in. (13 mm) strands at the sides and one 3/8 in. (9.5 mm) strand in the middle, as shown in Figures 2.7 and 2.8.

2.4.2 Shear design/ Strut and tie models

Shear reinforcement was designed with the aid of strut-and-tie models developed using force flow paths determined from elastic finite element analyses. Principal stresses were plotted for all models under both service and factored load levels for both shear and flexure loads. (See Figures 2.9 and 2.10 for typical examples.) These analyses were performed using 8-node isoparametric elements and nominal concrete properties.

Based on these plots and on strut-and-tie model theory [2,4] two different models were developed, one with inclined ties and another with a single vertical tie. Both models would be acceptable from a strength basis. However, the aim of the research project was to evaluate their performance with the different percentages of prestressing steel, as shown in Table 2.2, and to compare results.

Additional horizontal steel required in those overhangs with inclined tie models was provided with 7 gage wire.

The particular strut-and-tie models selected are shown in Figures 2.11 through 2.14. Tables 2.5 through 2.10 summarize the strut and tie forces.

It is important to mention that any shear contribution provided by concrete was not taken into account when proportioning the tie steel. In addition, tie forces were divided by a ϕ factor of 0.85 as in a typical ultimate strength design approach. For this reason, it was anticipated that these shear models would provide a very conservative design (lower bound solution).

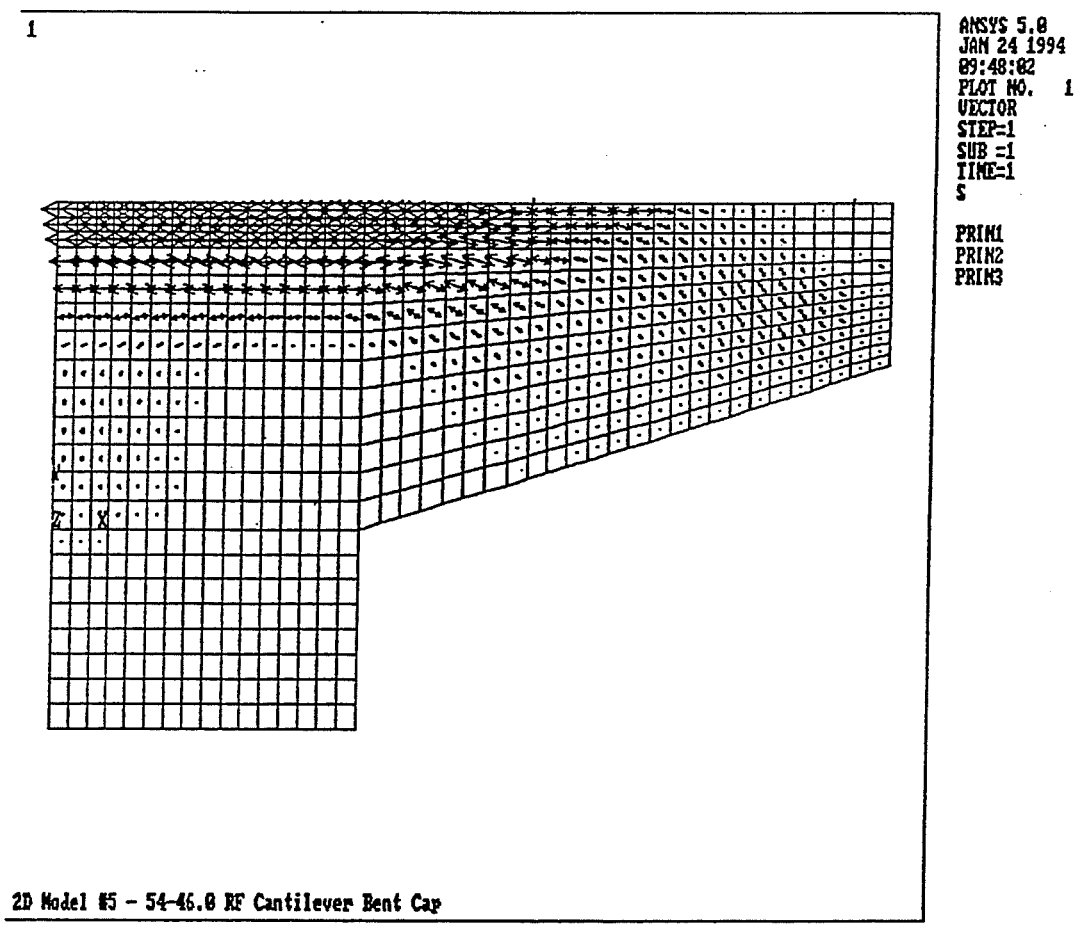


Figure 2.9 Principal Tensile Stresses for Specimen CO-PU-54S-TH under Flexure Service Loads

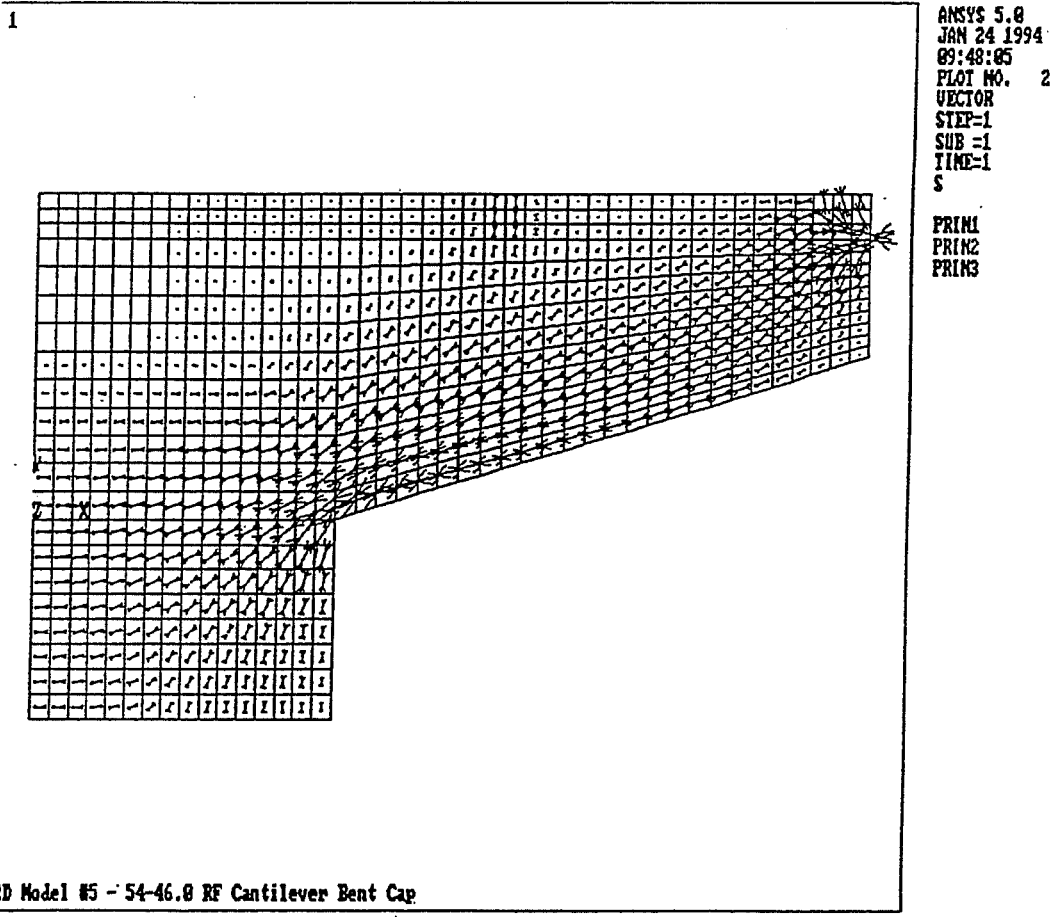


Figure 2.10 Principal Compressive Stresses for Specimen CO-PU-54S-TH under Flexure Service Loads

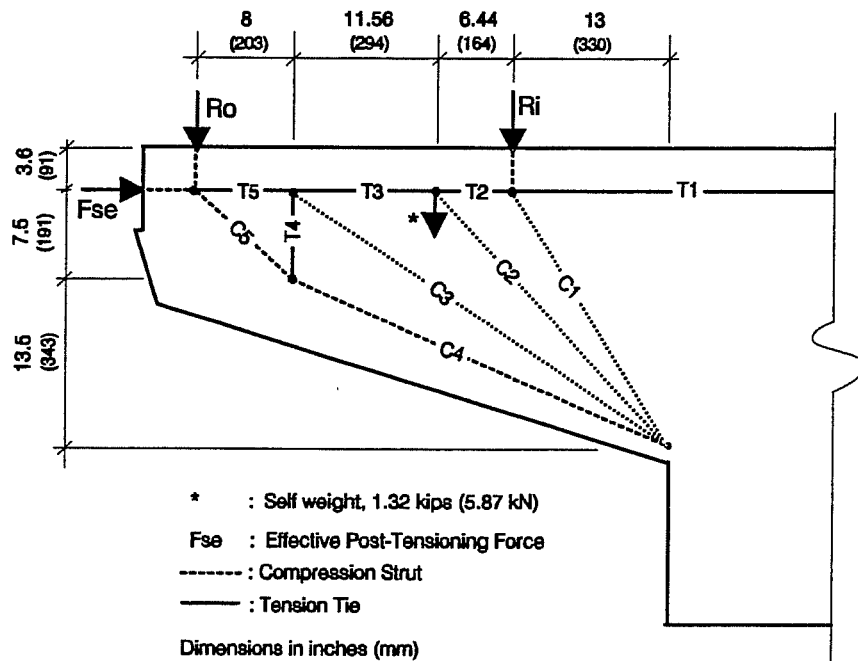


Figure 2.11 Strut and tie model for overhang CO-PU-54S-TH-V

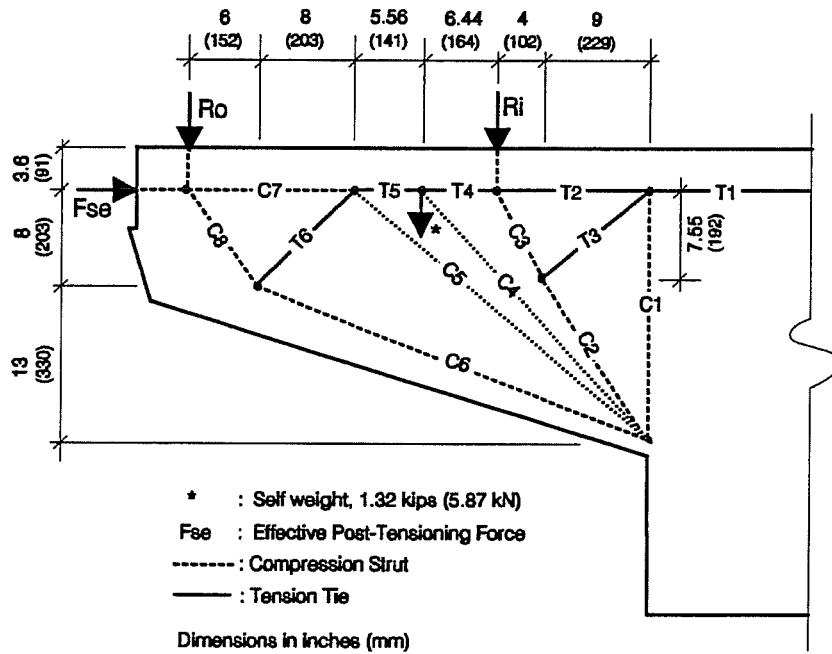


Figure 2.12 Strut and tie model for overhang CO-PU-54S-TH-I

Table 2.5 Strut and tie forces for overhang CO-PU-54S-TH-V

Strut or Tie force	Factored flexure loads applied *		Factored shear loads applied**	
	kips	(kN)	kips	(kN)
C1	-53.98	-(240.10)	-83.03	-(369.32)
C2	-2.34	-(10.41)	-2.34	-(10.41)
C3	-84.51	-(375.90)	-63.70	-(283.34)
C4	-102.97	-(458.01)	-77.61	-(345.21)
C5	-129.40	-(575.57)	-97.53	-(433.81)
T1	120.97	(538.07)	95.78	(426.03)
T2	92.56	(411.71)	52.08	(231.65)
T3	90.97	(404.63)	50.49	(224.58)
T4	47.39	(210.79)	35.72	(158.88)
T5	21.00	(93.41)	-2.25	-(10.01)

* Ro=88.5 kips (393.65 kN), Ri=45.9 kips (204.16 kN), Fse=73.4 kips (326.48 kN)

** Ro=66.7 kips (296.68 kN), Ri=70.6 kips (314.03 kN), Fse=73.4 kips (326.48 kN)

Note: Ro and Ri include simulated dead loads.

Table 2.6 Strut and tie forces for overhang CO-PU-54S-TH-I

Strut or Tie force	Factored flexure loads applied *		Factored shear loads applied**	
	kips	(kN)	kips	(kN)
C1	-3.37	-(14.99)	-5.17	-(23.00)
C2	-51.09	-(227.25)	-78.58	-(349.52)
C3	-51.98	-(231.21)	-79.96	-(355.66)
C4	-2.34	-(10.41)	-2.34	-(10.41)
C5	-69.56	-(309.40)	-52.42	-(233.16)
C6	-119.43	-(531.22)	-90.00	-(400.32)
C7	-7.02	-(31.22)	-23.37	-(103.95)
C8	-110.63	-(492.08)	-83.38	-(370.87)
T1	120.98	(538.12)	95.78	(426.03)
T2	116.97	(520.28)	89.61	(398.59)
T3	5.24	(23.31)	8.05	(35.81)
T4	92.57	(411.75)	52.07	(231.61)
T5	90.98	(404.68)	50.48	(224.54)
T6	63.27	(281.42)	47.68	(212.08)

* Ro=88.5 kips (393.65 kN), Ri=45.9 kips (204.16 kN), Fse=73.4 kips (326.48 kN)

** Ro=66.7 kips (296.68 kN), Ri=70.6 kips (314.03 kN), Fse=73.4 kips (326.48 kN)

Note: Ro and Ri include simulated dead loads.

Table 2.7 Strut and tie forces for overhang CO-PU-74S-TH-V

Strut or Tie force	Factored flexure loads applied *		Factored shear loads applied**	
	kips	(kN)	kips	(kN)
C1	-54.00	-(240.19)	-83.08	-(369.54)
C2	-2.34	-(10.41)	-2.34	-(10.41)
C3	-58.80	-(261.54)	-44.30	-(197.05)
C4	-129.14	-(574.41)	-97.33	-(432.92)
C5	-147.25	-(654.97)	-110.98	-(493.64)
C6	17.04	(75.79)	-11.95	-(53.15)
T1	94.10	(418.56)	68.84	(306.20)
T2	65.62	(291.88)	25.05	(111.42)
T3	64.03	(284.81)	23.46	(104.35)
T4	35.34	(157.19)	26.63	(118.45)

* Ro=88.5 kips (393.65 kN), Ri=45.9 kips (204.16 kN), Fse=100.64 kips (447.65 kN)

** Ro=66.7 kips (296.68 kN), Ri=70.6 kips (314.03 kN), Fse=100.64 kips (447.65 kN)

Note: Ro and Ri include simulated dead loads.

Table 2.8 Strut and tie forces for overhang CO-PU-74S-TH-I

Strut or Tie force	Factored flexure loads applied *		Factored shear loads applied**	
	kips	(kN)	kips	(kN)
C1	-7.75	-(34.47)	-11.92	-(53.02)
C2	-47.60	-(211.72)	-73.22	-(325.68)
C3	-49.51	-(220.22)	-76.15	-(338.72)
C4	-2.34	-(10.41)	-2.34	-(10.41)
C5	-45.29	-(201.45)	-34.13	-(151.81)
C6	-142.91	-(635.66)	-107.71	-(479.09)
C7	4.92	(21.88)	-21.08	-(93.76)
C8	-137.75	-(612.71)	-103.82	-(461.79)
T1	94.10	(418.56)	68.86	(306.29)
T2	84.18	(374.43)	53.60	(238.41)
T3	12.59	(56.00)	19.36	(86.11)
T4	65.63	(291.92)	25.07	(111.51)
T5	64.04	(284.85)	23.48	(104.44)
T6	38.00	(169.02)	28.64	(127.39)

* Ro=88.5 kips (393.65 kN), Ri=45.9 kips (204.16 kN), Fse=100.64 kips (447.65 kN)

** Ro=66.7 kips (296.68 kN), Ri=70.6 kips (314.03 kN), Fse=100.64 kips (447.65 kN)

Note: Ro and Ri include simulated dead loads.

Table 2.9 Strut and tie forces for overhang CO-PU-100S-TH-V

Strut or Tie force	Factored flexure loads applied *		Factored shear loads applied**	
	kips	(kN)	kips	(kN)
C1	-54.00	-(240.19)	-83.08	-(369.54)
C2	-2.34	-(10.41)	-2.34	-(10.41)
C3	-58.80	-(261.54)	-44.30	-(197.05)
C4	-129.14	-(574.41)	-97.33	-(432.92)
C5	-147.25	-(654.97)	-110.98	-(493.64)
C6	-18.31	-(81.44)	-47.30	-(210.39)
T1	58.74	(261.28)	33.48	(148.92)
T2	30.27	(134.64)	-10.31	-(45.86)
T3	28.68	(127.57)	-11.90	-(52.93)
T4	35.34	(157.19)	26.63	(118.45)

* Ro=88.5 kips (393.65 kN), Ri=45.9 kips (204.16 kN), Fse=136 kips (605 kN)

** Ro=66.7 kips (296.68 kN), Ri=70.6 kips (314.03 kN), Fse=136 kips (605 kN)

Note: Ro and Ri include simulated dead loads.

Table 2.10 Strut and tie forces for overhang CO-PU-100S-TH-I

Strut or Tie force	Factored flexure loads applied *		Factored shear loads applied**	
	kips	(kN)	kips	(kN)
C1	-7.75	-(34.47)	-11.92	-(53.02)
C2	-47.60	-(211.72)	-73.22	-(325.68)
C3	-49.51	-(220.22)	-76.15	-(338.72)
C4	-2.34	-(10.41)	-2.34	-(10.41)
C5	-45.29	-(201.45)	-34.13	-(151.81)
C6	-142.91	-(635.66)	-107.71	-(479.09)
C7	-30.44	-(135.40)	-56.44	-(251.05)
C8	-137.75	-(612.71)	-103.82	-(461.79)
T1	58.74	(261.28)	33.50	(149.01)
T2	48.82	(217.15)	18.24	(81.13)
T3	12.59	(56.00)	19.36	(86.11)
T4	30.27	(134.64)	-10.29	-(45.77)
T5	28.68	(127.57)	-11.88	-(52.84)
T6	38.00	(169.02)	28.64	(127.39)

* Ro=88.5 kips (393.65 kN), Ri=45.9 kips (204.16 kN), Fse=136 kips (605 kN)

** Ro=66.7 kips (296.68 kN), Ri=70.6 kips (314.03 kN), Fse=136 kips (605 kN)

Note: Ro and Ri include simulated dead loads.

2.4.3 Skin Reinforcement

Cantilever overhangs CO-PU-54S-TH-V and CO-PU-100S-TH-V were designed with an area of skin reinforcement of 0.59 in.^2 (380 mm^2), as per Frantz and Breen [6]. Calculation of the area of skin reinforcement based on that report includes all the face steel that is to be distributed over one-half of the effective depth of the member nearest the principal reinforcement. For the bottom half, supplementary steel (7 gage wire) was arbitrarily provided at a spacing of 3.09 in. (79 mm) as minimum reinforcement for shrinkage and temperature.

Face steel in models CO-PU-54S-TH-I and CO-PU-74S-TH (V&I) was not the result of a direct design but rather was the computation of the reinforcement in this area after the distribution of the main flexural steel (#2 reinforcing bars) in the top of the cage at a spacing of 3.09 in. (79 mm), and the addition of supplementary steel (7 gage wire) at the same spacing until reaching the bottom of the cage. The spacing corresponded to 18 in. (457 mm) in the prototype structure. By referring to Figure 2.4 and 2.6, and using the same criteria as described above, this gives an area of skin reinforcement of 0.29 in.^2 (187 mm^2) for the CO-PU-54S-TH-I model, and 0.34 in.^2 (219 in.^2) for the CO-PU-74-TH (V&I) models.

For the CO-PU-100S-TH-I overhang, even when it was not necessary for strength, some non-prestressed reinforcement was included in the detailing process for construction purposes. Minimum corner bars as well as minimum face steel were included in the design at a spacing of 3.09 in (79 mm) with the purpose of providing a working frame for the adequate placement and support of the stirrups and to facilitate handling of the cage. Spacing of the bars was selected arbitrarily as 3.09 in (79 mm) to be consistent with the other specimens. Based on this, and referring to Figure 2.8, the area of skin reinforcement in this model was calculated as 0.29 in.^2 (187 mm^2).

2.4.4 Post-tensioning Anchorage Zone Reinforcement

Prior to this series, a mock-up test was performed to define the adequate reinforcement that had to be provided in the post-tensioning anchorage zone. The mock-up test structure was a simply supported rectangular concrete beam, 44 in. x 18 in. x 13 in. (1118 mm x 457 mm x 330 mm), with minimum shear and flexural steel, and without bursting reinforcement in one end and with bursting reinforcement in the other end designed according to the NCHRP 10-29 proposed provisions [9]. During the test, some spalling was observed on the side without bursting

reinforcement, while the other end remained undamaged. As a result, bursting steel as shown in Figure 2.15 was used in all models of Series 1364-1A and 1364-1B.

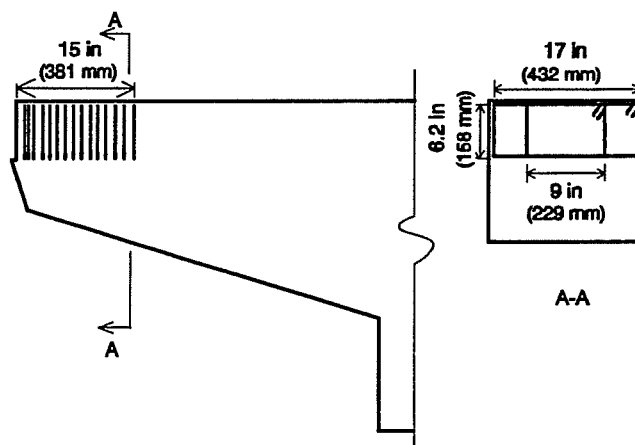


Figure 2.15 Detail of confinement reinforcement in bearing area of post-tensioning anchorage

2.4.5 Column design

The column was designed following basically the same reinforcement layout that was typical in TxDOT designs. Reinforcement bar and wire sizes were chosen with an area closest to $(1/5.5)^2$ of the area of the actual reinforcing bars. Figure 2.16 shows the column cage used in all models.

2.4.6 Fatigue considerations

Steel stress ranges (between full dead load and full dead load plus live load with

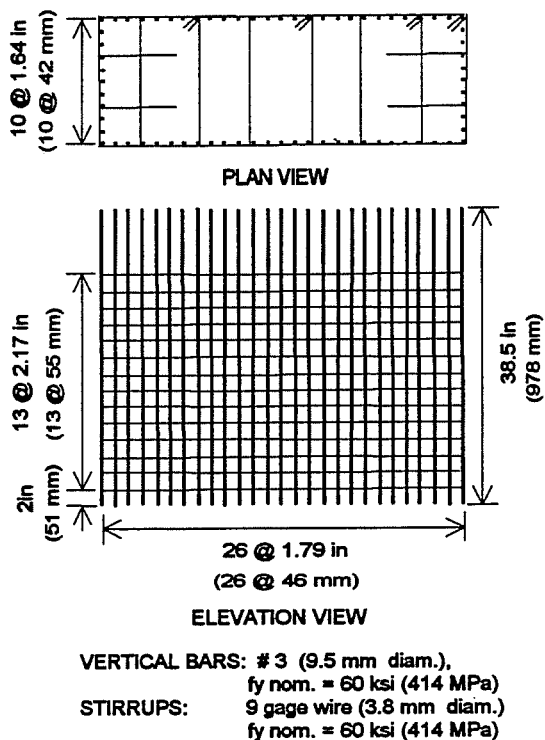


Figure 2.16 Column Cage

impact) and maximum steel stresses under service loads were of major concern during the design of the models. Table 2.11 shows the results of these calculations for every case. Under no circumstance was a stress allowed in excess of 0.70 of the specified tensile strength of the prestressing tendons or yield of the non-prestressed steel when full service loads were applied. Specimen CO-PU-74S-TH-V substantially exceeded the 15 ksi tendon stress range proposed by Wollman et. al. [10] while Specimen CO-PU-74S-TH-I was marginally above this stress range.

Table 2.11 Stress Ranges at service loads and Strand Stresses at full service loads

Model	Stress Range		fpt/fpu *
	ksi	(MPa)	
CO-PU-54S-TH-V	12.79	(88.19)	0.700
CO-PU-54S-TH-I	12.12	(83.57)	0.699
CO-PU-74S-TH-V	18.23	(125.70)	0.699
CO-PU-74S-TH-I	15.61	(107.63)	0.687
CO-PU-100S-TH-V	7.89	(54.40)	0.625
CO-PU-100S-TH-I	8.44	(58.19)	0.627

* fpt: Stress in strand at full service loads

fpu: Ultimate tensile stress of strand

2.5 MATERIALS

2.5.1 Concrete

The concrete strength typically used for the TxDOT post-tensioned pier cap design is 4000 psi (27.58 MPa) at time of prestressing and 5000 psi (34.48 MPa) at 28 days. Based on this, 5000 psi (34.48 MPa) at 28 days was selected for the test specimens and ordered from a local concrete supplier. Maximum aggregate size was 3/8 inches (9.5 mm) to allow the material to fit within the 0.41 inch (10.4 mm) cover and for adequate placement of the mix in the congested areas of the cage. To delay initial set and improve workability the mix included a retarder agent (Pozz. R) and a superplasticizer (Rheobuild). The design mix used, per cubic yard, is shown in Table 2.12.

Table 2.12 Concrete mix proportions

Description	Quantity*	
Type II Cement , lb (N)	564	(2509)
Aggregate-3/8 in.(9.5 mm), lb (N)	1463	(6507)
Sand, lb (N)	1631	(7255)
Water, lb (N)	200	(890)
Retarder additive, oz (ml)	25	(750)
Superplasticizer oz (ml)	45	(1350)
W/C ratio	0.35	(0.35)

* Quantities per cubic yard (0.76 cubic meters)

Consistency of the mix was determined by the use of slump tests. A great variability was found between mixes as presented in Table 2.13. The water-cement (W/C) ratio was calculated based on the mix component weights from the concrete supplier taking into account any extra water that the driver estimated to have added while transporting the mix. As can be concluded from this table, comparing the results from the initial slump test and the W/C ratio, it is very difficult to rely on the water and cement quantities said to be in the mix. This was recognized during casting operations. As a result, it was decided upon arrival of the concrete to add the water necessary to achieve a slump in the range of 3.5 in. (90 mm) to 5.5 in. (140 mm). In addition, superplasticizer, in excess of the initial 45 oz. (1350 ml), was then added to obtain a slump of approximately 8 inches (200 mm). The superplasticizer was added to improve workability.

Table 2.13 Concrete mix properties at time of casting

Model	Initial slump in. (mm)	Initial W/C*	Water added gal./cyd (l/m ³)	Superplasticizer added ** oz/cyd (ml/m ³)	Final slump in. (mm)	Final W/C
CO-PU-54S-TH	1 (25)	0.41	3 (15)	16 (632)	8.5 (216)	0.45
CO-PU-74S-TH	3.5 (89)	0.27	0 (0)	40 (1579)	8 (203)	0.27
CO-PU-100S-TH	5.5 (140)	0.37	0 (0)	21.3 (841)	7.5 (191)	0.37

* Based on the mix component weights from the concrete supplier and additional water added prior to arrival of the mix at the laboratory as reported by the driver.

** In addition to the 45 oz. (1350 ml) included in the mix design (See Table 2.12)

In spite of the great variability of apparent water content found between mixes very similar concrete strengths were obtained. Table 2.14 summarizes the average cylinder compressive strengths at the time of prestressing and at the day of testing. The cylinders tested were 6 inches (150 mm) by 12 inches (300 mm), and were loaded using neoprene pads. The results on each day are the average of two cylinder tests consecutively. A third cylinder was tested when very different strengths were obtained from the first two tests.

All cylinders and specimens were properly cured after casting.

Table 2.14 Concrete Cylinder Compressive Strengths

Model	Strength at time of prestressing psi (MPa)	Strength at time of testing psi (MPa)
CO-PU-54S-TH (V&I)	6146 (42.38)	6351 (43.79)
CO-PU-74S-TH (V&I)	6090 (41.99)	6400 (44.13)
CO-PU-100S-TH (V&I)	6300 (43.44)	6450 (44.47)

2.5.2 Passive Reinforcement

Reinforcement used in all test specimens for the overhang section was #2 deformed Swedish bars and 7 gage heat treated wire as longitudinal steel, and 10 gage heat treated wire as vertical steel. For construction of the column cage, #3 deformed bars were used for the vertical steel while 9 gage heat treated wires were used for the stirrups.

Bars and wires used in the three specimens were taken from the same lot. Number 10 and 9 wires were received in coils which had to be uncoiled, straightened, and cut to length.

Figures 2.17 and 2.18 show the stress-strain curves for #2 reinforcing bars and 7 gage wire.

2.5.3 Active Reinforcement

Prestressing steel consisted of 3/8 in. (9.5 mm) and 1/2 in. (13 mm) diameter, Grade 270 (1860 MPa), low relaxation 7-wire strands. The size utilized in a given model depended on the post-tensioning force requirements as explained in Section 2.4.1. Each size strand was taken from a single spool. Figures 2.19 and 2.20 show the stress-strain curves for the strands.

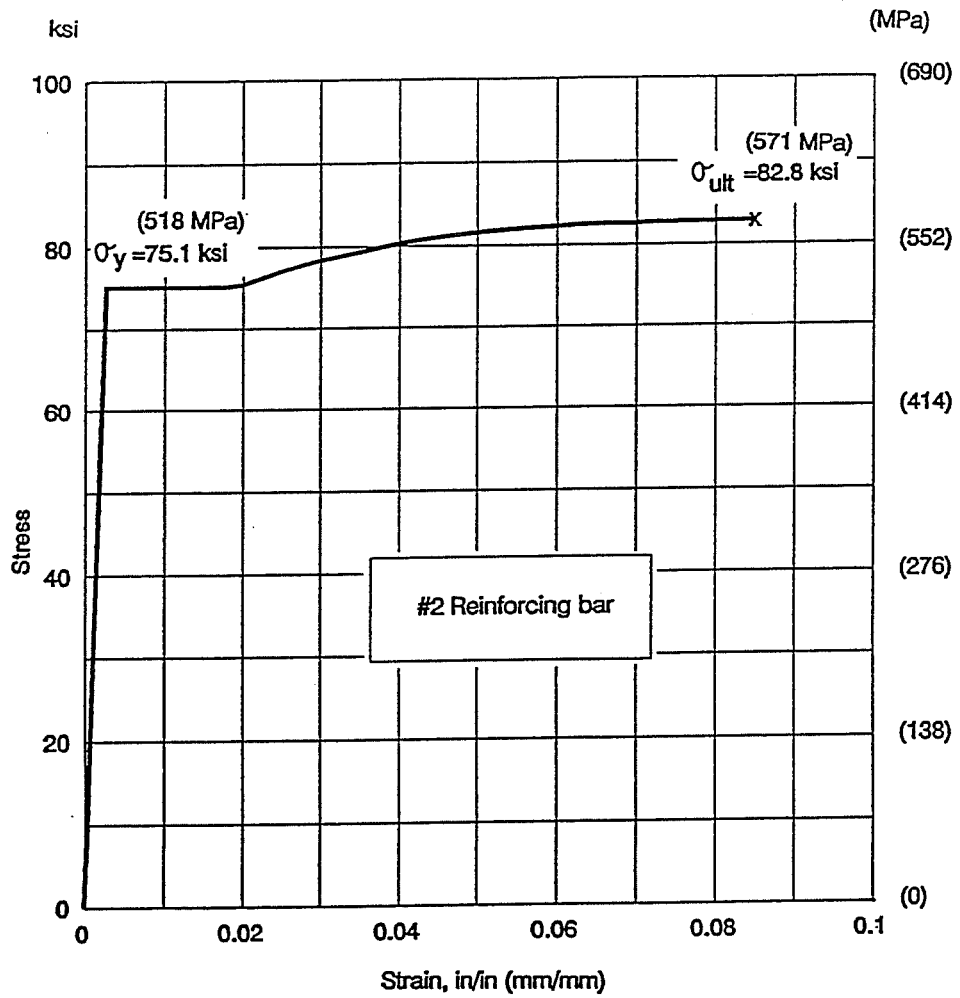


Figure 2.17 Stress-Strain Curve for #2 Reinforcing Bar [5]

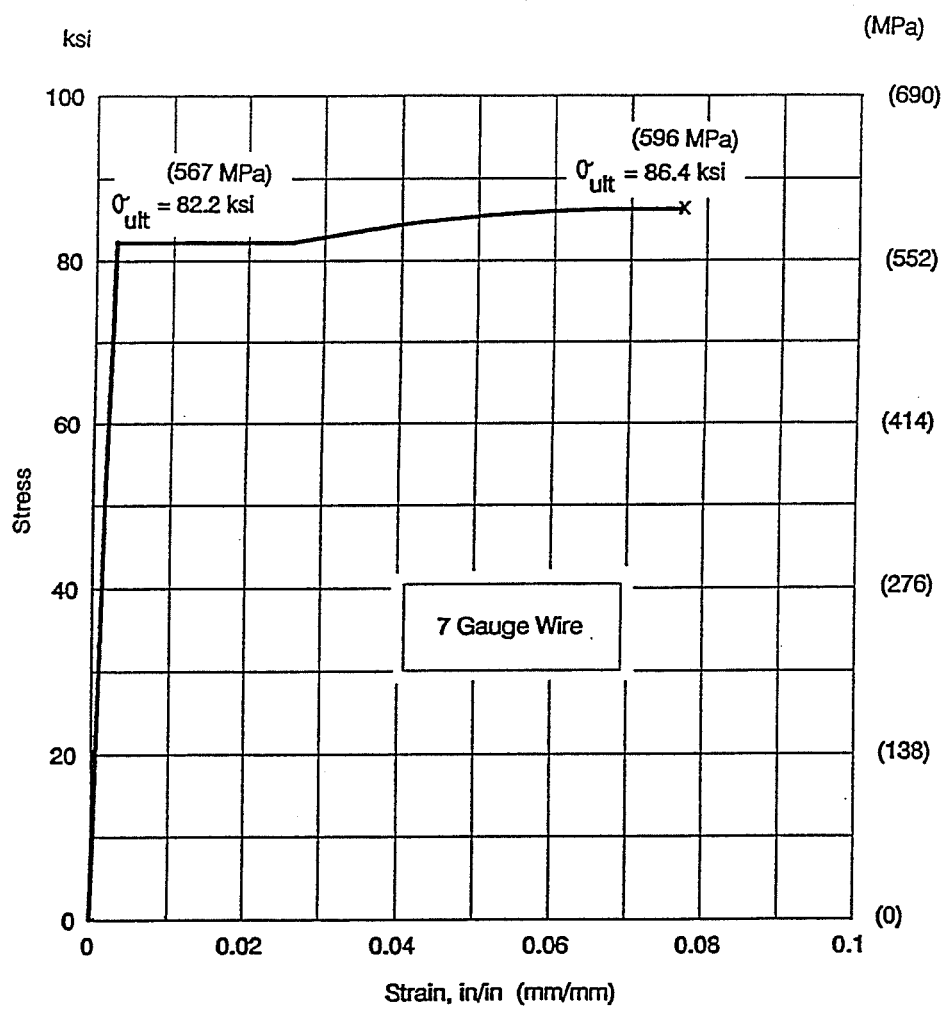


Figure 2.18 Stress-Strain Curve for 7 Gauge Wire [5]

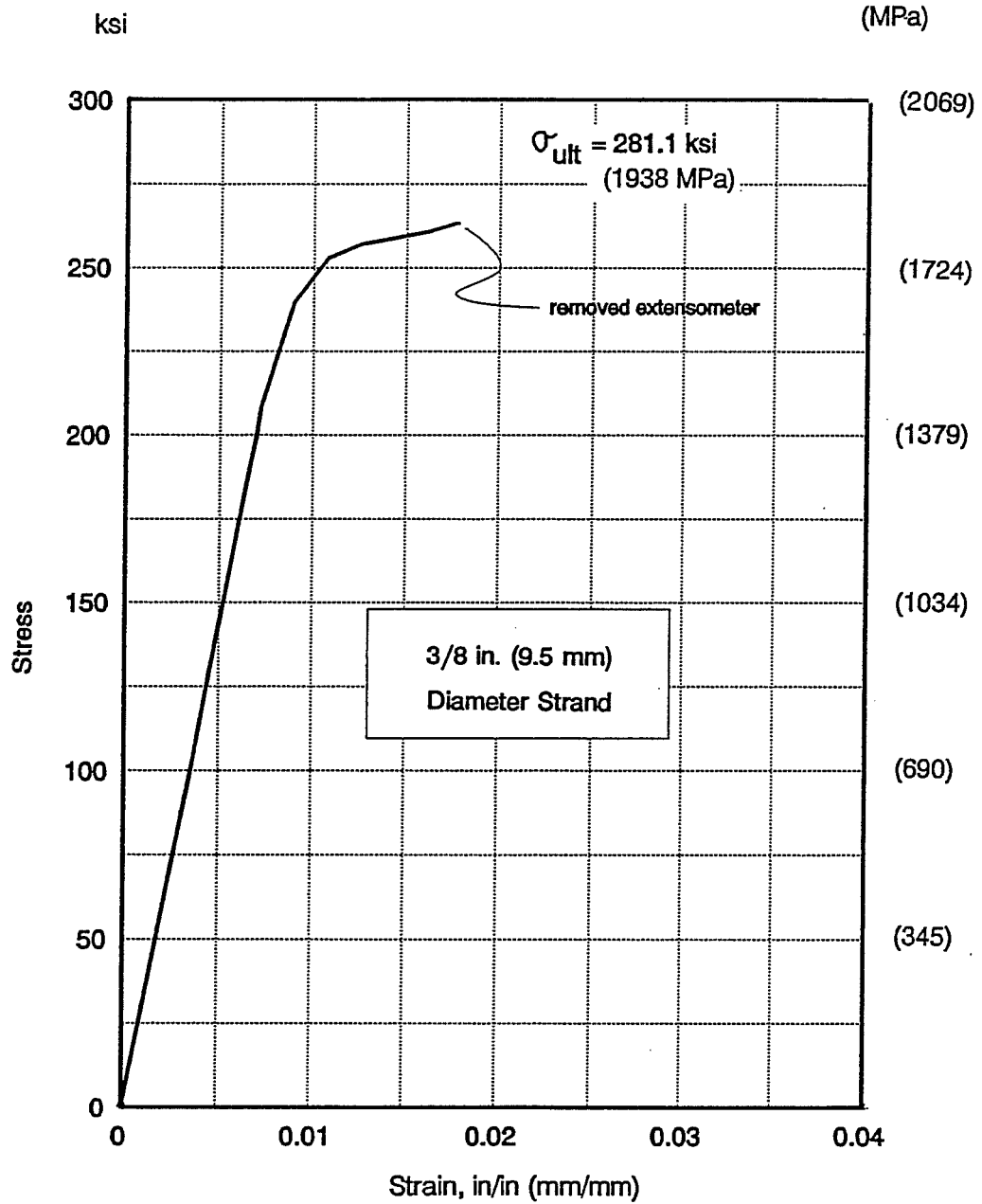


Figure 2.19 Stress-Strain Curve for 3/8 in. (9.5 mm) Strand

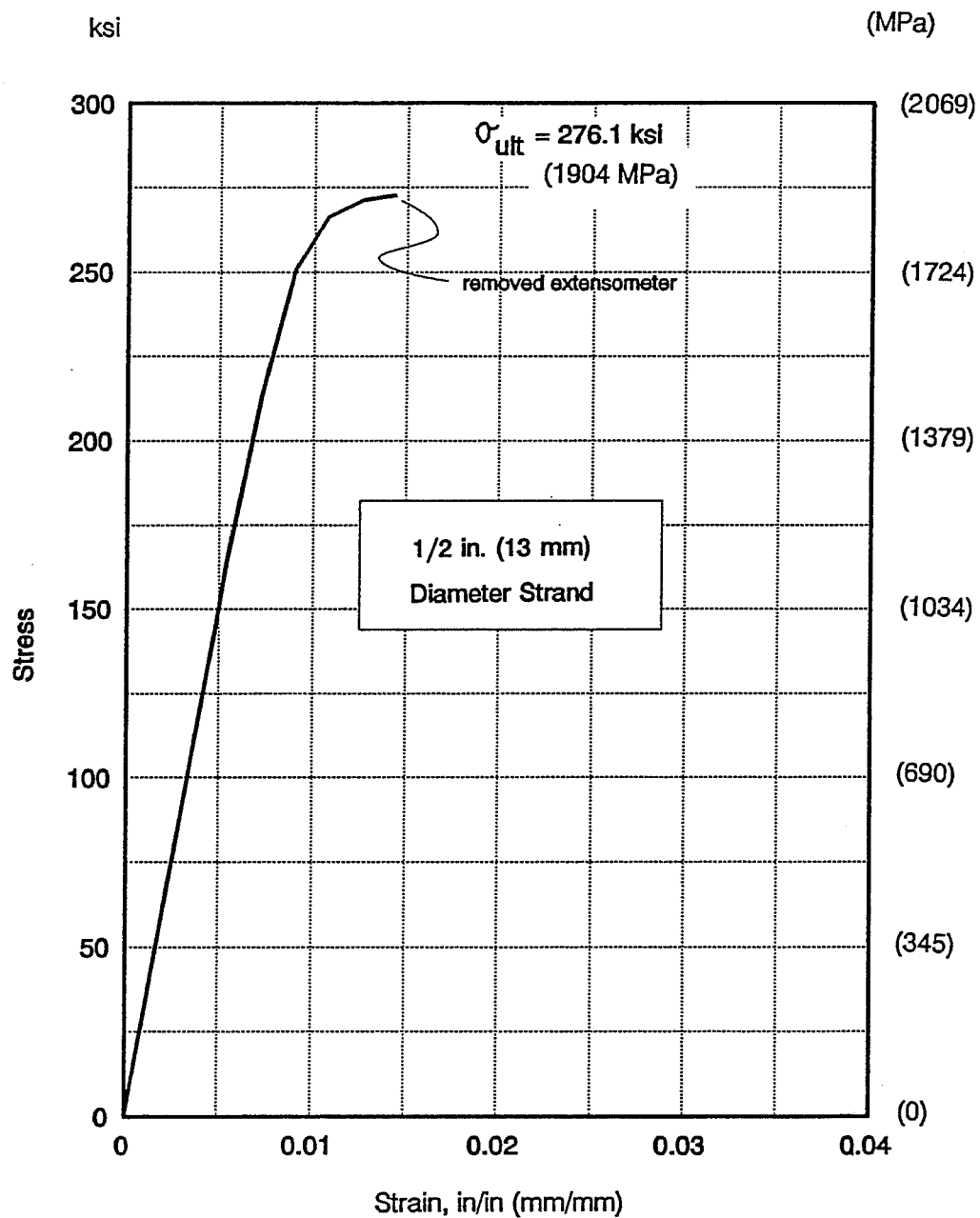


Figure 2.20 Stress-Strain Curve for 1/2 in. (13 mm) Strand [5]

2.5.4 Ducts and Prestressing Hardware

Ducts consisted of 3/4 in. (19 mm) semi-rigid galvanized steel conduit. Grout tubes were made of 1/2 in. (13 mm) diameter flexible hoses secured to the ducts with silicone caulk.

The anchorage hardware consisted of single steel bearing plates, 4 1/4 in. x 3 in. x 1 in. thick (108 mm x 76 mm x 25 mm) for each strand. Strands were anchored with commercial wedges and chucks. Threaded chucks with nuts that were prepared in the laboratory were used to minimize seating losses (see Figure 2.21.)

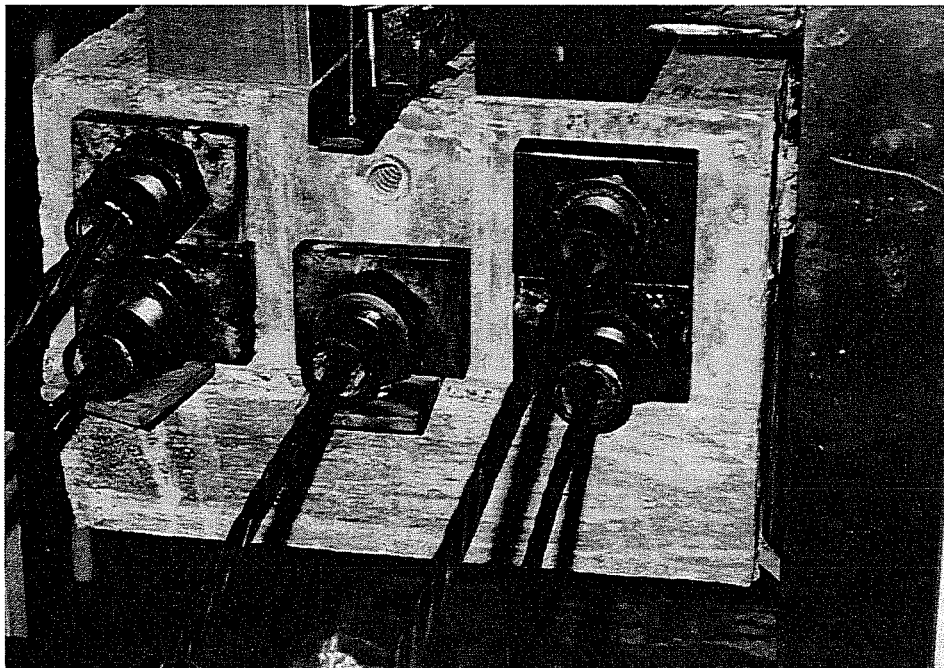


Figure 2.21 Prestressing Hardware for Models CO-PU-74S-TH (V&I)

2.5.5 Grout

Grout mix proportions were selected to allow an expansion of 2-4% and a W/C ratio of 0.44 to comply with AASHTO (Division II, Sec.10.6.4 [11]). For a 0.42 ft³ (0.0126 m³) batch the mix included 34.33 pounds (15.45 kg) of Type I Portland cement, 1.8 gallons of water (0.00684 m³) and 0.31 pounds (0.14 kg) of Interplast N, approximately 0.91 percent by weight of cement, as the

expansive additive. The expansive agent was added to prevent shrinkage and minimize bleeding. One batch was used for grouting of three strands, approximately 11 feet long (3.35 m) each. Table 2.15 shows grout cube strengths at the day of testing.

Table 2.15 Average Grout Compressive Strengths

Model	Strength psi (MPa)
CO-PU-54S-TH (V&I)	3202 (22.08)
CO-PU-74S-TH (V&I)	2289 (15.78)
CO-PU-100S-TH (V&I)	2936 (20.24)

2.5.6 T-heads

T-headed reinforcing bars or HR-bars (headed reinforcing bars) were used for all #2 flexural reinforcement. The design was based on recommendations from Norwegian Contractors [12,13,14] based on their experience in using T-headed reinforcing bars in highly congested cages in offshore concrete structures, especially as shear reinforcement.

In general, experience suggests the use of T-heads with 6 to 10 times the cross sectional area of the reinforcement bar [13] and a thickness of approximately 8/10 of the diameter of the bar. Heads may be square or circular. There are different ways of attaching them to the bars. The most commonly used is by friction welding where the head is rotated, forced onto the bar and heat is generated between the surfaces. "The weld is completed by the application of a forge force after the cessation of the rotation" [12]. Fatigue tests as well as pull-out tests have been performed and reported [12].

For this study, square heads were used on all #2 deformed bars with an approximate area of 0.50 in.^2 (323 mm^2) and a thickness of $1/4 \text{ in.}$ (6.4 mm), as shown in Figure 2.22. Fillet welding, $1/8 \text{ in.}$ (3.2 mm) thick, using an E70 electrode, was used between heads and bars. Special care was taken to check that every T-headed bar had at least the same cross sectional area in the weld region as in the bar itself. Figure 2.23 shows the use of T-headed reinforcing bars in Model CO-PU-74S-TH-V.

Four pull-out tests (elongation tests conducted by pulling in air with the bars anchored by the T-heads) were performed and results are summarized in Table 2.16. All T-headed bars developed yield stresses of at least 95% of the average of the original #2

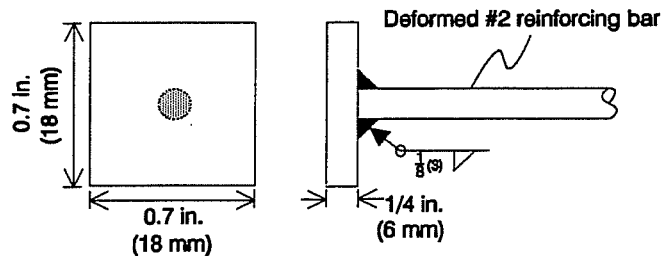


Figure 2.22 T-head dimensions

reinforcing bar and achieved ultimate stresses of at least 96% of the average of the original bars. One of the four tests resulted in breaking of the bar itself at a point far from the T-head. The other three tests resulted in failure of the weld material between the head and bar. Elongations were substantially reduced.

Table 2.16 Results from Tests of T-headed bars

Test No.	Yield stress ksi (MPa)	Ultimate stress ksi (MPa)	Strain at ultimate in/in (mm/mm)	Comments
1	73.57 (507.27)	85.64 (590.49)	0.068	failed in bar
2	74.14 (511.20)	81.58 (562.49)	0.027	broke in weld area
3	71.56 (493.41)	NA	NA	broke in weld area
4	72.42 (499.34)	80.15 (552.63)	0.017	broke in weld area
Average results from elongation tests of #2 bars without heads	75.1 (517.81)	82.8 (570.91)	0.085	

* NA: Not available

2.6 FABRICATION

As mention before, fabrication of all models was carried out at the Ferguson Structural Engineering Laboratory.

2.6.1 Formwork

Forms were made so that the models could be cast on their side (see Figure 2.24.) This was done to facilitate and control placement of the reinforcing cage, and casting and consolidation of the concrete mix. Reusable 3/4 in. (19 mm) plywood and 2 in. (50.8 mm) x 4 in. (101.6 mm) ribs were used. Before casting, the formwork was cleaned and lacquered with several layers of varnish.

2.6.2 Reinforcing Cage

All bars and wires were cut and bent at the laboratory except for all #3 deformed bars used in the column cages that were ordered from a local fabricator and were received with reasonable tolerance of approximately 3/8 inch (9.5 mm). Nylon and wire ties, 4 in. (101.6 mm) in length, were used to secure the cages.

The column cage was constructed first , followed by the placement of ducts. Rods were placed into the ducts to keep them straight while constructing the cage and during casting. This construction was followed by the placement of flexural steel, shear stirrups, anchorage reinforcement and additional horizontal steel. Ducts were then secured to the cage by the use of wire ties in various locations. In all cases the main longitudinal steel passed inside the vertical column bars. Stirrups were all closed and anchored at the top around a longitudinal bar.

Figures 2.3 through 2.8 show the steel cage layouts for all models. Plastic spacers, 0.41 in. thick (10.4 mm), were used on reinforcing bars parallel to the edges of the specimen to ensure adequate cover on all sides (see Figure 2.25.)



Figure 2.23 T-Headed Reinforcement in Model CO-PU-74S-TH-V

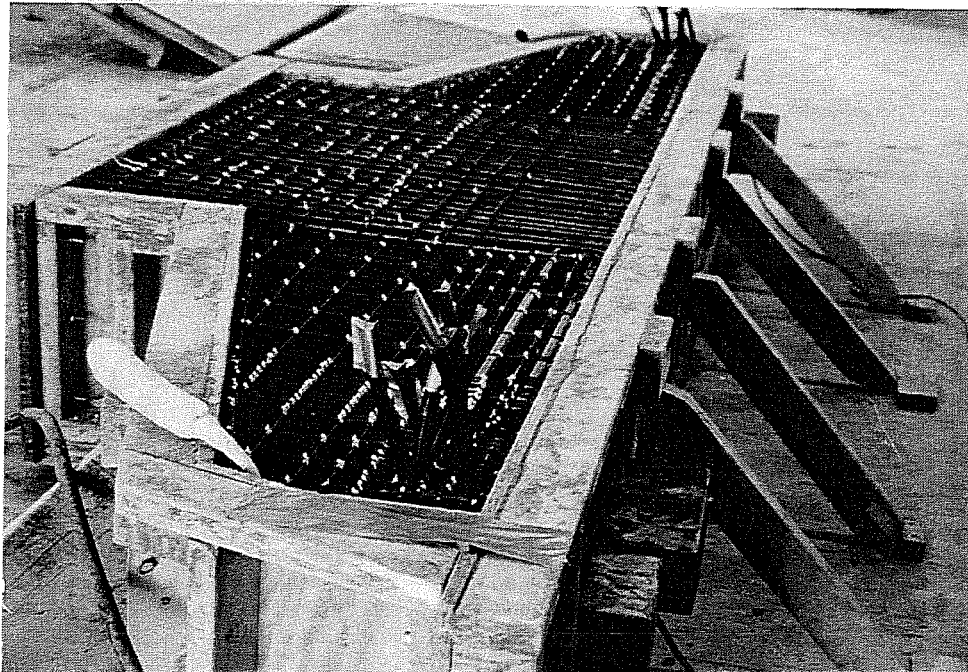


Figure 2.24 Formwork

2.6.3 Casting of Concrete

Concrete conforming with the mix described in Section 2.5.1 was ordered for all models, which were cast on different days. After receipt of the mix, the concrete slump was measured according to the ASTM C-143 procedure. Water and superplasticizer were added to achieve the desired slump of 8 inches (203 mm) as summarized in Table 2.13. Every model was cast in three layers with the use of a one cubic yard (0.76 m³) bucket hoisted by the overhead crane. Vibration was provided internally with flexible shaft vibrators, and externally with form vibrators to achieve good consolidation. Figure 2.26 shows casting of the CO-PU-54S-TH (V&I) overhangs. Adequate curing was provided by covering the models with wet burlap and plastic, maintaining adequate humidity and heat during the curing process. Twenty 6 in. (152 mm) x 12 in. (305 mm) cylinders per model were also cast in plastic molds according to ASTM C-31. They were also covered with burlap and plastic and maintained wet for approximately three to five days until forms were removed from the model.

No honeycombing was found in any of the specimens after stripping the forms.

2.6.4 Prestressing procedure

The stressing operations varied according to the characteristics of each model. In general the prestressing hardware and set-up for post-tensioning of the single strands consisted of a steel chair bearing on the corners of the bearing plate, a 30 ton (294 kN) hydraulic ram positioned at the end of the chair and centered over the strand, and a temporary anchor plate and wedges placed at the end of the ram. The ram force was applied in increments of approximately 5 percent of ultimate until the desired prestress was obtained. It was kept reasonably constant by adjusting the nut on the chuck to the desired position to overcome seating losses. The prestressing force was gradually released onto the anchorage system by reversing the ram direction, to ensure adequate seating of the wedges. All prestressing operations took place at one end (the "live end" or North end) of the models.

The force in the strands was checked and controlled to an acceptable degree by following a lift-off procedure and restressing as necessary. This operation was performed after all strands were initially stressed.

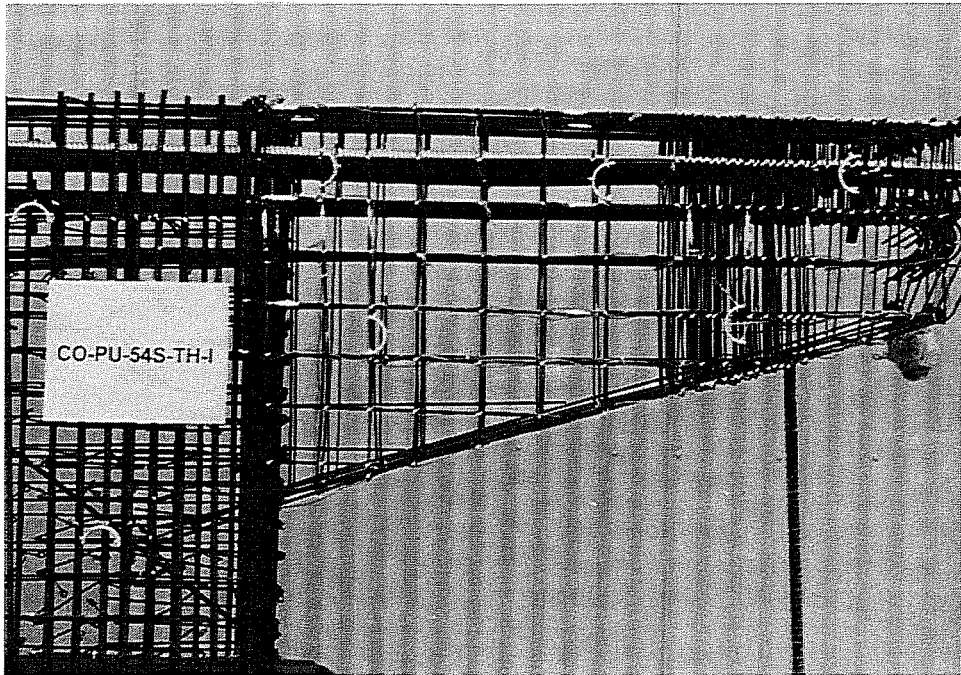


Figure 2.25 Reinforcement Cage for Model CO-PU-54S-TH-I

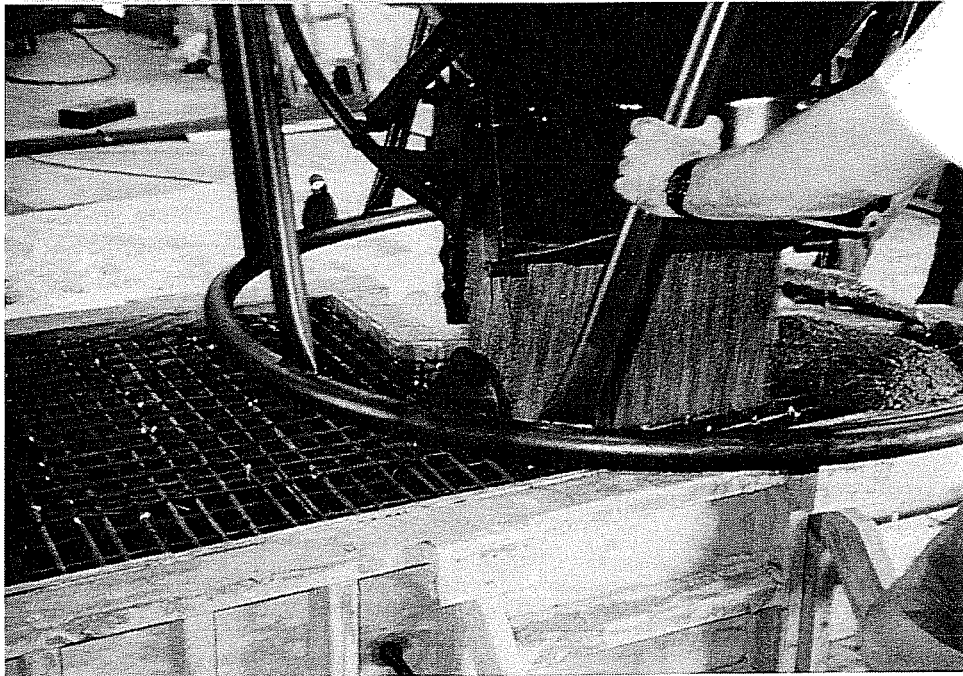


Figure 2.26 Casting of Specimen CO-PU-54S-TH

The lift-off operation can be better described by referring to Figure 2.27. A linear potentiometer attached to the ram was used to measure the elongation in the strand while the load was measured by an electronic pressure transducer. Both were plotted continuously. The plot showed an initial linear relationship between load and elongation, which prior to lift-off reflected only elongation in the portion of strand that was located between the anchorage wedges ("live end") and the temporary wedges located behind the ram. When the stress in this portion of strand equalled the stress in the strand inside the specimen, the force in the ram started pulling out the entire strand length ("dead end" to the temporary wedges) producing a change in the slope of the curve. The stress at which this break point occurred represented the actual stress in the tendon. Depending on the difference between this stress and the desired value, the nut in the anchorage system had to be adjusted, and the procedure was repeated (usually two to three times) until the desired stress was obtained. At no time was the stress in the strand allowed to exceed 75 percent of its ultimate tensile strength.

All specimens were grouted immediately after doing the lift-offs. Grout proportions are presented in Section 2.5.5. Water was added first, then the cement and finally the expansive agent. The materials were mixed for approximately four minutes. The grout was forced into the ducts, through the grout tubes, with the aid of a manual pump.

The grout was allowed to flow for a short period of time to eliminate any entrapped air in the conduit.

The exit grout tube was plugged first and additional grout was pumped into the duct before plugging the access side. Grout cubes were cast for every grout batch. Results are shown in Table 2.15.

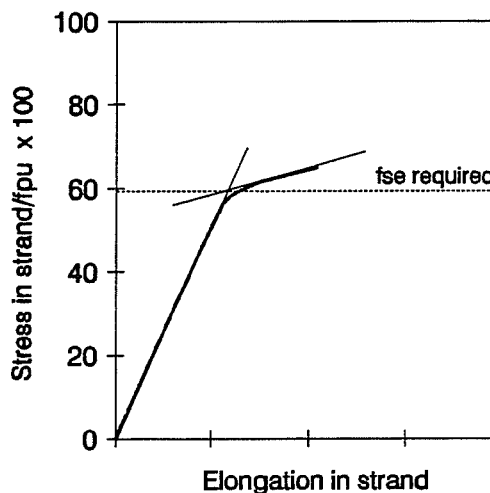


Figure 2.27 Example of plot obtained in a Lift-Off operation of a typical strand.

2.6.4.1 Models CO-PU-54S-TH (V&I)

Prestressing force for the 54 percent post-tensioned overhangs was provided by the use of a single row of three 1/2 in. (13 mm) diameter strands located at 3.6 in. (91 mm) from the top extreme fiber of the section. Initial stresses (before losses) and final stresses (after losses) were checked at every stage to define the appropriate stressing sequence. All models, including those 74 and 100 percent post-tensioned, were stressed to only 59 percent of the tensile strength of the tendons to simulate all losses that would occur in the prototype structure during its service life. This was done due to the short period of time (4 to 5 days) between prestressing of the models and testing.

The prestressing sequence for the 54 percent prestressed models was performed as follows:

- a) Application of simulated dead load (additional dead load required due to scale relations) ,
- b) Stressing of middle tendon,
- c) Stressing of right edge tendon,
- d) Stressing of left edge tendon,
- e) Performance of lift-off tests in the order of tendons in b), c), d),
- f) Grouting of tendons, and
- g) Placing of screw jacks between model and rams to avoid undesirable upward deflections due to any possible overnight losses in hydraulic force.

2.6.4.2 Models CO-PU-74S-TH (V&I)

For these overhangs, the prestressing force was provided by the use of two rows of prestressing tendons, one centered at 2 inches (51 mm) from the extreme fiber of the section and the other at 5 inches (127 mm) . The top row consisted of two 1/2 in. (13 mm) diameter strands, and the bottom row of two 3/8 in. (9.5 mm) diameter strands and one 1/2 in. (13 mm) diameter strand.

As for the 54 percent prestressed overhangs, initial and final stresses were calculated and compared with allowable values (AASHTO [15]). The stressing sequence was performed as described below:

- a) Application of simulated dead load through loading rams,

- b) Stressing of middle tendon, 1/2 in. (13 mm), bottom row,
- c) Stressing of left edge tendon, 1/2 in. (13 mm), top row,
- d) Stressing of right edge tendon, 1/2 in. (13 mm), top row,
- e) Application of simulated back span dead loads through loading rams,
- f) Stressing of left edge tendon, 3/8 in. (9.5 mm), bottom row,
- g) Stressing of right edge tendon, 3/8 in. (9.5 mm), bottom row,
- h) Performance of lift-off tests in the order of tendons in b), c), d), f), g),
- i) Grouting of tendons, and
- j) Placing of screw jacks between model and rams to avoid undesirable upward deflections due to any possible overnight losses in hydraulic force.

2.6.4.3 Models CO-PU-100S-TH (V&I)

Two rows of prestressing strands were used to provide the 100 percent post-tensioning of these overhangs. The top row consisted of three 1/2 in. (13 mm) diameter strands located at 2.22 in. (56 mm) from the extreme fiber of the section, and the bottom row of two 1/2 in. (13 mm) diameter strands and one 3/8 in. (9.5 mm) diameter strand at 5.22 in. (133 mm) from the extreme fiber.

Once again, as in the previous models, stresses were checked against allowable values and the stressing sequence was defined and finally performed as follows:

- a) Application of simulated dead load through loading rams,
- b) Stressing of middle tendon, 3/8 in. (9.5 mm), bottom row,
- c) Stressing of left edge tendon, 1/2 in. (13 mm), bottom row,
- d) Stressing of right edge tendon, 1/2 in. (13 mm), bottom row,
- e) Application of simulated back span dead loads through loading rams,
- f) Stressing of middle tendon, 1/2 in. (13 mm), top row,
- g) Stressing of left edge tendon, 1/2 in. (13 mm), top row,
- h) Stressing of right edge tendon, 1/2 in. (13 mm), top row,
- i) Performance of lift-off tests in the order of tendons in b), c), d), f), g), h),
- j) Grouting of tendons, and
- k) Placing of screw jacks between model and rams to avoid undesirable upward deflections due to any possible overnight losses in hydraulic force.

2.7 INSTRUMENTATION

2.7.1 Deflections

Overhang deflections were measured with linear potentiometers connected to the data acquisition system. Tip deflection measurements were backed up with the use of digital gages. In addition, dial gages were placed at the column base as shown in Figure 2.28 with the purpose of monitoring the behavior of the model at this level and recording any important deflections that had to be subtracted from the top measurements.

At the tip of the overhangs, 6 in. (152 mm) linear potentiometers were used while at the middle and at the column section these were 2 in. (51 mm) linear potentiometers.

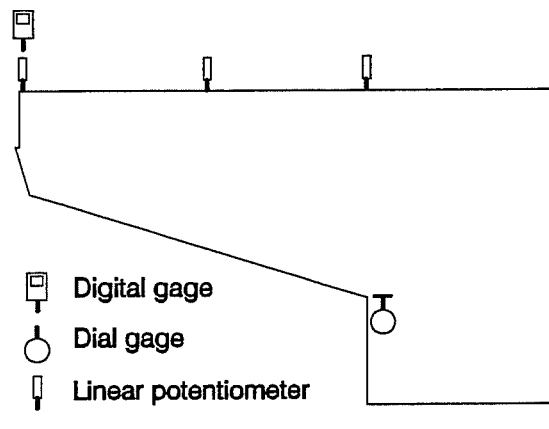
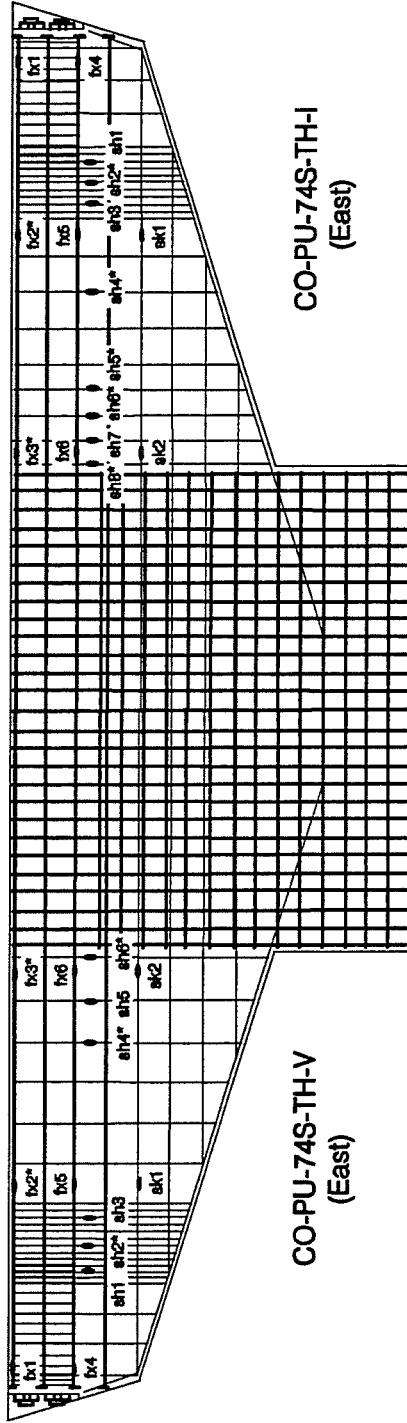


Figure 2.28 Location of Linear potentiometers, Digital gages and Dial gages

2.7.2 Strains

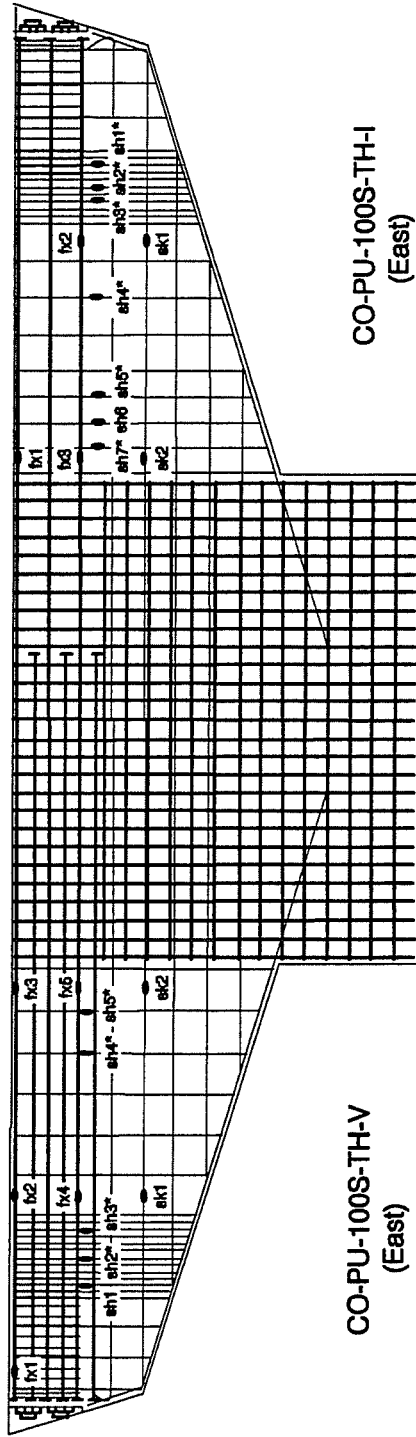
Several strain gages were used to monitor the stresses in reinforcing steel. Typically, 0.2 in. (5 mm) strain gages were used on all longitudinal steel and 0.08 in. (2 mm) strain gages on all shear reinforcement. Figures 2.29 , 2.30 and 2.31 show the location of these gages in the models.



All strain gages in east side face of cage unless noted:

- sh : 2 mm strain gage in sheer stirrup (10 gage wire)
- sk: 5 mm strain gage in skin reinforcement (7 gage wire)
- fx: 5 mm strain gage in flexural reinforcement (#2 reinforcing bar)
- sh*: an additional strain gage was placed in interior stirrup at same height.
- fx*: an additional strain gage was placed in interior middle flexural bar at same distance from column face.

Figure 2.30 Location of Strain Gages for models CO-PU-74S-TH (V & I)



All strain gages in east side face of cage unless noted:

- sh : 2 mm strain gage in shear stirrup (10 gage wire)
- sk: 5 mm strain gage in skin reinforcement (7 gage wire)
- fx: 5 mm strain gage in flexural reinforcement (#2 reinforcing bar)
- sh*: an additional strain gage was placed in interior stirrup at same height.
- fx*: an additional strain gage was placed in interior middle flexural bar at same distance from column face.

Figure 2.31 Location of Strain Gages for models CO-PU-100S-TH (V & I)

2.8 TEST SET-UP

Specimens were tested in the loading frame shown in Figure 2.32. This consisted of a W12x120 (12 in. (305 mm) x 120 lb/ft (1.75 kN/m)), grade 50 (345 MPa) steel beam used to give support to the rams and four grade 50 (345 MPa) steel cross beams which transmitted the force to the reaction floor through the use of rod groups attached to the ends.

With this test set-up the model had to be placed first, leveled and hydrostoned, before the beam with the rams and the cross beams could be placed and properly aligned. This was not an inconvenience due to the simplicity of the system.

The specimens were loaded using 100 ton (981 kN) hydraulic rams. The exterior rams (RO loads) were controlled together and independently from the interior rams (RI loads), which also acted together. Each group was operated with a manual pump, and the load was recorded with the use of a pressure transducer connected to a data acquisition system and to a voltmeter.

2.9 TESTING PROCEDURE

2.9.1 Loading

Loading was applied in discrete increments as shown in Table 2.17. The "RO" loads were the outer loads applied to the overhang, at 39 inches (991 mm) from the column face, and the "RI" loads were the inner loads, at 13 inches (330 mm) from the column face. Loads required to increase model density based on scale relations (Section 2.3.2(4)) were applied as additional dead load (load step 1) using the same loading rams.

The loading sequence included various cycles, which are described below:

- a) Loading from dead load to service flexure load, then unloading to dead load,
- b) Loading from dead load to service shear load, then unloading to dead load,
- c) Loading from dead load to service flexure load, continuing to factored flexure load, then unloading to dead load,
- d) Loading from dead load to service shear load, continuing to factored shear load, then unloading to dead load,
- e) Loading from dead load to service flexure load, then to factored flexure load and continuing to ultimate flexure load.

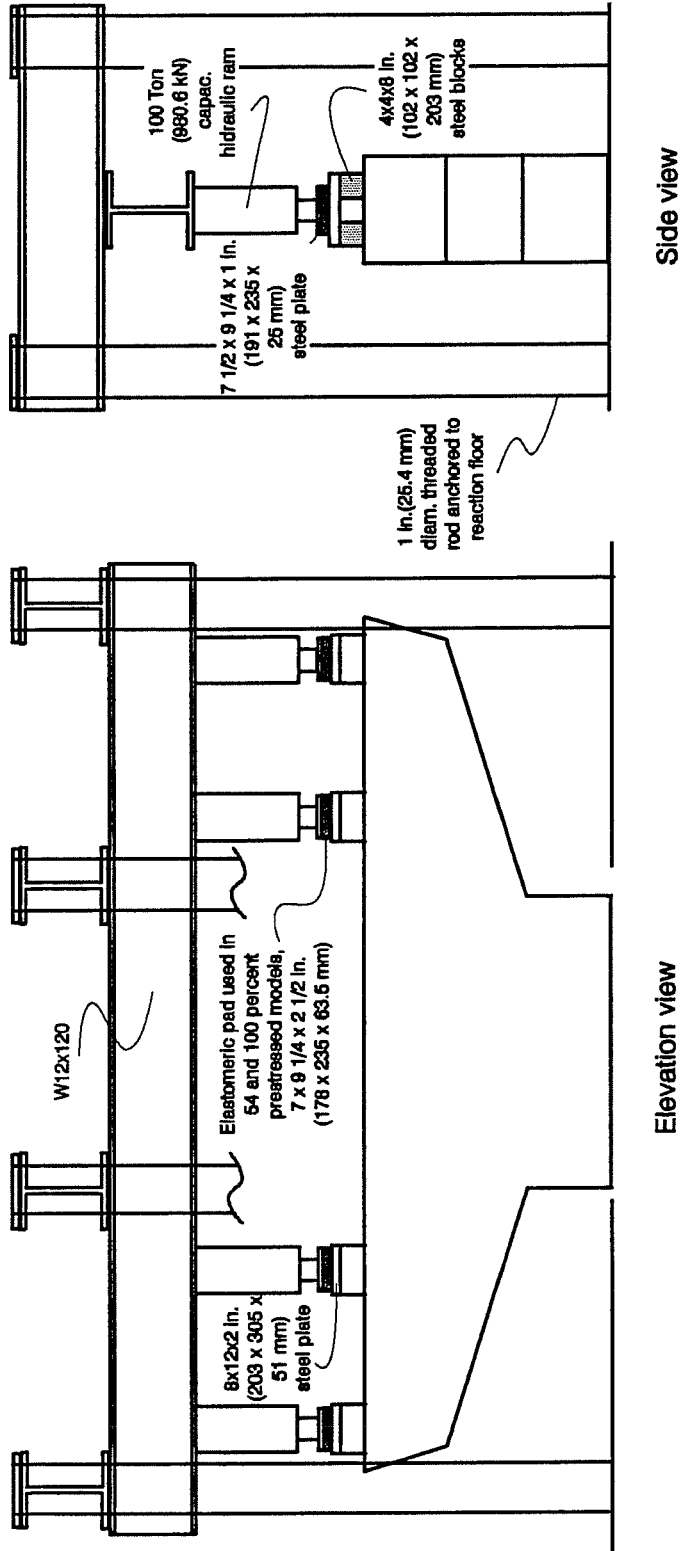


Figure 2.32 Test Set-up

Table 2.17 Load Steps

Load step	Ri		Ri + simulated dead load		Ro		Ro + simulated dead load		Description
	kips	(kN)	kips	(kN)	kips	(kN)	kips	(kN)	
0	0.0	(0.0)	0.00	(0.0)	0.0	(0.0)	0.00	(0.0)	
1	0.0	(0.0)	4.48	(19.9)	0.0	(0.0)	1.46	(6.5)	simul. dead load
2	4.0	(17.8)	8.48	(37.7)	4.0	(17.8)	5.46	(24.3)	
3	8.0	(35.6)	12.48	(55.5)	8.0	(35.6)	9.46	(42.1)	
4	12.0	(53.4)	16.48	(73.3)	12.0	(53.4)	13.46	(59.9)	
5	16.0	(71.2)	20.48	(91.1)	16.0	(71.2)	17.46	(77.7)	
6	19.5	(86.7)	23.98	(106.7)	19.5	(86.7)	20.96	(93.2)	back span loads
7	20.0	(89.0)	24.48	(108.9)	20.0	(89.0)	21.46	(95.5)	
8	24.0	(106.8)	28.48	(126.7)	24.0	(106.8)	25.46	(113.2)	
9	28.0	(124.5)	32.48	(144.5)	28.0	(124.5)	29.46	(131.0)	
10	32.0	(142.3)	36.48	(162.3)	32.0	(142.3)	33.46	(148.8)	
11	36.0	(160.1)	40.48	(180.1)	36.0	(160.1)	37.46	(166.6)	
12	39.0	(173.5)	43.48	(193.4)	39.0	(173.5)	40.46	(180.0)	both spans
13	38.7	(172.2)	43.18	(192.1)	40.0	(177.9)	41.46	(184.4)	
14	37.7	(167.8)	42.20	(187.7)	44.0	(195.7)	45.46	(202.2)	
15	36.7	(163.4)	41.22	(183.4)	48.0	(213.5)	49.46	(220.0)	
16	35.1	(156.3)	39.62	(176.2)	52.0	(231.3)	53.46	(237.8)	
17	34.1	(151.7)	38.58	(171.6)	55.5	(246.9)	56.96	(253.4)	service flexure
18	39.0	(173.5)	43.48	(193.4)	39.0	(173.5)	40.46	(180.0)	both spans
19	40.0	(177.9)	44.48	(197.8)	40.0	(177.9)	41.46	(184.4)	
20	44.0	(195.7)	48.48	(215.6)	44.0	(195.7)	45.46	(202.2)	
21	45.0	(200.2)	49.48	(220.1)	45.0	(200.2)	46.46	(206.7)	service shear
22	39.0	(173.5)	43.48	(193.4)	39.0	(173.5)	40.46	(180.0)	both spans
23	38.7	(172.2)	43.18	(192.1)	40.0	(177.9)	41.46	(184.4)	
24	37.7	(167.8)	42.20	(187.7)	44.0	(195.7)	45.46	(202.2)	
25	36.7	(163.4)	41.22	(183.4)	48.0	(213.5)	49.46	(220.0)	
26	35.1	(156.3)	39.62	(176.2)	52.0	(231.3)	53.46	(237.8)	
27	34.1	(151.7)	38.58	(171.6)	55.5	(246.9)	56.96	(253.4)	service flexure

Table 2.17 Load Steps (continuation...)

Load step	Ri		Ri + simulated dead load		Ro		Ro + simulated dead load		Description
	kips	(kN)	kips	(kN)	kips	(kN)	kips	(kN)	
28	34.2	(152.1)	38.68	(172.0)	56.0	(249.1)	57.46	(255.6)	
29	35.0	(155.5)	39.45	(175.5)	60.0	(266.9)	61.46	(273.4)	
30	35.7	(159.0)	40.22	(178.9)	64.0	(284.7)	65.46	(291.2)	
31	36.5	(162.4)	40.99	(182.3)	68.0	(302.5)	69.46	(309.0)	
32	37.3	(165.8)	41.76	(185.8)	72.0	(320.3)	73.46	(326.8)	
33	38.1	(169.3)	42.53	(189.2)	76.0	(338.0)	77.46	(344.5)	
34	38.8	(172.7)	43.31	(192.6)	80.0	(355.8)	81.46	(362.3)	
35	39.6	(176.1)	44.08	(196.1)	84.0	(373.6)	85.46	(380.1)	
36	40.1	(178.4)	44.58	(198.3)	86.6	(385.2)	88.06	(391.7)	factored flexure
37	39.0	(173.5)	43.48	(193.4)	39.0	(173.5)	40.46	(180.0)	both spans
38	40.0	(177.9)	44.48	(197.8)	40.0	(177.9)	41.46	(184.4)	
39	44.0	(195.7)	48.48	(215.6)	44.0	(195.7)	45.46	(202.2)	
40	45.0	(200.2)	49.48	(220.1)	45.0	(200.2)	46.46	(206.7)	service shear
41	48.0	(213.5)	52.48	(233.4)	48.0	(213.5)	49.46	(220.0)	
42	52.0	(231.3)	56.48	(251.2)	52.0	(231.3)	53.46	(237.8)	
43	56.0	(249.1)	60.48	(269.0)	56.0	(249.1)	57.46	(255.6)	
44	60.0	(266.9)	64.48	(286.8)	60.0	(266.9)	61.46	(273.4)	
45	64.0	(284.7)	68.48	(304.6)	64.0	(284.7)	65.46	(291.2)	
46	64.8	(288.2)	69.28	(308.2)	64.8	(288.2)	66.26	(294.7)	factored shear
47	39.0	(173.5)	43.48	(193.4)	39.0	(173.5)	40.46	(180.0)	both spans
48	36.7	(163.2)	41.18	(183.2)	48.0	(213.5)	49.46	(220.0)	
49	34.1	(151.7)	38.58	(171.6)	55.5	(246.9)	56.96	(253.4)	service flexure
50	35.0	(155.7)	39.48	(175.6)	60.0	(266.9)	61.46	(273.4)	
51	36.5	(162.4)	40.98	(182.3)	68.0	(302.5)	69.46	(309.0)	
52	38.1	(169.5)	42.58	(189.4)	76.0	(338.0)	77.46	(344.5)	
53	40.1	(178.4)	44.58	(198.3)	86.6	(385.2)	88.06	(391.7)	factored flexure
54	40.4	(179.6)	44.85	(199.5)	88.0	(391.4)	89.46	(397.9)	
55	41.1	(183.0)	45.62	(202.9)	92.0	(409.2)	93.46	(415.7)	

Table 2.17 Load Steps (continuation...)

Load step	Ri		Ri + simulated dead load		Ro		Ro + simulated dead load		Description
	kips	(kN)	kips	(kN)	kips	(kN)	kips	(kN)	
56	41.9	(186.4)	46.39	(206.4)	96.0	(427.0)	97.46	(433.5)	
57	42.7	(189.9)	47.17	(209.8)	100.0	(444.8)	101.46	(451.3)	
58	43.5	(193.3)	47.94	(213.2)	104.0	(462.6)	105.46	(469.1)	
59	44.2	(196.7)	48.71	(216.7)	108.0	(480.4)	109.46	(486.9)	
60	45.0	(200.2)	49.48	(220.1)	112.0	(498.2)	113.46	(504.7)	
61	45.8	(203.6)	50.25	(223.5)	116.0	(516.0)	117.46	(522.5)	
62	46.5	(207.0)	51.02	(227.0)	120.0	(533.8)	121.46	(540.3)	
63	47.3	(210.5)	51.80	(230.4)	124.0	(551.6)	125.46	(558.0)	
64	48.1	(213.9)	52.57	(233.8)	128.0	(569.3)	129.46	(575.8)	
65	48.9	(217.3)	53.34	(237.3)	132.0	(587.1)	133.46	(593.6)	
66	49.6	(220.8)	54.11	(240.7)	136.0	(604.9)	137.46	(611.4)	
67	50.4	(224.2)	54.88	(244.1)	140.0	(622.7)	141.46	(629.2)	
68	51.2	(227.6)	55.66	(247.6)	144.0	(640.5)	145.46	(647.0)	
69	51.9	(231.1)	56.43	(251.0)	148.0	(658.3)	149.46	(664.8)	
70	52.7	(234.5)	57.20	(254.4)	152.0	(676.1)	153.46	(682.6)	
71	53.5	(237.9)	57.97	(257.9)	156.0	(693.9)	157.46	(700.4)	
72	54.3	(241.4)	58.74	(261.3)	160.0	(711.7)	161.46	(718.2)	
73	55.0	(244.8)	59.51	(264.7)	164.0	(729.5)	165.46	(736.0)	
74	55.8	(248.2)	60.29	(268.2)	168.0	(747.3)	169.46	(753.8)	
75	56.6	(251.7)	61.06	(271.6)	172.0	(765.1)	173.46	(771.6)	
76	57.3	(255.1)	61.83	(275.0)	176.0	(782.8)	177.46	(789.3)	
77	58.1	(258.5)	62.60	(278.5)	180.0	(800.6)	181.46	(807.1)	
78	58.9	(262.0)	63.37	(281.9)	184.0	(818.4)	185.46	(824.9)	
79	59.7	(265.4)	64.15	(285.3)	188.0	(836.2)	189.46	(842.7)	
80	60.4	(268.8)	64.92	(288.8)	192.0	(854.0)	193.46	(860.5)	
81	60.8	(270.5)	65.30	(290.5)	194.0	(862.9)	195.46	(869.4)	
82	61.2	(272.3)	65.69	(292.2)	196.0	(871.8)	197.46	(878.3)	
83	61.6	(274.0)	66.07	(293.9)	198.0	(880.7)	199.46	(887.2)	

For the models CO-PU-100S-TH (V&I) , due to the fact that no cracking was observed while following steps a) and b) above, additional cycles were performed to evaluate the behavior of existing cracks at service level. To do this, the steps that are presented below were followed between steps b) and c) above:

- b') Loading from dead load to service flexure load, continuing to first crack, and then unloading to dead load,
- b'') Loading from dead load to service flexure load, continuing until cracks were observed in both overhangs and both sides, and then unloading to dead load.

Testing of models CO-PU-54S-TH (V&I) was performed in three days. Referring to the load cycles that were described above, the first day of testing included cycles a) and b), the second day cycle c), and the third day the overhangs were tested to ultimate loads, cycles d) and e). Models CO-PU-74S-TH (V&I) were tested in two days. The first included cycles a), b) and c), and the second day cycles d) and e). Finally, models CO-PU-100S-TH (V&I) were also tested in two days. The first including load cycles a), b), b''), b'') and c), and the second including d) and e).

Table 2.18 shows the age of concrete for every model at the time of prestressing and at testing operations.

Table 2.18 Age of Concrete

Model	Age of concrete at prestressing (days)	Age of concrete at first day testing (days)
CO-PU-54S-TH (V&I)	16	22
CO-PU-74S-TH (V&I)	13	20
CO-PU-100S-TH (V&I)	15	21

Models CO-PU-74S-TH (V&I) were tested without elastomeric pads between the loading rams and steel bearing plates. As will be discussed in Chapters 3 and 4, this presented a problem for loads higher than factored loads, because friction forces were developed, limiting the deflection of the overhang and providing additional moment at the column face which acted opposite to that from applied loads. As a result, models CO-PU-54S-TH (V&I) and CO-PU-100S-TH (V&I) were tested with the 2 1/2 in. (63.5 mm) thick reinforced elastomeric bearing pads as illustrated in Figure 2.32.

2.9.2 Crack readings and deflections

Crack widths were read with a crack measurement device having a smallest division of 0.001 in. (0.025 mm). Accuracy of reading, defined as half the smallest division, was ± 0.0005 in. (0.013 mm).

Crack readings were taken when the first cracking occurred and at every major step (service shear, service flexure, etc). After service load only maximum crack widths were measured.

Deflections from digital and dial gages were recorded by hand and compared, where applicable, with those from linear potentiometers.

CHAPTER 3 TEST RESULTS

Six concrete overhang structures with mixed reinforcement were tested under static loading. The specimens included two overhangs with 74 percent of the main flexural reinforcement prestressed, two with 54 percent of the main flexural reinforcement prestressed and two with approximately 100 percent of the flexural reinforcement prestressed, tested in that order. Three of the overhangs, one per each percentage of prestressing, were tested to failure.

The same loading sequence was used for all models, except for the 100 percent prestressed overhangs where two additional service load cycles were included (see Section 2.9.1).

All models were oriented in the test set-up such that overhangs designed using "inclined ties", in the strut and tie modelling, were always located at the North end, corresponding to the "live end" for prestressing.

Testing was performed during three days for the overhangs with 54 percent prestressed reinforcement and two days for the others. Between days of testing, applied loads were released and only dead loads were maintained overnight. Typically the first day of testing included load cycles in the service range, while the second and third days included testing to factored loads and then to failure.

Scans of data using the Data Acquisition System, including strain readings from strain gages, deflections from linear potentiometers and loading from pressure transducers, were taken at every load step as shown in Table 2.17, until failure. Tip deflections from digital gages precision of 0.0001 in. (0.0025 mm), as well as column settlement from dial gages having a precision of 0.0005 in. (0.013 mm), were recorded with the same frequency. Documentation of crack widths and crack patterns was performed at every major load step as described later. In addition, several photographs were taken at every major load level (service shear, service flexure, etc.).

Models CO-PU-74S-TH (V&I) were tested without elastomeric pads between the loading rams and steel plates. This presented a problem for loads higher than factored loads since some friction forces were developed, limiting the deflection of the overhang and providing an additional moment at the column face which acted opposite to that from applied loads. As will be discussed in Chapter 4, this was considered one of the causes of the additional capacity observed in these

overhangs. As a result, models CO-PU-54S-TH (V&I) and CO-PU-100S-TH (V&I) were tested with the 2 1/2 in. (63.5 mm) thick reinforced elastomeric bearing pads shown in Figure 2.32 This eliminated the restraint problem for these specimens.

In the following sections, the response of all overhang structures to the applied loads is discussed in detail in terms of load versus deflection, cracking, and failure modes.

3.1 LOAD VERSUS DEFLECTION RESPONSE

Linear potentiometers and digital gages were mounted on a steel reference frame. This frame was supported independently of the test specimens and loading system.

Figures 3.1 to 3.3 show the individual applied moment-deflection responses for all models. Particular deflections and loads have been indicated in these figures for all major load levels. Plots for models CO-PU-54S-TH-I, CO-PU-74S-TH-I, and CO-PU-100S-TH-V do not represent the behavior of such overhangs to complete failure since these models could be loaded only to the level of ultimate load of the other overhang for each specimen. The scales for the graphs were intentionally held constant for comparative purposes. In the overhang CO-PU-74S-TH-V, discontinuities in the plot above factored load levels were mainly due to the lack of elastomeric pads, as explained before. In this case, built-up friction forces between rams and steel plates were suddenly relieved (whether in part or in whole is unknown) at certain load steps due to the horizontal movement of the overhang. These restraining forces were a function of the rigidity of the loading frame and the lack of shear deformation capacity of the bearing system. The modified loading system for the other models, where elastomeric pads were used, greatly relieved these restraining forces. Figure 3.4 shows the horizontal deformation of the elastomeric pad in model CO-PU-100S-TH-V.

In all cases, the initial deflection measurements were made before prestressing operations. No corrections of the tip deflection were made based on column settlement or deflections at the top of the overhang at the column face, since deflections at these locations were negligible. In addition, no normalization of results based on concrete strength were performed since all models were tested at very similar cylinder compressive strengths as was reported in Section 2.5.1. Tip deflections used in the moment-deflection plots were taken in all cases from linear potentiometer data since there was a perfect correlation with the results from digital gages. As an example of this correlation, Figure 3.5 shows the results for the CO-PU-54S-TH models.

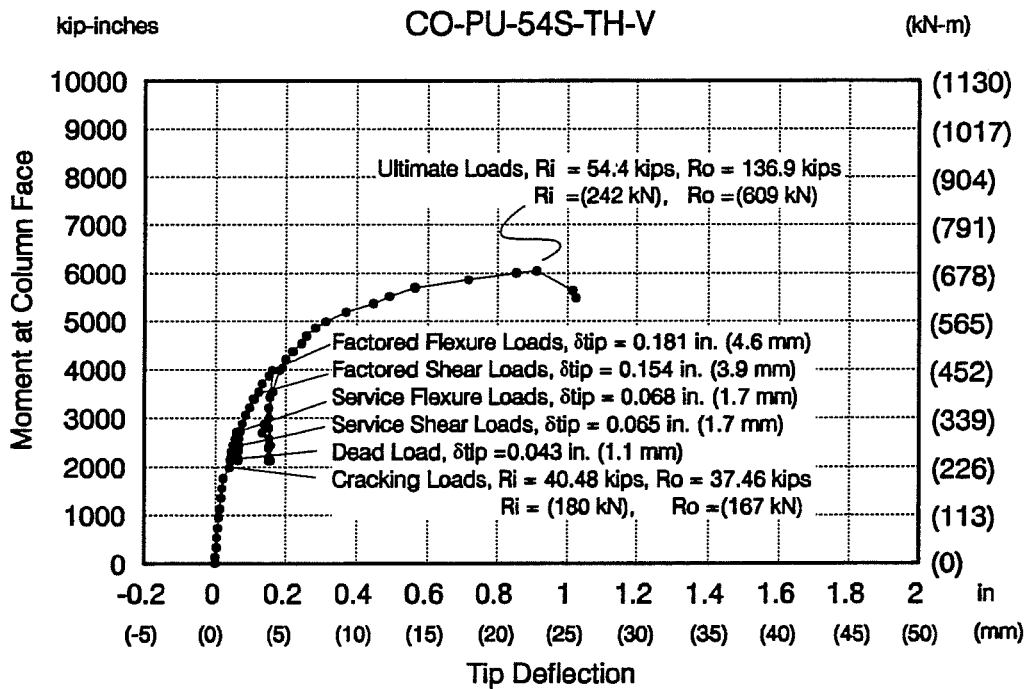
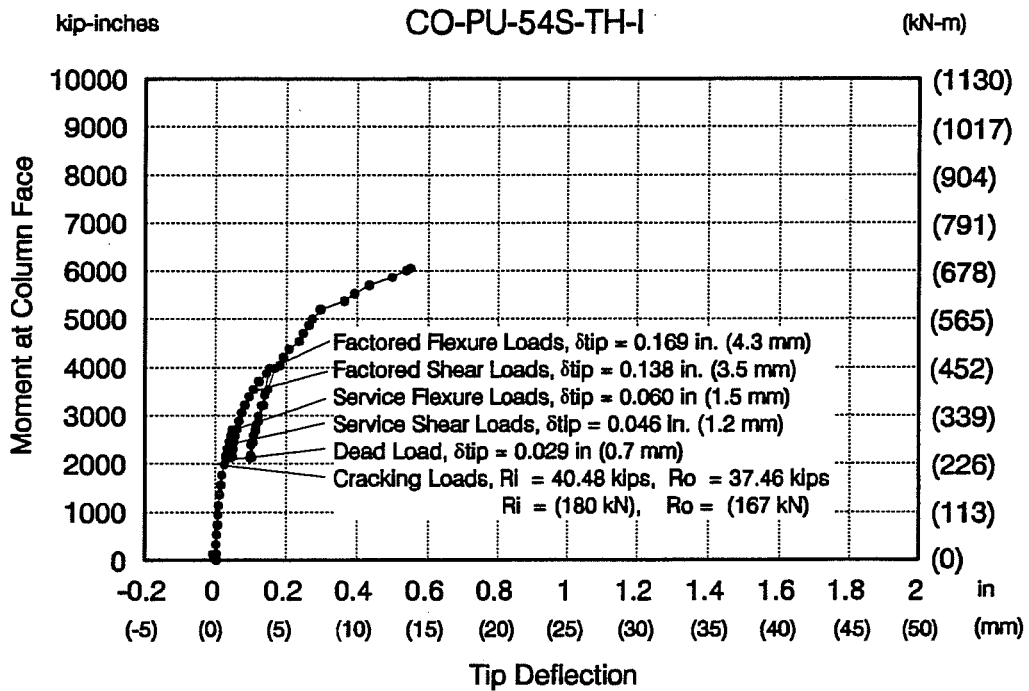


Figure 3.1 Moment-Deflection Response for Models CO-PU-54S-TH (V&I)

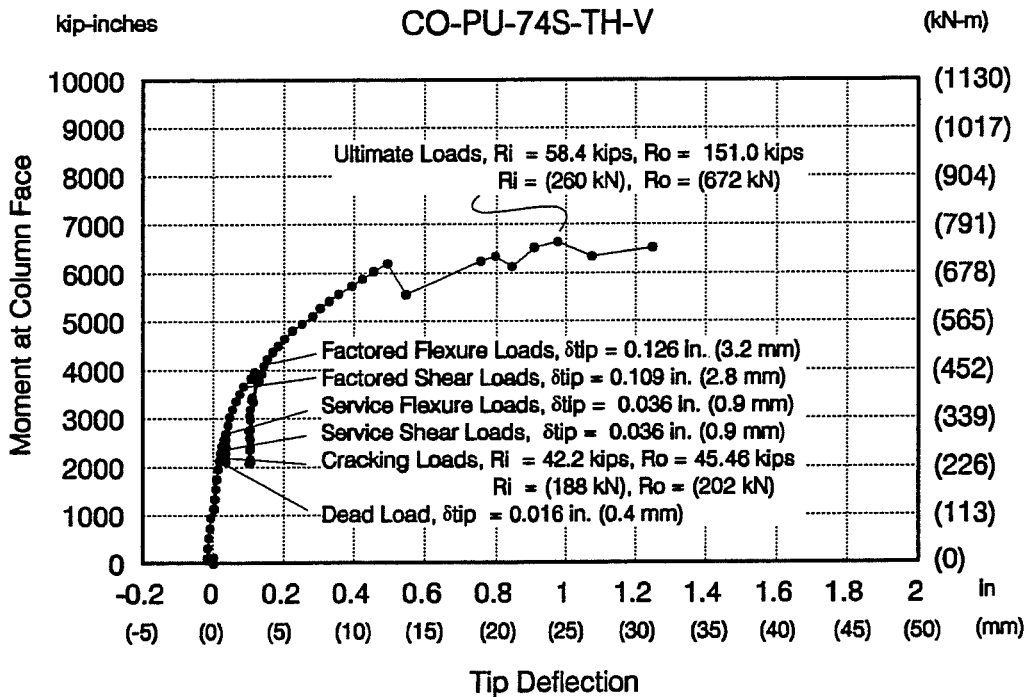
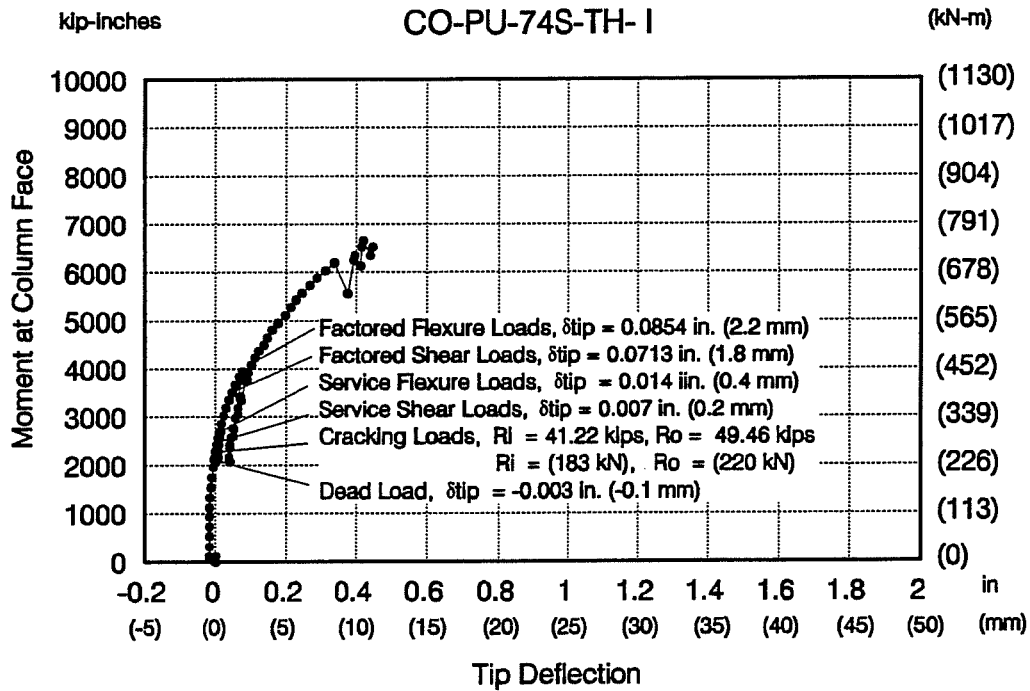


Figure 3.2 Moment-Deflection Response for Models CO-PU-74S-TH (V&I)

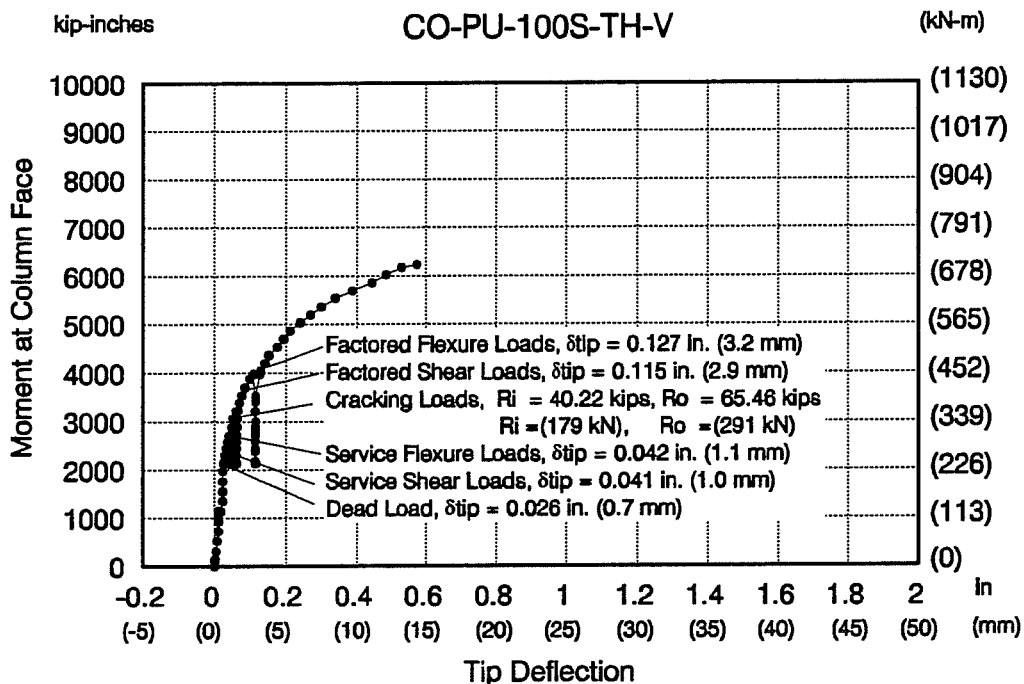
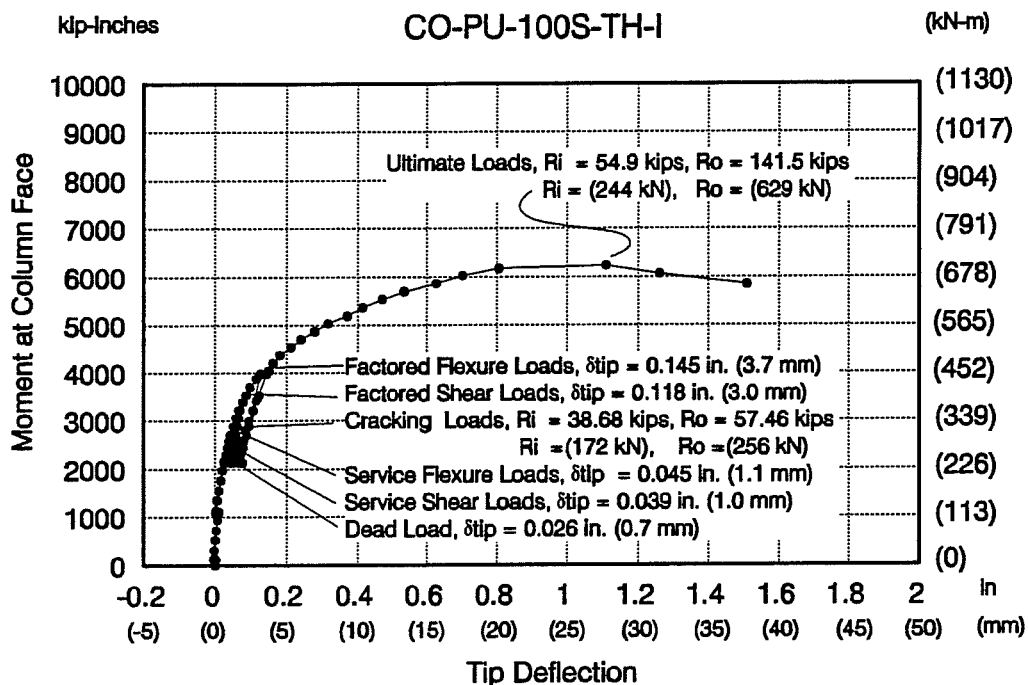


Figure 3.3 Moment-Deflection Response for Models CO-PU-100S-TH (V&I)

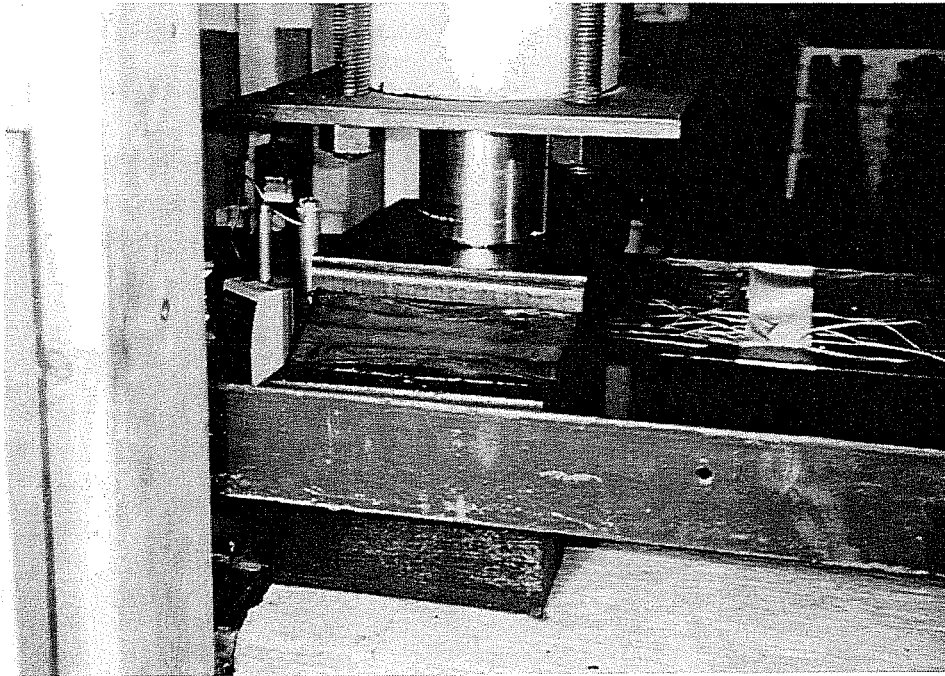


Figure 3.4 Use of Elastomeric Pads in Model CO-PU-100S-TH-V

From the moment-deflection curve for model CO-PU-54S-TH-V, it can be observed that the behavior was basically linear until cracking occurred. After this load stage, gradual non-linear behavior began with some plastic behavior seen near the peak load. A clear point of onset of yielding in the main flexural reinforcement was observed approximately at an applied moment of 5000 kip-inches (565 kN-m), 23 percent above factored flexure load level. Crushing was extensive at failure loads which did not allow for large plastic deformations. As discussed later, a post-mortem investigation found evidence of one #2 reinforcing bar broken in the top layer of the main flexural reinforcement and signs of yielding in all other # 2 reinforcing bars. At ultimate loads, tip deflection was 0.914 inches (23 mm), corresponding to a ratio of tip deflection to overhang length of 0.020 ($\Delta=L/50$). Failure occurred at a moment of 6046 kip-inches (683 kN-m), at approximately 48 percent above factored flexure load level.

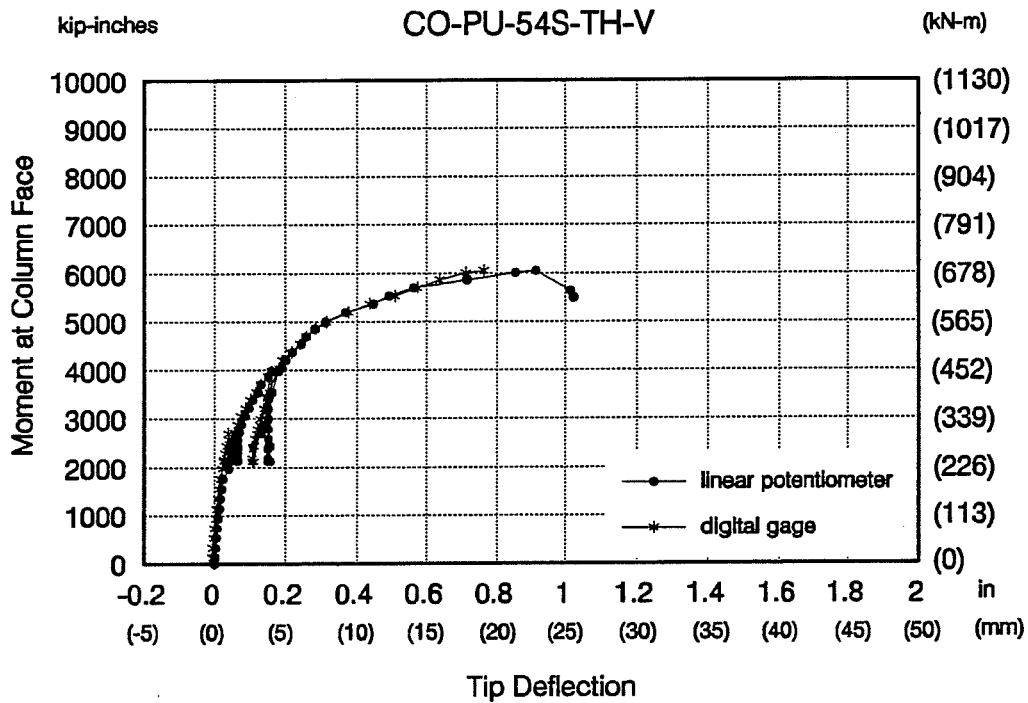
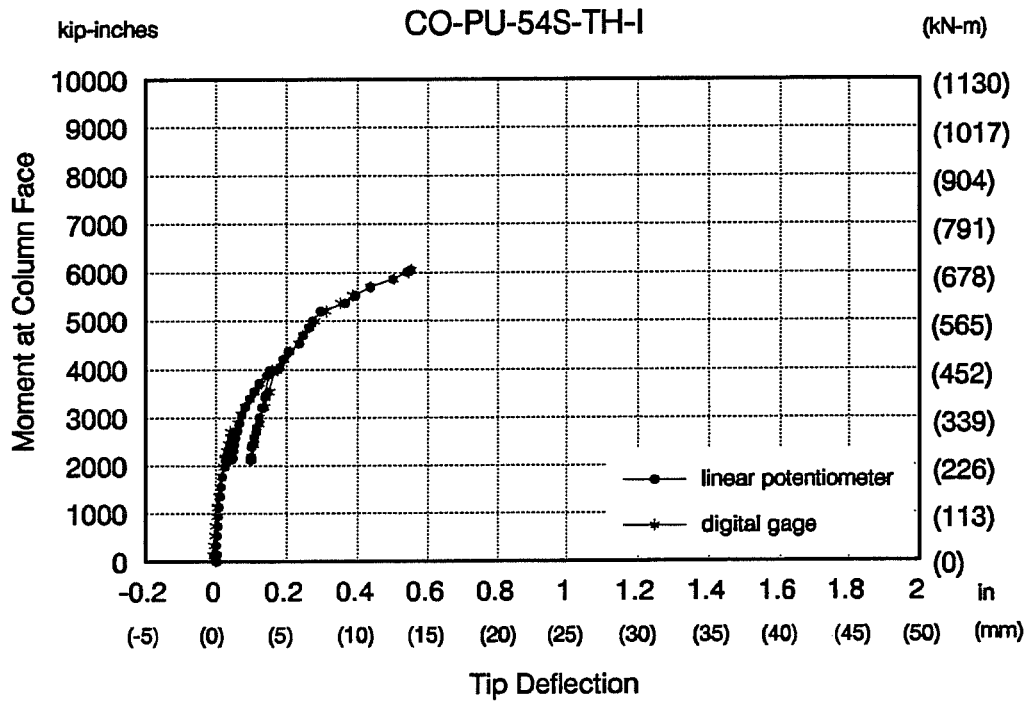


Figure 3.5 Comparison of Data from Linear Potentiometers and Digital Gages for the Moment-Deflection Response of Models CO-PU-54S-TH (V&I)

Behavior of model CO-PU-54S-TH-I also presented a linear relationship between moment and deflection until cracking load, then again gradually non-linear behavior took place. A clear point of onset of yielding in the main flexural reinforcement is shown in Figure 3.1 at an applied moment of 5200 kip-inches (588 kN-m), approximately 28 percent above factored flexure load level. Crack patterns were very similar to those in model CO-PU-54S-TH-V. No significant plastic deformations took place since this model was not tested to failure. Ultimate moment capacity was calculated, by analytical methods, to be approximately 5 percent above the ultimate moment capacity of the companion overhang.

Model CO-PU-74S-TH-V behaved basically linear up to cracking loads, then non-linear behavior began with plastic deformations seen near ultimate loads. No clear point of beginning of yielding of the reinforcing steel could be observed. Continuity in the plot was lost at the beginning of plastic behavior due to the problem with the built up friction forces between loading rams and model, as explained above. In spite of that, the test continued until a tip deflection at ultimate of 0.99 inches (25 mm) was reached. This corresponded to a ratio of tip deflection to overhang length of 0.022 ($\Delta=L/45$). Failure occurred at an applied moment of 6648 kip-inches (751 kN-m), approximately 63 percent above factored flexure load level.

Response of model CO-PU-74S-TH-I showed very similar characteristics of linear and non-linear behavior to the companion overhang. However, after cracking this model was more stiff. Calculated ultimate capacity for this model was approximately 10 percent higher than that for model CO-PU-74S-TH-V.

Model CO-PU-100S-TH-I presented a very smooth curve of moment versus tip deflection, up to failure. Again, a linear relationship was observed up to cracking loads, followed by non-linear behavior with large plastic deformations near ultimate loads. Onset of yielding in the reinforcing steel could not be precisely defined. Failure of this model occurred at an applied moment of 6232 kip-inches (704 kN-m), 53 percent above factored flexure load level. This corresponded to a tip deflection of 1.11 in. (28 mm), and a tip deflection to overhang length ratio of 0.024 ($\Delta=L/42$). It is obvious comparing this plot, Figure 3.3, with the moment-deflection response of model CO-PU-74S-TH-V, Figure 3.2, that there is an enormous advantage of using the elastomeric pads between rams and specimen.

Finally, model CO-PU-100S-TH-V presented very similar linear and non-linear behavior to that described for all the previous models, showing to be somewhat more stiff than model

CO-PU-100S-TH-I. The calculated ultimate capacity for this model was approximately 4 percent higher than that for model CO-PU-100S-TH-I.

Comparison of moment-deflection response for all overhangs is presented in Figure 3.6. For this figure, the curve for model CO-PU-74S-TH-V was smoothed above factored load level by eliminating some data points that were considered to be caused by the sudden loss of friction forces between rams and bearing plates.

Analyzing this plot, it can be observed that deflections in the elastic region and up to the service flexure load level were very similar for all models, showing minimal effect from the different reinforcement patterns and amounts of post-tensioning force. After this load level, model CO-PU-54S-TH-V showed the lowest stiffness and ductility. This behavior was expected when compared to the CO-PU-100S-TH-I model (of very similar ultimate capacity) since the different amounts of prestressed reinforcement were found to be in direct proportion with the amount of cracking. As explained later, for a higher post-tensioning force, fewer cracks were observed.

Model CO-PU-74S-TH-V, in spite of having the smallest moment capacity of all models, as predicted by analytical methods, showed a higher moment capacity and more stiffness than models CO-PU-54S-TH-V and CO-PU-100S-TH-I. The reason associated with this behavior was the already-mentioned friction forces between rams and bearing plates.

3.2 CRACKING

Cracking loads for each model are presented in Table 3.1. First cracking corresponds to the load step where cracking was first visually observed. However, this is somewhat subjective since cracks may not be immediately seen when they originate.

To identify cracks and document their location on the model faces, a 4 in. (100 mm) x 4 in. (100 mm) grid system was drawn on each side. In addition, a horizontal line was drawn at approximately one inch (25 mm) from the top of the specimens, at the approximate location of the top flexural reinforcing bar. Each line was identified by an alphabetical letter A through G from top to bottom, including A' for the additional horizontal line.

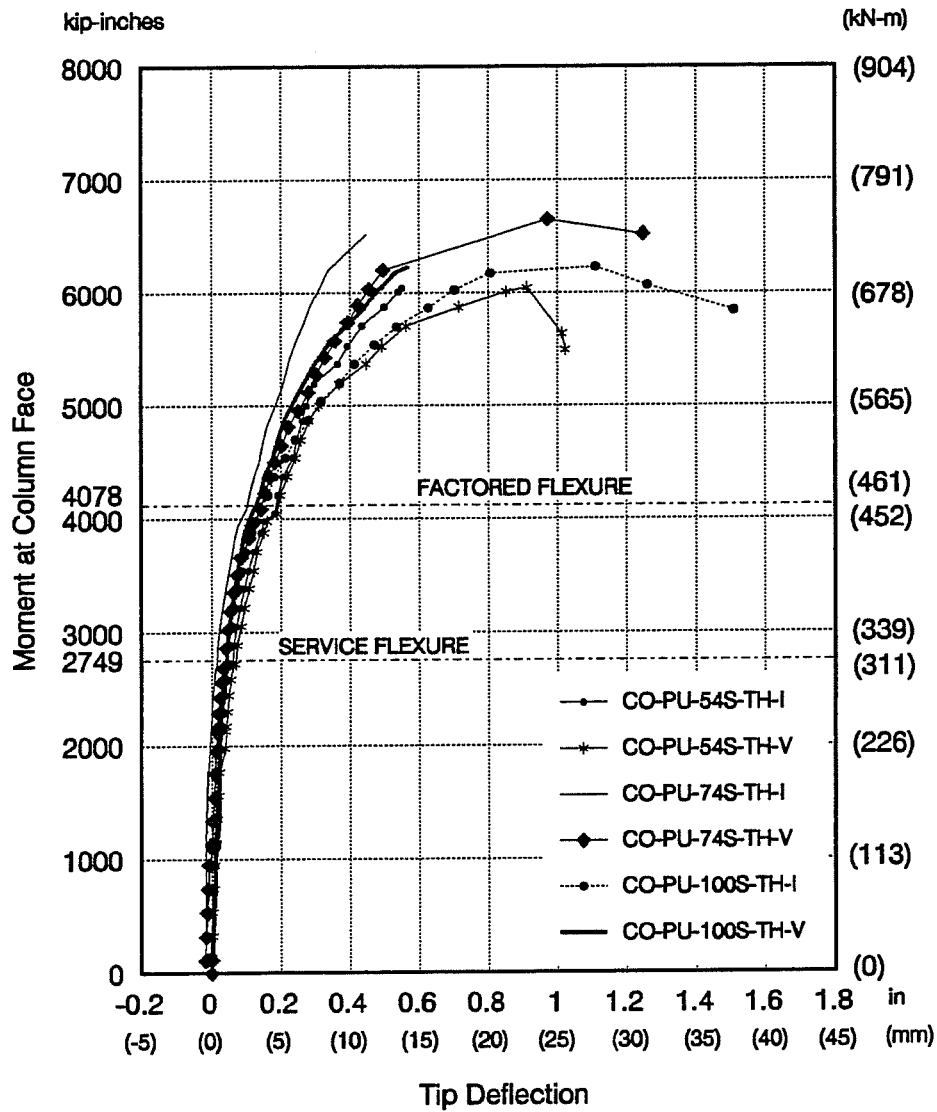


Figure 3.6 Comparison of Moment - Deflection curves.

Table 3.1 Cracking and Failure loads

Model	Cracking loads						Failure loads					
	Ro kips (kN)	Ri kips (kN)	Moment kip-in (kN-m)	Mcr / Mdead *	Mcr / Mserv. flex.**		Ro kips (kN)	Ri kips (kN)	Moment (Mn) kip-in (kN-m)	Mn / Mu/0.9 ****		
CO-PU-54S-TH-V	37.46 (166.6)	40.48 (180.1)	1987 (224.49)	0.92	0.72		136.9 (608.9)	54.4 (242.0)	6046 (683.07)	1.33		
CO-PU-54S-TH-I	37.46 (166.6)	40.48 (180.1)	1987 (224.49)	0.92	0.72		—	—	—	—		
CO-PU-74S-TH-V	45.46 (202.2)	42.2 (187.7)	2322 (262.34)	1.07	0.84		151 (671.6)	58.4 (259.8)	6648 (751.09)	1.47		
CO-PU-74S-TH-I	49.46 (220.0)	41.22 (183.3)	2465 (278.49)	1.14	0.90		—	—	—	—		
CO-PU-100S-TH-V	65.46 (291.2)	40.22 (178.9)	3076 (347.52)	1.42	1.12		—	—	—	—		
CO-PU-100S-TH-I	57.46 (255.6)	38.68 (172.0)	2750 (310.69)	1.27	1.00		141.5 (629.4)	54.9 (244.2)	6232 (704.09)	1.37		

* Mdead = 2169 k-in (245 kN-m)

** Mservice flexure = 2749 k-in (311 kN-m)

*** Mu/0.9 = 4531 k-in (512 kN-m). In design of the specimens a reduction factor of 0.9 was used for flexure. Considering that in these laboratory experiments all materials and dimensions were carefully controlled, test results were compared against the value Mu/0.9 to be more consistent.

At specific load steps, cracks were detected with the unaided eye and marked. Cracks as small as 0.001 in. (0.025 mm) could be seen and documented. Crack measurements were made with a crack measurement device with an accuracy of ± 0.0005 inches (0.013 mm). An attempt was made to measure each crack at the same location at every load stage.

3.2.1 Models CO-PU-54S-TH (V&I)

Cracking in model CO-PU-54S-TH-V (located in the South side) occurred first on the west side of the overhang, at load step 11, $R_o=37.46$ kips (167 kN) and $R_i=40.48$ kips (180. kN), just before the application of the complete dead load. The East side cracked at load step 12, corresponding to dead load.

First cracking in model CO-PU-54S-TH-I (located in the North side) also occurred on the West side at load step 11, corresponding to 92 percent of dead load and 72 percent of service flexure load, as shown in Table 3.1. The East side cracked later at load step 14, while loading to service flexure load.

Complete readings of all crack widths (all cracks, all grid levels) were performed at first cracking, service flexure loads and service shear loads. Only the maximum width of each crack was measured at dead loads - load steps (LS) 18, 22, 37 -, at 24 percent above service flexure loads (service flexure plus) - LS 32 -, at factored flexure - LS 36 -, at second time service shear - LS 40 -, at factored shear - LS 46 -, third time service flexure - LS 49 -, and at factored flexure - LS 53-. No crack readings were performed above factored flexure loads.

Figures 3.7 and 3.8 show the crack pattern and crack numbering (the numbers indicate the order in which they appeared) for these overhangs at factored flexure loads. Tables 3.2 to 3.5 show the maximum crack width of every crack at every major load step. Shaded areas in these tables emphasize the "major" cracks (cracks that showed a maximum crack width for the particular side of the overhang at any given load step).

Crack widths on the top face of the specimens were always checked. No crack width was found to exceed those on the side faces. These results were true for all models.

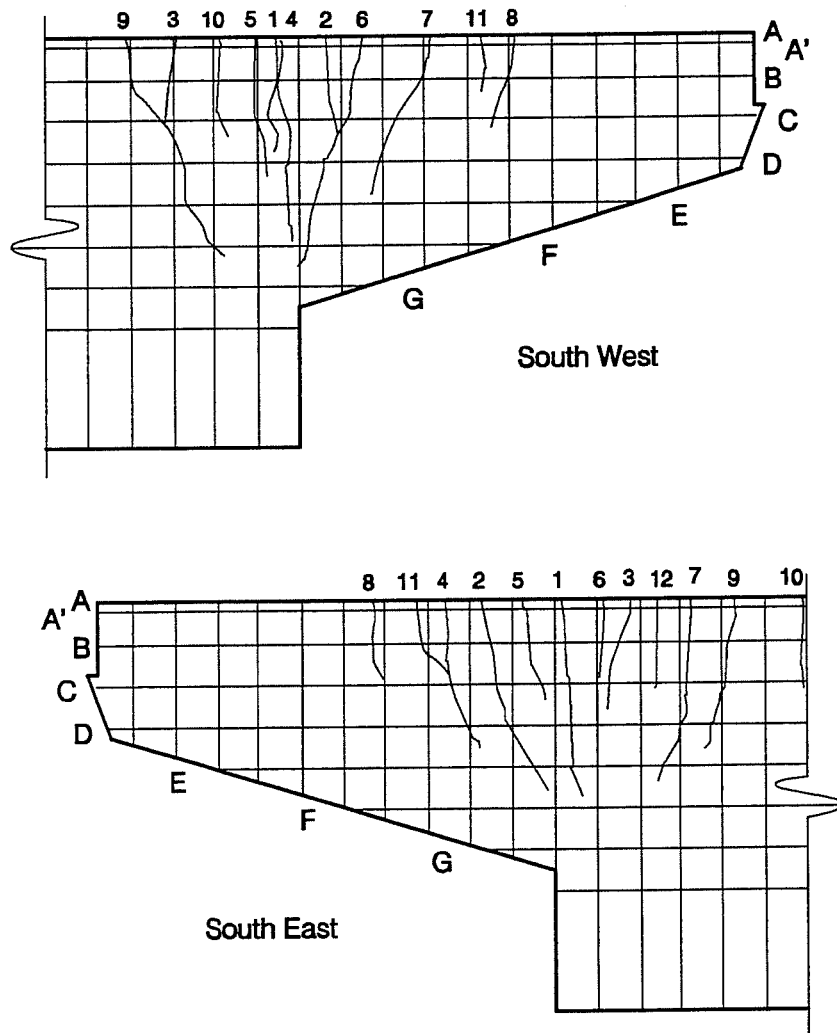


Figure 3.7 Crack Number and Location on East and West sides of CO-PU-54S-TH-V overhang.

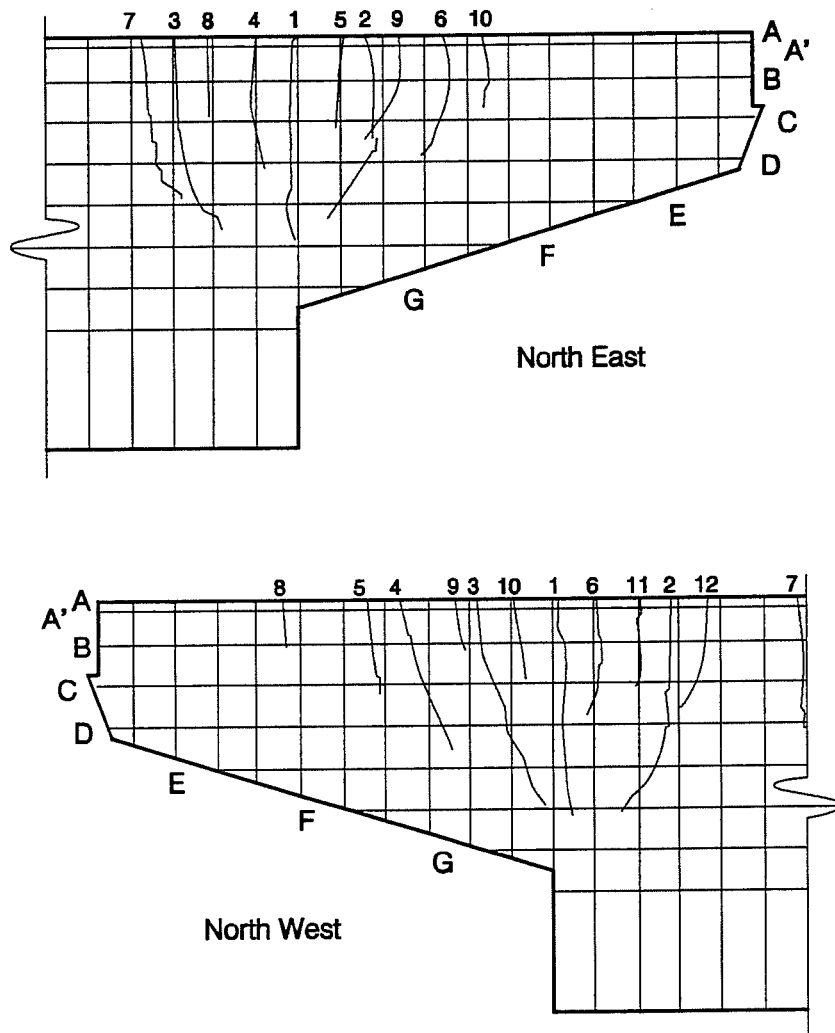


Figure 3.8 Crack Number and Location on East and West sides of CO-PU-54S-TH-I overhang.

Table 3.3 Maximum Crack Width Readings for Overhang CO-PU-54S-TH-V (West Side)

Load Stage	West Side				Maximum Crack Width, inches											
	RI	Ro	Moment at Face of Column		Crack Number											
	kips	kips	kip-inches		1	2	3	4	5	6	7	8	9	10	11	12
cracking	40.48	37.16	1987													
Dead Load plus	42.2	45.48	2322		0.0026											
(2) Service Flexure	38.57	58.97	2749		0.003 A	0.0025										
(3) Dead Load *	43.47	40.47	2169		0.002	0.0015										
(4) Service Shear	49.97	48.97	2507		0.0025	0.002										
(5) Dead Load *	43.47	40.47	2169		0.0025	0.002										
(6) Service Flexure	38.57	58.97	2749		0.0035	0.0025	0.001 C									
Service Flexure plus *	41.76	73.46	3408		0.005	0.005	0.004	0.003 C	0.0045	0.0035	0.0035	0.002				
(7) Factored Flexure *	46.18	88.52	4078		0.005	0.0045	0.005	0.003 C	0.008	0.006	0.005	0.002	0.0025	0.003	0.002	
(8) Dead Load *	43.47	40.47	2169		0.003	0.004	0.0025	0.0015 C	0.002	0.0025	0.0035	0.001	0.002	0.002	0.001	
(9) Service Shear *	49.97	48.97	2507		0.004	0.0045	0.003	0.0015	0.003	0.0035	0.001	0.002	0.0025	0.003	0.001	
(10) Factored Shear *	70.92	68.82	3554		0.005	0.005	0.003	0.002	0.004	0.0055	0.006	0.002	0.0025	0.0025	0.002	
(12) Service Flexure *	38.57	58.97	2749		0.0025	0.0045	0.0035	0.002	0.003	0.0035	0.0045	0.001	0.0025	0.0025	0.0015	
(13) Factored Flexure *	46.18	88.52	4078		0.0035	0.007	0.004	0.003	0.0055	0.006	0.007	0.003	0.0025	0.005	0.0035	

Load Stage	West Side				Maximum Crack Width (mm)											
	RI	Ro	Moment at Face of Column		Crack Number											
	(kN)	(kN)	(kN-m)		1	2	3	4	5	6	7	8	9	10	11	12
cracking	(180.1)	(166.6)	(224.5)													
Dead Load plus	(187.7)	(202.2)	(262.4)		(0.025)											
(2) Service Flexure	(171.6)	(253.4)	(310.6)		(0.064)	(0.064)										
(3) Dead Load *	(193.4)	(180.0)	(245.1)		(0.061)	(0.038)										
(4) Service Shear	(222.3)	(208.9)	(283.3)		(0.064)	(0.057)										
(5) Dead Load *	(193.4)	(180.0)	(245.1)		(0.064)	(0.051)										
(6) Service Flexure	(171.6)	(253.4)	(310.6)		(0.089)	(0.064)	(0.051)	(0.025 C)								
Service Flexure plus *	(185.7)	(326.8)	(385.1)		(0.127)	(0.127)	(0.102)	(0.076 C)	(0.114)	(0.089)	(0.089)	(0.051)				
(7) Factored Flexure *	(205.4)	(393.7)	(460.8)		(0.127)	(0.165)	(0.127)	(0.076 C)	(0.152)	(0.152)	(0.127)	(0.051)	(0.064)	(0.076)	(0.051)	
(8) Dead Load *	(193.4)	(180.0)	(245.1)		(0.076)	(0.102)	(0.064)	(0.038 C)	(0.051)	(0.064)	(0.089)	(0.025)	(0.051)	(0.051)	(0.025)	
(9) Service Shear *	(222.3)	(208.9)	(283.3)		(0.102)	(0.114)	(0.076)	(0.038)	(0.076)	(0.076)	(0.089)	(0.025)	(0.051)	(0.076)	(0.025)	
(10) Factored Shear *	(315.5)	(297.2)	(401.6)		(0.127)	(0.127)	(0.076)	(0.051)	(0.102)	(0.140)	(0.152)	(0.051)	(0.064)	(0.064)	(0.051)	
(12) Service Flexure *	(171.6)	(253.4)	(310.6)		(0.064)	(0.114)	(0.089)	(0.051)	(0.076)	(0.089)	(0.114)	(0.025)	(0.064)	(0.064)	(0.038)	
(13) Factored Flexure *	(205.4)	(393.7)	(460.8)		(0.089)	(0.176)	(0.102)	(0.076)	(0.140)	(0.152)	(0.176)	(0.076)	(0.064)	(0.127)	(0.089)	

* Only maximum crack width was measured, usually at level A unless otherwise noted.

Table 3.4 Maximum Crack Width Readings for Overhang CO-PU-54S-TH-I (East Side)

Load Stage	East Side		Maximum Crack Width, Inches																						
	RI kips	Ro kips	Moment at Face of Column kip-inches	Crack Number																					
				1	2	3	4	5	6	7	8	9	10	11	12										
Dead Load plus	42.2	45.46	2322	0.001																					
(2) Service Flexure	38.57	56.97	2749	0.0025	0.0005	0.0015																			
(3) Dead Load *	43.47	40.47	2169	0.002	0.0005	0.001																			
(4) Service Shear	48.97	46.97	2507	0.0025 A	0.0015 A	0.0015																			
(5) Dead Load *	43.47	40.47	2169	0.0015 A	0.001	0.0015																			
(6) Service Flexure	38.57	56.97	2749	0.0025	0.002	0.0015																			
Service Flexure plus *	41.76	73.46	3408	0.0035 A	0.0025	0.0025	0.004	0.003	0.0005																
(7) Factored Flexure *	46.16	66.52	4078	0.005 A	0.0035	0.005	0.005 A	0.0035	0.0025	0.003	0.003	0.003	0.003	0.002	0.001	0.001	0.001	0.001	0.001	0.001	0.001	0.001	0.001	0.001	0.001
(8) Dead Load *	43.47	40.47	2169	0.0035	0.002	0.0025	0.001	0.001	0.001	0.001	0.002	0.001	0.001	0.001	0.001	0.001	0.001	0.001	0.001	0.001	0.001	0.001	0.001	0.001	0.001
(9) Service Shear *	48.97	46.97	2507	0.0025 A	0.002	0.0025	0.0025 A	0.002	0.001	0.002	0.001	0.002	0.001	0.001	0.001	0.001	0.001	0.001	0.001	0.001	0.001	0.001	0.001	0.001	0.001
(10) Factored Shear *	70.92	66.82	3554	0.005 A	0.003	0.003	0.0035 A	0.003	0.002	0.003	0.002	0.003	0.002	0.003	0.002	0.003	0.0025	0.0035	0.0025	0.0035	0.0025	0.0035	0.0025	0.0035	0.0025
(12) Service Flexure *	38.57	56.97	2749	0.003 A	0.0025	0.0025	0.0035 A	0.002	0.001	0.0015	0.0015	0.0015	0.0015	0.0015	0.0015	0.0015	0.0015	0.0015	0.0015	0.0015	0.0015	0.0015	0.0015	0.0015	0.0015
(13) Factored Flexure *	46.16	66.52	4078	0.006 A	0.004	0.0035	0.006 A	0.0045	0.0035	0.0045	0.0035	0.0045	0.0035	0.0045	0.0035	0.0045	0.0035	0.0045	0.0035	0.0045	0.0035	0.0045	0.0035	0.0045	0.0035

Load Stage	East Side		Moment at Face of Column (kN-m)	Maximum Crack Width (mm)																					
	RI (kN)	Ro (kN)		Crack Number																					
				1	2	3	4	5	6	7	8	9	10	11	12										
Dead Load plus	(187.7)	(202.2)	(282.4)	(0.025)																					
(2) Service Flexure	(171.6)	(253.4)	(310.6)	(0.064)	(0.013)	(0.038)																			
(3) Dead Load *	(193.4)	(180.0)	(245.1)	(0.051)	(0.019)	(0.025)																			
(4) Service Shear	(222.3)	(208.6)	(283.3)	(0.064 A)	(0.038 A)	(0.038)																			
(5) Dead Load *	(193.4)	(180.0)	(245.1)	(0.038 A)	(0.025)	(0.038)																			
(6) Service Flexure	(171.6)	(253.4)	(310.6)	(0.064)	(0.051)	(0.038)																			
Service Flexure plus *	(185.7)	(326.6)	(385.1)	(0.089 A)	(0.064)	(0.064)	(0.102)	(0.076)	(0.013)																
(7) Factored Flexure *	(205.4)	(393.7)	(460.8)	(0.327 A)	(0.089)	(0.127)	(0.127 A)	(0.089)	(0.064)	(0.064)	(0.076)	(0.076)	(0.076)	(0.051)	(0.064)	(0.051)	(0.064)	(0.051)	(0.064)	(0.051)	(0.064)	(0.051)	(0.064)	(0.051)	(0.064)
(8) Dead Load *	(193.4)	(180.0)	(245.1)	(0.089)	(0.051)	(0.064)	(0.025)	(0.025)	(0.025)	(0.025)	(0.025)	(0.025)	(0.025)	(0.025)	(0.025)	(0.025)	(0.025)	(0.025)	(0.025)	(0.025)	(0.025)	(0.025)	(0.025)	(0.025)	(0.025)
(9) Service Shear *	(222.3)	(208.6)	(283.3)	(0.064 A)	(0.051)	(0.064)	(0.064 A)	(0.064 A)	(0.064)	(0.064)	(0.064)	(0.064)	(0.064)	(0.064)	(0.064)	(0.064)	(0.064)	(0.064)	(0.064)	(0.064)	(0.064)	(0.064)	(0.064)	(0.064)	(0.064)
(10) Factored Shear *	(315.5)	(297.2)	(401.6)	(0.127 A)	(0.076)	(0.076)	(0.140 A)	(0.076)	(0.051)	(0.076)	(0.051)	(0.076)	(0.051)	(0.076)	(0.051)	(0.076)	(0.051)	(0.076)	(0.051)	(0.076)	(0.051)	(0.076)	(0.051)	(0.076)	(0.051)
(12) Service Flexure *	(171.6)	(253.4)	(310.6)	(0.076 A)	(0.064)	(0.064)	(0.064 A)	(0.064)	(0.064)	(0.064)	(0.064)	(0.064)	(0.064)	(0.064)	(0.064)	(0.064)	(0.064)	(0.064)	(0.064)	(0.064)	(0.064)	(0.064)	(0.064)	(0.064)	(0.064)
(13) Factored Flexure *	(205.4)	(393.7)	(460.8)	(0.152 A)	(0.102)	(0.089)	(0.152 A)	(0.114)	(0.089)	(0.114)	(0.089)	(0.114)	(0.089)	(0.114)	(0.089)	(0.114)	(0.089)	(0.114)	(0.089)	(0.114)	(0.089)	(0.114)	(0.089)	(0.114)	(0.089)

* Only maximum crack width was measured, usually at level A unless otherwise noted.

Table 3.5 Maximum Crack Width Readings for Overhang CO-PU-54S-TH-1 (West Side)

CO-PU-54S-TH-1	West Side		Maximum Crack Width (inches)																	
	Load Stage	RI kips	Ro kips	Moment at Face of Column kip-inches	Crack Number															
					1	2	3	4	5	6	7	8	9	10	11	12				
	cracking	40.48	37.48	1867	0.0015															
	Dead Load plus	42.2	45.46	2322	0.0025															
	(2) Service Flexure	38.57	56.97	2748	0.0025	0.0025	0.001													
	(3) Dead Load *	43.47	40.47	2168	0.002	0.0015	0.001													
	(4) Service Shear	49.97	48.97	2507	0.003	0.0025	0.001													
	(5) Dead Load *	43.47	40.47	2168	0.0025	0.002	0.0025	0.001												
	(6) Service Flexure	38.57	56.97	2748	0.005	0.002	0.0045	0.0015												
	Service Flexure plus *	41.76	73.46	3408	0.006	0.002	0.0045	0.002	0.0015	0.004	0.0015									
	(7) Factored Flexure *	48.18	86.52	4078	0.006	0.005	0.0095	0.003	0.003	0.008	0.003	0.002	0.0025	0.0005	0.004	0.0025				
	(8) Dead Load *	43.47	40.47	2168	0.0035	0.003	0.0025	0.0025	0.001	0.003	0.002	0.001	0.002	0.002	0.002	0.002	0.002	0.002	0.0015	
	(9) Service Shear *	49.97	48.97	2507	0.003	0.003	0.0035	0.002	0.001	0.0035	0.002	0.001	0.002	0.0015	0.001	0.002	0.002	0.002	0.002	
	(10) Factored Shear *	70.92	66.82	3554	0.006	0.0055	0.0045	0.003	0.002	0.005	0.003	0.003	0.001	0.003	0.005	0.0045	0.0005	0.0045	0.0025	
	(12) Service Flexure *	38.57	56.97	2748	0.0045	0.004	0.0035	0.003	0.002	0.0045	0.003	0.002	0.0045	0.003	0.0025	0.0035	0.003	0.003	0.002	
	(13) Factored Flexure *	48.18	86.52	4078	0.0065	0.005	0.005	0.004	0.004	0.0065	0.0035	0.0025	0.0035	0.006	0.0065	0.0035	0.006	0.0065	0.003	

CO-PU-54S-TH-1	West Side		Maximum Crack Width (mm)																	
	Load Stage	RI (kN)	Ro (kN)	Moment at Face of Column (kN-m)	Crack Number															
					1	2	3	4	5	6	7	8	9	10	11	12				
	cracking	180.1	166.6	224.5	0.038															
	Dead Load plus	187.7	202.2	282.4	0.064															
	(2) Service Flexure	171.6	253.4	310.9	0.076	0.064	0.025													
	(3) Dead Load *	183.4	180.0	245.1	0.051	0.051	0.038	0.025												
	(4) Service Shear	222.3	208.9	283.3	0.076	0.051	0.064	0.025												
	(5) Dead Load *	183.4	180.0	245.1	0.064	0.051	0.064	0.025												
	(6) Service Flexure	171.6	253.4	310.9	0.064	0.051	0.064	0.038												
	Service Flexure plus *	185.7	328.6	385.1	0.127	0.051	0.114	0.051	0.038	0.102	0.038									
	(7) Factored Flexure *	205.4	393.7	460.8	0.152	0.127	0.165	0.076	0.076	0.152	0.076	0.152	0.051	0.064	0.127	0.102	0.064	0.038		
	(8) Dead Load *	183.4	180.0	245.1	0.089	0.076	0.064	0.064	0.025	0.076	0.025	0.076	0.051	0.051	0.051	0.051	0.051	0.051	0.038	
	(9) Service Shear *	222.3	208.9	283.3	0.076	0.076	0.089	0.051	0.025	0.089	0.051	0.025	0.038	0.025	0.051	0.051	0.051	0.051	0.051	
	(10) Factored Shear *	315.5	297.2	401.6	0.152	0.140	0.114	0.076	0.051	0.127	0.076	0.076	0.025	0.064	0.127	0.114	0.064	0.051		
	(12) Service Flexure *	171.6	253.4	310.9	0.114	0.102	0.089	0.076	0.051	0.114	0.076	0.076	0.025	0.064	0.089	0.076	0.064	0.051		
	(13) Factored Flexure *	205.4	393.7	460.8	0.165	0.127	0.127	0.102	0.102	0.165	0.089	0.089	0.064	0.089	0.165	0.165	0.089	0.076		

* Only maximum crack width was measured, usually at level A unless otherwise noted.

3.2.2 Models CO-PU-74S-TH (V&I)

First cracking occurred in overhang CO-PU-74S-TH-V at the East and West sides at load step 14, $R_o=45.46$ kips (202 kN) and $R_i=42.20$ kips (188 kN), corresponding to 7 percent above dead load and 84 percent of the service flexure load, as shown in Table 3.1. For overhang CO-PU-74S-TH-I first cracking occurred also simultaneously at both sides at load step 15, $R_o=41.22$ kips (183 kN) and $R_i=49.46$ kips (220 kN).

Complete crack width readings were taken at first cracking - LS 14 and 15 -, service flexure loads - LS 17 and 27 -, and service shear loads - LS 21 -. Only the maximum width of each crack was recorded at dead loads - LS 18, 37 -, 24 percent above service flexure loads (service flexure plus) - LS 32 -, factored flexure - LS 36-, second time service shear - LS 40 -, factored shear - LS 46 -, third time service flexure - LS 49 -, and at factored flexure loads - LS 53 -.

As for the previous models, Figures 3.9 and 3.10 show the crack pattern and crack numbering for these overhangs at factored flexure loads. Tables 3.6 to 3.9 show the maximum crack width of every crack at every major load step. Shaded areas in these tables emphasize the "major" cracks.

3.2.3 Models CO-PU-100S-TH (V&I)

Cracking started on the West side of overhang CO-PU-100S-TH-I, located at the North end, at load step 28, $R_o=57.46$ kips (256 kN) and $R_i=38.68$ kips (172 kN), just above service flexure load. For the same model, cracking on the East side occurred at load step 31, $R_o=69.46$ kips (309 kN) and $R_i=40.99$ kips (182 kN), midway between service flexure and factored flexure load.

For overhang CO-PU-100S-TH-V cracking started also on the West side at load step 30, $R_o=65.46$ kips (291 kN) and $R_i=40.22$ kips (179 kN), corresponding to 12 percent above service flexure load. Cracking on the East side took place at load step 31, $R_o=69.46$ kips (309 kN) and $R_i=40.99$ kips (182 kN).

Testing of these models included the addition of two load cycles at service loads after first cracking as explained in Section 2.9.1. This was done to observe the behavior of existing cracks at these load levels.

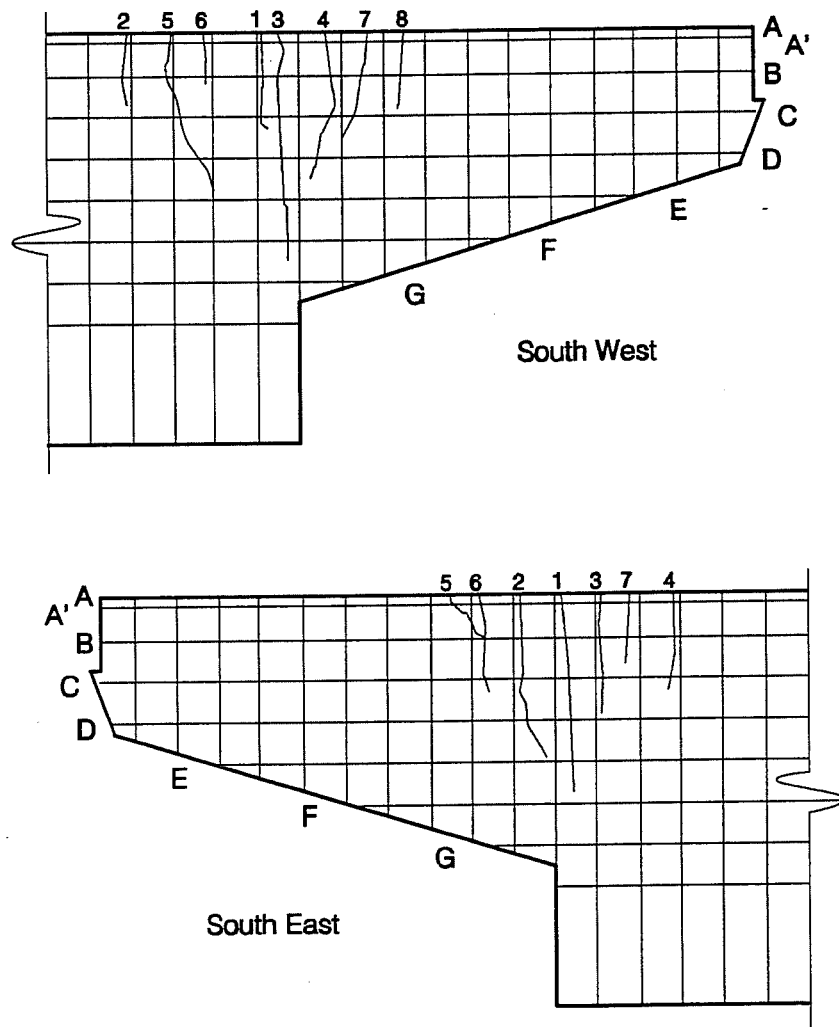


Figure 3.9 Crack Number and Location on East and West sides of CO-PU-74S TH-V overhang.

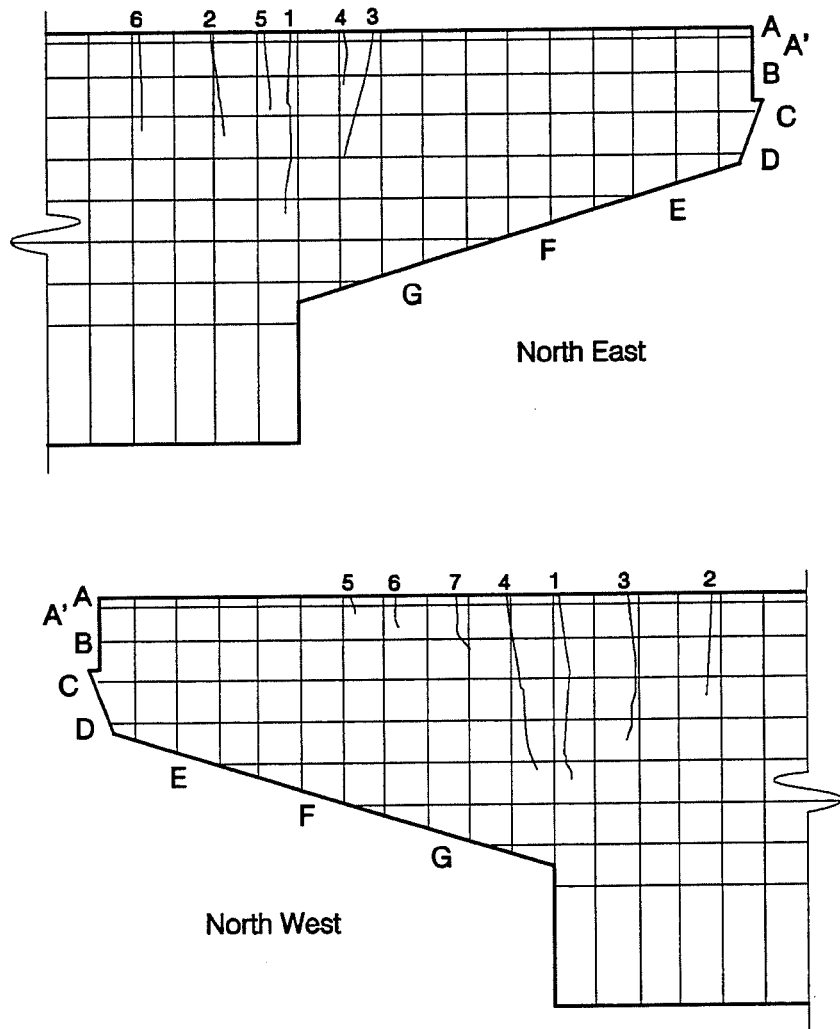


Figure 3.10 Crack Number and Location on East and West sides of CO-PU-74S-TH-I overhang.

Table 3.6 Maximum Crack Width Readings for Overhang CO-PU-74S-TH-V (East Side)

CO-PU-74S-TH-V	East Side				Maximum Crack Width, inches													
	Load Stage	RI kips	Ro kips	Moment at Face of Column kip-inches	Crack Number													
					1	2	3	4	5	6	7	8						
cracking	42.2	45.46	2322															
Dead Load plus	41.22	48.46	2485															
(2) Service Flexure	38.57	56.97	2749		0.0015 A													
(3) Dead Load *	43.47	40.47	2169		0.003 A													
(4) Service Shear	48.97	46.97	2507		0.0025 A													
(6) Service Flexure	38.57	56.97	2749		0.003 A													
Service Flexure plus *	41.76	73.46	3408		0.005 A	0.004	0.004	0.005	0.002	0.005 B	0.0045							
(7) Factored Flexure *	48.18	88.52	4078		0.007 A	0.005	0.008	0.005	0.002	0.005 B	0.0015 B							
(8) Dead Load	43.47	40.47	2169		0.003	0.0025	0.0025	0.0025	0.002 B	0.0005	0.0015							
(9) Service Shear	49.97	46.97	2507		0.003 A	0.0025	0.002	0.003	0.001 A	0.002	0.002							
(10) Factored Shear *	70.92	66.82	3554		0.005 A	0.005	0.005 A	0.004 A	0.0015 A	0.003	0.002							
(12) Service Flexure *	38.57	56.97	2749		0.005 A	0.004	0.005	0.004	0.001	0.002	0.003							
(13) Factored Flexure *	48.18	88.52	4078		0.006	0.005	0.006	0.005	0.002	0.004	0.004							

CO-PU-74S-TH-V	East Side				Maximum Crack Width (mm)													
	Load Stage	RI (kN)	Ro (kN)	Moment at Face of Column (kN-m)	Crack Number													
					1	2	3	4	5	6	7	8						
cracking	187.7	202.2	262.4															
Dead Load plus	183.3	220.0	278.5															
(2) Service Flexure	171.9	253.4	310.9		0.013													
(3) Dead Load *	193.4	180.0	245.1		0.016 A													
(4) Service Shear	222.3	208.9	283.3		0.017 A													
(6) Service Flexure	171.9	253.4	310.9		0.016 A													
Service Flexure plus *	185.7	326.8	395.1		0.017 A	0.102	0.102	0.102	0.051	0.127 B	0.114							
(7) Factored Flexure *	205.4	393.7	480.8		0.017 A	0.127	0.152	0.127	0.051	0.127 B	0.114							
(8) Dead Load	193.4	180.0	245.1		0.016	0.064	0.064	0.064	0.051 B	0.038	0.038 B							
(9) Service Shear	222.3	208.9	283.3		0.016	0.064	0.064	0.064	0.051	0.076	0.051							
(10) Factored Shear *	315.5	297.2	401.8		0.127 A	0.127	0.127 A	0.102 A	0.038 A	0.076	0.051							
(12) Service Flexure *	171.9	253.4	310.9		0.127 A	0.102	0.127	0.102	0.051	0.127	0.076							
(13) Factored Flexure *	205.4	393.7	480.8		0.152	0.127	0.152	0.127	0.051	0.127	0.102							

* Only maximum crack width was measured, usually at level A unless otherwise noted.

Table 3.7 Maximum Crack Width Readings for Overhang CO-PU-74S-TH-V (West Side)

Load Stage	West Side				Maximum Crack Width, inches								
	RI	Ro	Moment at Face of Column		Crack Number								
	kips	kips	kips-inches	kips-inches	1	2	3	4	5	6	7	8	
cracking	42.2	45.46	2322		0.002								
Dead Load plus	41.22	46.46	2465		0.003	0.0015							
(2) Service Flexure	38.57	56.97	2748		0.002	0.0015 A'							
(3) Dead Load *	43.47	40.47	2168		0.004	0.0015 A'							
(4) Service Shear	49.97	46.97	2507		0.0045	0.0015							
(5) Service Flexure	38.57	56.97	2748		0.0045	0.0015							
Service Flexure plus *	41.76	73.46	3408		0.006	0.003	0.005 A'	0.005					
(7) Factored Flexure *	48.18	86.52	4078		0.008 A'	0.008 A'	0.008 A'	0.008 A'	0.005 A'	0.008	0.005	0.008	0.0035
(8) Dead Load	43.47	40.47	2168		0.003 A'	0.002	0.002	0.002	0.002	0.001	0.002 A'	0.001	0.001
(9) Service Shear	49.97	46.97	2507		0.004 A'	0.002	0.0025	0.003 A'	0.002	0.002 A'	0.002 A'	0.0015	0.0015
(10) Factored Shear *	70.62	66.82	3554		0.0075	0.004	0.005 A'	0.005 A'	0.004 B	0.005	0.004	0.002	0.002
(12) Service Flexure *	38.57	56.97	2748		0.008	0.003	0.004 A'	0.005 A'	0.003 A'	0.005	0.003 A'	0.0015	0.0015
(13) Factored Flexure *	46.18	88.52	4078		0.007	0.004	0.005 A'	0.007 A'	0.005 A'	0.006	0.006	0.004	0.004

Load Stage	West Side				Maximum Crack Width (mm)								
	RI	Ro	Moment at Face of Column		Crack Number								
	(kN)	(kN)	(kN-m)	(kN-m)	1	2	3	4	5	6	7	8	
cracking	(187.7)	(202.2)	(282.4)		(0.051)								
Dead Load plus	(183.3)	(220.0)	(276.5)		(0.076)	(0.038)							
(2) Service Flexure	(171.6)	(253.4)	(310.6)		(0.102)	(0.038 A')							
(3) Dead Load *	(193.4)	(180.0)	(245.1)		(0.102)	(0.038 A')							
(4) Service Shear	(222.3)	(208.9)	(283.3)		(0.114)	(0.038)							
(5) Service Flexure	(171.6)	(253.4)	(310.6)		(0.114)	(0.038)							
Service Flexure plus *	(185.7)	(326.8)	(385.1)		(0.152)	(0.076)	(0.127 A)	(0.127)					
(7) Factored Flexure *	(205.4)	(393.7)	(460.6)		(0.203)	(0.152)	(0.127 A)	(0.152 A)	(0.127 A)	(0.152)	(0.127)	(0.089)	(0.089)
(8) Dead Load	(193.4)	(180.0)	(245.1)		(0.102 A)	(0.051)	(0.051)	(0.051)	(0.051)	(0.025)	(0.051 A)	(0.025)	(0.025)
(9) Service Shear	(222.3)	(208.9)	(283.3)		(0.102 A)	(0.051)	(0.051)	(0.051)	(0.051)	(0.051)	(0.051 A)	(0.051)	(0.051)
(10) Factored Shear *	(315.5)	(297.2)	(401.6)		(0.161)	(0.102)	(0.127 A)	(0.127 A)	(0.102 B)	(0.127)	(0.102)	(0.051)	(0.051)
(12) Service Flexure *	(171.6)	(253.4)	(310.6)		(0.152)	(0.076)	(0.102 A)	(0.127 A)	(0.076 A)	(0.127)	(0.076 A)	(0.038)	(0.038)
(13) Factored Flexure *	(205.4)	(393.7)	(460.6)		(0.176)	(0.102)	(0.127 A)	(0.178 A)	(0.127 A)	(0.152)	(0.152)	(0.102)	(0.102)

* Only maximum crack width was measured, usually at level A unless otherwise noted.

Table 3.8 Maximum Crack Width Readings for Overhang CO-PU-74S-TH-I (East Side)

Load Stage	East Side				Maximum Crack Width, Inches						
	RI	Ro	Moment at Face of Column	Crack Number	1	2	3	4	5	6	7
	kips	kips	Kip-inches								
cracking	41.22	48.48	2465		0.001						
(2) Service Flexure	38.57	56.97	2749		0.002						
(3) Dead Load	43.47	40.47	2189		0.002						
(4) Service Shear	49.97	46.97	2507		0.0025						
(6) Service Flexure	38.57	56.97	2749		0.0035						
Service Flexure plus *	41.76	73.46	3408		0.005	0.0035	0.002				
(7) Factored Flexure *	46.18	86.52	4076		0.008	0.0045	0.005	0.004 A'	0.0035	0.003 A'	
(8) Dead Load	43.47	40.47	2189		0.0025 A'	0.002	0.0015 B	0.001	0.001	0.0015 A'	
(9) Service Shear	49.97	46.97	2507		0.002	0.002	0.002 A'	0.001	0.001	0.0015 A'	
(10) Factored Shear *	70.92	66.82	3554		0.005	0.004	0.004 A'	0.003 C	0.0035 C	0.003 A'	
(12) Service Flexure *	38.57	56.97	2749		0.004	0.003	0.003	0.002 A'	0.002	0.002 A'	
(13) Factored Flexure *	46.18	86.52	4076		0.005	0.004	0.004	0.004 A'	0.004	0.004	0.003

Load Stage	East Side				Maximum Crack Width (mm)						
	RI	Ro	Moment at Face of Column	Crack Number	1	2	3	4	5	6	7
	(kN)	(kN)	(kN-m)								
cracking	(183.3)	(220.0)	(278.5)		(0.025)						
(2) Service Flexure	(171.6)	(253.4)	(310.6)		(0.051)						
(3) Dead Load	(183.4)	(180.0)	(245.1)		(0.051)						
(4) Service Shear	(222.3)	(208.9)	(283.3)		(0.064)						
(6) Service Flexure	(171.6)	(253.4)	(310.6)		(0.064)						
Service Flexure plus *	(185.7)	(326.8)	(395.1)		(0.127)	(0.089)	(0.051)				
(7) Factored Flexure *	(205.4)	(393.7)	(480.6)		(0.152)	(0.114)	(0.127)	(0.102 A')	(0.089)	(0.076 A')	
(8) Dead Load	(183.4)	(180.0)	(245.1)		(0.064 A')	(0.051)	(0.038 B)	(0.025)	(0.025)	(0.038 A')	
(9) Service Shear	(222.3)	(208.9)	(283.3)		(0.051)	(0.051)	(0.051 A')	(0.025)	(0.025)	(0.038 A')	
(10) Factored Shear *	(315.5)	(287.2)	(401.6)		(0.127)	(0.102)	(0.102 A')	(0.076 C)	(0.089 C)	(0.076 A')	
(12) Service Flexure *	(171.6)	(253.4)	(310.6)		(0.102)	(0.076)	(0.076)	(0.051 A')	(0.051)	(0.051 A')	
(13) Factored Flexure *	(205.4)	(393.7)	(480.6)		(0.127)	(0.102)	(0.102)	(0.102 A')	(0.102)	(0.102)	(0.076)

* Only maximum crack width was measured, usually at level A unless otherwise noted.

Table 3.9 Maximum Crack Width Readings for Overhang CO-PU-74S-TH-I (West Side)

CO-PU-74S-TH-I	West Side						Maximum Crack Width, Inches									
	Load Stage	RI kips	Ro kips	Moment at Face of Column kip-inches	Crack Number											
					1	2	3	4	5	6	7					
cracking	41.22	48.48	2485													
(2) Service Flexure	38.57	58.87	2149		0.0015											
(3) Dead Load	43.47	40.47	2189		0.0025	0.001										
(4) Service Shear	48.97	46.97	2507		0.002	0.0015										
(6) Service Flexure	38.57	58.87	2149		0.003	0.002										
Service Flexure plus *	41.76	73.46	3408		0.0045	0.002	0.004	0.003	0.002							
(7) Factored Flexure *	48.18	88.52	4078		0.007	0.005	0.007	0.009	0.0025	0.0015	0.0035					
(8) Dead Load	43.47	40.47	2189		0.002	0.001	0.002	0.004	0.002	0.001 A'	0.0015					
(9) Service Shear	49.97	46.97	2507		0.0035	0.003	0.0025	0.004	0.002	0.001 A'	0.001					
(10) Factored Shear *	70.82	68.82	3554		0.006	0.004	0.006	0.005	0.001	0.0015	0.002 A'					
(12) Service Flexure *	38.57	58.87	2149		0.005	0.004	0.0045	0.008	0.0015	0.001	0.002					
(13) Factored Flexure *	46.18	88.52	4078		0.008	0.006	0.008	0.002	0.002	0.002	0.003					

CO-PU-74S-TH-I	West Side						Maximum Crack Width (mm)									
	Load Stage	RI (kN)	Ro (kN)	Moment at Face of Column (kN-m)	Crack Number											
					1	2	3	4	5	6	7					
cracking	183.3	220.0	278.5													
(2) Service Flexure	171.6	253.4	310.6		0.039											
(3) Dead Load	183.4	180.0	245.1		0.064	0.025										
(4) Service Shear	222.3	208.9	263.3		0.051	0.038										
(6) Service Flexure	171.6	253.4	310.6		0.051	0.051										
Service Flexure plus *	185.7	328.6	385.1		0.114	0.051	0.102	0.076	0.051							
(7) Factored Flexure *	205.4	383.7	460.8		0.178	0.127	0.178	0.228	0.064	0.038	0.089					
(8) Dead Load	193.4	180.0	245.1		0.051	0.025	0.051	0.102	0.051	0.025 A'	0.038					
(9) Service Shear	222.3	208.9	263.3		0.089	0.076	0.064	0.102	0.051	0.025 A'	0.025					
(10) Factored Shear *	315.5	287.2	401.6		0.152	0.102	0.152	0.127	0.038	0.025	0.051 A'					
(12) Service Flexure *	171.6	253.4	310.6		0.127	0.102	0.114	0.152	0.038	0.025	0.051					
(13) Factored Flexure *	205.4	383.7	460.8		0.203	0.152	0.152	0.228	0.051	0.025	0.076					

* Only maximum crack width was measured, usually at level A unless otherwise noted.

Complete crack width readings were recorded at first cracking, dead load (second time), 7 percent above dead load (dead load plus), and service flexure load (second time). Only the maximum width of each crack was recorded at factored flexure load - LS 36 -, dead load - LS 22", 37, 47 -, service shear - LS 40 -, factored shear - LS 46 -, service flexure - LS 49 - and factored flexure load - LS 53 -.

Again, Figures 3.11 and 3.12 show the crack pattern and crack numbering for these overhangs at factored flexure load. Tables 3.10 to 3.13 show the maximum crack width of every crack at every major load step. Shaded areas in these tables emphasize the "major" cracks.

3.2.4 Nature of Cracking and Comparison of Models

Figure 3.13 shows the "major" cracks at service flexure load level for all models, except for models CO-PU-100S-TH where no cracks were visible at this load stage.

In general, flexural and flexural/shear cracks predominated. Failure in all cases was caused by the opening of a major flexural/shear crack (or two in the case of model CO-PU-54S-TH-V South West side) close to the face of the column. Table 3.14 shows a comparison of cracking for all overhangs, in terms of number of cracks and nature, at service flexure, factored flexure and ultimate flexure load levels. In this table flexural cracks have been included into the flexural/shear crack classification. The number and identification of predominant cracks at failure are indicated with reference to Figures 3.7, 3.9 and 3.12 to show the approximate location. Pure shear cracks were never major and typically appeared between points of application of load, well above factored flexure load level.

Analyzing these results it can be noticed that as the post-tensioning force in the model decreased, the number of cracks increased. This is especially clear at service flexure and at factored flexure load levels. These results were somewhat expected from the experience with fully prestressed beams and ordinary reinforced concrete beams. Referring to Figures 3.7 to 3.12, it is observed that for the CO-PU-100S-TH (V&I) models, cracks were concentrated around the critical section at the column face, with an average crack spacing of approximately 5-6 inches (127-152 mm). Cracking in models CO-PU-54S-TH (V&I), with more cracks present, show a better distribution of cracks in the total length of the overhangs, with an average crack spacing of approximately 2-3 inches (51-76 mm). Models CO-PU-74S-TH (V&I) showed an average crack spacing in between the models described before of approximately 4-5 inches (102 -127 mm).

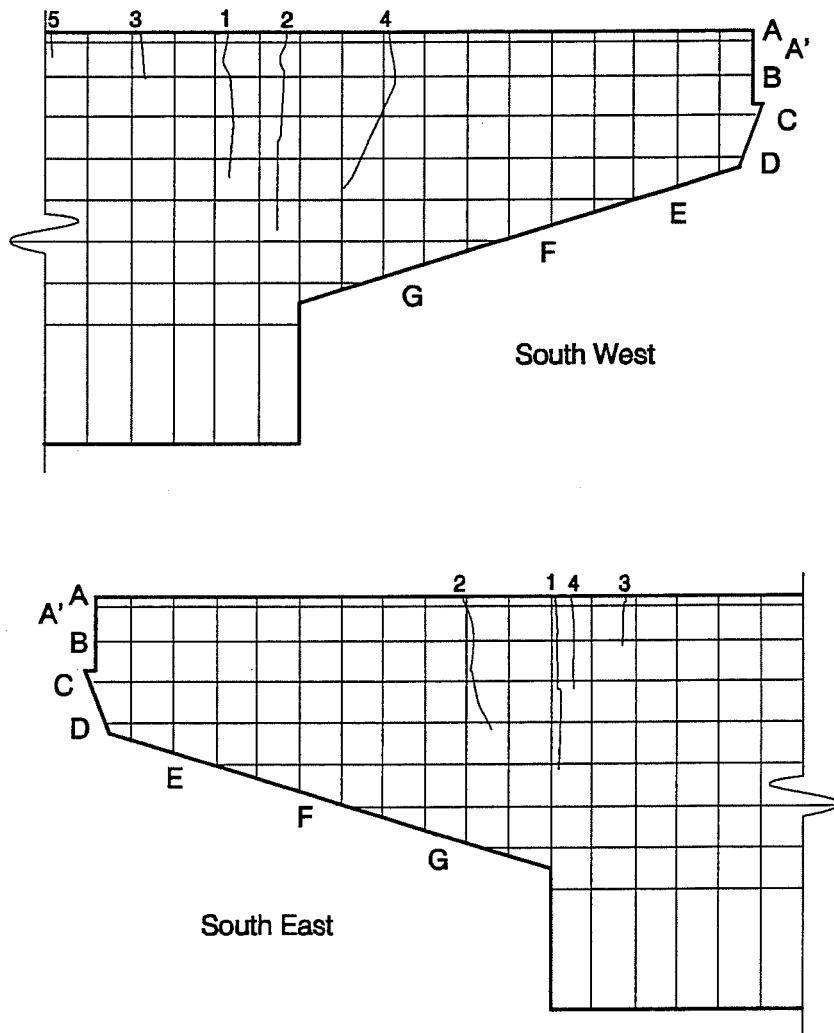


Figure 3.11 Crack Number and Location on East and West sides of CO-PU-100S-TH-V overhang.

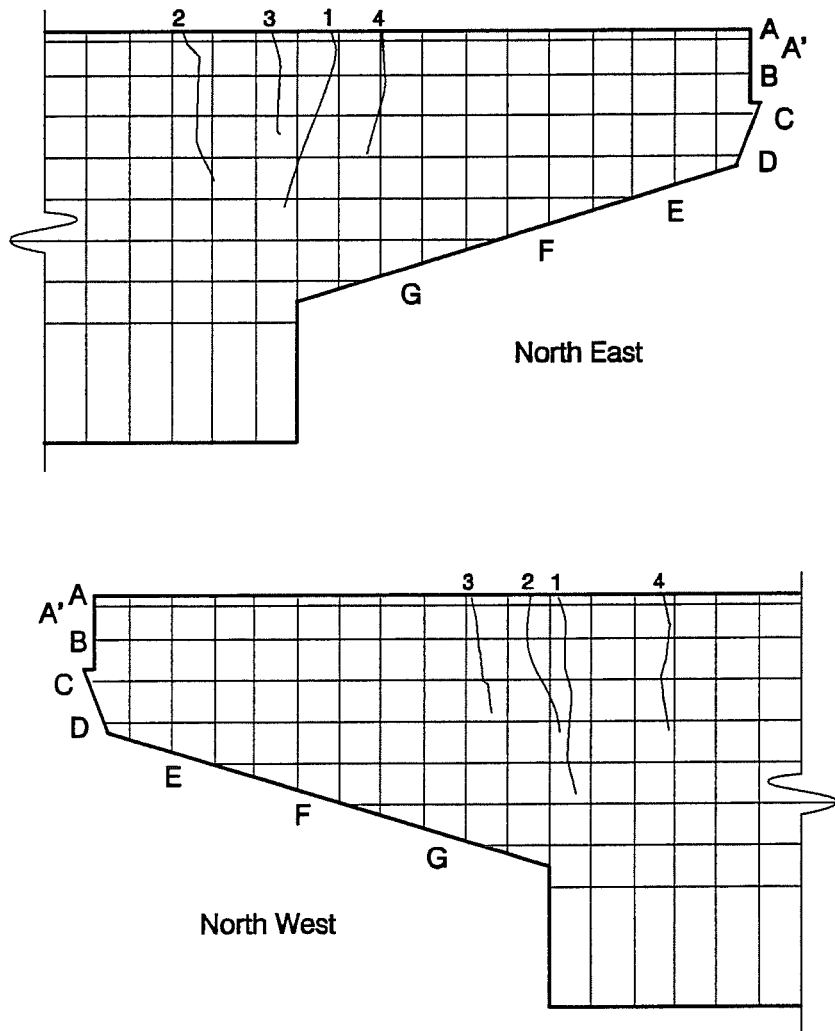


Figure 3.12 Crack Number and Location on East and West sides of CO-PU-100S-TH-I overhang.

Table 3.10 Maximum Crack Width Readings for Overhang CO-PU-100S-TH-V (East Side)

CO-PU-100S-TH-V		East Side				Maximum Crack Width, Inches				
Load Stage	RI kips	Ro kips	Moment at Face of Column kip-inches	Crack Number	1	2	3	4	5	
service flexure plus	40.69	69.46	3242		0.0015					
Dead Load **	43.47	40.47	2169		0.0005					
Service Flexure **	38.57	58.97	2749		0.001					
Service Flexure plus **	40.69	69.46	3242		0.0025					
(7) Factored Flexure *	46.18	88.52	4078		0.003	0.001	0.0005			
(8) Dead Load *	43.47	40.47	2169		0.0005	0.0005	0.0005			
(9) Service Shear *	49.97	48.97	2507		0.0005	0.0005	0.0005			
(10) Factored Shear *	70.92	68.82	3554		0.001	0.001	0.001	0.0005		
(11) Dead Load*	43.47	40.47	2169		0.001	0.001	0.001	0.001		
(12) Service Flexure *	38.57	58.97	2749		0.001	0.001	0.001	0.001		
(13) Factored Flexure *	46.18	88.52	4078		0.0025	0.003	0.0005	0.002		

CO-PU-100S-TH-V		East Side				Maximum Crack Width (mm)				
Load Stage	RI (kN)	Ro (kN)	Moment at Face of Column (kN-m)	Crack Number	1	2	3	4	5	
service flexure plus	(182.3)	(309.0)	(368.3)		(0.038)					
Dead Load **	(193.4)	(180.0)	(245.1)		(0.013)					
Service Flexure **	(171.6)	(253.4)	(310.6)		(0.025)					
Service Flexure plus **	(182.3)	(309.0)	(368.3)		(0.064)					
(7) Factored Flexure *	(205.4)	(393.7)	(460.6)		(0.076)	(0.025)	(0.013)			
(8) Dead Load *	(183.4)	(180.0)	(245.1)		(0.013)	(0.013)	(0.013)			
(9) Service Shear *	(222.3)	(208.9)	(283.3)		(0.013)	(0.013)	(0.013)			
(10) Factored Shear *	(315.5)	(287.2)	(401.6)		(0.025)	(0.025)	(0.013)			
(11) Dead Load*	(183.4)	(180.0)	(245.1)		(0.025)	(0.025)	(0.025)			
(12) Service Flexure *	(171.6)	(253.4)	(310.6)		(0.025)	(0.025)	(0.025)			
(13) Factored Flexure *	(205.4)	(393.7)	(460.6)		(0.084)	(0.076)	(0.013)	(0.051)		

* Only maximum crack width was measured, usually at level A unless otherwise noted.

** This load sequence was followed in specimen CO-PU-100S-TH only.

Table 3.1.1 Maximum Crack Width Readings for Overhang CO-PU-100S-TH-V (West Side)

CO-PU-100S-TH-V		West Side				Maximum Crack Width, inches				
Load Stage	RI kips	Ro kips	Moment at Face of Column kip-inches	Crack Number	1	2	3	4	5	
Cracking	40.22	65.48	3076		0.0015					
Dead Load **	43.47	40.47	2169		0.0005					
Dead Load plus **	42.2	45.48	2322		0.0005					
Service Flexure **	38.57	59.97	2749		0.001					
Service Flexure plus **	40.22	65.48	3076		0.002					
Service Flexure plus plus **	40.99	69.48	3242		0.002	0.0028				
Dead Load * *	43.47	40.47	2169		0.001	0.0015				
Service Flexure * *	38.57	59.97	2749		0.001	0.0015				
Service Flexure plus * *	40.88	69.48	3242		0.002	0.003				
(7) Factored Flexure *	46.16	88.52	4078		0.008 A	0.006	0.001	0.005		
(8) Dead Load *	43.47	40.47	2169		0.002 A	0.002 A	0.0005	0.001		
(9) Service Shear *	49.97	48.97	2507		0.002 A	0.002	0.0005	0.001		
(10) Factored Shear *	70.92	68.92	3554		0.005 A	0.008	0.0005	0.003	0.0005	
(11) Dead Load *	43.47	40.47	2169		0.002 A	0.002	0.0005	0.001	0.0005	
(12) Service Flexure *	38.57	59.97	2749		0.003 A	0.003	0.0005	0.0015	0.0005	
(13) Factored Flexure *	46.16	88.52	4078		0.0075 A	0.0085	0.0005	0.005	0.0005	

CO-PU-100S-TH-V		West Side				Maximum Crack Width (mm)				
Load Stage	RI (kN)	Ro (kN)	Moment at Face of Column (kN-m)	Crack Number	1	2	3	4	5	
Cracking	(178.6)	(281.2)	(347.6)		(0.038)					
Dead Load **	(183.4)	(180.0)	(245.1)		(0.013)					
Dead Load plus **	(187.7)	(202.2)	(282.4)		(0.013)					
Service Flexure **	(171.0)	(253.4)	(310.9)		(0.025)					
Service Flexure plus **	(176.6)	(281.2)	(347.6)		(0.051)					
Service Flexure plus plus **	(182.3)	(308.0)	(385.3)		(0.061)	(0.064)				
Dead Load * *	(183.4)	(180.0)	(245.1)		(0.025)	(0.038)				
Service Flexure * *	(171.0)	(253.4)	(310.9)		(0.051)	(0.076)				
Service Flexure plus * *	(182.3)	(308.0)	(385.3)		(0.051)	(0.076)				
(7) Factored Flexure *	(205.4)	(393.7)	(480.8)		(0.152 A)	(0.182)	(0.025)	(0.127)		
(8) Dead Load *	(183.4)	(180.0)	(245.1)		(0.051 A)	(0.051 A)	(0.015)	(0.025)		
(9) Service Shear *	(222.3)	(208.9)	(283.3)		(0.051 A)	(0.051 A)	(0.015)	(0.025)		
(10) Factored Shear *	(315.5)	(287.2)	(401.6)		(0.127 A)	(0.152)	(0.015)	(0.076)	(0.013)	
(11) Dead Load *	(183.4)	(180.0)	(245.1)		(0.051 A)	(0.051)	(0.015)	(0.025)	(0.013)	
(12) Service Flexure *	(171.0)	(253.4)	(310.9)		(0.076 A)	(0.076)	(0.015)	(0.038)	(0.013)	
(13) Factored Flexure *	(205.4)	(393.7)	(480.8)		(0.181 A)	(0.165)	(0.015)	(0.127)	(0.013)	

* Only maximum crack width was measured, usually at level A unless otherwise noted.
 ** This load sequence was followed in specimen CO-PU-100S-TH only.

Table 3.12 Maximum Crack Width Readings for Overhang CO-PU-100S-TH-I (East Side)

CO-PU-100S-TH-I	East Side				Maximum Crack Width, Inches			
	Load Stage	RI Kips	Ro Kips	Moment at Face of Column Kip-inches	Crack Number			
					1	2	3	4
	service flexure plus	40.89	69.46	3242	0.002			
	Dead Load **	43.47	40.47	2169	0.0005			
	Service Flexure **	38.57	58.97	2149	0.0015			
	Service Flexure plus **	40.99	69.46	3242	0.003			
	(7) Factored Flexure *	46.18	88.52	4078	0.006 A	0.0025	0.0055 A	0.007
	(8) Dead Load *	43.47	40.47	2169	0.001 A	0.0005	0.001 A	0.0015
	(9) Service Shear *	49.97	48.87	2507	0.002 A	0.001 A	0.0015 A	0.001
	(10) Factored Shear *	70.92	68.82	3554	0.0035 A	0.003 A	0.005 A	0.003
	(11) Dead Load *	43.47	40.47	2169	0.001	0.0005	0.001 A	0.001
	(12) Service Flexure *	38.57	58.97	2149	0.0015	0.001 A	0.002 A	0.0015
	(13) Factored Flexure *	46.18	88.52	4078	0.006	0.004 A	0.0065 A	0.0065

CO-PU-100S-TH-I	East Side				Maximum Crack Width (mm)			
	Load Stage	RI (kN)	Ro (kN)	Moment at Face of Column (kN-m)	Crack Number			
					1	2	3	4
	service flexure plus	(182.3)	(309.0)	(888.3)	(0.051)			
	Dead Load **	(183.4)	(180.0)	(245.1)	(0.013)			
	Service Flexure **	(171.6)	(253.4)	(310.6)	(0.039)			
	Service Flexure plus **	(182.3)	(309.0)	(888.3)	(0.076)			
	(7) Factored Flexure *	(205.4)	(393.7)	(460.8)	(0.152 A)	(0.064)	(0.140 A)	(0.178)
	(8) Dead Load *	(183.4)	(180.0)	(245.1)	(0.025 A)	(0.013)	(0.025 A)	(0.039)
	(9) Service Shear *	(222.3)	(208.9)	(283.3)	(0.057 A)	(0.025 A)	(0.038 A)	(0.025)
	(10) Factored Shear *	(315.5)	(297.2)	(401.6)	(0.089 A)	(0.076 A)	(0.127 A)	(0.076)
	(11) Dead Load *	(183.4)	(180.0)	(245.1)	(0.025)	(0.013)	(0.025 A)	(0.025)
	(12) Service Flexure *	(171.6)	(253.4)	(310.6)	(0.038)	(0.025 A)	(0.051 A)	(0.038)
	(13) Factored Flexure *	(205.4)	(393.7)	(460.8)	(0.152)	(0.102 A)	(0.165 A)	(0.165)

* Only maximum crack width was measured, usually at level A unless otherwise noted.

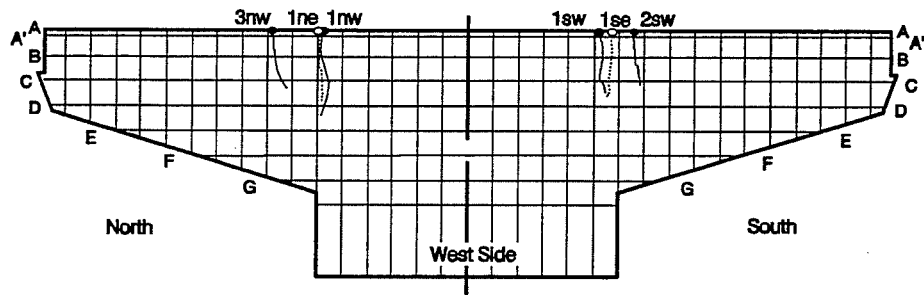
** This load sequence was followed in specimen CO-PU-100S-TH only.

Table 3.13 Maximum Crack Width Readings for Overhang CO-PU-100S-TH-I (West Side)

Load Stage	West Side			Maximum Crack Width, inches			
	RI kips	Ro kips	Moment at Face of Column kip-inches	Crack Number 1	2	3	4
cracking	38.68	57.48	2750	0.001			
service flexure plus **	38.45	61.48	2910	0.0015			
service flexure plus plus **	40.22	65.48	3078	0.002	0.0018		
Dead Load **	43.47	40.47	2189	0.0005	0.0005		
Dead Load plus **	42.2	45.48	2322	0.0006	0.0005		
Service Flexure **	38.57	58.97	2749	0.001	0.001		
Service Flexure plus **	40.22	65.48	3078	0.002	0.0018		
Service Flexure plus plus **	40.99	69.48	3242	0.002	0.0028		
Dead Load **	43.47	40.47	2189	0.001	0.001		
Service Flexure **	38.57	58.97	2749	0.0015	0.002		
Service Flexure plus **	40.99	69.48	3242	0.0028	0.002		
Service Flexure plus plus **	46.16	88.52	4078	0.007	0.0075 A	0.003	0.0075
(7) Factored Flexure *	43.47	40.47	2189	0.0016	0.002 A	0.0005	0.0015
(8) Dead Load *	49.97	48.97	2507	0.002	0.002 A	0.001	0.003
(9) Service Shear *	70.92	68.82	3554	0.0065	0.008 A	0.002	0.005
(10) Factored Shear *	43.47	40.47	2189	0.003	0.0025 A	0.001	0.002
(11) Dead Load *	38.57	58.97	2749	0.0035	0.003 A	0.002	0.003
(12) Service Flexure *	46.16	88.52	4078	0.01	0.0075 A	0.006	0.006
(13) Factored Flexure *							

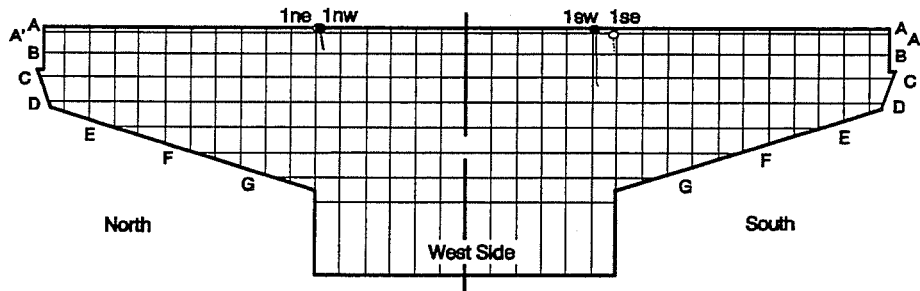
Load Stage	West Side			Maximum Crack Width (mm)			
	RI (kN)	Ro (kN)	Moment at Face of Column (kN-m)	Crack Number 1	2	3	4
cracking	(172.0)	(255.6)	(310.8)	(0.025)			
service flexure plus **	(175.9)	(273.4)	(328.6)	0.039			
service flexure plus plus **	(178.9)	(281.2)	(347.6)	0.051	0.039		
Dead Load **	(183.4)	(180.0)	(245.1)	0.013	0.013		
Dead Load plus **	(187.7)	(202.2)	(262.4)	0.019	0.019		
Service Flexure **	(171.6)	(253.4)	(310.6)	0.025	0.025		
Service Flexure plus **	(178.9)	(281.2)	(347.6)	0.051	0.051		
Service Flexure plus plus **	(182.3)	(308.0)	(389.3)	0.064	0.064		
Dead Load **	(183.4)	(180.0)	(245.1)	0.025	0.025		
Service Flexure **	(171.6)	(253.4)	(310.6)	0.039	0.039		
Service Flexure plus **	(182.3)	(308.0)	(389.3)	0.064	0.064		
(7) Factored Flexure *	(205.4)	(393.7)	(480.6)	0.118	0.118 A	0.076	0.191
(8) Dead Load *	(193.4)	(180.0)	(245.1)	0.039	0.051 A	0.013	0.039
(9) Service Shear *	(222.3)	(203.9)	(283.3)	0.051	0.051 A	0.025	0.076
(10) Factored Shear *	(315.5)	(287.2)	(401.6)	0.165	0.165 A	0.051	0.127
(11) Dead Load *	(183.4)	(180.0)	(245.1)	0.076	0.064 A	0.025	0.051
(12) Service Flexure *	(171.6)	(253.4)	(310.6)	0.069	0.076 A	0.051	0.076
(13) Factored Flexure *	(205.4)	(393.7)	(480.6)	0.254	0.191 A	0.152	0.152

* Only maximum crack width was measured, usually at level A, unless otherwise noted.
 ** This load sequence was followed in specimen CO-PU-100S-TH only.



CO-PU-54S-TH-I

CO-PU-54S-TH-V



CO-PU-74S-TH-I

CO-PU-74S-TH-V

- location of maximum crack width on West side of specimen
- location of maximum crack width on East side of specimen

Figure 3.13 "Major" Cracks at Service Flexure Loads.

Table 3.14 Comparison of Cracking

Model	Side	Number of cracks at service flexure load level			Number of cracks at factored flexure load level			Cracks at failure***		Number of predominant cracks at failure	Identification and location of predominant cracks at failure
		Flexural/ shear*		Flexural/ shear		Flexural/ Shear	shear				
		Flexural/ shear*	shear**	Flexural/ shear	shear						
CO-PU-54S-TH-V	SE	1	0	12	0	0	20	1	1	1	#2 (Figure 3.7)
	SW	3	0	11	0	0	17	0	2	2	#2 and #6 (Fig.3.7)
	NE	3	0	10	1	1	14	2	---	---	---
	NW	4	0	12	0	0	17	1	---	---	---
CO-PU-74S-TH-V	SE	1	0	7	0	0	11	0	1	1	#2 (Figure 3.9)
	SW	2	0	8	0	0	10	0	1	1	#4 (Figure 3.9)
	NE	1	0	6	0	0	13	0	---	---	---
	NW	2	0	7	0	0	12	0	---	---	---
CO-PU-100S-TH-V	SE	0	0	4	0	0	14	1	---	---	---
	SW	0	0	4	0	0	10	0	---	---	---
	NE	0	0	4	0	0	6	0	1	1	#4 (Figure 3.12)
	NW	0	0	4	0	0	6	0	0	1	#3 (Figure 3.12)

* Flexural/shear cracks include those in column as shown in Figures 3.7 to 3.12.

** Shear cracks in overhang structure only - any shear crack in the column is not included.

*** For models CO-PU-54S-TH-I, CO-PU-74S-TH-I and CO-PU-100S-TH-V cracking is at failure loads of the other overhang in the specimen.

From Table 3.14, it can also be observed that in those models with skin reinforcement designed according to Frantz and Breen (models CO-PU-54S-TH-V and CO-PU-100S-TH-V) there was a considerable increase in the number of cracks from factored flexure load level to ultimate flexure loads, showing that distribution was still taking place at high loads.

3.3 FAILURE MODES

All models experienced flexural failure dominated by the opening of major cracks close to the face of the column, with crushing and spalling of the concrete in the compression zone. Table 3.1 summarizes the failure loads of each model .

For overhang CO-PU-54S-TH-V, crushing was first observed at the South East side, at load step 64, $R_o=128$ kips (569 kN) and $R_i=48.1$ kips (214 kN). Crushing extended the width of the specimen, causing a compression failure at an applied moment of 6046 kip-inches (683 kN-m), $R_o=136.9$ kips (609 kN) and $R_i=54.4$ kips (242 kN). Failure was characterized by fair ductility, $\Delta/L = 0.020$, as was shown in the moment deflection response. A post mortem investigation found one broken #2 reinforcing bar in the top layer of steel, and signs of yielding in the other non-prestressed flexural reinforcement. Stirrups were undamaged, as well as the strands. Figures 3.14 and 3.15 show the condition of this model at failure. Overhang CO-PU-54S-TH-I was not tested to complete failure since its capacity was higher than its companion overhang.

For overhang CO-PU-74S-TH-V there was a loud popping sound heard after load stage 63, $R_o=127.01$ kips (565 kN) and $R_i=46.92$ kips (209 kN). Following this, in the next load step, there was evidence of concrete spalling and crushing at the bottom of the overhang/column junction. Two load steps later (loads corresponding to load step 67 in Table 2.17) there was a loud sound and the frame vibrated. After three additional load steps, another loud sound was heard and then at load stage $R_o=149.06$ kips (663 kN) and $R_i=54.39$ kips (242 kN), some dust was evident from the cracked section followed by a sound, as non-prestressed reinforcement broke in the tension zone. At this stage extensive crushing had taken place in the compression region. The test ended at this load step. Inspection of this specimen after testing showed one #2 reinforcing bar broken in the first row of steel from the top. All other #2 reinforcing bars showed areas of significant yielding deformations. No strands were found broken. Stirrups were undamaged. Popping sounds were imputed to the sudden losses of built-up friction forces be-

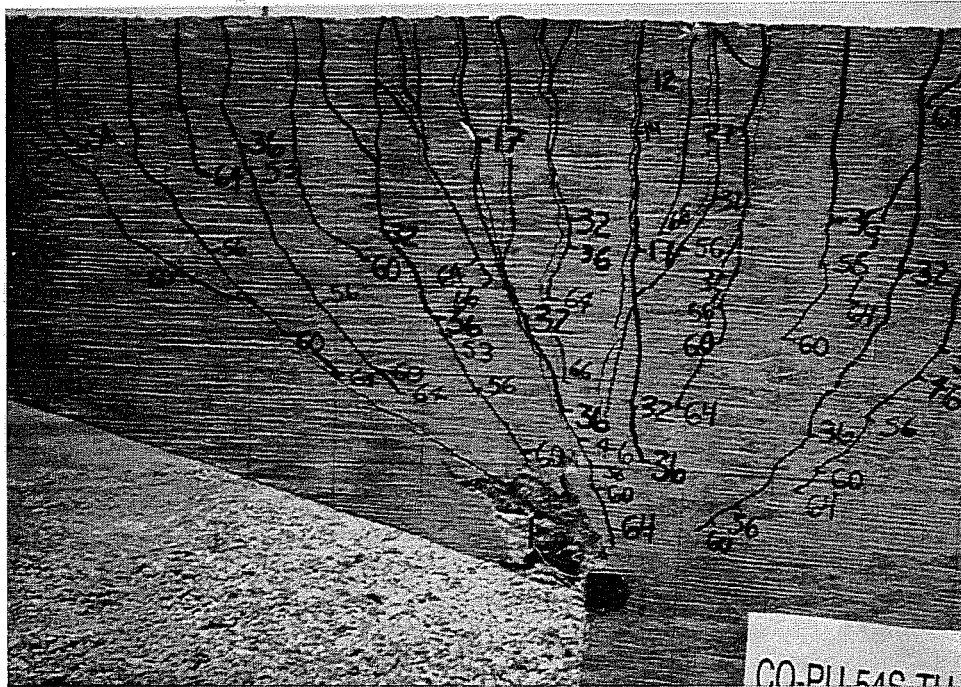


Figure 3.14 Crack Distribution in Model CO-PU-54S-TH-V (East) After Failure

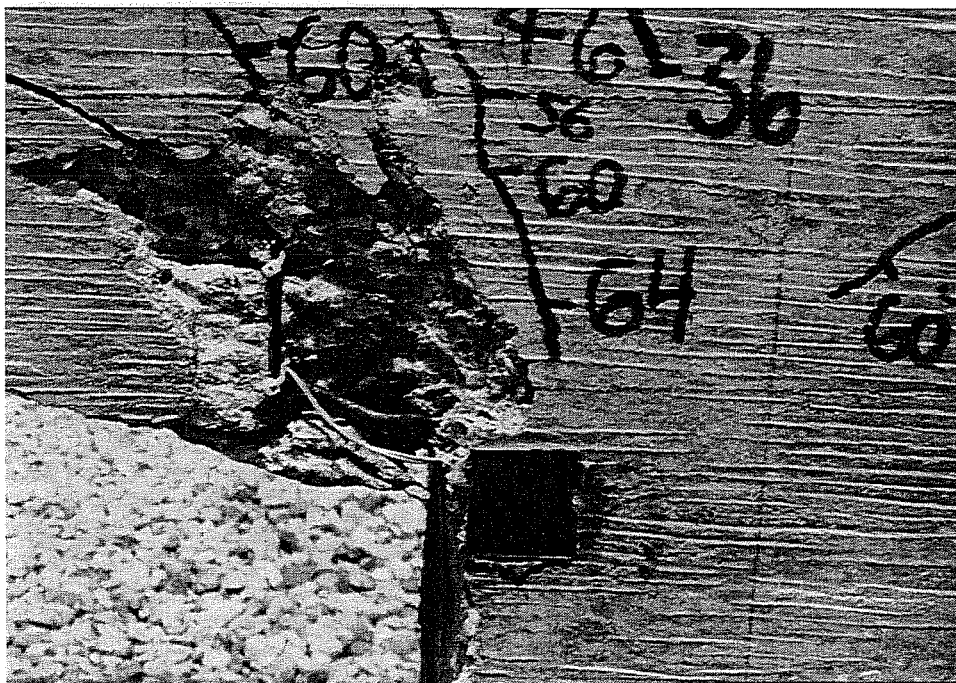


Figure 3.15 Crushing in Model CO-PU-54S-TH-V (East)

tween bearing plates. Figures 3.16 and 3.17 show the failure conditions of this overhang. Model CO-PU-74S-TH-I was not tested to failure.

Failure of the model CO-PU-100S-TH-I started at load step 67, $R_o = 141.46$ kips (629 kN) and $R_i = 54.88$ kips (244 kN), with spalling at the bottom of the overhang/column interface, as happened on the previous models. In the next load step, there was a loud popping sound evidencing the breaking of some reinforcing bars, and more spalling. This was observed after considerable tip deflections had taken place. The test was stopped at this point. Inspection of this specimen after testing showed all #2 reinforcing bars failed in the first, second and third rows, from the top. Two of the three 7 gage wires in the top row were also broken. Stirrups were undamaged and no strands were found broken. Figures 3.18 and 3.19 show the failure conditions of this overhang. Overhang CO-PU-100S-TH-V was not tested to failure.

All post-mortem investigations were performed with the use of a jackhammer being careful to not damage the reinforcing bars.

3.4 REINFORCEMENT STRAINS

Strain gage data was summarized and grouped for better interpretation. For a description of the strain gages for each specimen refer to Section 2.7.2.

Figures 3.20, 3.21 and 3.22 show with a circle those gages with microstrain readings in excess of 270. To facilitate the study of results these strain gages have been identified as "Effective Strain Gages." Gages with readings less than 270 microstrains, "negligible readings", are also shown in the same figures but without a circle and are tabulated for easy identification. Bad strain gages refer to those gages from which it was not possible to obtain acceptable readings, or any readings at all.

The limit of 270 microstrains was chosen arbitrarily - about 10 percent of the yield strain of the reinforcing bars and wires - with the sole purpose of having a better and more clear presentation of data. This allowed for easier identification of those bars and wires that experienced large elastic or plastic deformations. Results from gages with negligible readings would show as vertical lines in plots of applied load versus microstrain that are introduced below.

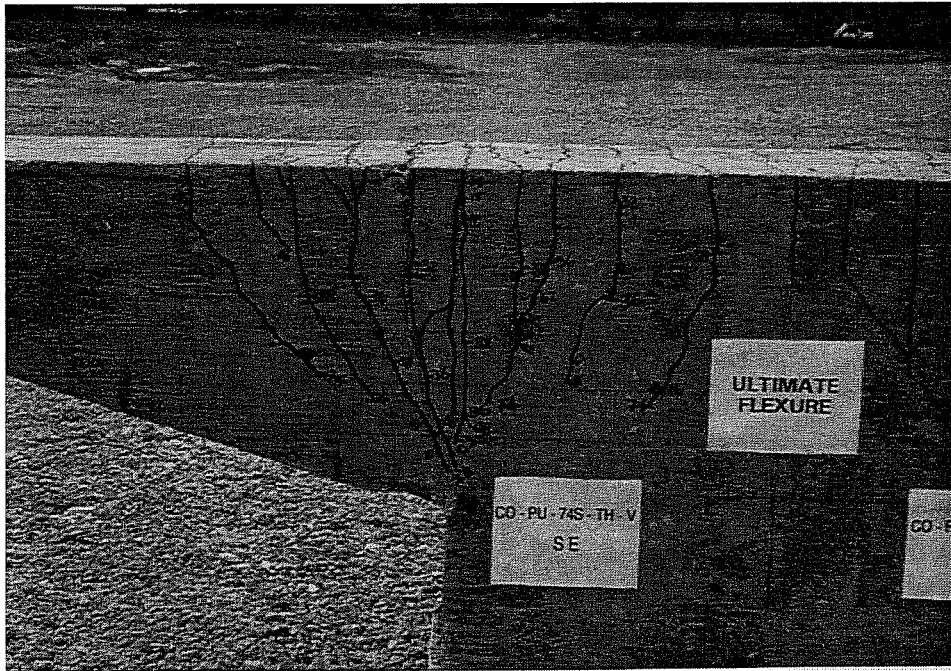


Figure 3.16 Crack Distribution in Model CO-PU-74S-TH-V (East) After Failure

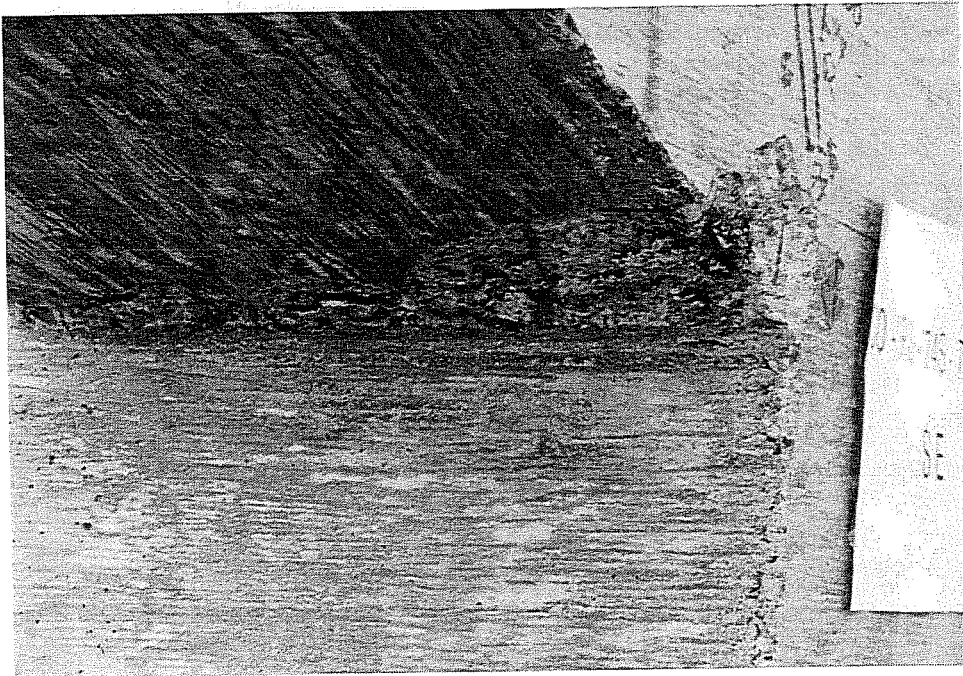


Figure 3.17 Crushing in Model CO-PU-74S-TH-V (East)

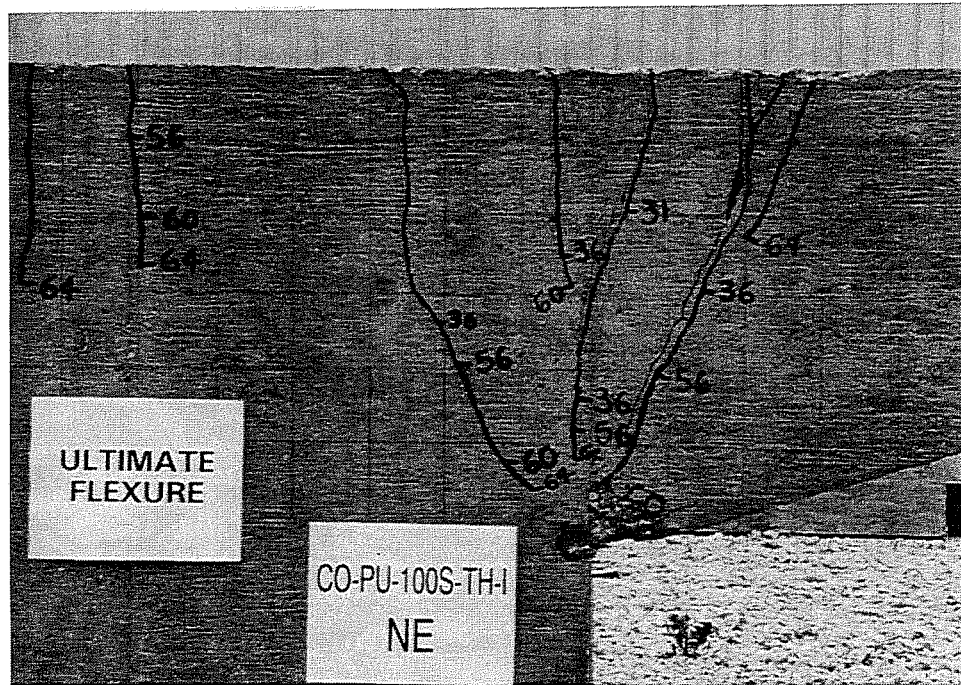


Figure 3.18 Crack Distribution in Model CO-PU-100S-TH-I (East) After Failure

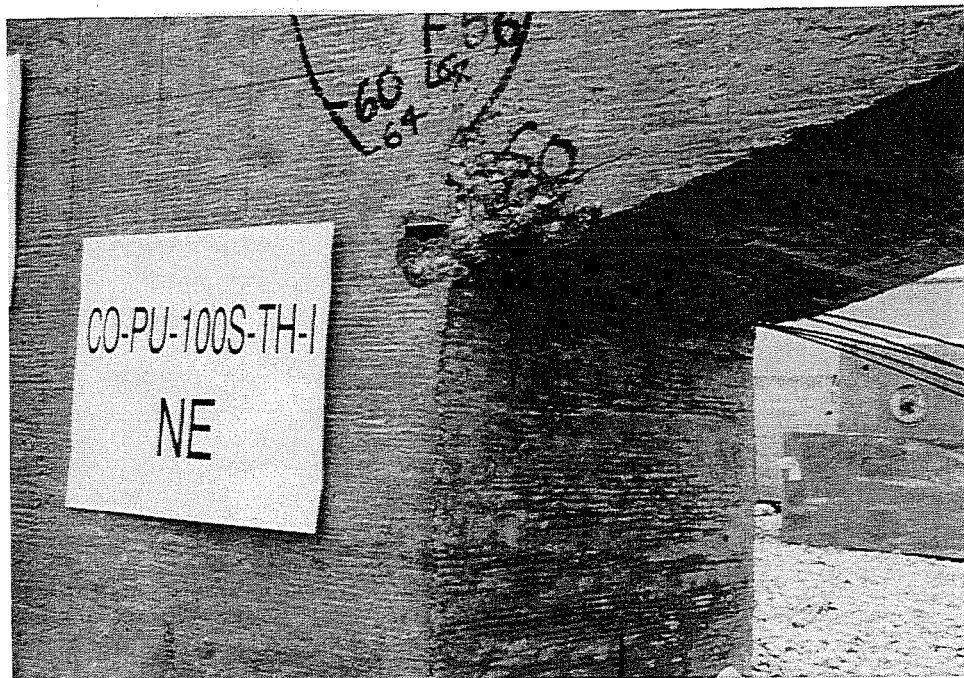
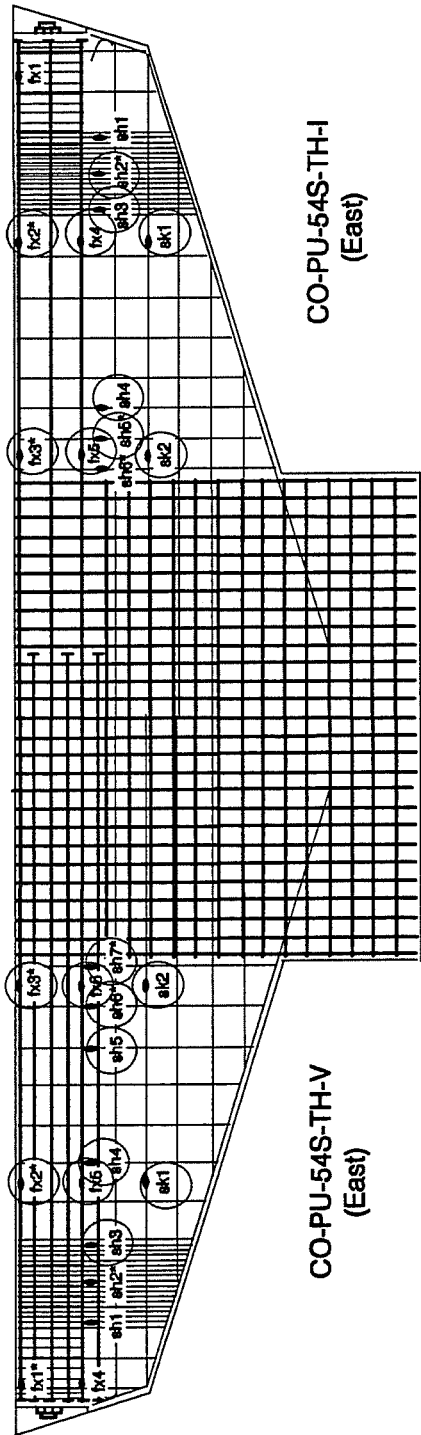
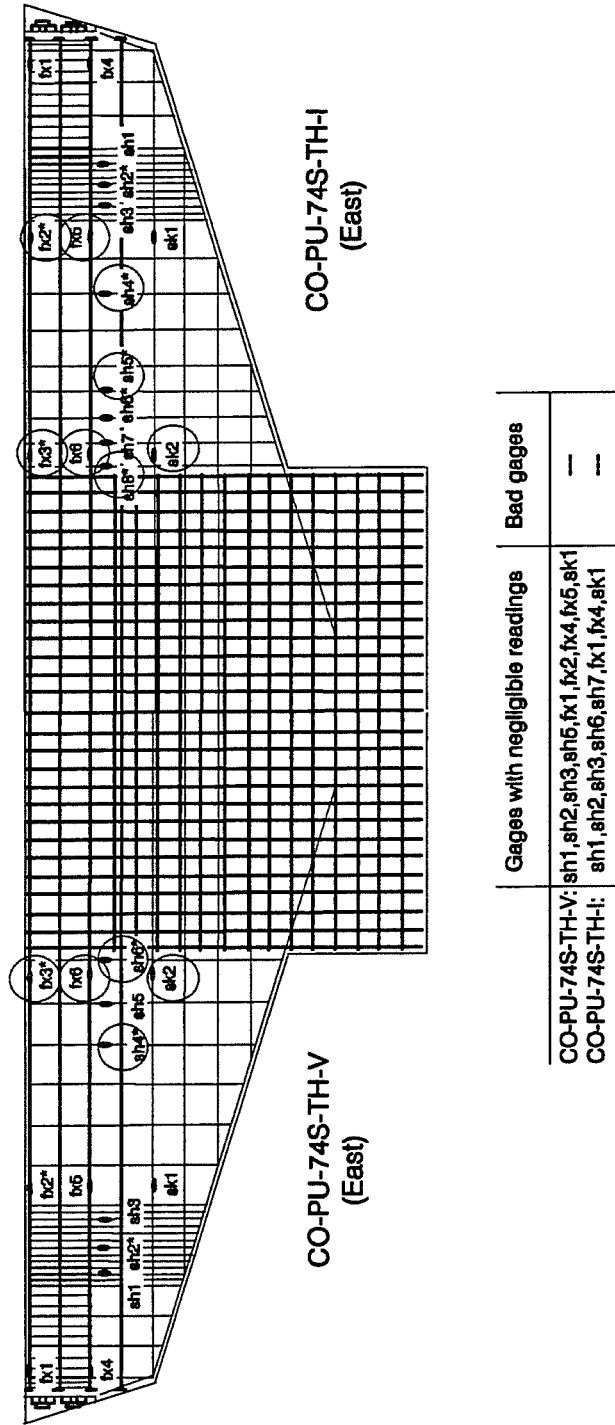


Figure 3.19 Crushing in Model CO-PU-100S-TH-I (East)



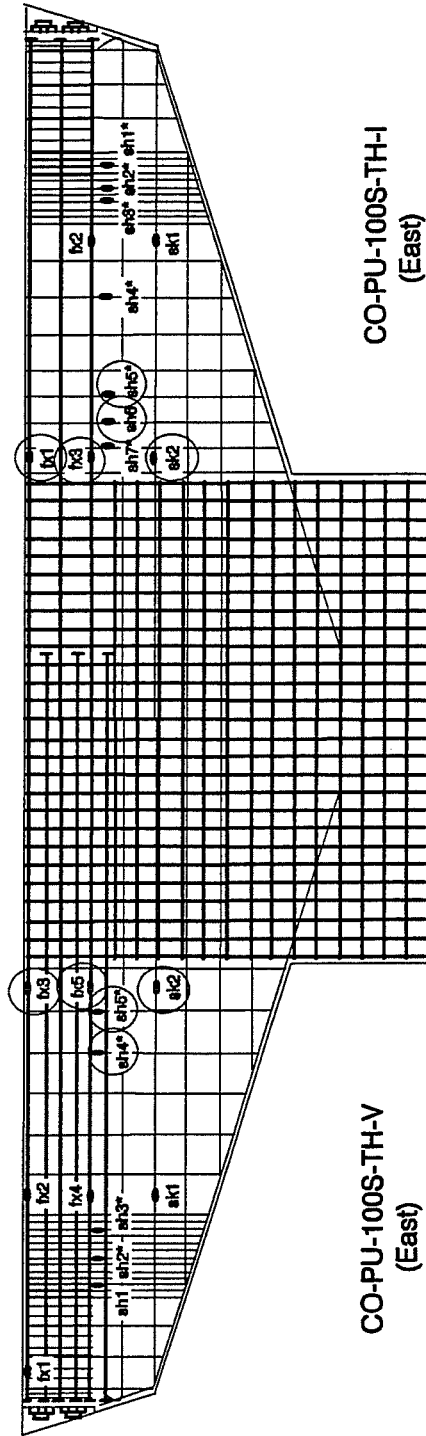
	Gages with negligible readings	Bad gages
CO-PU-54S-TH-V:	sh1,sh2,fx1	fx4
CO-PU-54S-TH-I:	sh1,sh6,fx1	—

Figure 3.20 Effective Strain Gages for Models CO-PU-54S-TH (V & I)



	Gages with negligible readings	Bad gages
CO-PU-74S-TH-V:	sh1, sh2, sh3, sh5, fx1, fx2, fx4, fx5, sk1	--
CO-PU-74S-TH-I:	sh1, sh2, sh3, sh6, sh7, fx1, fx4, sk1	--

Figure 3.2.1 Effective Strain Gages for models CO-PU-74S-TH (V & I)



	Gages with negligible readings	Bad gages
CO-PU-100S-TH-V:	fx1,fx2,fx4,sh1,sh2,sh3,sk1	--
CO-PU-100S-TH-I:	fx2,sh1,sh2,sh3,sh4,sh7,sk1	--

Figure 3.22 Effective Strain Gages for Models CO-PU-100S-TH (V & I)

All strain gage data was set to zero strain at the beginning of the test, before prestressing operations. Any strain due to prior shrinkage and creep of concrete is not reflected in the strain gage results.

Effective strain gages have been classified in groups depending on their location in non-prestressed flexural reinforcement (#2 reinforcing bars, horizontal), skin reinforcement (7 gage wire, horizontal) and vertical steel (10 gage wire). Non-prestressed flexural reinforcement strain gage data has been plotted for every model against the applied moment at the column face. Shear reinforcement strain gage data, depending on the location of the gages, has been plotted against the total applied loads (R_o and R_i) or against the outer load only (R_o). Figures 3.23 through 3.43 show the plots for all "effective" strain gages of models CO-PU-54S-TH (V&I), CO-PU-74S-TH (V&I), and CO-PU-100S-TH (V&I).

Analysis of these results is presented in Chapter 4. An obvious observation is the conservativeness of the shear models used in all overhangs. From all models it is clear that up to factored flexure loads there was no significant contribution of any shear reinforcement.

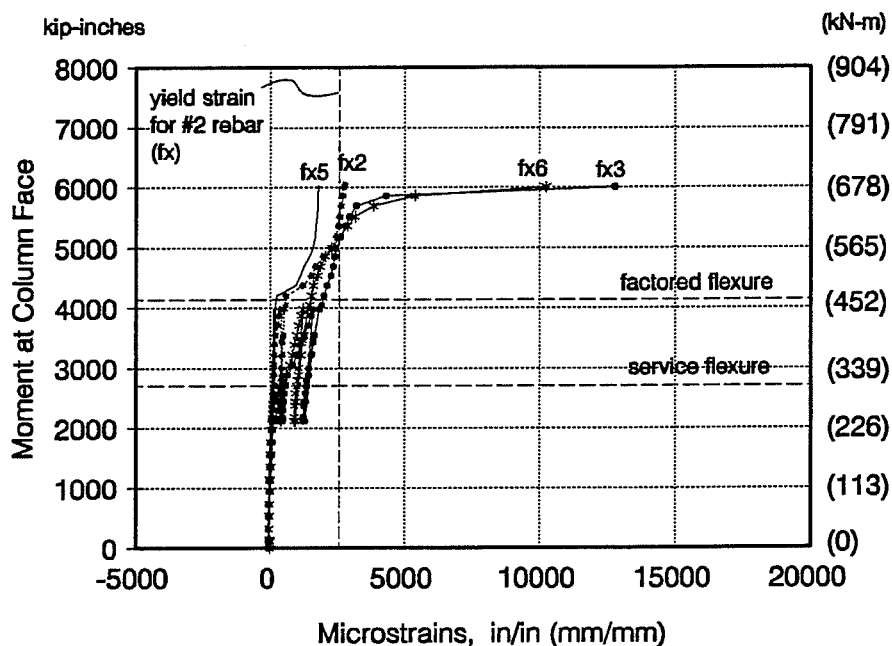


Figure 3.23 Resultant Moment vs. Strain in Effective Strain Gages in Flexural Bars for Model CO-PU-54S-TH-V

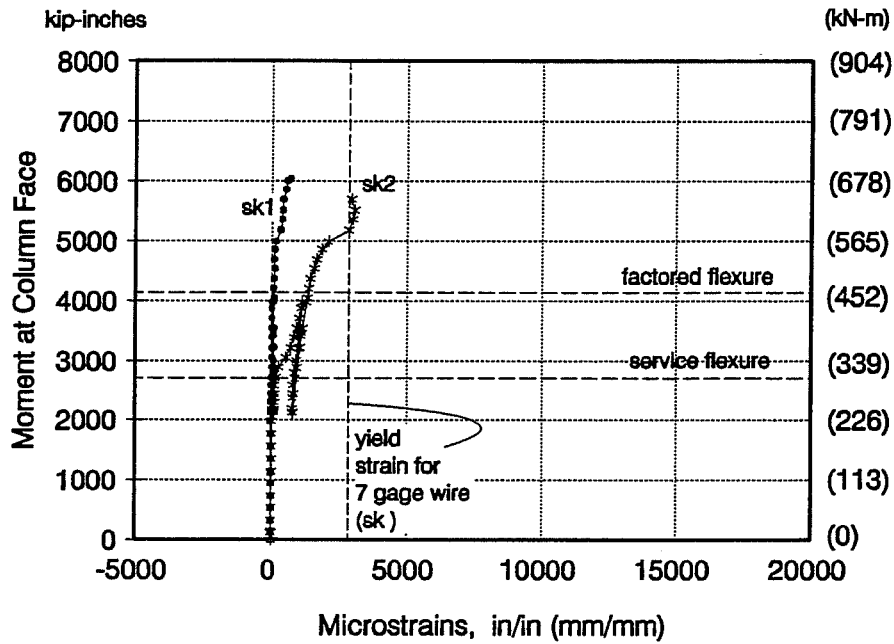


Figure 3.24 Resultant Moment vs. Strain in Effective Strain Gages in Skin Reinforcement for Model CO-PU-54S-TH-V

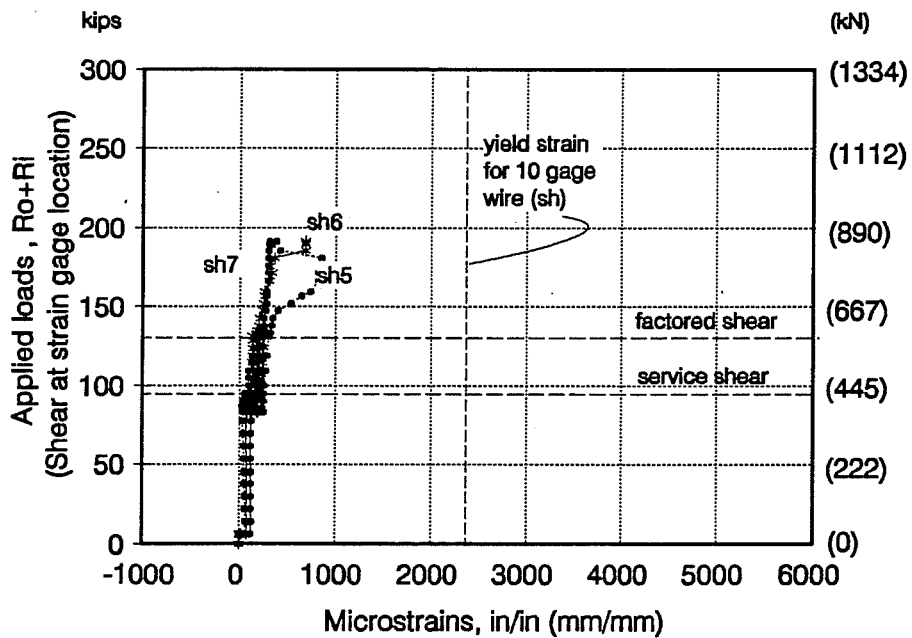


Figure 3.25 Resultant Load vs. Strain in Effective Strain Gages in Shear Reinforcement for Model CO-PU-54S-TH-V

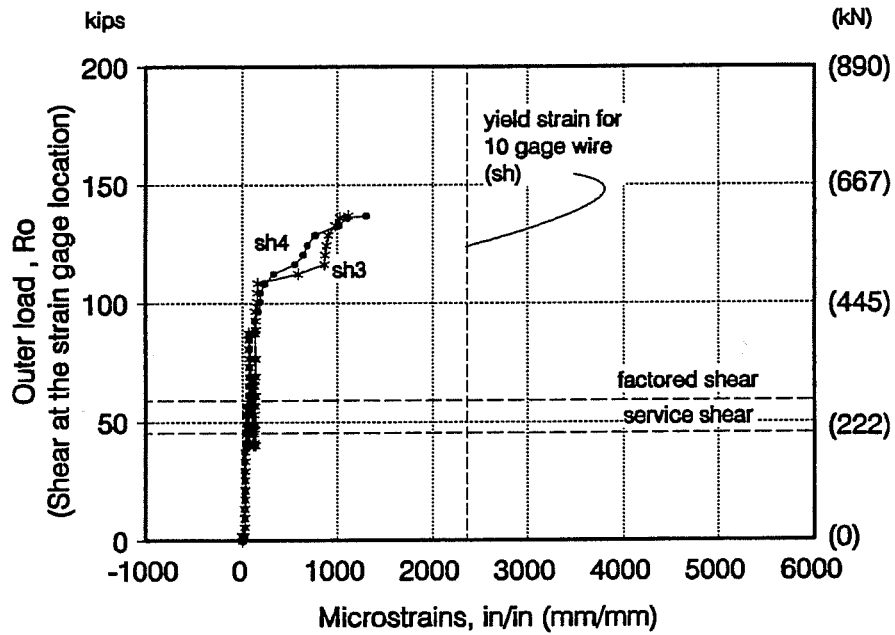


Figure 3.26 Resultant Load vs. Strain in Effective Strain Gages in Shear reinforcement for Model CO-PU-54S-TH-V (continuation...)

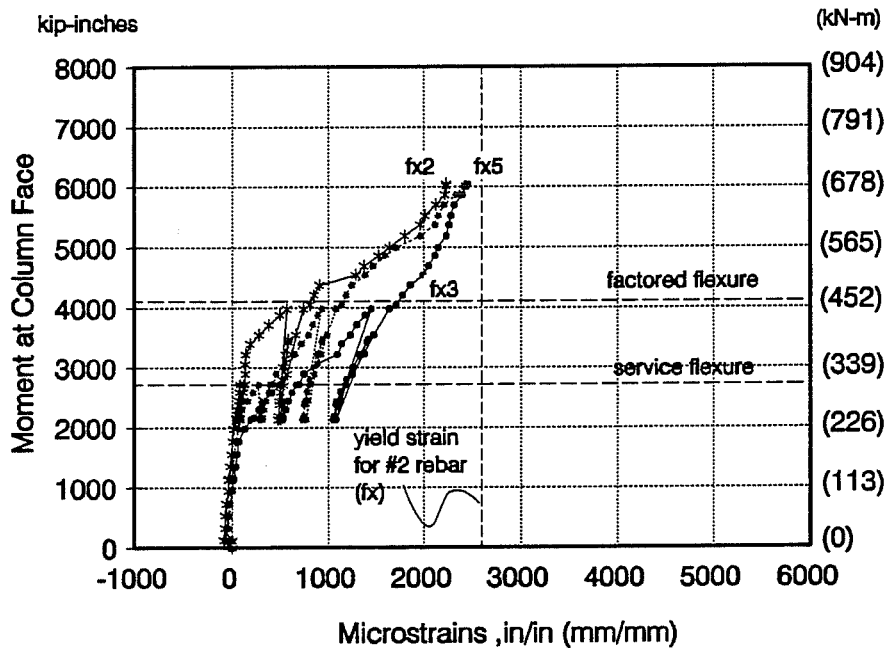


Figure 3.27 Resultant Moment vs. Strain in Effective Strain Gages in Flexural Bars for Model CO-PU-54S-TH-I

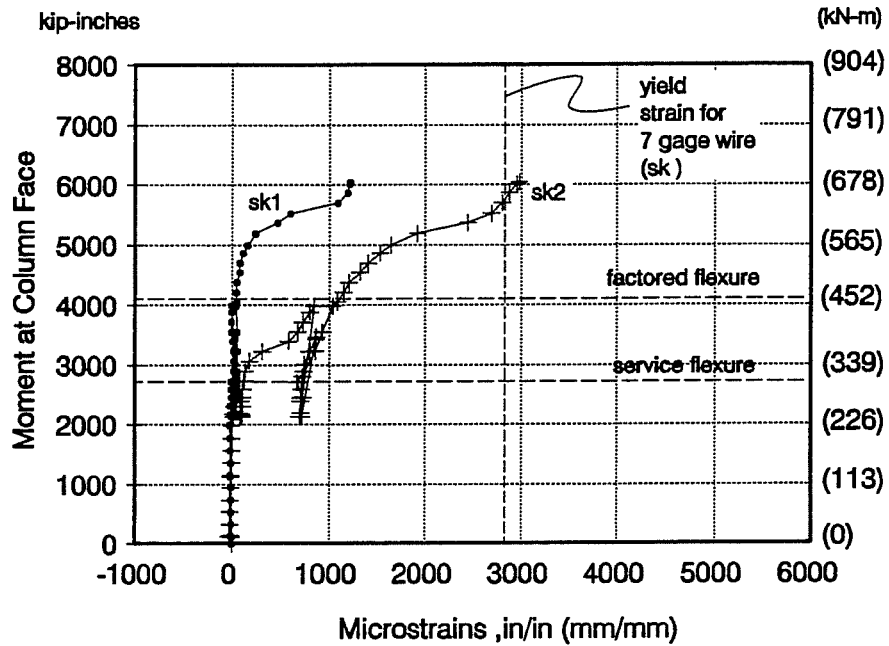


Figure 3.28 Resultant Moment vs. Strain in Effective Strain Gages in Skin Reinforcement for Model CO-PU-54S-TH-I

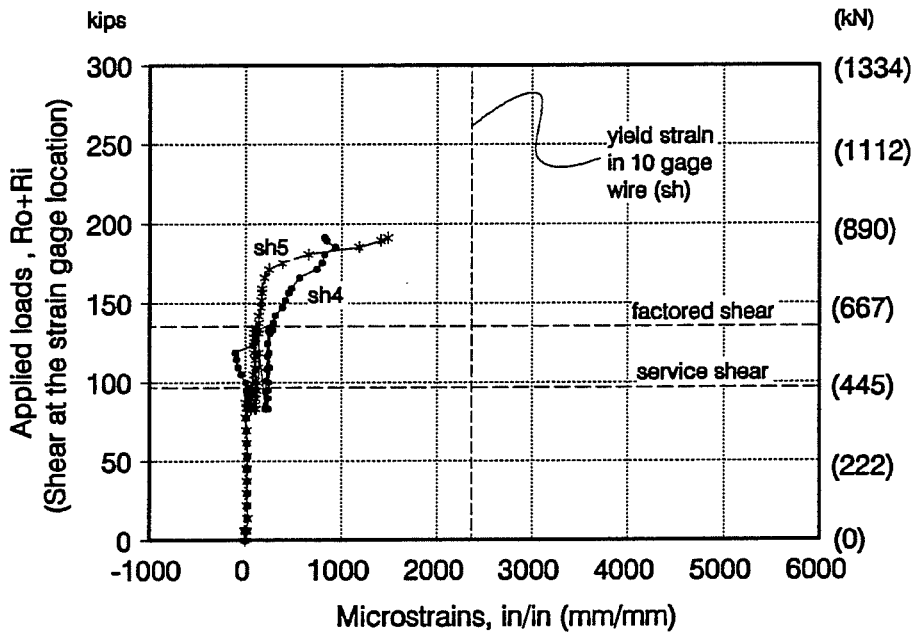


Figure 3.29 Resultant Load vs. Strain in Effective Strain Gages in Shear Reinforcement for Model CO-PU-54S-TH-I

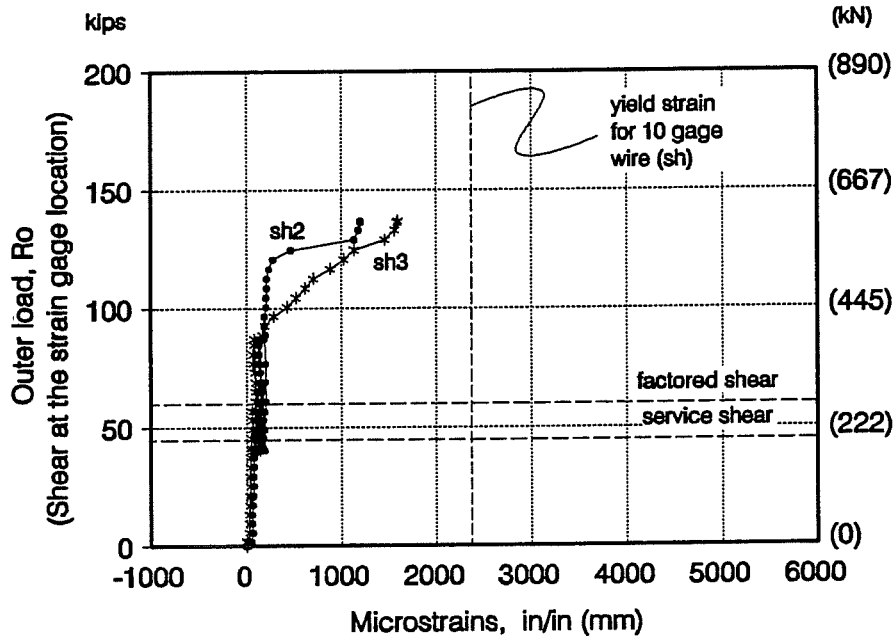


Figure 3.30 Resultant Load vs. Strain in Effective Strain Gages in Shear Reinforcement for Model CO-PU-54S-TH-I (continuation...)

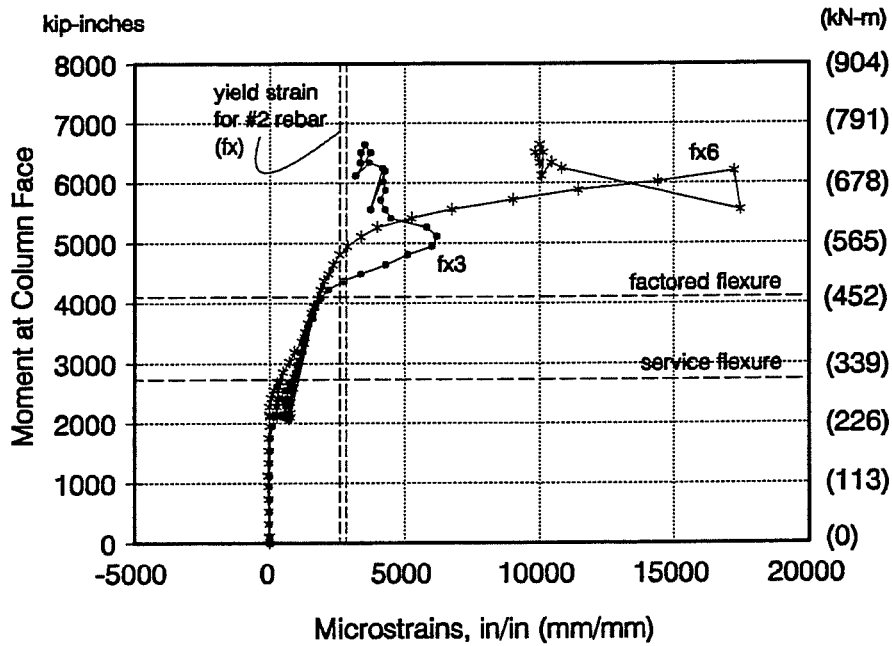


Figure 3.31 Resultant Moment vs. Strain in Effective Strain Gages in Flexural Bars for Model CO-PU-74S-TH-V

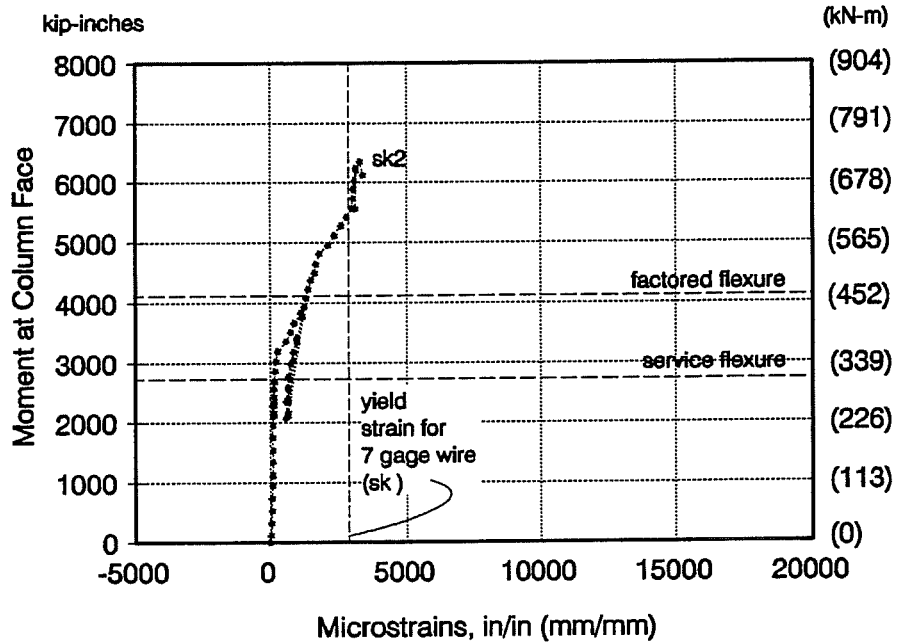


Figure 3.32 Resultant Moment vs. Strain in Effective Strain Gages in Skin Reinforcement for Model CO-PU-74S-TH-V

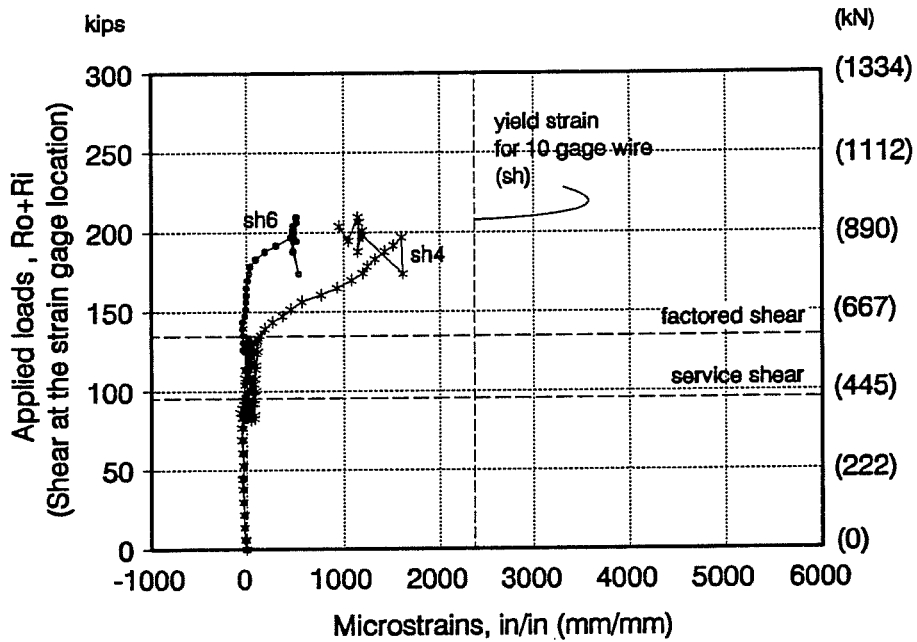


Figure 3.33 Resultant Load vs. Strain in Effective Strain Gages in Shear Reinforcement for Model CO-PU-74S-TH-V

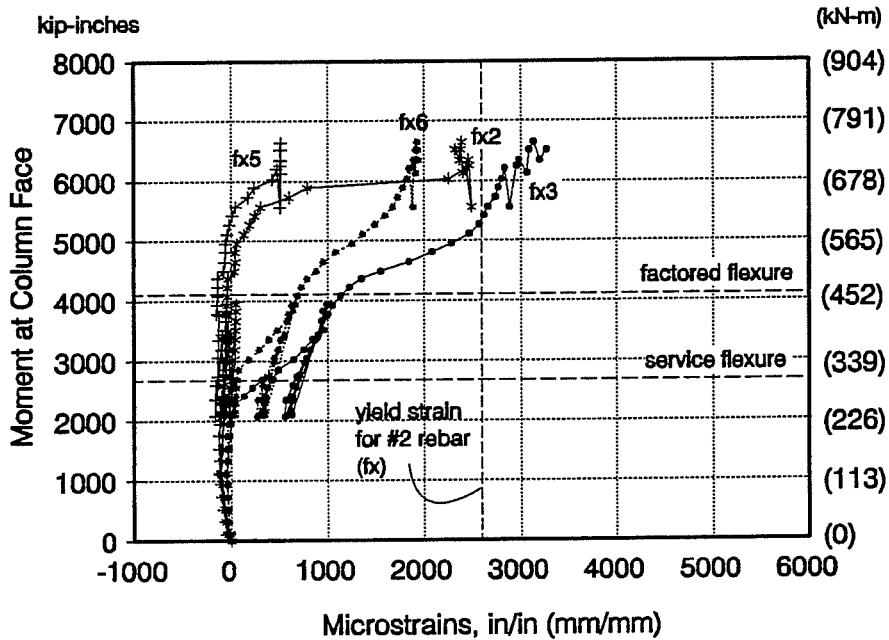


Figure 3.34 Resultant Moment vs. Strain in Effective Strain Gages in Flexural Bars for Model CO-PU-74S-TH-I

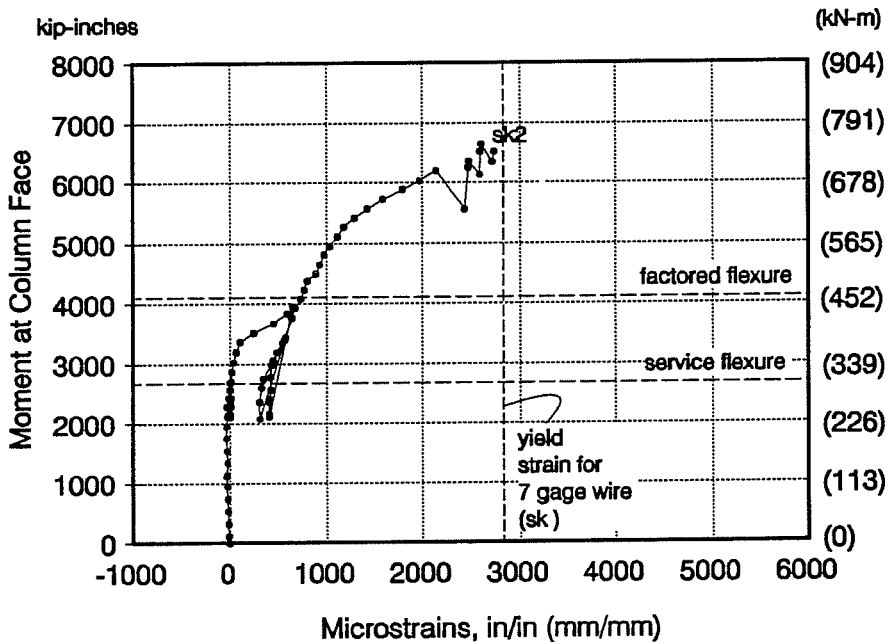


Figure 3.35 Resultant Moment vs. Strain in Effective Strain Gages in Skin Reinforcement for Model CO-PU-74S-TH-I

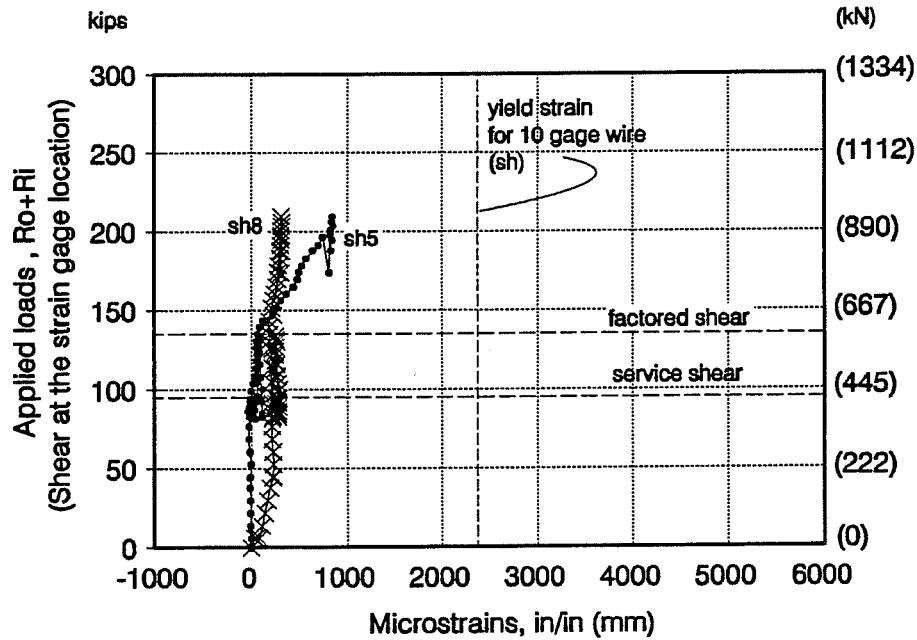


Figure 3.36 Resultant Load vs. Strain in Effective Strain Gages in Shear Reinforcement for Model CO-PU-74S-TH-I

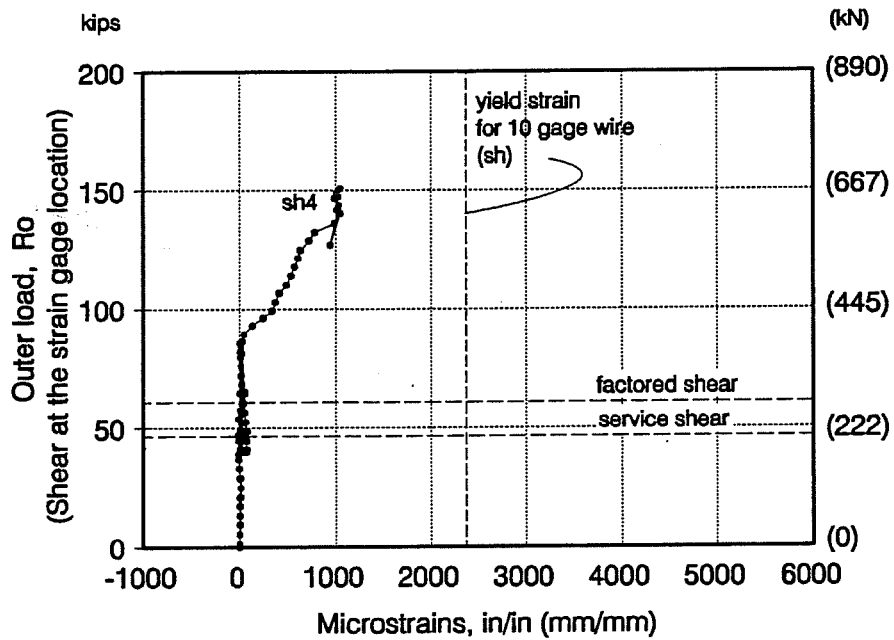


Figure 3.37 Resultant Load vs. Strain in Effective Strain Gages in Shear Reinforcement for Model CO-PU-74S-TH-I (continuation...)

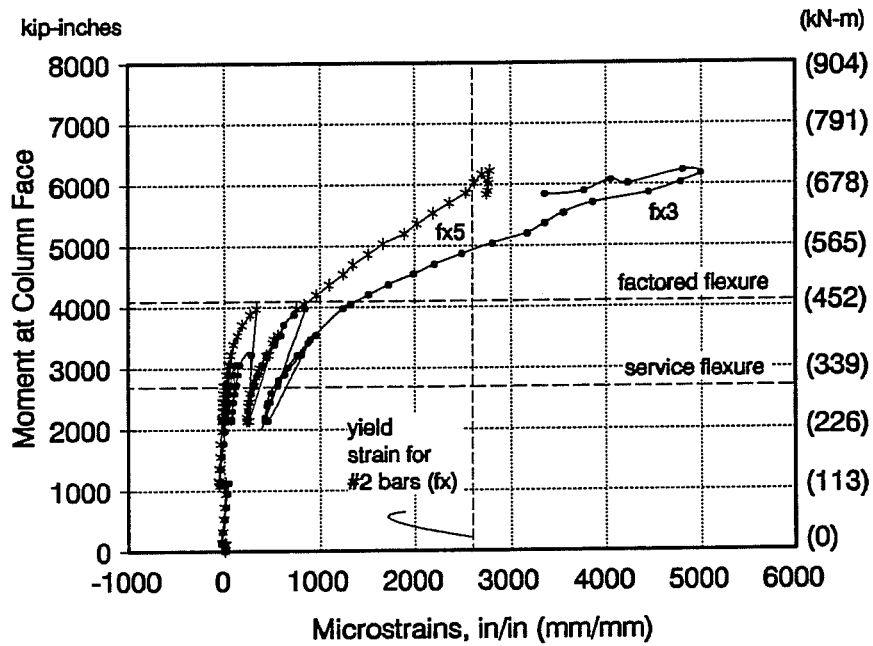


Figure 3.38 Resultant Moment vs. Strain in Effective Strain Gages in Flexural Bars for Model CO-PU-100S-TH-V

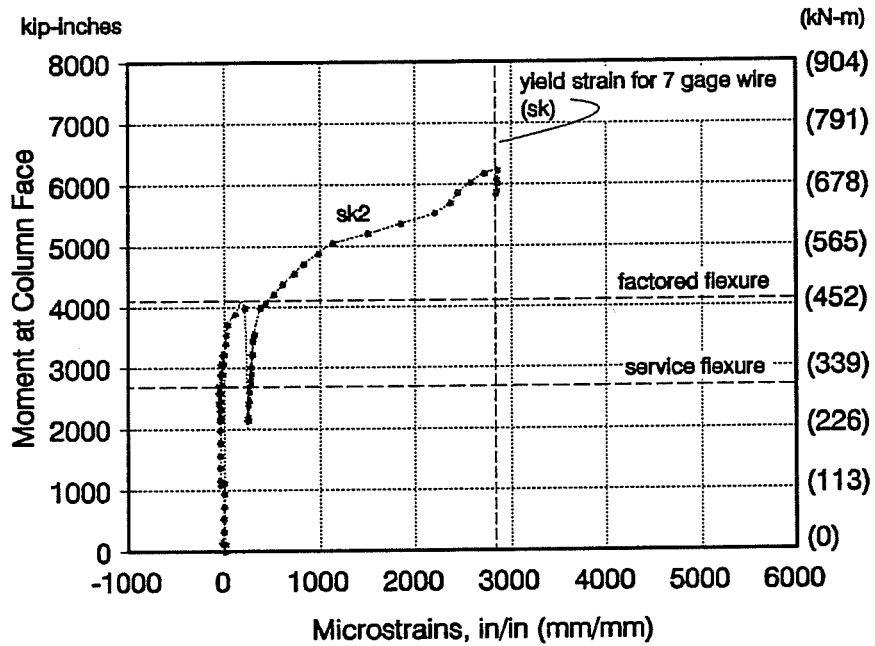


Figure 3.39 Resultant Moment vs. Strain in Effective Strain Gages in Skin Reinforcement for Model CO-PU-100S-TH-V

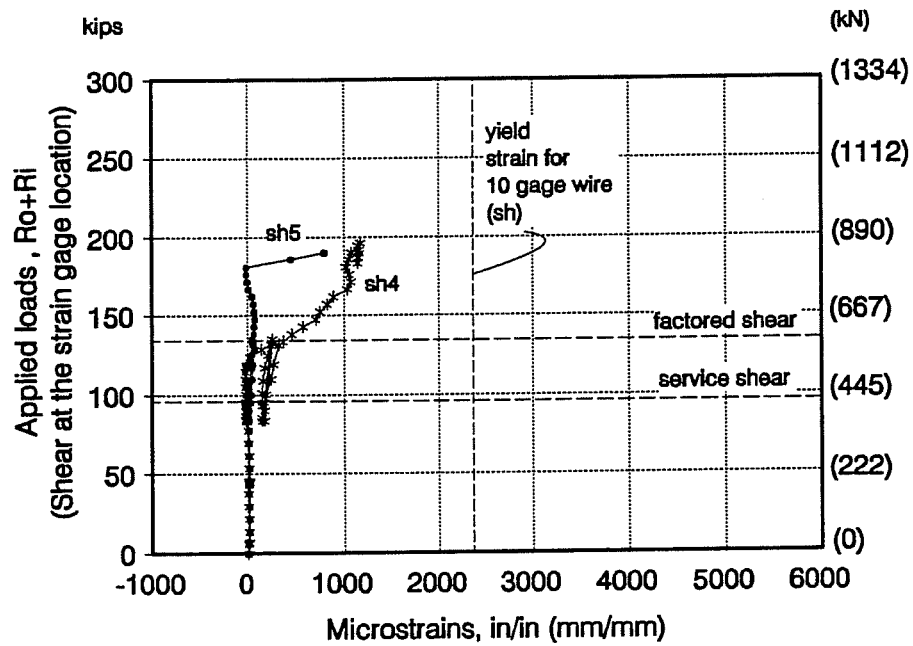


Figure 3.40 Resultant Load vs. Strain in Effective Strain Gages in Shear Reinforcement for Model CO-PU-100S-TH-V

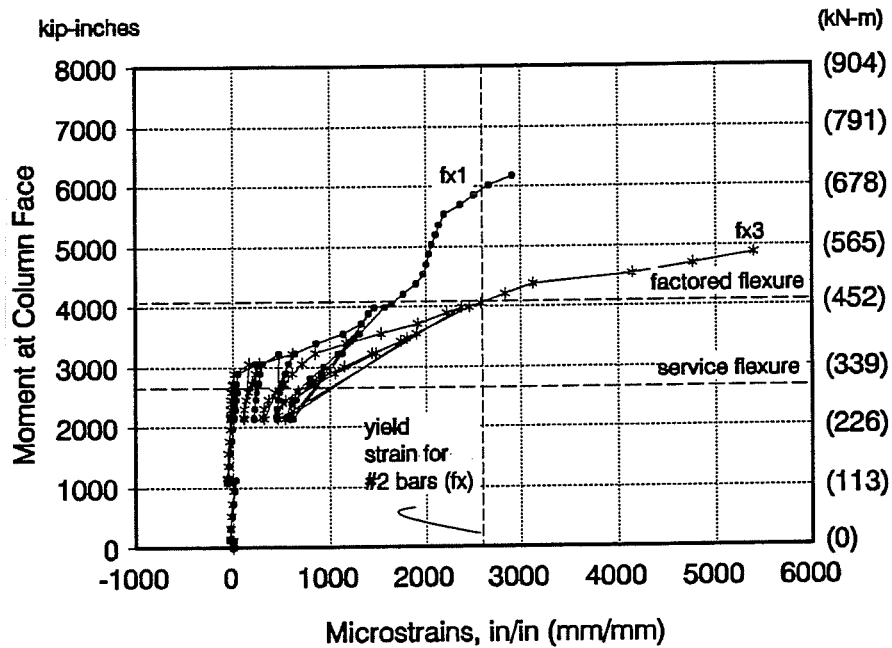


Figure 3.41 Resultant Moment vs. Strain in Effective Strain Gages in Flexural Bars for Model CO-PU-100S-TH-I

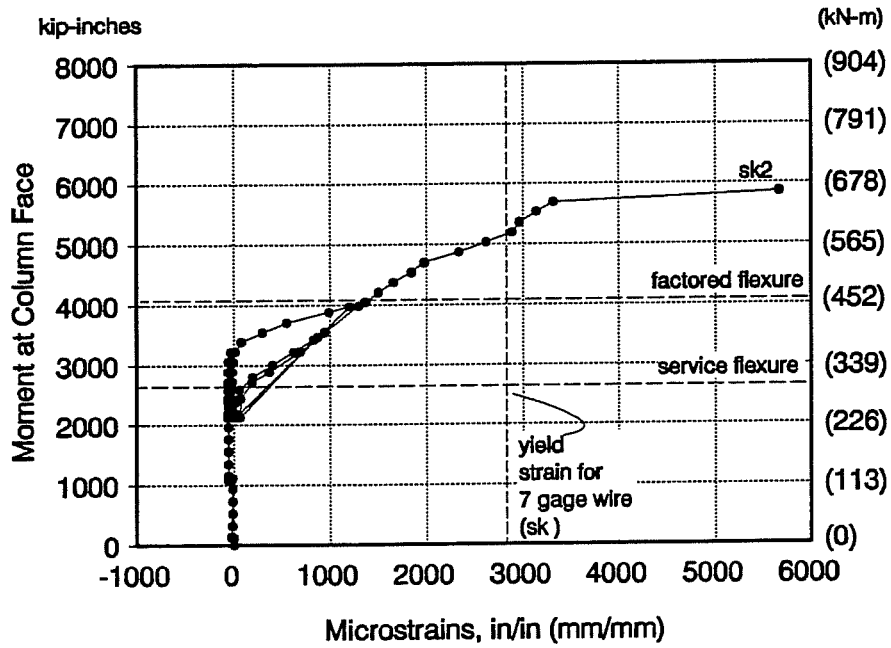


Figure 3.42 Resultant Moment vs. Strain in Effective Strain Gages in Skin Reinforcement for Model CO-PU-100S-TH-I

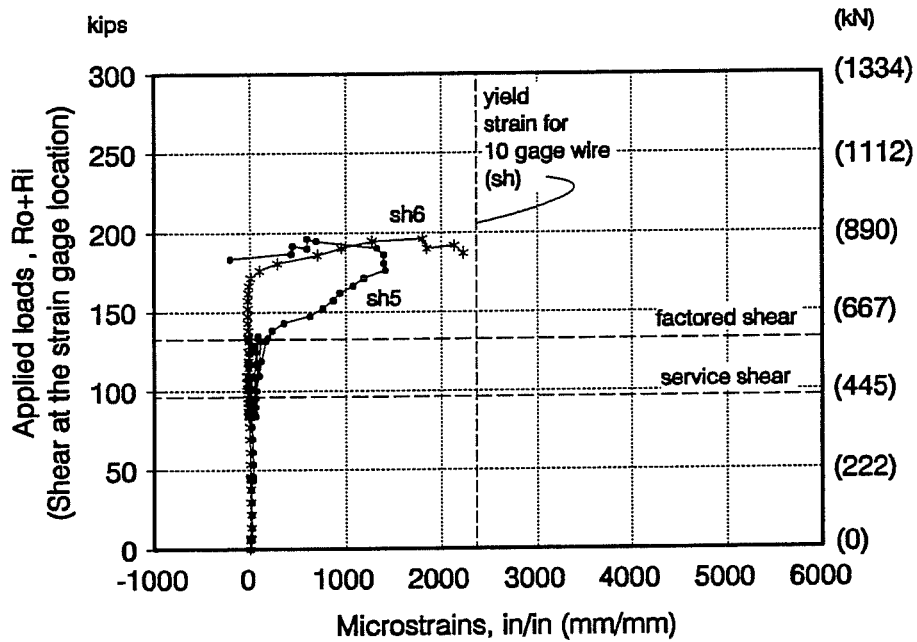


Figure 3.43 Resultant Load vs. Strain in Effective Strain Gages in Shear Reinforcement for Model CO-PU-100S-TH-I

CHAPTER 4

ANALYSIS OF RESULTS

Test results presented in Chapter 3 are analyzed and compared to previous experimental results as well as theoretical and allowable values. The discussion includes analysis of deflections, cracking and ultimate capacities and behavior. Predictions based on current codes of practice, such as AASHTO [11,15] and ACI [16], for conventionally reinforced and fully prestressed structures, are evaluated and compared with the performance of structures with a mixture of non-prestressed and prestressed reinforcement. Results showing the use of T-headed reinforcing bars as well as various amounts of skin reinforcement are included and conclusions are drawn based on their influence on the constructability and structural behavior of the members.

4.1 DEFLECTIONS

Tip deflections for all overhangs at all major load levels are summarized in Table 4.1. In this table, ratios of tip deflection to overhang length are included as an indicator of the stiffnesses and ductility of the models. In these results, service load deflections refer to those measured after two cycles of service loading, corresponding to load cycle c) as described in Section 2.9.1.

To evaluate the model performances at service load level, results were prepared in a graphic form as shown in Figure 4.1. As can be noticed, all results from Series 1364-1A were also included. This was done to provide assistance in understanding the nature of the transition between conventionally reinforced to fully prestressed structures, as given by those structures designed with a mixture of prestressed and non-prestressed reinforcement. Specifically, those models from Series 1364-1A corresponded to overhangs CO-RU (Reinforced concrete design), CO-PU-74S (Mixed reinforced concrete design, similar to overhangs CO-PU-74S-TH with the only difference being the use of standard hooks in non-prestressed flexural reinforcement instead of T-heads), CO-PU-100S (Fully prestressed concrete design similar to models CO-PU-100S-TH with the difference in the vertical tie side, as defined in Section 2.4.2, being the use of minimum skin reinforcement instead of the skin reinforcement suggested by Frantz and Breen, and using standard hooks instead of T-heads in the minimum non-prestressed horizontal reinforcement provided), and CO-PS-100S (Prestressed concrete design based on allowable stresses for flexure).

Table 4.1 Comparison of Tip Deflections at Major Load Levels

Model	Dead Load		Service Shear Loads		Service Flexure Loads		Factored Shear Loads		Factored Flexure Loads		Ultimate Loads	
	Tip deflection	Δ^*	Tip deflection	Δ	Tip deflection	Δ	Tip deflection	Δ	Tip deflection	Δ	Tip deflection	Δ
	in (mm)	l	in (mm)	l	in (mm)	l	in (mm)	l	in (mm)	l	in (mm)	l
CO-PU-54S-TH-V	0.043 (1.09)	0.0009	0.065 (1.65)	0.0014	0.068 (1.73)	0.0015	0.154 (3.91)	0.0033	0.161 (4.60)	0.0039	0.914 (23.22)	0.0199
CO-PU-54S-TH-I	0.029 (0.74)	0.0006	0.046 (1.17)	0.0010	0.060 (1.52)	0.0013	0.138 (3.51)	0.0030	0.169 (4.29)	0.0037	--	--
CO-PU-74S-TH-V	0.018 (0.41)	0.0003	0.036 (0.91)	0.0008	0.036 (0.91)	0.0008	0.109 (2.77)	0.0024	0.126 (3.20)	0.0027	0.960 (25.15)	0.0215
CO-PU-74S-TH-I	-0.003 (-0.08)	-0.0001	0.007 (0.18)	0.0002	0.014 (0.36)	0.0003	0.071 (1.81)	0.0016	0.085 (2.17)	0.0019	--	--
CO-PU-100S-TH-V	0.026 (0.66)	0.0006	0.041 (1.04)	0.0006	0.042 (1.07)	0.0006	0.115 (2.92)	0.0025	0.127 (3.23)	0.0028	--	--
CO-PU-100S-TH-I	0.028 (0.69)	0.0006	0.039 (0.99)	0.0008	0.045 (1.14)	0.0010	0.118 (3.00)	0.0028	0.145 (3.68)	0.0032	1.110 (28.19)	0.0241

* Δ : Tip deflection
 l : Overhang length, 46 in. (1.17 m)

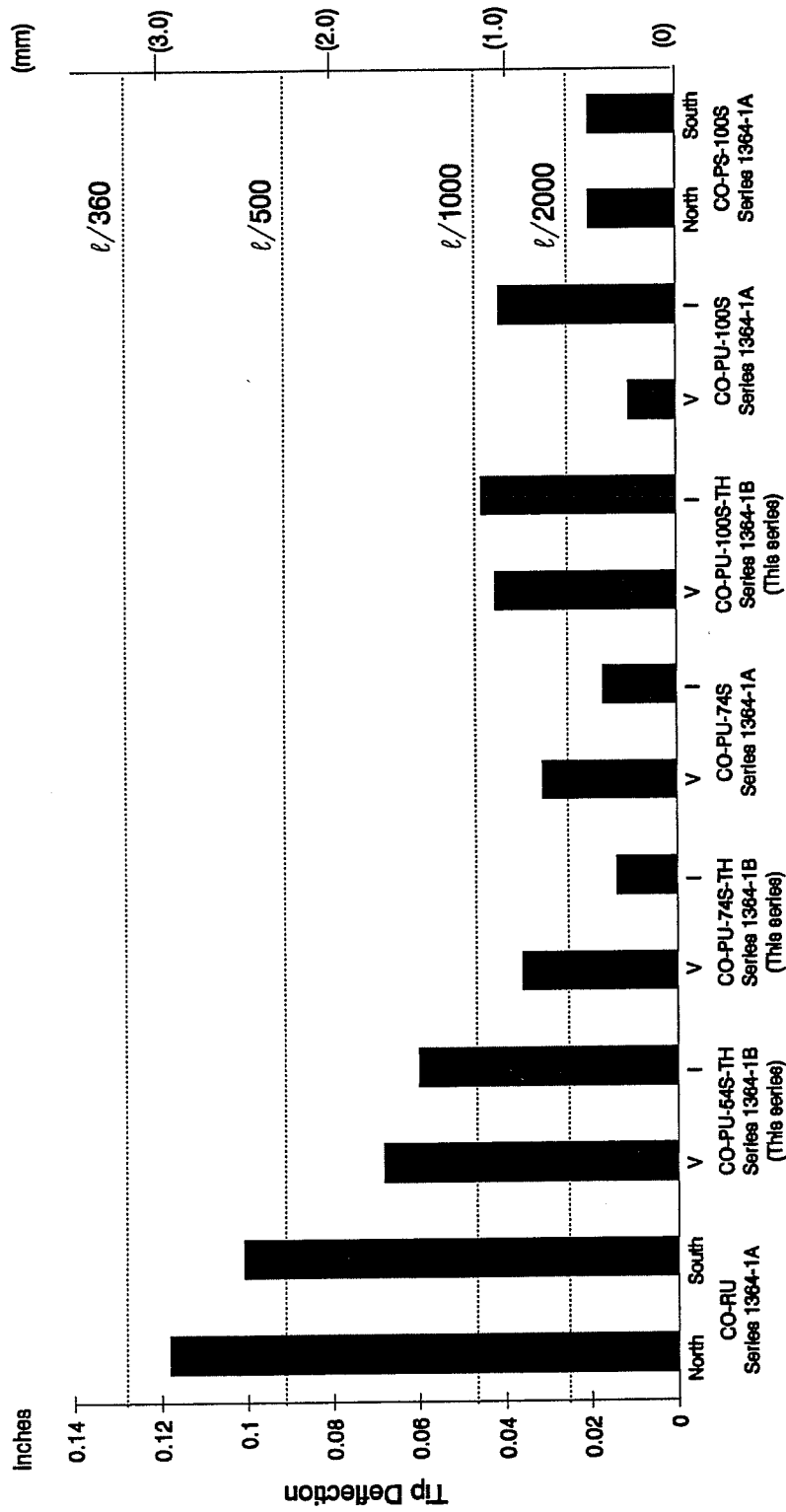


Figure 4.1 Tip deflections at service flexure load level

Figure 4.1 shows a trend between deflections and the amount of post-tensioning in the models. In general, as the post-tensioning force in the models increases, the deflections at service load level decrease. The exception was observed for models CO-PU-74S-TH (V&I) (This series) and CO-PU-74S (V&I) (Series 1364-1A) where service load deflections were less than those for the fully prestressed models designed with ultimate strength governing flexure. It is believed that this behavior was due to the lack of elastomeric pads between bearing plates and loading rams, which allowed for the friction forces to build up in those areas. In this respect it has to be remembered that only models CO-RU (Series 1364-1A), CO-PU-54S-TH (V&I) (This series) and CO-PU-100S-TH (V&I) (This series) were tested with pads. Those three specimens had the highest tip deflections so restraint seems to be a factor in the behavior of all other specimens at the very small deflection levels.

Regarding the acceptability of deflections when compared with the typical service flexure live load limit of $L/360$ for serviceability of concrete structures, in all cases deflections were below that value. In fact, all prestressed structures were well below that limit by factors of two to ten.

4.2 MOMENT VERSUS DEFLECTION RESPONSE

Comparison of moment - deflection responses for the three specimens of this study was presented in Figure 3.6. In general, deflections in the elastic region and up to the service flexure load level were very similar for all the overhangs, showing minimal effect from the different patterns of non-prestressed and prestressed reinforcement. Above this load level, model CO-PU-54S-TH-V showed the lowest stiffness and ductility. As was explained in Chapter 3, this behavior was expected when compared to the CO-PU-100S-TH-I model (of very similar ultimate capacity) since the different amounts of prestressed reinforcement were found to be in direct proportion to the amount of cracking, and therefore the degradation of the stiffness of the structure. Generally, at higher post-tensioning forces, fewer cracks were observed, and as a result stiffer structures were attained.

Models CO-PU-74S-TH demonstrated a higher stiffness than all the other models, but it was concluded that this behavior was mainly due to the restraining friction forces between bearing plates and loading rams.

4.3 CRACKING LOAD PREDICTIONS

Theoretical values for cracking loads were calculated using Equation 4.1. This formulation assumes that cracks occur when the maximum tensile stress at the critical section reaches the modulus of rupture f_r of concrete.

$$M_{cr} = \left(f_r + \frac{A_{ps} f_{pe}}{A_g} \right) \frac{I}{c} + A_{ps} f_{pe} e \quad [4.1]$$

where:

- M_{cr} : cracking moment
- A_{ps} : area of active reinforcement in tension zone,
- A_g : gross area of section,
- f_{pe} : effective stress in active reinforcement (after losses),
- I : moment of inertia of uncracked concrete cross section,
- c : distance to the extreme tensile fiber measured from the centroid of the cross section,
- e : eccentricity of the centroid of active reinforcement measured from the centroid of the cross section

Table 4.2 summarizes the results of the test data and the theoretical values calculated using two different modulus of rupture values, $7.5\sqrt{f'_c}$ ($0.62\sqrt{f'_c}$ MPa) and $6\sqrt{f'_c}$ ($0.5\sqrt{f'_c}$ MPa). The concrete cylinder compressive strengths used for these calculations are those presented in Table 2.14. As shown, a concrete modulus of rupture of $6\sqrt{f'_c}$ ($0.5\sqrt{f'_c}$ MPa) generally gave better predictions for the cracking moment of the models. In these calculations it was assumed that no losses had taken place in the post-tensioning force in the few days between stressing and testing.

Table 4.2 Cracking Moments

Model	Predicted Cracking Moment		Test Cracking Moment kip in (kN-m)	Mcr/ Mserv. flex **
	Using $f_r = 7.5\sqrt{f'_c}$ (0.62 $\sqrt{f'_c}$) kip-in (kN-m)	Using $f_r = 6\sqrt{f'_c}$ (0.5 $\sqrt{f'_c}$) kip-in (kN-m)		
CO-PU-54S-TH-V	2221 (251.0) -0.89- *	1978 (223.5) -1.00-	1987 (224.5)	0.72
CO-PU-54S-TH-I	2221 (251.0) -0.89-	1978 (223.5) -1.00-	1987 (224.5)	0.72
CO-PU-74S-TH-V	2599 (293.5) -0.89-	2356 (266.0) -0.99-	2465 (278.5)	0.84
CO-PU-74S-TH-I	2599 (293.5) -0.95-	2356 (266.0) -1.04-	2465 (278.5)	0.90
CO-PU-100S-TH-V	3089 (349.0) -0.99-	2845 (321.5) -1.08-	3076 (347.5)	1.12
CO-PU-100S-TH-I	3089 (349.0) -0.89-	2845 (321.5) -0.96-	2744 (310.0)	1.00
Average ratio	-0.92-	-1.01-	—	—

* Values between dashes are ratios of test to predicted cracking moments

** Mserv. flexure = 2749 kip-in (310.6 kN-m)

4.4 CRACK WIDTHS

4.4.1 Allowable versus Test

In Chapter 3, crack patterns and maximum crack widths were presented for all overhangs. To better interpret these results and compare them against expected and allowable values, data was organized and plotted depending on those cracks that were evident after the first cycle of loading or after the subsequent load cycles. To do this, some terms were introduced:

Virgin Loading: Load steps where the different load levels had been reached for the first time. These include first time: cracking, dead load, service shear load, service flexure load, and factored flexure load. Referring to Table 2.17, these corresponded to load steps 12, 17, 21, and 36, in addition to the load step for first cracking.

Complete loading: All load steps where crack width readings were performed up to the first time factored flexure loads. This includes load cycles a), b), and c) as described in Section 2.9.1., without considering the final load step to dead loads after reaching the factored flexure load level.

Major Cracks: Cracks in a particular overhang side that presented the largest width in any load step, from cracking to first time factored flexure load level. These corresponded to those cracks shown in shaded areas in Tables 3.2 through 3.13.

Figures 4.2 to 4.7 present the individual plots for all "Major Cracks", in all models, after "Virgin Loading". For every overhang, major cracks were plotted independently as shown in the top of each figure and then combined as shown in the lower part of each figure to produce a summary plot. The heavy dashed line in the lower part of each figure connects points of maximum crack width at every load level and defines the "Maximum Crack Width Envelope."

Comparison of the Overhang Crack Width Envelopes based on Virgin Loading for the specimens of this series is shown in Figure 4.8. In this plot the level of service flexure moment, 2749 kip-in (310.6 kN-m), and the acceptable AASHTO service load crack width for moderate exposure have been indicated. Any crack width envelope passing below the line of service flexure moment and right of the line of acceptable crack width is violating the limiting crack width, as set (indirectly by a z factor as discussed later) in the AASHTO provisions [15] for reinforced concrete structures under moderate exposure conditions. In viewing Figure 4.8 it must also be realized that since the level of accuracy of crack readings was 0.0005 in. (0.013 mm) the acceptable crack width of 0.0028 in. (0.071 mm) should be rounded to 0.003 in. (0.076 mm) when comparing with measurements. Thus the crack width limit is shown as a shaded bar between the theoretical 0.0028 in. (0.071 mm) and the experimental equivalent 0.003 in. (0.076 mm).

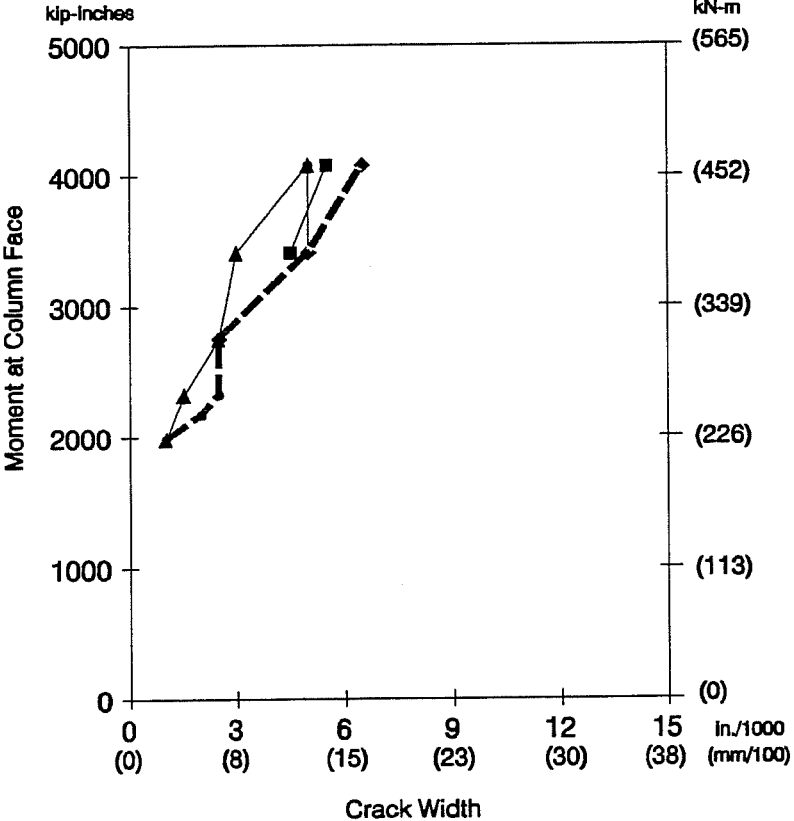
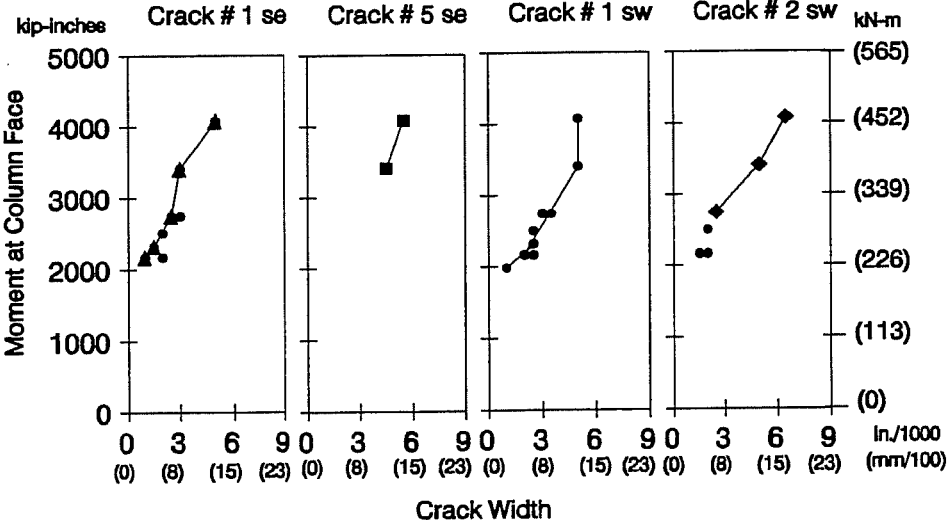


Figure 4.2 Crack plots for CO-PU-54S-TH-V overhang with "virgin" loading curves, (above) "Major" crack plots, (below) "Crack Width Envelope"

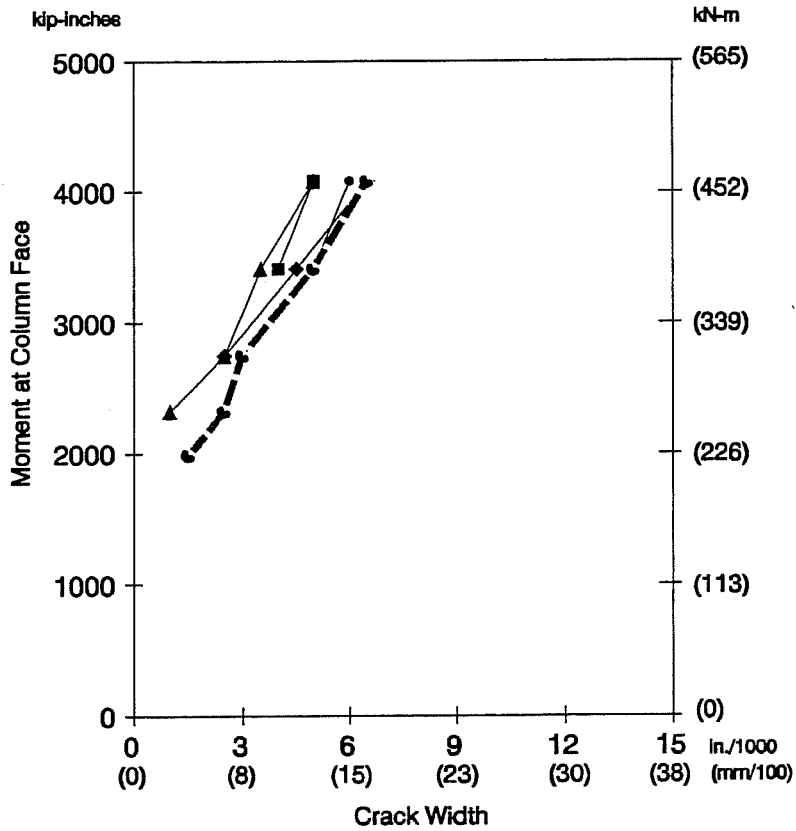
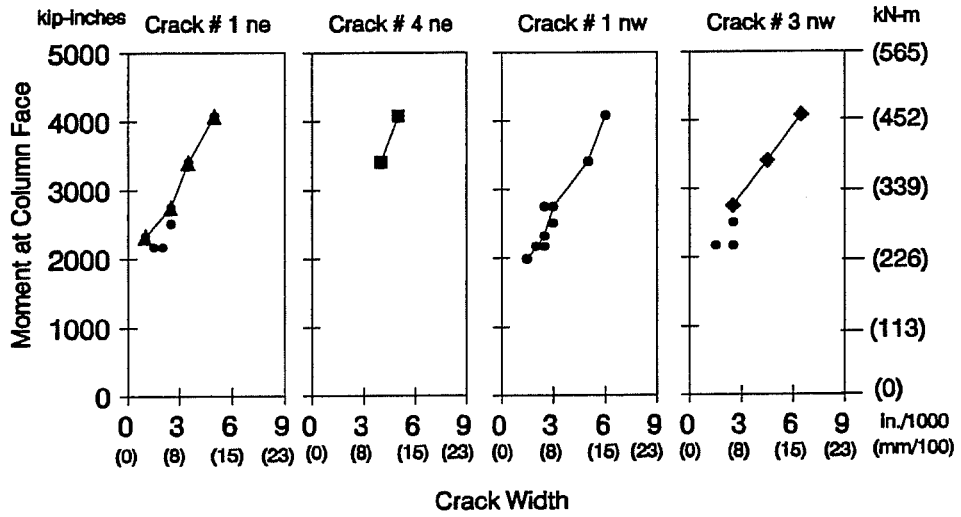


Figure 4.3 Crack plots for CO-PU-54S-TH-I overhang with "virgin" loading curves, (above) "Major" crack plots, (below) "Crack Width Envelope"

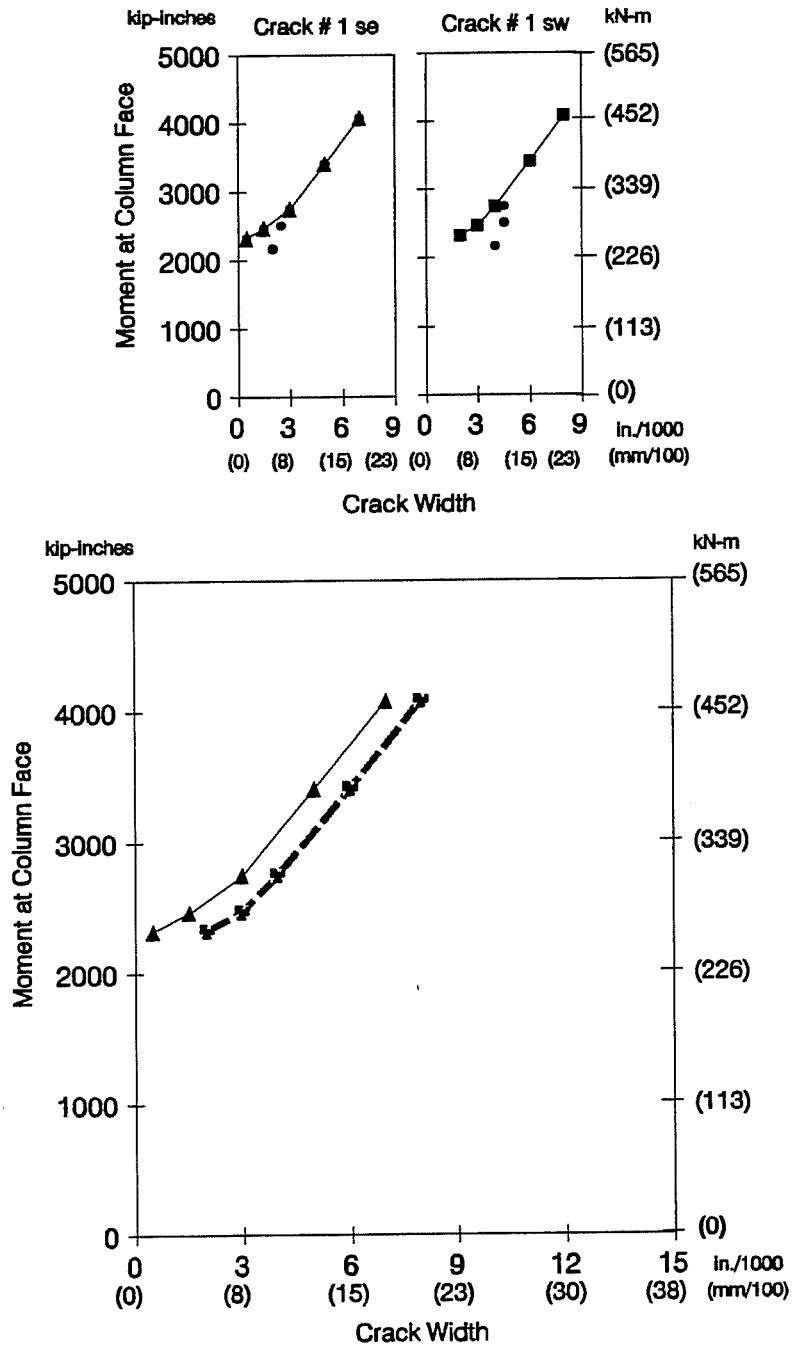


Figure 4.4 Crack plots for CO-PU-74S-TH-V overhang with "virgin" loading curves, (above) "Major" crack plots, (below) "Crack Width Envelope"

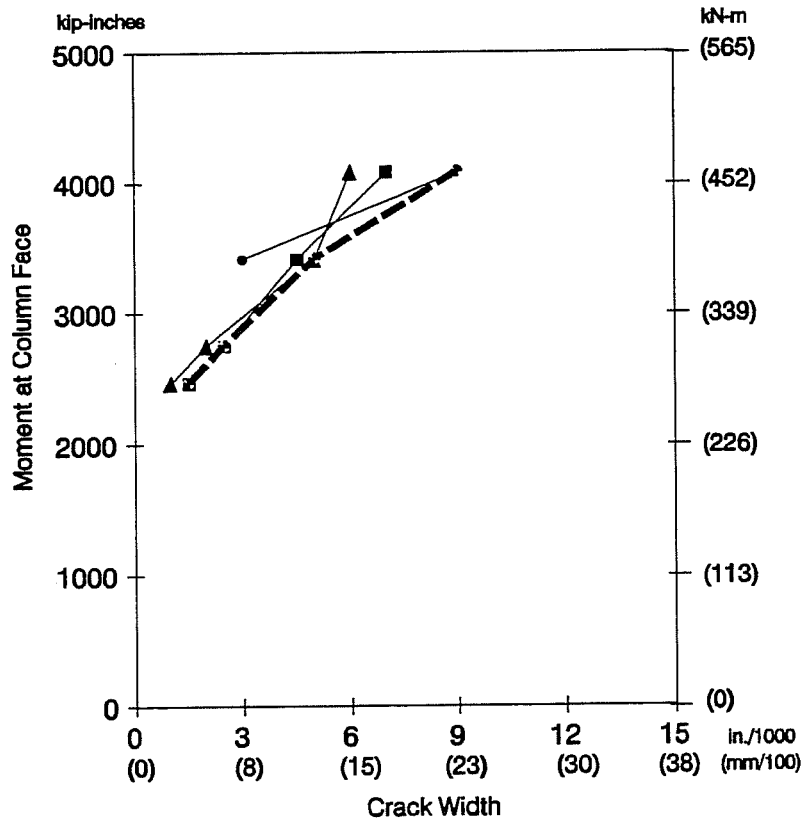
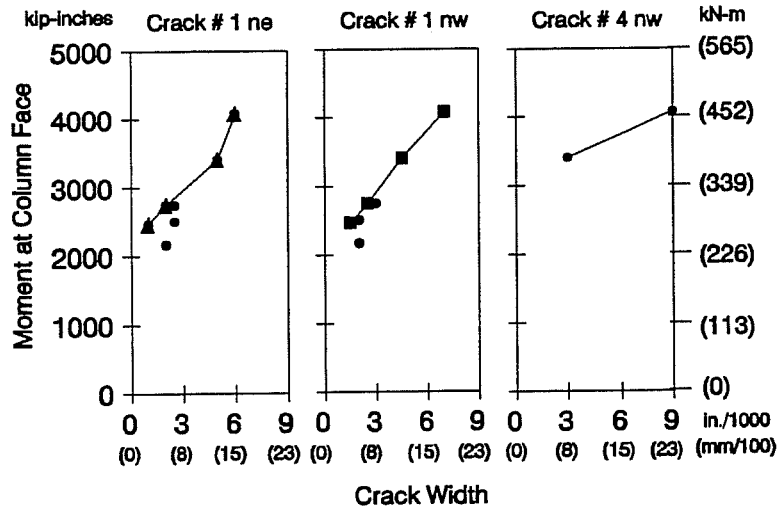


Figure 4.5 Crack plots for CO-PU-74S-TH-I overhang with "virgin" loading curves, (above) "Major" crack plots, (below) "Crack Width Envelope"

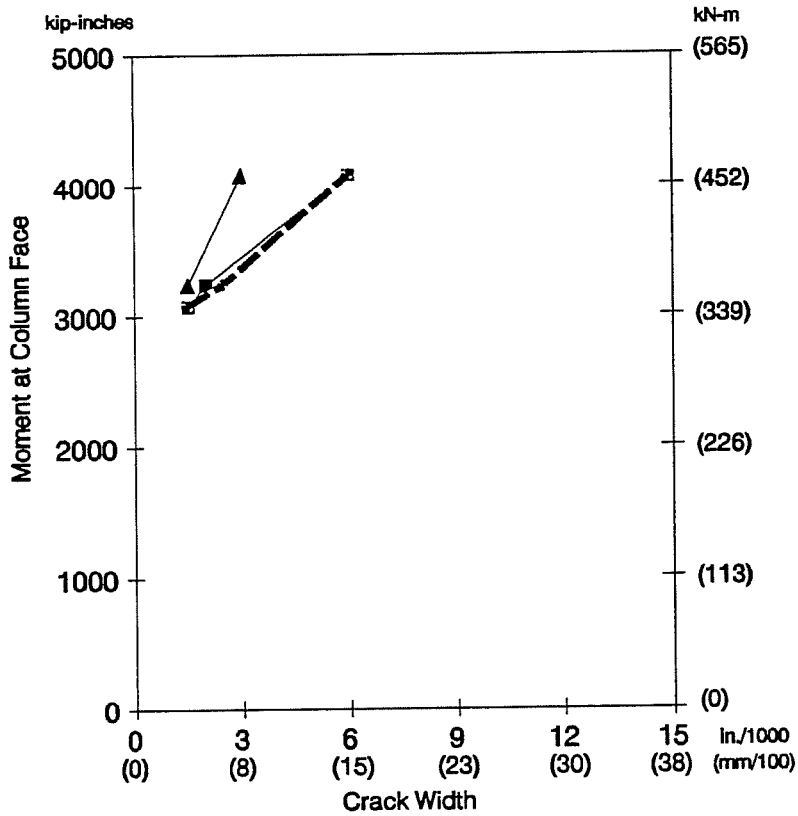
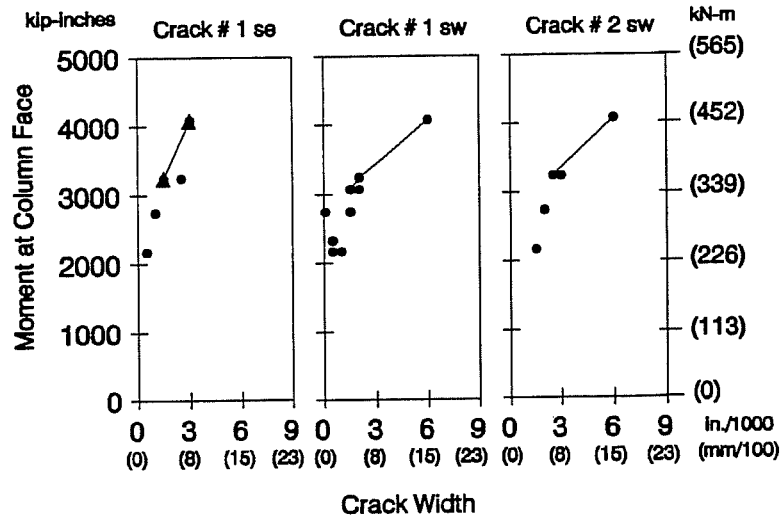


Figure 4.6 Crack plots for CO-PU-100S-TH-V overhang with "virgin" loading curves, (above) "Major" crack plots, (below) "Crack Width Envelope"

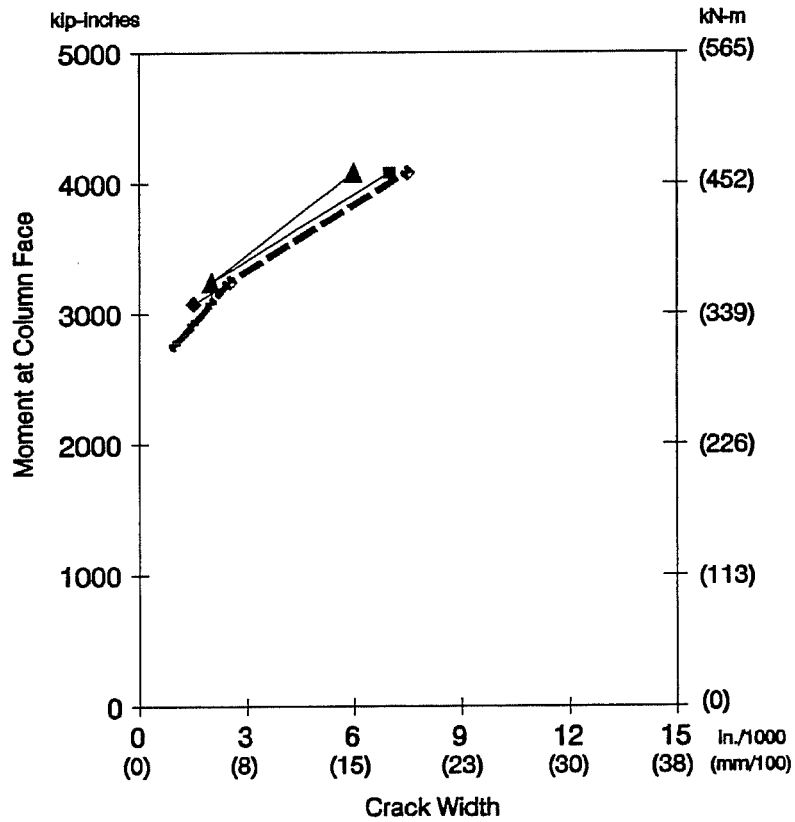
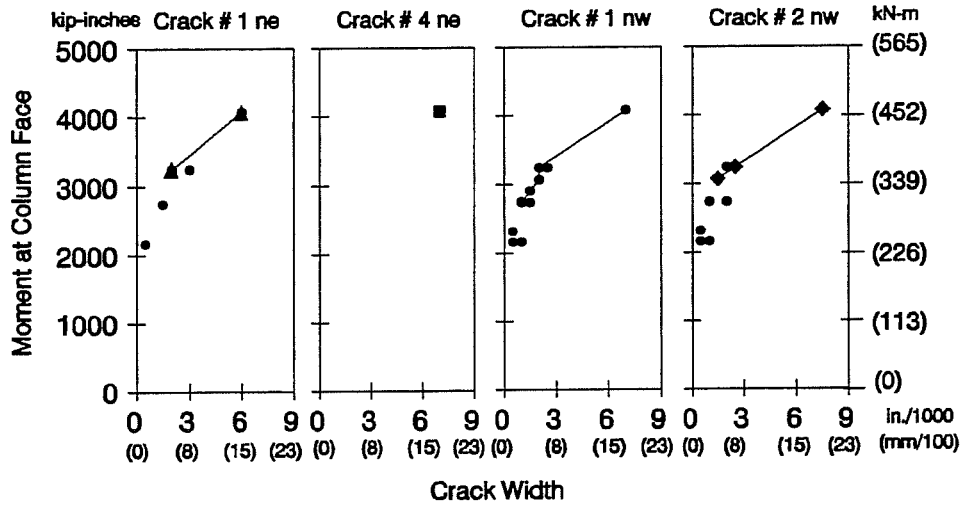


Figure 4.7 Crack plots for CO-PU-100S-TH-I overhang with "virgin" loading curves, (above) "Major" crack plots, (below) "Crack Width Envelope"

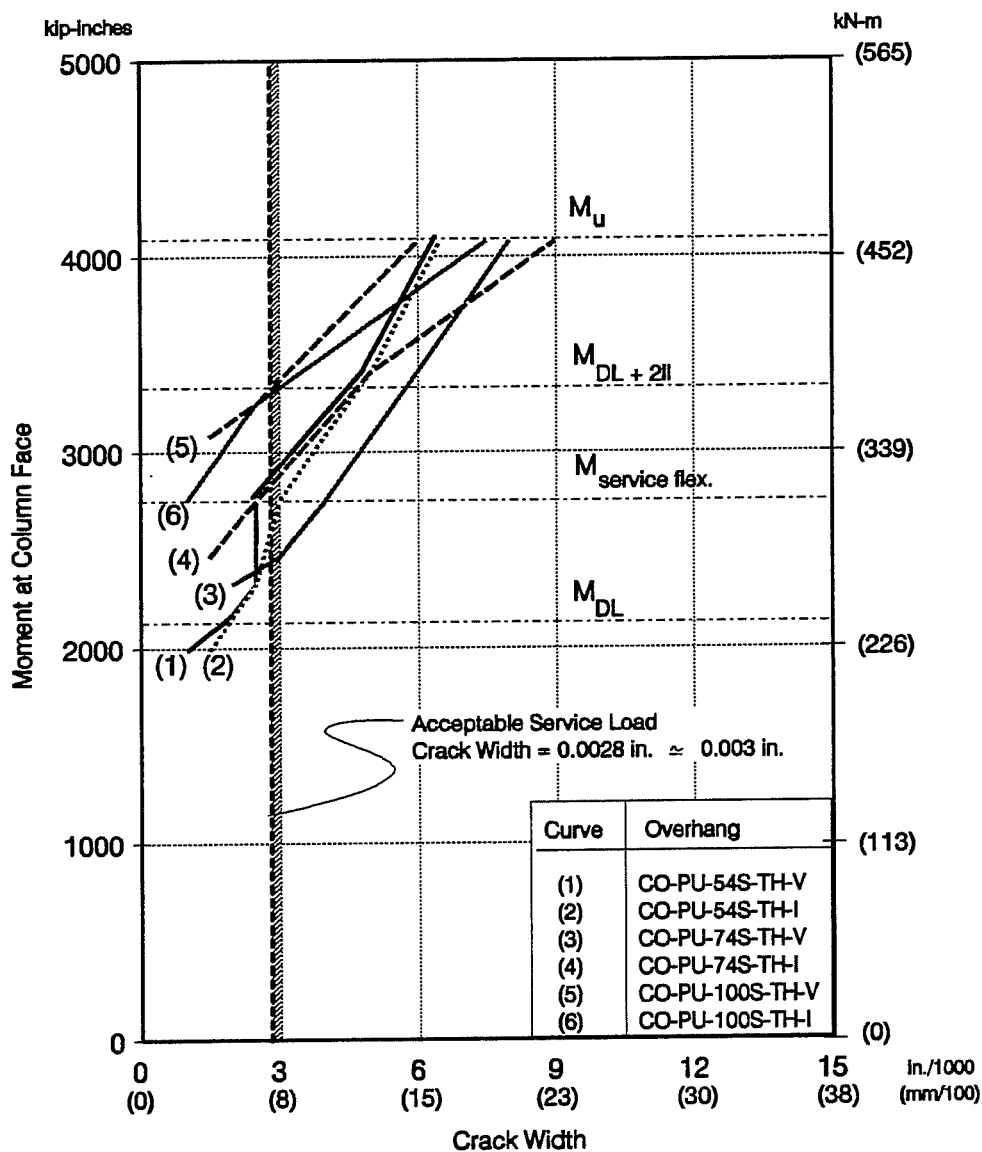


Figure 4.8 Comparison of Overhang "Crack Width Envelopes" based on "virgin" loading curves.

It should be emphasized that there is still not a clear definition as to what should be an adequate limiting value for maximum crack widths of concrete structures designed with a mixture of prestressed and non-prestressed reinforcement. A discussion in this sense, including comparison of provisions in different codes of practice, is presented in Section 4.4.3. In this section, results from Chapter 3 are compared only against current provisions of the AASHTO code for serviceability of reinforced concrete structures under service loads.

AASHTO provisions for reinforced concrete structures recommend for members in moderate exposure conditions that the factor "z" in Equation 4.2 should not exceed 170 kips per inch (29.8 kN/mm).

$$z = f_s (d_c A)^{1/3} \quad [4.2]$$

where:

z: quantity limiting distribution of flexural reinforcement

f_s : tensile stress in reinforcement at service loads $\approx 0.6 f_y$

f_y : specified yield strength of reinforcement

A: average effective concrete area surrounding a reinforcing bar

d_c : thickness of concrete cover measured from extreme tension fiber to center of the closest bar or wire

Using the expression proposed by Gergely and Lutz (as included in the ACI-318-89 code, Section 10.6.4 [16]), Equation 4.3, this value of z corresponds to a crack width of 0.0155 in. (0.397 mm) for the prototype structure and 0.0028 in. (0.071 mm) for the models at 1/5.5 scale.

$$w = 0.076 \beta f_s (d_c A)^{1/3} \quad [4.3]$$

where:

w: crack width in units of 0.001 in.

β : 1.2 for beams

A, f_s , and d_c as defined above

Analyzing the data shown in Figure 4.8 it can be observed, considering an accuracy of ± 0.0005 in. (0.013 mm) in all crack width readings, that at service flexure load levels only the model CO-PU-74S-TH-V exceeded the allowable value of 0.0028 in. ≈ 0.003 in. (0.07 mm) and even that model exceeded the limit by only approximately 25 percent. Models CO-PU-54S-TH (V&I) as well as model CO-PU-74S-TH-I performed well with values at the limit or close to the limit at service flexure loads. For models CO-PU-100S-TH (V&I), since they were uncracked at service flexure loads, their performance in terms of crack widths was obviously very good. After service loading, crack widths in these models were approximately 33 percent smaller than those from the other specimens at the same load levels. All models showed similar rates of increase of crack widths with respect to loading.

In the same way, "Major Cracks" were plotted against "Complete Loading". Figures 4.9 to 4.14 show the crack width plots for all specimens. Once again, these figures show in the upper part the individual plots for each major crack, and in the lower part the combination of data with the resulting "Maximum Crack Width Envelopes."

Comparison of all Overhang Crack Width Envelopes based on "Complete Loading" is shown in Figure 4.15. It can be observed in this plot, again considering an accuracy of ± 0.0005 in. (0.013 mm) for all crack width readings, that model CO-PU-74S-TH-V exceeded the allowable service load level value by approximately 43 percent. Model CO-PU-54S-TH-V exceeded that value by approximately 7 percent after the application of full service flexure loads. All other models performed within allowable limits. In general, as the percentage of post-tensioning force in the specimens increased, the maximum crack width decreased, as expected.

An important observation when analyzing the results from models CO-PU-74S-TH-V is that the major cracks in this overhang originated and propagated in the beam structure very close to the column face. In this region, because of the way the model was constructed (placing the overhang non-prestressed flexural bars inside of the column cage) a larger cover existed, which corresponded to approximately double that assumed in design of 0.41 in. (10.4 mm). Since cover thickness is an important variable affecting crack widths, this factor was considered one of the major causes of the very large crack widths observed in that area.

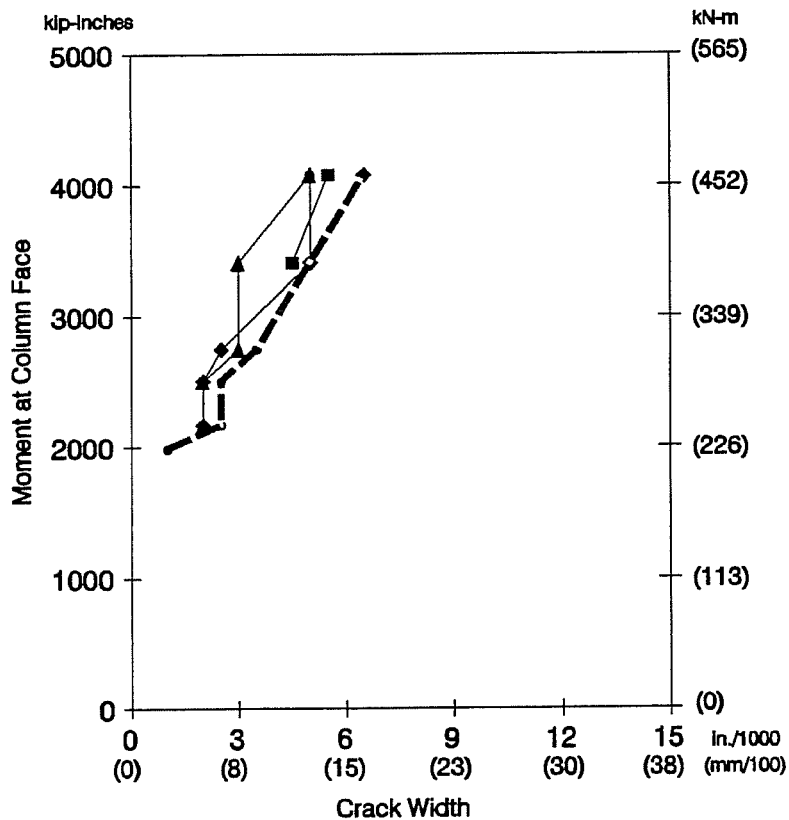
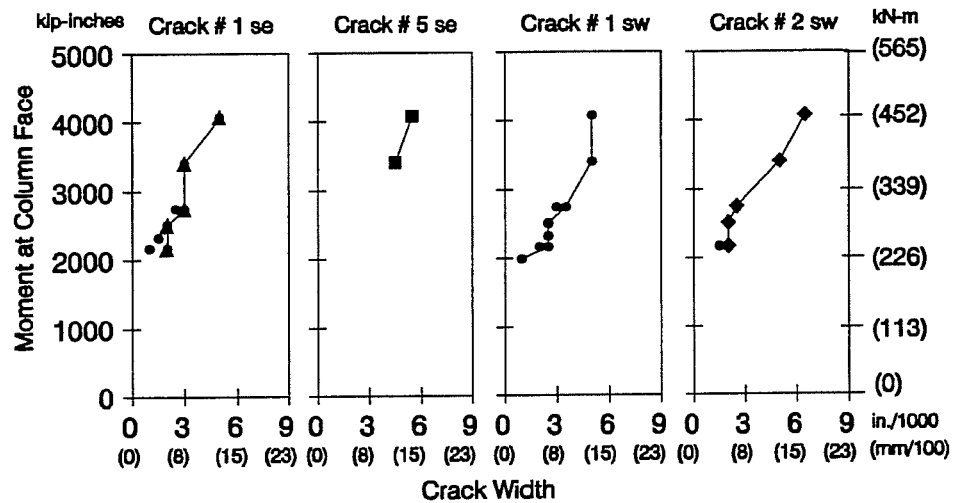


Figure 4.9 Crack plots for CO-PU-54S-TH-V overhang with "complete" loading curves, (above) "Major" crack plots, (below) "Crack Width Envelope"

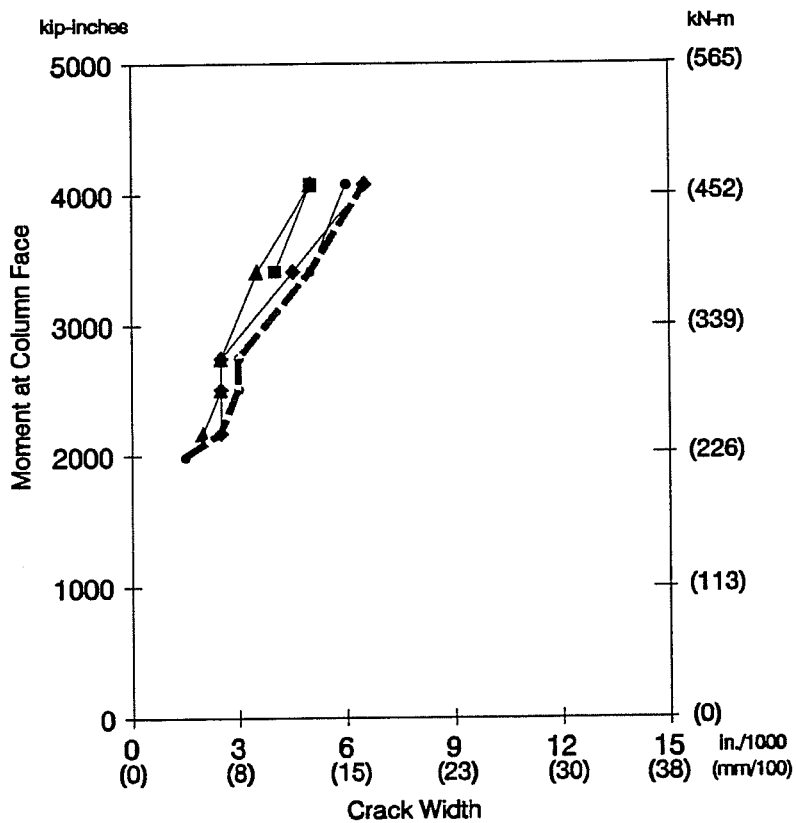
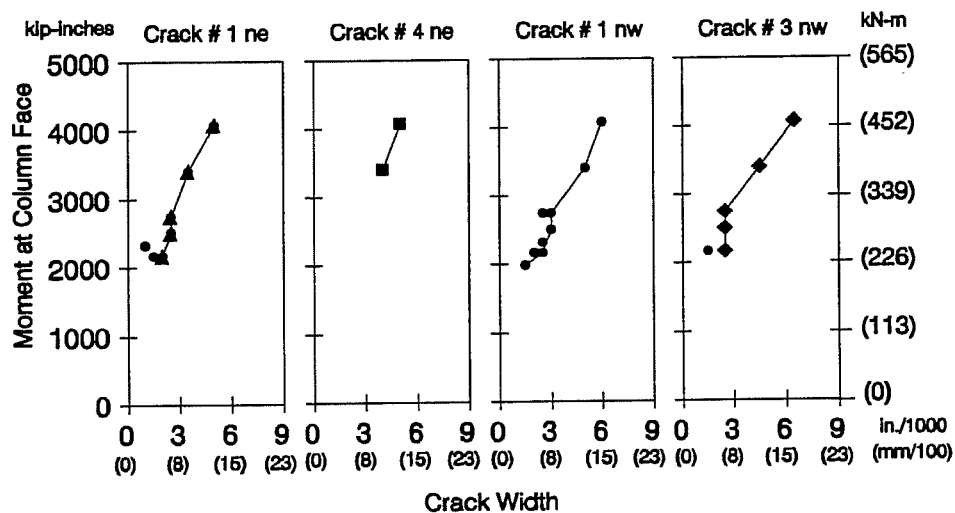


Figure 4.10 Crack plots for CO-PU-54S-TH-I overhang with "complete" loading curves, (above) "Major" crack plots, (below) "Crack Width Envelope"

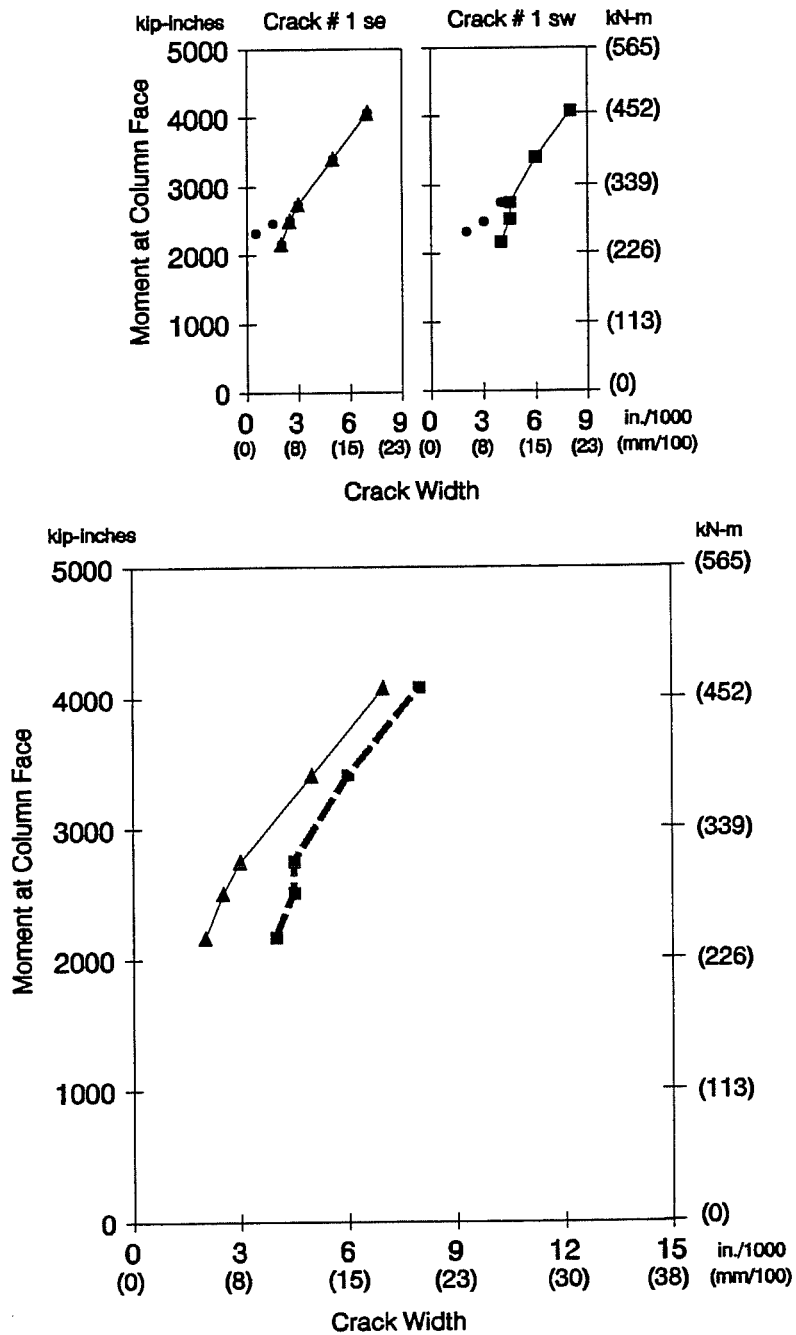


Figure 4.11 Crack plots for CO-PU-74S-TH-V overhang with "complete" loading curves, (above) "Major" crack plots, (below) "Crack Width Envelope"

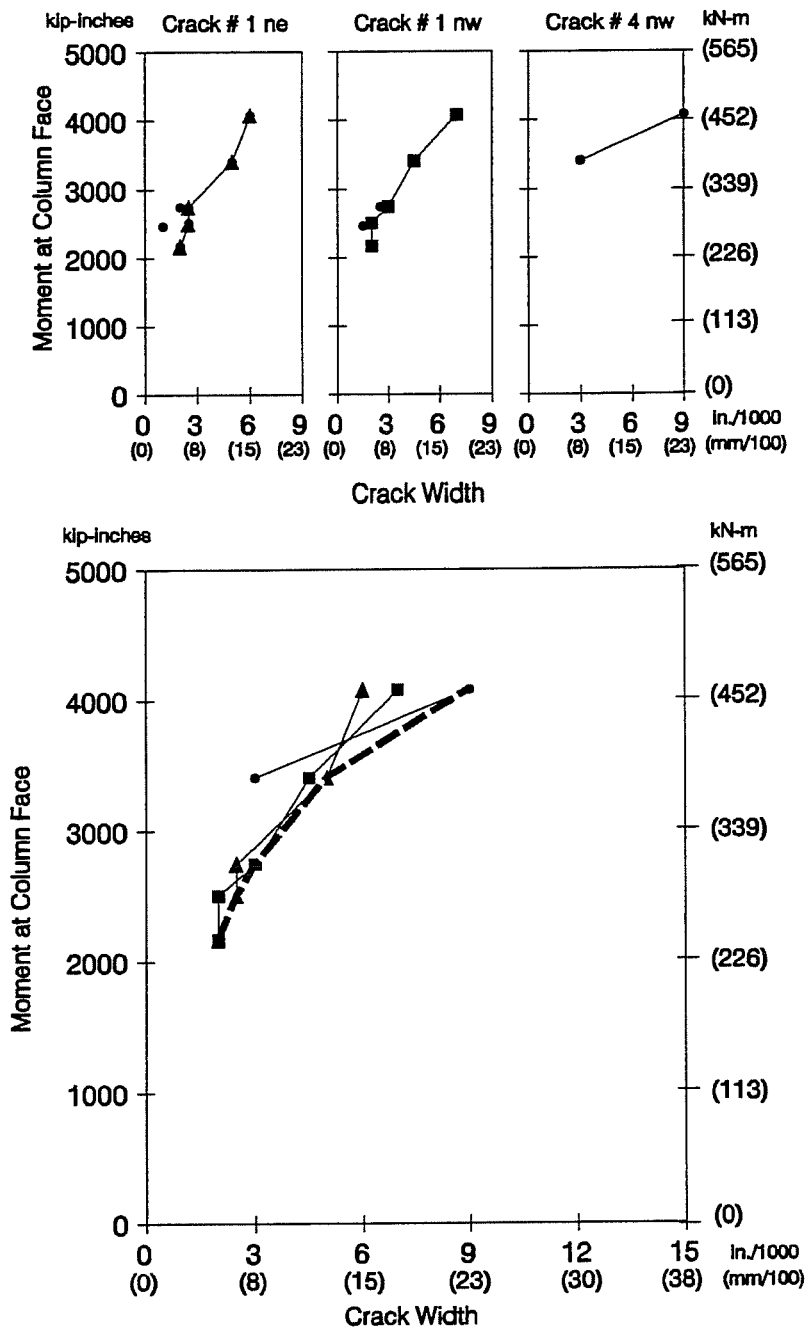


Figure 4.12 Crack plots for CO-PU-74S-TH-I overhang with "complete" loading curves, (above) "Major" crack plots, (below) "Crack Width Envelope"

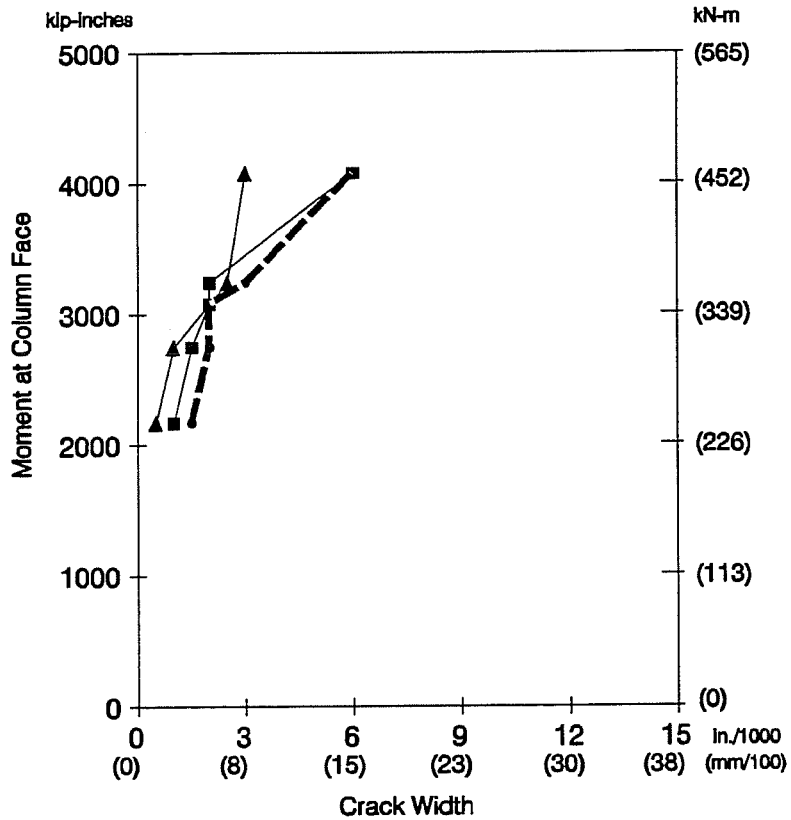
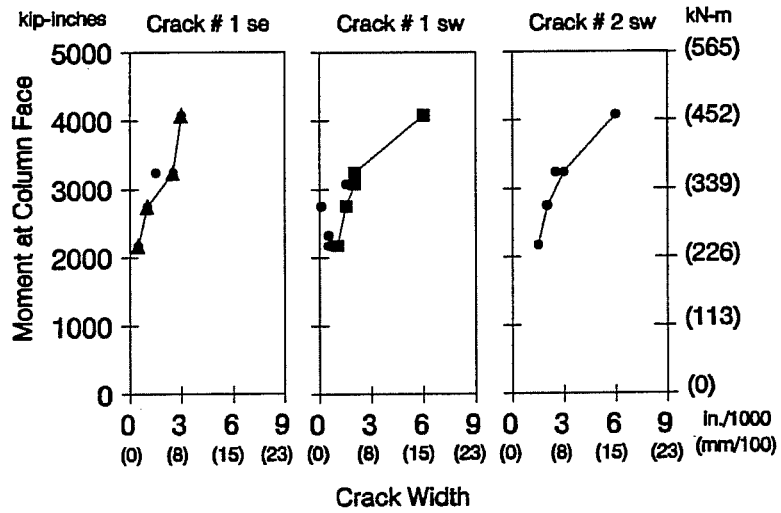


Figure 4.13 Crack plots for CO-PU-100S-TH-V overhang with "complete" loading curves, (above) "Major" crack plots, (below) "Crack Width Envelope"

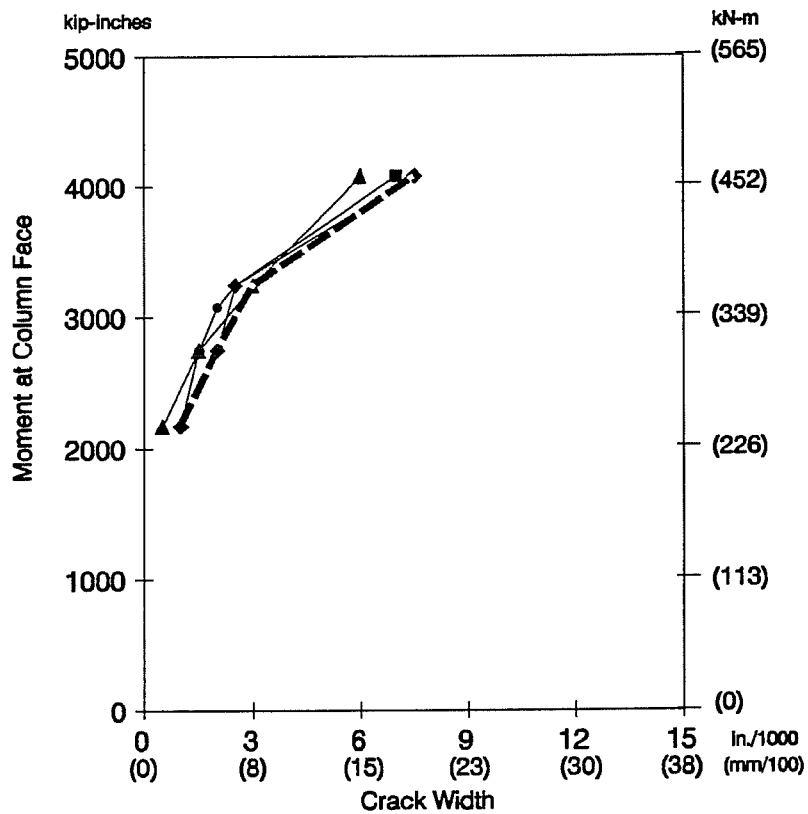
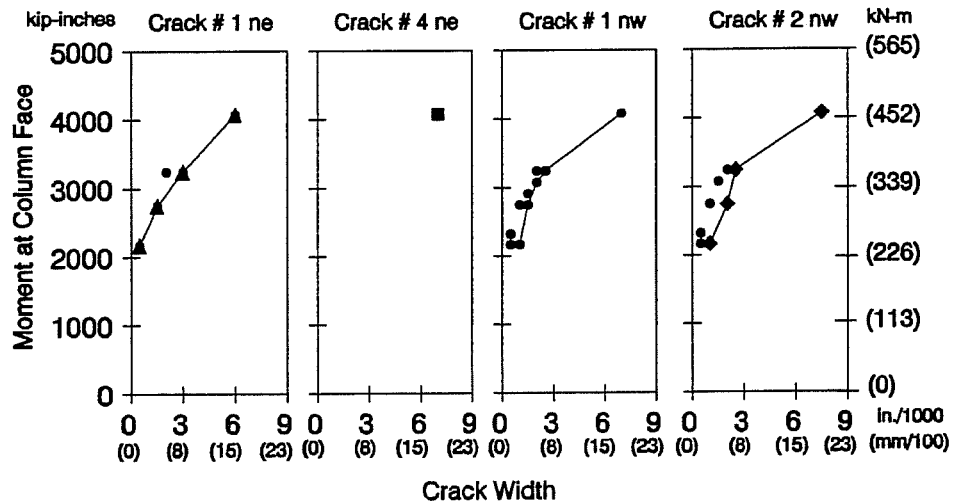


Figure 4.14 Crack plots for CO-PU-100S-TH-I overhang with "complete" loading curves, (above) "Major" crack plots, (below) "Crack Width Envelope"

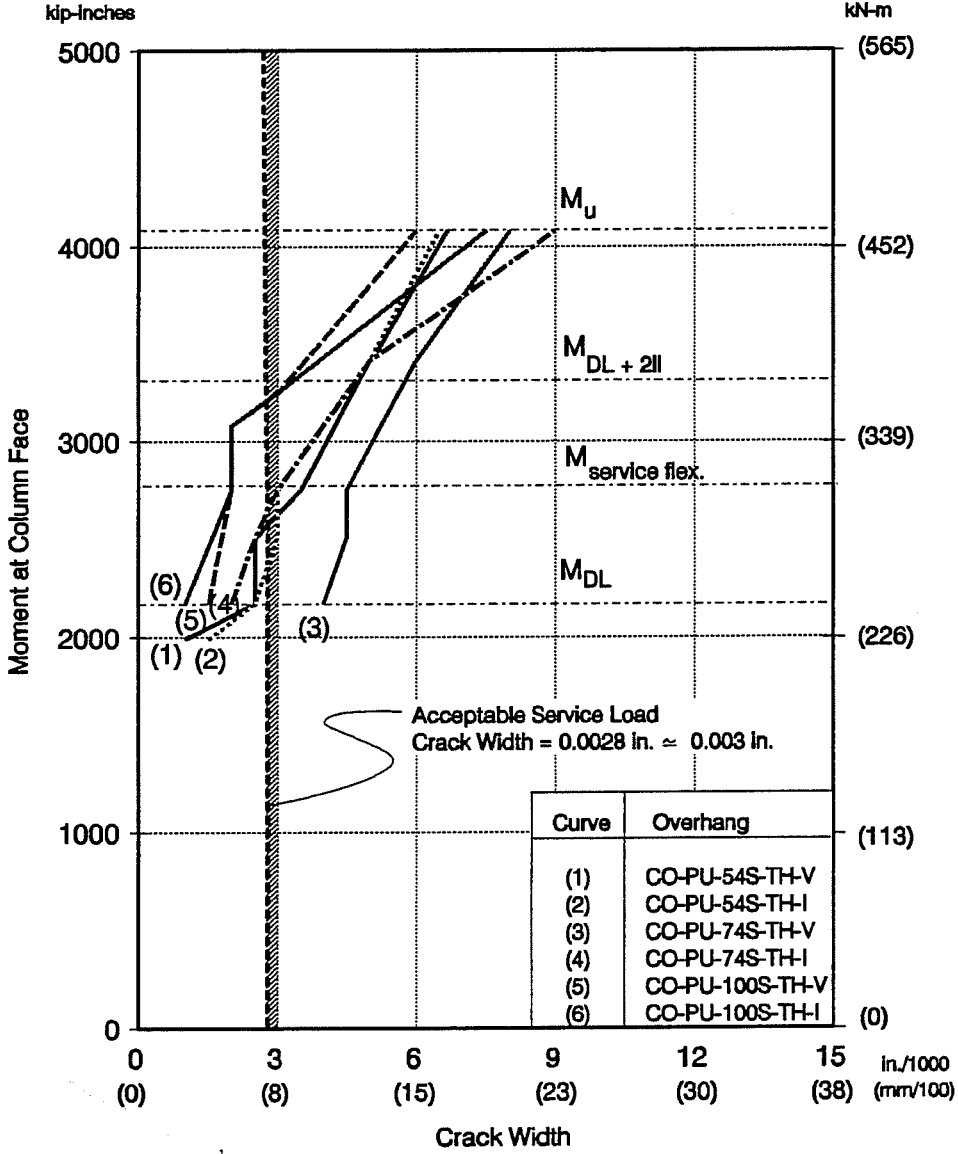


Figure 4.15 Comparison of Overhang "Crack width Envelopes" based on "complete" loading curves.

4.4.2 Predictions versus Test

Determination of the most probable maximum crack width on the tension face of the overhangs was carried out with the use of three equations. The first was introduced before as Equation 4.3 which was adopted in the ACI 318-89 Building Code [16]. This equation was originally recommended by Gergely and Lutz [17], and was simplified for design purposes by ACI. The second equation, Equation 4.4, is actually the original equation by Gergely and Lutz. The third equation, Equation 4.5, corresponds to an improved equation also suggested by those investigators [17].

As reported by Gergely and Lutz, Equation 4.5 is the preferred equation for the calculation of the most probable maximum crack width in the tension face of the beam. Equation 4.4 was suggested, and later adopted by ACI, because it was slightly simpler than Equation 4.5, recognizing that results may not be quite as good.

$$w = 0.076 \frac{h_2}{h_1} f_s (d_c A)^{1/3} \quad [4.4]$$

$$w = 0.091 \frac{h_2}{h_1} (f_s - 5) (d_c A)^{1/3} \quad [4.5]$$

where:

- w: crack width in units of 0.001 in.
- A = Ae/m : average effective concrete area around a reinforcing bar, in²
- Ae = 2 b' (h-d) : effective area of tension concrete surrounding tensile reinforcement, in²
- m: number of tensile reinforcing bars
- b': width of beam at centroid of tensile reinforcement, in.
- h: overall depth of beam, in.
- d; effective depth of beam to centroid of tensile reinforcement, in.
- d_c: thickness of concrete cover measured from extreme tension fiber to center of bar or wire located closest thereto, in.

- f_s : steel stress in non-prestressed reinforcement calculated by elastic cracked section theory, ksi
- $h_2 = h - kd$
- $h_1 = d - kd$
- k : distance from neutral axis to compression face divided by the effective depth of beam.

Equations 4.3 to 4.5 were developed for reinforced concrete structures. To apply them to post-tensioned structures some modifications had to be made. To this end, variables involved were manipulated until acceptable predictions were obtained when compared to test results.

For the calculation of A (average effective concrete area surrounding a reinforcing bar), the factor m (number of bars) was calculated using three different methods:

a) Considering the actual number of all non-prestressed bars in the tension zone, independent of the size of those bars; and considering the post-tensioning tendon as if it were a non-prestressed bar of the largest size of non-prestressed reinforcement present.

b) Considering the total area of steel in the tension zone, including the area of all prestressed reinforcement (irrespective of the degree of prestress as recommended by Suri et. al. [18]) and all non-prestressed reinforcement, and dividing that total area of reinforcing steel by the area of the largest size non-prestressed reinforcement bar present, and

c) Considering the total area of non-prestressed reinforcement in the tension zone, adding the post-tensioning tendons as if they were non-prestressed bars of the largest size non-prestressed reinforcement present, and dividing that total area of reinforcing steel by the area of the largest size non-prestressed reinforcement bar present.

This analysis was performed using test results from models CO-PU-54S-TH (V&I) and CO-PU-74S-TH (V&I). Models CO-PU-100S-TH (V&I) were not considered since these overhangs were uncracked at service load level. Table 4.3 shows the results after the comparison of the three options. To obtain these results all other variables involved in the crack width calculations were maintained constant. As can be noticed, options a) and b) gave in general the best predictions. The exception was observed when using option b) for model CO-PU-74S-TH-V where the prediction differed considerably from test results. Considering that option a) was

consistent and gave acceptable predictions which were most of the time conservative, with an average ratio of test results to predicted values of 0.96, this was the procedure selected.

Table 4.3 Values of Test vs. Predicted Maximum Crack Widths based on three options to account for prestressed and non-prestressed reinforcement

Model	Ratio of Test to Predicted Crack Width*		
	Option a)	Option b)	Option c)
CO-PU-54S-TH-V	0.89	0.92	0.89
CO-PU-54S-TH-I	0.89	0.89	0.81
CO-PU-74S-TH-V	1.1	1.32	1.1
CO-PU-74S-TH-I	0.97	1.02	0.88
Average ratio	0.96	1.04	0.92

* Test results based on complete loading. See Table 4.4

In addition to the above, two other variables were studied to adapt the Gergely and Lutz expressions to post-tensioned structures. These were the steel stress and the effective depth of beam. For these variables it was not necessary to test several options since the first trial gave very good results. The first, the steel stress, was taken as the steel stress in the non-prestressed reinforcement calculated by elastic cracked section theory, irrespective of the effective prestress in the tendons. The second, the effective depth, was calculated based on the location of the centroid of the primary flexural reinforcement (ignoring skin steel).

Table 4.4 shows the predicted crack widths for each overhang using Equations 4.3, 4.4, and 4.5 with the proposed modifications as discussed above. In the same table results are compared with test data and allowable values. For models CO-PU-54S-TH (V&I) and CO-PU-74S-TH (V&I) the three equations were very similar in predicting the most probable maximum crack widths, within ± 13 percent of the test results in the worst cases. Since models CO-PU-100S-TH (V&I) were not cracked at service flexure loads, predictions differed significantly from the zero test values. In this respect, it has to be recognized that cracks were not visually detected

in the overhangs until they reached a minimum of 0.001 in. (0.025 mm), and in models CO-PU-100S-TH (V&I) cracks were first observed just above service flexure loads. This suggests that small cracks could have existed in those overhangs at service flexure load level, which could give a better agreement with predicted values.

Based on the results above, it can be concluded that the use of any of the three expressions for the prediction of the most probable maximum crack widths can be applied with reasonable, if not excellent, accuracy to structural concrete if the modifications are considered. It has to be recognized that scatter in crack widths is always very large even in ordinary reinforced concrete structures [17]. In fact, in the derivation of the Gergely and Lutz expression (Equation 4.3) 10 percent of the data exceeded 1.5 times the crack width predicted by the equation, while two percent were less than 0.5 times the calculated width [19].

In summary, recommendations to apply the Gergely and Lutz expressions to structures with a mixture of prestressed and non-prestressed reinforcement are:

a) For the calculation of A_e , the effective area of concrete surrounding the tension reinforcement, it is recommended to use the actual number of non-prestressed bars present in the tension zone, and then add to that number an equivalent non-prestressed bar of the largest size present to account for each bonded prestressed strand.

b) The steel stress should be that for the non-prestressed reinforcement calculated by elastic cracked section theory.

c) The effective depth of beam should be calculated based on the primary flexural reinforcement (ignoring skin steel).

It has to be clear that results presented herein refer to models using single straight strands as tendons. It is not known at this stage if these results could be extrapolated to models with multi-strand tendons or with high strength bars instead of strands.

For the procedure above, steel stresses were determined using a program in the form of a spreadsheet. The program was developed by Bradley Wood specifically for the models in Series 1364-1A and Series 1364-1B.

Table 4.4 Predicted Crack Widths versus Test Results

Model	Predicted Crack Width						Test Results				Allowable service load crack width as per AASHTO[15]	
	EQ. 4.3**		EQ. 4.4**		EQ. 4.5**		Maximum crack width at full service loads		Complete Loading		in.	(mm)
	in.	(mm)	in.	(mm)	in.	(mm)	in.	(mm)	in.	(mm)		
							Virgin Loading					
CO-PU-54S-TH-V	0.0038 -0.92-*	(0.0965) -0.92-	0.0039 -0.90-	(0.0991) -0.90-	0.0039 -0.89-	(0.0998) -0.89-	0.0030	(0.0762)	0.0035	(0.0889)	0.0028	(0.0711)
CO-PU-54S-TH-I	0.0034 -0.89-	(0.0854) -0.89-	0.0035 -0.87-	(0.0879) -0.87-	0.0035 -0.87-	(0.0876) -0.87-	0.0030	(0.0762)	0.0030	(0.0762)	0.0028	(0.0711)
CO-PU-74S-TH-V	0.0041 -1.10-	(0.1035) -1.10-	0.0042 -1.08-	(0.1060) -1.08-	0.0041 -1.10-	(0.1039) -1.10-	0.0040	(0.1016)	0.0045	(0.1143)	0.0028	(0.0711)
CO-PU-74S-TH-I	0.0031 -0.97-	(0.0786) -0.97-	0.0032 -0.93-	(0.0821) -0.93-	0.0031 -0.98-	(0.0776) -0.98-	0.0025	(0.0635)	0.0030	(0.0762)	0.0028	(0.0711)
CO-PU-100S-TH-V	0.0012	(0.0301)	0.0013	(0.0331)	0.0006	(0.0153)	0.0000	(0.0000)	0.0000	(0.0000)	0.0028	(0.0711)
CO-PU-100S-TH-I	0.0013	(0.0328)	0.0014	(0.0364)	0.0007	(0.0181)	0.0000	(0.0000)	0.0000	(0.0000)	0.0028	(0.0711)

* Values between dashes are ratios of test under complete loading to predicted crack widths.

** Refer to Section 4.4.1 and 4.4.2

4.4.3 Brief Discussion on Maximum Crack Width limits

The purpose of this section is to provide and compare provisions in different codes of practice with respect to crack width limits in structural concrete structures. No attempt is made to define, from basic performance characteristics such as corrosion protection, what should be an adequate limiting value for maximum crack widths in concrete structures designed with a mixture of prestressed and non-prestressed reinforcement. Such a study is outside the scope of the present study but is important and should be undertaken.

In the previous sections, test results were compared against the allowable maximum crack width at service load level based on current AASHTO Standard Specifications for Highway Bridges for the serviceability of ordinary reinforced concrete structures under moderate exposure conditions. This was done basically because TxDOT typically bases their bridge designs on the AASHTO Specifications and these do not yet provide provisions for concrete structures designed with a mixture of prestressed and non-prestressed reinforcement. The limiting value for the maximum crack width was calculated as 0.0155 in. (0.394 mm) for the prototype structure and 0.0028 in. (0.071 mm) for the models, assuming linear scaling of cracks as proposed by Borges and Lima [20].

When studying the serviceability requirements in the AASHTO Specifications, it is important to recognize that AASHTO also provides more strict limits for those structures which would be subjected to severe exposure conditions. In this case the AASHTO Specifications recommend that the value of "z", as shown in Equation 4.2 above, should not exceed 130 kips per inch (23 kN/mm), corresponding to a calculated crack width of 0.0119 in. (0.302 mm) for the prototype structure and 0.0022 in. \approx 0.002 in. (0.055 mm) for the models.

In a like manner, provisions in the ACI-318-89 Building Code, in terms of crack width limits, are also expressed exclusively for the treatment of non-prestressed reinforced concrete structures. The ACI Code recommends maximum values of z of 175 kips per inch (31 kN/mm) for interior exposure and 145 kips per inch (25 kN/mm) for exterior exposure, which correspond to maximum crack widths of 0.016 in. (0.406 mm) and 0.013 in. (0.330 mm) for the prototype structure; and 0.0029 in. \approx 0.003 in. (0.074 mm) and 0.0024 in. \approx 0.0025 in. (0.060 mm) for the models, respectively.

To date, US bridge or building design codes have not specifically addressed limits for maximum crack widths in concrete structures using a mixture of prestressed and non-prestressed

reinforcement for flexure, which have been designed using the ultimate strength approach. In fact, these structures are not yet explicitly allowed under those standards. It is clear though, that crack widths in these structures should probably not exceed the limits for ordinary reinforced concrete structures. Moreover, it is anticipated that when considering the higher vulnerability of prestressed reinforcement to corrosion and the high level of risk that is involved, those limitations should possibly be more severe.

Looking at the Canadian Standards Association code (CSA Committee A23.3, Design of Concrete Structures for Buildings 1984 [21]), it is observed that this code already includes some provisions for structures designed with a mixture of prestressed and non-prestressed reinforcement. With respect to crack width limits, maximum values of z of 117 kips per inch (20 kN/mm) for interior exposure and 88 kips per inch (15 kN/mm) for exterior exposure are recommended. These values represent 67 percent and 60 percent, respectively, of those limits established by the CSA code and the ACI 318-89 code, since limits in both are the same for conventionally reinforced concrete structures. In terms of crack widths, these values correspond to 0.011 in. (0.270 mm) and 0.008 in. (0.200 mm) for the prototype structure and 0.002 in. (0.051 mm) and 0.0014 in. (0.037 mm) for the models.

In the same way, the current European Standard, CEB-FIP Model Code for Concrete Structures 1990 [22], developed by the Comité Euro-International du Béton, also establishes some limits on maximum crack widths for mixed reinforced concrete structures (Section 7.4). In this code instead of checking for full service load crack widths as in AASHTO, ACI and CSA, checks are performed with respect to the "frequent load level," which includes the dead load plus the frequently occurring live load. Using recommendations for parking areas, since this code does not explicitly provide provisions for bridge structures, the frequent load combination corresponds to 70 percent of the characteristic live load (the latter is the value which is not likely to be exceeded during more than 5 percent of the projected life of the structure). Recommendations in the CEB code in terms of crack width limits for post-tensioned members are summarized in Table 4.5. It can be noticed that for a structure that is to be in a humid environment, this code recommends the same crack width limit as the CSA code of 0.008 in. (0.2 mm).

Table 4.5 Summary of CEB-FIP-90 Crack Width Limits for Post-tensioned Structures under frequent load combination [22]

Exposure class	Limiting crack width**	
	in.	(mm)
1. Dry environment	0.008*	(0.2)
2. Humid environment	0.008*	(0.2)
3. Humid environment with frost and de-icing agents. 4. Sea-Water environment	a) No tension is allowed within the section, or b) if tension is accepted, impermeable ducts or coating of the tendons should be applied; in this case $w_{lim} = 0.008$ in. (0.2 mm)*	
5. Aggressive chemical environment	No tension is allowed within the section.	

* Corresponding limit in models at a 1/5.5 scale is 0.0014 in. (0.036 mm)

** For a cover equal to the minimum recommended by CEB.

It has to be recognized that the CEB-FIP 1990 Code has not yet been adopted for actual operational codes in Europe. Instead, the CEB-FIP 1978 Code [23] is being used as the base for Eurocode 2. Table 4.6 summarizes the recommendations in that earlier version of the CEB-FIP Code. As can be observed in these tables, exposure conditions were modified in the latest version as well as the maximum crack width limits. For example, for a structure under usual exterior exposure conditions without frost or deicing agents, the CEB-FIP 78 provisions recommend a maximum crack width limit of 0.004 in (0.1 mm). This is half the value that now is recommended for the same structure in the CEB-FIP-90 Code. Both sets are very stringent when compared to the AASHTO and ACI values.

Table 4.6 Summary of CEB-FIP-78 Crack Width Limits for Post-tensioned Structures under frequent load combination [23]

Exposure Conditions	Limiting crack width***	
	in.	(mm)
1. Mild - Interior Exposure - Low humidity exterior exposure	0.008*	(0.2)
2. Moderate - High humidity or slightly corrosive interior exposure. - Running water - Ordinary Soil exposure - Usual exterior exposure	0.004**	(0.1)
3. Severe - Seawater exposure - Deicing chemicals - Corrosive gases and soils	No tension allowed in concrete	No tension allowed in concrete

* Corresponding limit in models is 0.0014 in. (0.036 mm)

** Corresponding limit in models is 0.0007 in. (0.018 mm)

*** For a cover equal to the minimum recommended by CEB

To visualize how these crack width limits compare with test results, Figure 4.15 (which was presented before showing the comparison of overhang crack width envelopes based on complete loading curves) is reproduced in Figure 4.16. In this case controlling limits for maximum crack widths from each of the various standards are included. Controlling exposure conditions for the subject structures were selected corresponding to moderate exposure, exterior exposure, or dry or humid environment depending on the code.

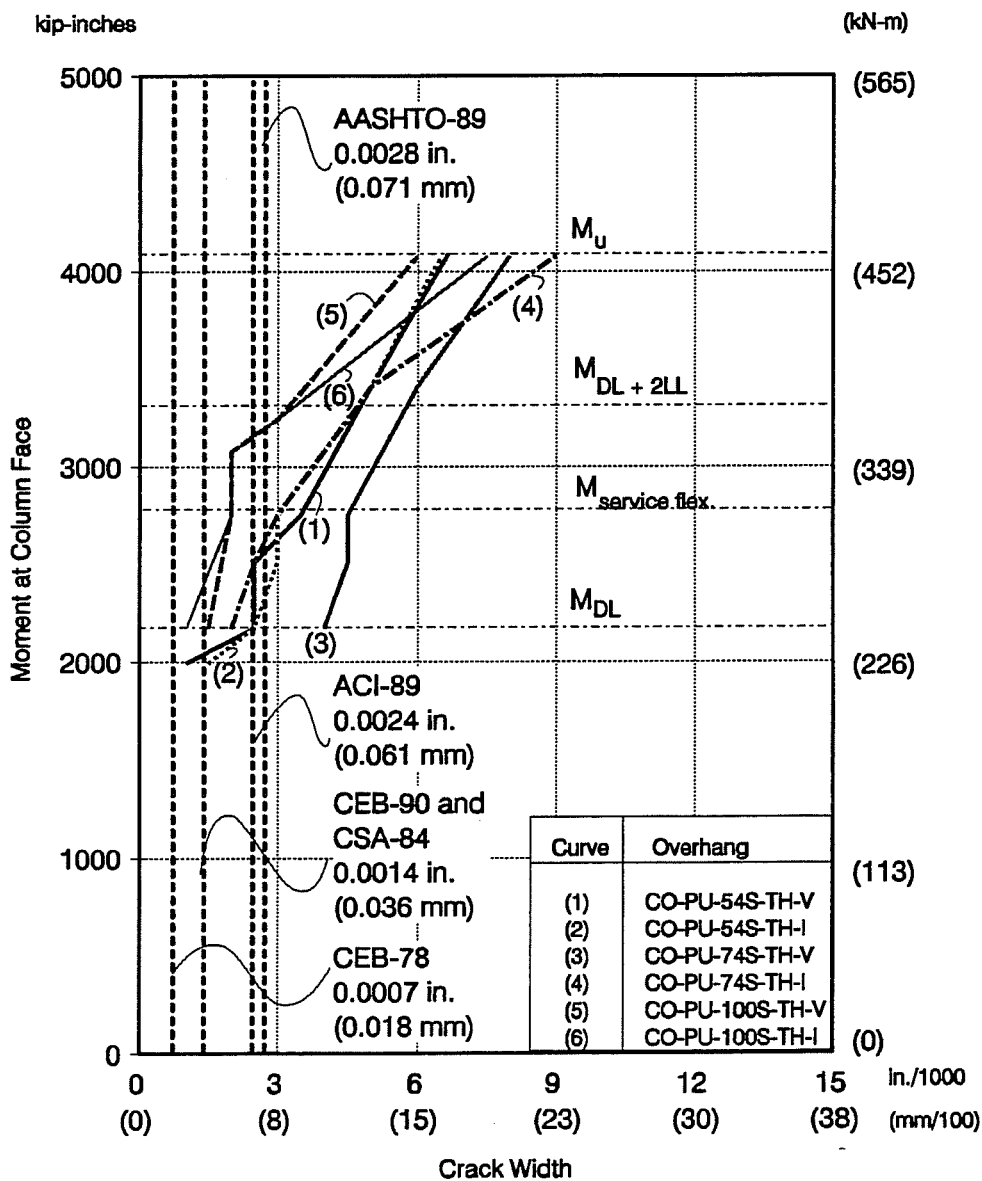


Figure 4.16 Performance of overhangs in terms of scaled maximum crack widths when compared to allowable values in different codes of practice (Overhang "Crack Width Envelopes" based on "complete" loading curves).

Analyzing the results in this figure, considering an accuracy in the crack width readings of ± 0.0005 in. (0.013), it can be observed that only overhangs CO-PU-100S-TH (V&I) met most of the codes, except for the CEB-FIP-78 where even these models were marginally above the limit. Models CO-PU-54S-TH (V&I) and CO-PU-74S-TH-I were approximately 200 percent above the limiting value set in CEB-FIP-90 and CSA. Model CO-PU-74S-TH-V was approximately 280 percent above that limit.

As can be noticed, crack width limits as established by the CEB-FIP-90 and the CSA codes were the same for these structures (designed with a mixture of prestressed and non-prestressed reinforcement) and corresponded to approximately half of the limiting values set in AASHTO and ACI, which are provisions exclusively for reinforced concrete structures. CEB-FIP-78 code provisions were more severe corresponding, in this case, to a maximum crack width limit of half that proposed in the new CEB-FIP-90 and CSA codes. This plot clearly shows the concern in those foreign codes for the presence of cracks in structures with any amount of prestressed reinforcement.

When analyzing the results above, it has to be recognized that the CSA crack width limits for structures designed with a mixture of prestressed and non-prestressed reinforcement, which would be under exterior exposure conditions, could be influenced by the widespread use of salt due to the severe climate. In much of Texas, for example, those limits could possibly be much less severe.

4.5 PERFORMANCE OF SKIN REINFORCEMENT

Results from various models, which were designed and detailed using different amounts of skin reinforcement, were compared and evaluated to determine the differences that the various amounts of face steel made in controlling crack widths at service load levels, and in general to evaluate skin reinforcement performance on the overall behavior of the specimens.

Four overhangs from this series (Series 1364-1B), overhangs CO-PU-54S-TH (V&I) and CO-PU-100S-TH (V&I) were selected to perform these analyses. Models CO-PU-74S-TH (V&I) were not considered since they were used to evaluate the performance of T-headed reinforcement bars.

As a summary of the design procedures actually utilized, face steel in models CO-PU-54S-TH-V and CO-PU-100S-TH-V was proportioned using the amount of skin reinforcement proposed by Frantz and Breen [6]. This corresponded with an area of skin reinforcement of 0.59 in² (381 mm²). Models CO-PU-54S-TH-I and CO-PU-100S-TH-I, as explained in Section 2.4.3, were not designed specifically for an area of skin reinforcement. Rather the skin steel reinforcement was calculated based on the side face reinforcing steel that was provided as part of the flexural design as well as the reinforcing steel provided in the detailing process for supporting stirrups. These models had an area of skin reinforcement of 0.29 in² (187 mm²).

Using the individual results from each overhang, two direct comparisons were made:

a) Model CO-PU-54S-TH-V versus Model CO-PU-54S-TH-I

These models were tested as part of the same specimen. Ultimate flexural capacities differed by six percent, as calculated by analytical methods. As mentioned previously, model CO-PU-54S-TH-I differed from model CO-PU-54S-TH-V since it did not include skin steel as per Frantz and Breen but it included some horizontal steel in the inside of the section to account for the horizontal component of the inclined tie that was used in the strut and tie model as presented in Section 2.4.2.

Table 4.7 shows the results from these models at each grid level at dead loads, at service shear load and at service flexure load. As can be noticed, considering an accuracy in the crack width readings of ± 0.0005 in. (0.013 mm), no significant differences were observed between the models. It has to be pointed out that, with very few exceptions, maximum crack widths were always at the top of the overhangs (at the locations of the extreme tension fibers).

With respect to crack patterns it is possible to refer to Figures 3.13, 3.7 and 3.8. From these figures, it can be noticed that at service flexure and factored flexure load levels these models were very similar. Above those load levels, as documented in Table 3.14, an average of three more flexural-shear cracks were observed on both sides of model CO-PU-54S-TH-V when compared with its companion overhang.

b) Model CO-PU-100S-TH-V (This series) versus model CO-PU-100S-TH-I (This series)

These models were tested as part of the same specimen. Ultimate flexural capacities differed by only four percent (as calculated by analytical methods).

Table 4.7 Maximum Crack Width at each grid level in models CO-PU-54S-TH-V and CO-PU-54S-TH-I
(Above: US Customary units, Below: SI Units)

Level **	Model CO-PU-54S-TH-V, Ask = 0.59 in2										Model CO-PU-54S-TH-I, Ask = 0.29 in2																			
	Dead Load					Service Shear					Service Flexure					Dead Load					Service Shear					Service Flexure				
	(LS 12*)					(LS 21*)					(LS 27*)					(LS 12*)					(LS 21*)					(LS 27*)				
	SE	SW	in	in	in	SE	SW	in	in	in	SE	SW	in	in	in	NE	NW	in	in	in	NE	NW	in	in	in	NE	NW	in	in	in
A	0.0005	0.0010	0.0020	0.0025	0.0025	0.0025	0.0025	0.0025	0.0025	0.0030	0.0030	0.0030	0.0030	0.0035	0.0035	--	0.0015	0.0015	0.0015	0.0015	0.0020	0.0020	0.0020	0.0025	0.0030	0.0025	0.0025	0.0025	0.0030	0.0030
A'	0.0010	0.0010	0.0015	0.0025	0.0025	0.0022	0.0030	0.0030	0.0030	0.0030	0.0025	0.0025	0.0025	0.0030	0.0030	--	0.0015	0.0015	0.0015	0.0015	0.0025	0.0025	0.0025	0.0025	0.0025	0.0015	0.0015	0.0015	0.0025	0.0025
B	--	0.0005	0.0010	0.0020	0.0020	0.0010	0.0015	0.0020	0.0020	0.0020	0.0010	0.0015	0.0020	0.0020	0.0020	--	--	--	--	--	0.0015	0.0015	0.0015	0.0015	0.0015	0.0015	0.0015	0.0015	0.0025	0.0025
C	--	--	0.0005	0.0010	0.0010	0.0005	0.0005	0.0010	0.0010	0.0010	0.0010	0.0010	0.0010	0.0010	0.0010	--	--	--	--	--	0.0010	0.0010	0.0010	0.0010	0.0010	0.0010	0.0010	0.0010	0.0020	0.0020
D	--	--	--	--	--	--	--	--	--	--	--	--	--	--	--	--	--	--	--	--	--	--	--	--	--	--	--	--	0.0010	0.0015
E	--	--	--	--	--	--	--	--	--	--	--	--	--	--	--	--	--	--	--	--	--	--	--	--	--	--	--	--	--	--

Level **	Model CO-PU-54S-TH-V, Ask = 380 mm2										Model CO-PU-54S-TH-I, Ask = 187 mm2																			
	Dead Load					Service Shear					Service Flexure					Dead Load					Service Shear					Service Flexure				
	(LS 12*)					(LS 21*)					(LS 27*)					(LS 12*)					(LS 21*)					(LS 27*)				
	SE	SW	(mm)	(mm)	(mm)	SE	SW	(mm)	(mm)	(mm)	SE	SW	(mm)	(mm)	(mm)	NE	NW	(mm)	(mm)	(mm)	NE	NW	(mm)	(mm)	(mm)	NE	NW	(mm)	(mm)	(mm)
A	0.013	0.025	0.051	0.064	0.064	0.064	0.064	0.064	0.064	0.089	0.064	0.064	0.064	0.089	--	0.038	0.038	0.038	0.038	0.051	0.051	0.051	0.051	0.051	0.064	0.064	0.064	0.064	0.064	
A'	0.025	0.025	0.038	0.064	0.064	0.056	0.076	0.076	0.076	0.076	0.064	0.064	0.064	0.076	0.076	--	0.038	0.038	0.038	0.038	0.064	0.064	0.064	0.064	0.064	0.038	0.038	0.038	0.064	0.064
B	--	0.013	0.025	0.051	0.051	0.025	0.038	0.038	0.038	0.051	0.025	0.038	0.038	0.051	0.051	--	--	--	--	--	0.038	0.038	0.038	0.038	0.038	0.038	0.038	0.038	0.051	0.051
C	--	--	0.013	0.025	0.025	0.013	0.013	0.013	0.013	0.025	0.013	0.013	0.013	0.025	0.025	--	--	--	--	--	0.025	0.025	0.025	0.025	0.025	0.025	0.025	0.025	0.025	0.025
D	--	--	--	--	--	--	--	--	--	--	--	--	--	--	--	--	--	--	--	--	--	--	--	--	--	--	--	--	0.025	0.038
E	--	--	--	--	--	--	--	--	--	--	--	--	--	--	--	--	--	--	--	--	--	--	--	--	--	--	--	--	--	--

* Refer to Table 2.17

** Refer to Figures 3.7 and 3.8

As reported previously, these models first cracked above service flexure load level. For this reason, it was obviously not possible to obtain any data with respect to the performance of skin reinforcement at service loads. In spite of that, an important contribution of the skin reinforcement, proportioned as per Frantz and Breen, was observed at high load levels up to ultimate loads. As shown in Figures 3.11 and 3.12, both models exhibited the same number of cracks at factored flexure load. At ultimate loads model CO-PU-100S-TH-V showed approximately double the number of cracks. These results can be observed in Figure 4.17, and in Table 3.14 where the number of cracks at each major load stage are summarized.

Based on the above discussion, it can be concluded that skin reinforcement for these type of structures, designed as per Frantz and Breen, does not provide significant improvement for crack control at service and factored load levels. However, it provides a great deal of distribution of cracks above these loads up to ultimate. Considering that the distribution of cracks at these load levels is certainly beneficial and healthy (which provides a better distribution of the tensile forces in the horizontal steel and better overall ductility in the member), it is concluded that the minimum reinforcement suggested by Frantz and Breen should be used.

It is very important to recognize, that recommendations by Frantz and Breen were actually developed for deep structures in which the maximum crack width would not occur in the extreme tensile fibers, as it did in most of the models tested as part of this series, but somewhere in the face of the structure between the locations of the flexural reinforcement. In all models, the major crack width was at the level of the main flexural reinforcement. Thus, the skin steel provided in all models was sufficient to control side face cracking.

4.6 PERFORMANCE OF T-HEADED REINFORCEMENT

T-headed reinforcing bars were used for the main flexural reinforcement #2 bars, as an alternative for the commonly used standard hooks. The purpose was to evaluate their performance in crack control, in reducing congestion in anchorage areas, and in improving constructability of the reinforcing cages, when compared to results from Series 1364-1A.

To this end, models CO-PU-74S-TH (V&I) were designed, constructed and tested maintaining the same characteristics of models CO-PU-74S (V&I) from Series 1364-1A, but only replacing the standard hooks with T-heads. By maintaining all the other variables in the project without change, performance of T-headed reinforcement could be adequately evaluated.

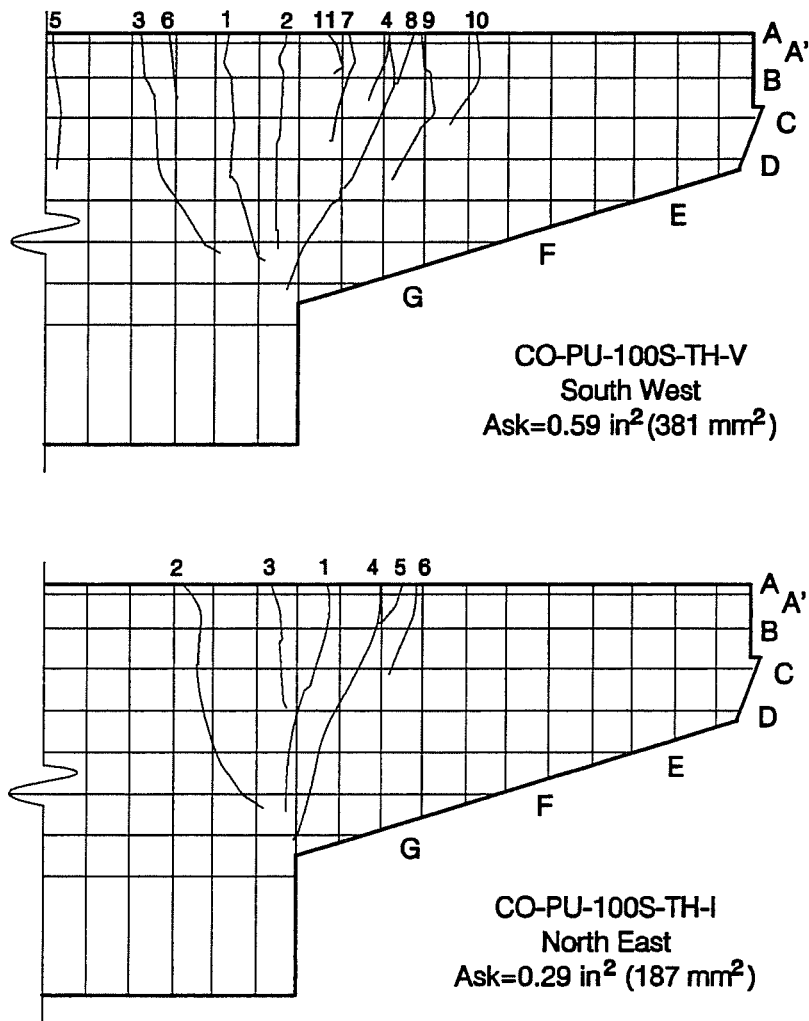


Figure 4.17 Comparison of Crack Patterns in Models CO-PU100S-TH-V and CO-PU-100S-TH-I at failure

Analyzing the results in terms of constructability, T-headed reinforcing bars were found to reduce significantly the time necessary to build the reinforcing cages. Additionally, they proved to be very helpful for facilitating placement of the post-tensioning anchorage zone reinforcement. Congestion in the anchorage area was reduced by approximately 50 percent, resulting in better placement and consolidation of the concrete mix .

With respect to crack control at service load levels, no major improvements were observed. Both specimens CO-PU-74S-TH (V&I) and CO-PU-74S (V&I) showed very similar cracking patterns and maximum crack widths. Additionally, the overall behavior up to ultimate loads was very similar. Figure 4.18 shows a comparison of the moment-deflection response of these models.

After analyzing the strain gage data, Figure 3.2 (gage fx1), it can be observed that the strain in the reinforcing bar near the location of the head was negligible throughout the entire range of static loading. This showed, as expected, that reinforcing bars were already developed before any tensile force would reach the heads. This was true for all models. Based on these results one could even question the need for any special anchorage system at the end of the non-prestressed reinforcement. In this respect, it has to be recognized that different patterns of cracking may occur during the service life of the structure due to the variable conditions to which this type of overhang structure is exposed, including other load cycles. It is anticipated that any crack forming near the end of the cantilever would create additional stresses in the reinforcing bars that would call for enough development of the tension force to avoid any slippage. More research needs to be conducted including fatigue performance of the specimens to better conclude this subject.

Concentrating on the comparison between the use of standard hooks and T-heads, it can be concluded from the above discussion that in general for this type of application, T-heads:

- improve considerably the constructability of the cages
- reduce congestion in anchorage areas by more than 50 percent
- improve placement and consolidation of the concrete mix in the anchorage areas
- do not provide any improvements in terms of crack control.

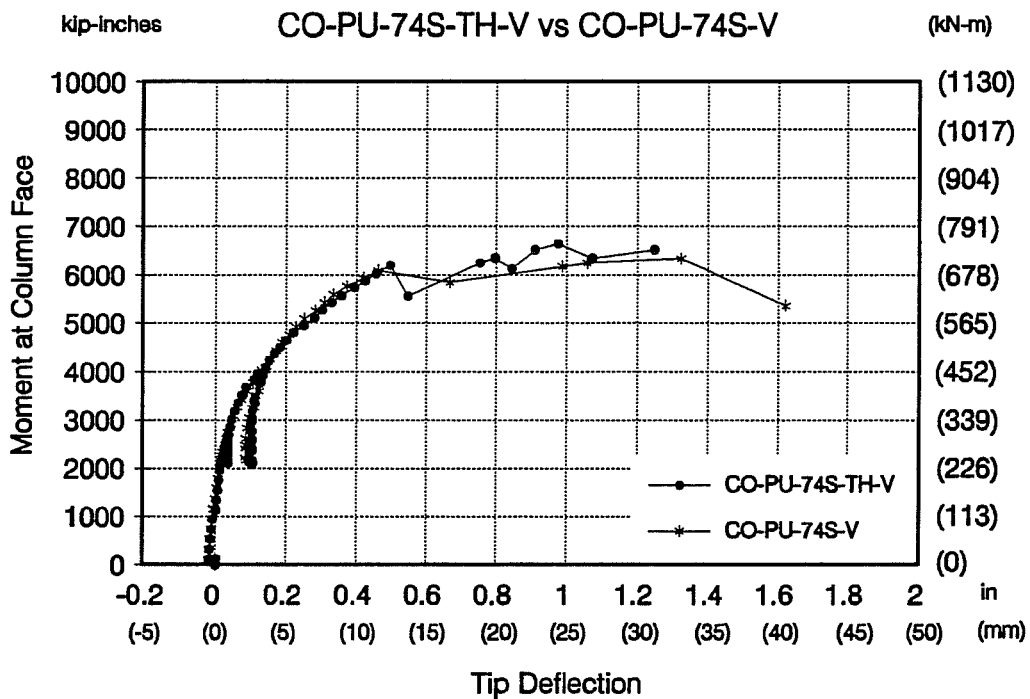
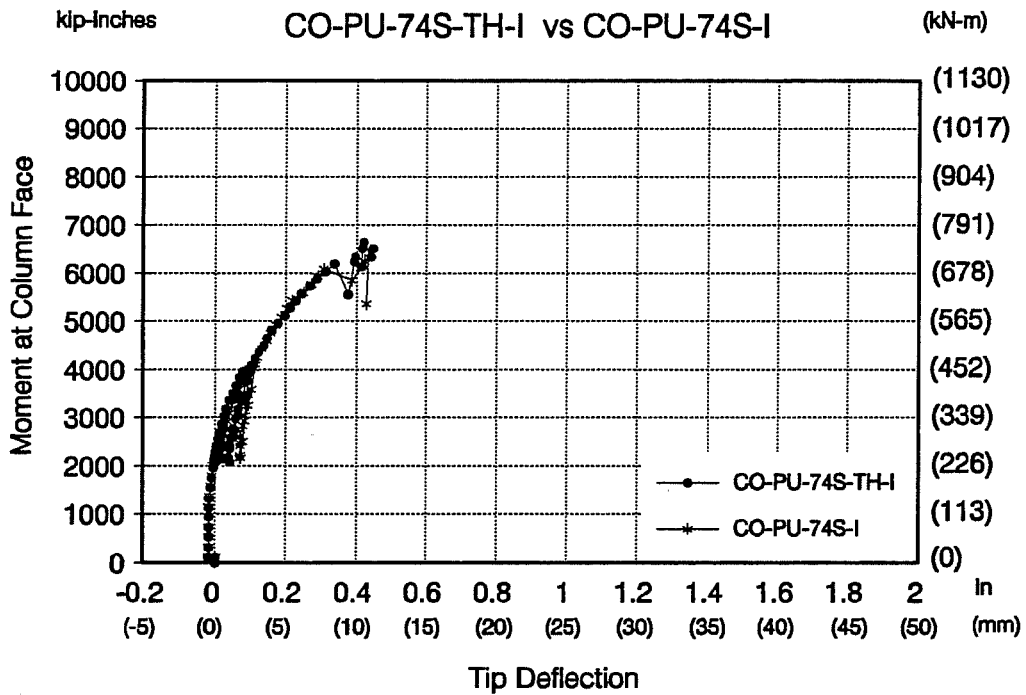


Figure 4.18 Comparison of Moment-Deflection responses of Models CO-PU-74S-TH (V&I) using T-heads versus Models CO-PU-74S (V&I) using Standard Hooks.

4.7 STRESS RANGES

Stress ranges for all models were presented in Table 2.11 and were briefly discussed in Section 2.4.6.

As mentioned in that section, Wollmann, et. al. [10] recommended that for structures which have to withstand a minimum of two million cycles, stress ranges should not exceed 14.5 ksi (between the load levels of full dead load and full dead load plus live load with impact). A similar limiting value was reported by other investigators [24].

Based on these recommendations, the CO-PU-54S-TH (V&I) models as well as the CO-PU-100S-TH (V&I) models were adequate in terms of fatigue life, with values below the limit. On the other hand, model CO-PU-74S-TH-I was marginally above and model CO-PU-74S-TH-V was substantially above, with a stress range of 18.2 ksi.

Some recommendations to improve the fatigue design life of these models would be either to provide additional non-prestressed flexural reinforcement in the tensile zone, or rearrange the prestressing steel to be farther away from the extreme tensile face of the specimen, which could require the use of an increased area of prestressed reinforcement. Either of these solutions could be part of a design that would also contribute to a better distribution and control of cracks.

4.8 ULTIMATE FLEXURAL CAPACITY

Predicted flexural capacities were calculated based on a strain compatibility analysis, as well as with the use of approximate formulations for ultimate capacity recommended in the 1990 Interim specifications of the AASHTO-89 code and the ACI-318-89 code. Table 4.8 shows a comparison of the predicted capacities versus test results.

The strain compatibility analysis was performed assuming a linear strain profile over the depth of the beam. In this analysis, actual stress-strain properties for concrete and prestressed and non-prestressed reinforcement were used. Any reinforcement present in the critical section (face of the column), either in tension or compression, was taken into account. The criteria for the calculation of the ultimate moment corresponded to the occurrence of a strain in the concrete extreme compressive fiber of 0.003 in./in. (mm/mm). For the calculation of the ultimate moment an equivalent rectangular stress block was assumed.

Table 4.8 Model Flexural Capacities

Model	Predicted Flexural Capacity (Mn)			Test Capacity (Mn) kip-in (kN-m)
	Strain-Compatibility kip-in (kN-m)	AASHTO [11] kip-in (kN-m)	ACI-318-89 kip-in (kN-m)	
CO-PU-54S-TH-V	5252 (593.5) -1.15- *	5814 (657.0) -1.04-	5200 (588.0) -1.16-	6046 (683.0)
CO-PU-54S-TH-I	5606 (633.5)	5975 (675.0)	5574 (630.0)	NA **
CO-PU-74S-TH-V	4799 (542.0) -1.39-	5039 (569.0) -1.32-	4752 (537.0) -1.40-	6648 (751.0)
CO-PU-74S-TH-I	5356 (605.0)	5610 (634.0)	5258 (594.0)	NA
CO-PU-100S-TH-V	5969 (674.5)	6129 (692.5)	5814 (657.0)	NA
CO-PU-100S-TH-I	5730 (647.5) -1.09-	5882 (664.5) -1.06-	5596 (632.0) -1.11-	6232 (704.0)
Average	-1.21-	-1.14-	-1.22-	—
Average without considering model CO-PU-74S-TH-V***	-1.12-	-1.05-	-1.14-	—

* Values between dashes are ratios of test to predicted capacities.

** NA: Not applicable

*** This model was tested without elastomeric pads, which affected the ultimate capacity.

Approximate predictions based on AASHTO (1990 Interim specifications) were performed without considering the contribution from any reinforcement in compression, as it is not included in the recommended formulations. On the other hand, calculations based on ACI-318-89 (Section 18.7.2) did take into account that reinforcement.

Analyzing these results, it can be noticed that the prediction of the capacity based on AASHTO was in general the most accurate. The results from the strain compatibility analysis did not give a better prediction of the capacity, contrary to what might be expected. This analysis

predicts maximum tensile stresses in the non-prestressed steel of approximately two percent, which in fact during testing and based on the post-mortem investigations (which showed breaking of the bars at failure) were observed to be higher.

For the model CO-PU-74S-TH-V there is a large difference between predicted flexural capacities and test. The reason for these results was associated with the problem of extra friction forces between the steel bearing plates. In fact, it was at ultimate loads that this problem was most pronounced.

CHAPTER 5 CONSTRUCTABILITY AND ECONOMICS

5.1 CONSTRUCTABILITY

Constructability of the overhangs in Series 1364-1A and in this series, Series 1364-1B, was of major concern throughout this experimental program. Results from Series 1364-1A showed important differences between those models designed following current AASHTO provisions (for reinforced concrete and fully prestressed concrete members) when compared to those structures designed with the ultimate strength approach governing for flexure and a mixture of prestressed and non-prestressed reinforcement. In general, ease of construction varied with the amount of steel (prestressed and non-prestressed) in the models. When more steel was present, particularly as in the non-prestressed structures, construction of the cages took longer and the difficulty in placing the concrete mix was increased.

Results from this series (corresponding only to models designed with the strength design approach and a mixture of prestressed and non-prestressed reinforcement) showed a similar relationship between constructability and amount of reinforcement. However, in this case differences between models were not really significant. The major difference was found when compared to those models in Series 1364-1A, since the constructability of all models in Series 1364-1B was notably improved with the use of T-headed reinforcing bars.

T-headed reinforcement was found to reduce significantly the time necessary to build the reinforcing cages, was shown to ease placement of the post-tensioning anchorage zone reinforcement, and resulted in improved placement and consolidation of the concrete mix in anchorage areas. Conservatively, it was estimated that T-headed bars improved the time of construction of the reinforcing cages by at least 30 percent.

Independent of the use of T-headed reinforcement, when compared to the other models of Series 1364-1B, models CO-PU-54S-TH (V&I) were the most time consuming with respect to the construction of the reinforcing cages. However, because of the smaller quantity of post-tensioning reinforcement, these overhangs were the easiest to prestress and grout. As a result, the overall time of construction of these cages including all post-tensioning operations, was just slightly greater than the time of construction of all the other models of Series 1364-1B, including CO-PU-74S-TH (V&I) and CO-PU-100S-TH (V&I).

Models CO-PU-74S-TH (V&I) were not too different from the CO-PU-54S-TH (V&I) models. These overhangs did not include the skin reinforcement suggested by Frantz and Breen, which resulted in easier construction of the cages, but prestressing operations took more time and effort than models CO-PU-54S-TH (V&I).

Reinforcing cages for models CO-PU-100S-TH (V&I) were the easiest of the Series 1364-1B models to construct. These cages were the least congested. However, placement and tying of the ducts, and placement of the grout tubes was more difficult. Additionally, prestressing operations were performed in double the time when compared with models CO-PU-54S-TH (V&I), which suggested a direct relationship between the time to perform prestressing operations and the amount of prestressed reinforcement in the models. As a result, the time to construct these models was just slightly below the time to construct overhangs CO-PU-54S-TH (V&I) and CO-PU-74S-TH (V&I).

With respect to the ease of placement and adequate consolidation of the concrete mix, all models of Series 1364-1B showed very similar characteristics. The major advantage was in fact the use of T-headed reinforcement.

When the overall combined specimens of Series 1364-1A and 1364-1B are considered, constructability of the specimens with a mix of non-prestressed and prestressed flexural reinforcement was significantly better than either the non-prestressed specimens or the fully prestressed specimens.

5.2 ECONOMICS

To evaluate and compare the overhangs with respect to their estimated costs, reinforcing bars and wires in the models had to be converted into prototype reinforcement. Reinforcing bars were selected depending on the scaled bar area (model bar area multiplied by 5.5²), and the yield strength that would be used in design, 60 ksi (414 MPa). The equivalent non prestressed bars for the prototype structures were selected as shown below:

<u>Model</u>	<u>Prototype</u>
1 - # 2 reinforcing bar	1.15 - # 11 reinforcing bars
1 - 7 gage wire	1.3 - # 8 reinforcing bars
1 - 10 gage wire	1 - # 6 reinforcing bar

The prestressed reinforcement in the models, which consisted on 1/2 in. (13 mm) diam. strands and 3/8 in. (9.5) diam. strands, was converted into 19-0.6 in. (15 mm) diam. strand tendons, 12-0.6 in. (15 mm) diam. strand tendons or 7-0.6 in. (15 mm) diam. strand tendons, depending on the prototype post-tensioning force requirements. This was done since some of the tendon sizes were found to be common in TxDOT designs.

Tables 5.1 and 5.2 show the quantities of non-prestressed and prestressed reinforcement per model, respectively. A summary of total quantities is presented in Table 5.3.

Figure 5.1 shows the comparison of the total reinforcing weights per overhang. Here all results from Series 1364-1A were included. As can be observed, overhangs CO-PU-74S-TH (V&I) did not differ much from overhangs CO-PU-100S-TH (V&I), and as expected, overhangs CO-PU-54S-TH (V&I) presented the highest total reinforcement quantity of the six structures in Series 1364-1B.

Table 5.1 Non-Prestressed Reinforcement Quantities in Prototype Overhangs
(Above: US customary units, Below: SI units)

Model	#6 rebar		#8 rebar		#11 rebar		Total non-prestressed reinforcement
	ft	lb	ft	lb	ft	lb	lb
CO-PU-54S-TH-V	2238	3362	319	853	748	3974	8188
CO-PU-54S-TH-I	2212	3322	934	2494	612	3251	9068
CO-PU-74S-TH-V	1963	2948	251	669	323	1716	5333
CO-PU-74S-TH-I	1987	2985	665	1777	323	1716	6477
CO-PU-100S-TH-V	1963	2948	396	814	272	1445	5207
CO-PU-100S-TH-I	1987	2985	524	1400	136	723	5107

Model	#6 rebar		#8 rebar		#11 rebar		Total non-prestressed reinforcement
	(m)	(kg)	(m)	(kg)	(m)	(kg)	(kg)
CO-PU-54S-TH-V	(682)	(1513)	(97)	(384)	(228)	(1788)	(3685)
CO-PU-54S-TH-I	(674)	(1495)	(285)	(1123)	(187)	(1463)	(4080)
CO-PU-74S-TH-V	(598)	(1327)	(76)	(301)	(98)	(772)	(2400)
CO-PU-74S-TH-I	(606)	(1343)	(203)	(800)	(98)	(772)	(2915)
CO-PU-100S-TH-V	(598)	(1327)	(121)	(366)	(83)	(650)	(2343)
CO-PU-100S-TH-I	(606)	(1343)	(160)	(630)	(41)	(325)	(2298)

Table 5.2 Prestressed Reinforcement Quantities in Prototype Overhangs
(Above: US customary units, Below: SI units)

Model	7 strand tendon *		12 strand tendon *		19 strand tendon *		Total prestressed reinforcement
	ft	lb	ft	lb	ft	lb	lb
CO-PU-54S-TH-V	20	104	0	0	60	851	955
CO-PU-54S-TH-I	20	104	0	0	60	851	955
CO-PU-74S-TH-V	0	0	20	178	80	1135	1313
CO-PU-74S-TH-I	0	0	20	178	80	1135	1313
CO-PU-100S-TH-V	20	104	0	0	120	1701	1805
CO-PU-100S-TH-I	20	104	0	0	120	1701	1805

Model	7 strand tendon *		12 strand tendon *		19 strand tendon *		Total prestressed reinforcement
	(m)	(kg)	(m)	(kg)	(m)	(kg)	(kg)
CO-PU-54S-TH-V	(6)	(47)	(0)	(0)	(18)	(383)	(430)
CO-PU-54S-TH-I	(6)	(47)	(0)	(0)	(18)	(383)	(430)
CO-PU-74S-TH-V	(0)	(0)	(6)	(80)	(24)	(511)	(591)
CO-PU-74S-TH-I	(0)	(0)	(6)	(80)	(24)	(511)	(591)
CO-PU-100S-TH-V	(6)	(47)	(0)	(0)	(37)	(765)	(812)
CO-PU-100S-TH-I	(6)	(47)	(0)	(0)	(37)	(765)	(812)

* 0.6 in. (15 mm) diameter strands

Table 5.3 Summary of Reinforcement Quantities in Prototype Overhangs
(Above: US customary units, Below: SI units)

Model	Non-prestressed reinforcement		Prestressed reinforcement		Total	
	lb	(kg)	lb	(kg)	lb	(kg)
CO-PU-54S-TH-V	8188	(3685)	955	(430)	9143	(4114)
CO-PU-54S-TH-I	9068	(4081)	955	(430)	10023	(4510)
CO-PU-74S-TH-V	5333	(2400)	1313	(591)	6646	(2991)
CO-PU-74S-TH-I	6477	(2915)	1313	(591)	7790	(3506)
CO-PU-100S-TH-V	5207	(2343)	1805	(812)	7012	(3155)
CO-PU-100S-TH-I	5107	(2298)	1805	(812)	6912	(3110)

Based on these results, cost estimates presented by Armstrong [5] in Series 1364-1A, which were obtained from a local construction company (Austin Bridge & Road, Inc.), and T-headed reinforcement costs obtained from a Canadian supplier [25], were used to compare the overhangs. These results are shown in Figure 5.2. Again, all overhangs from Series 1364-1A were included for comparison purposes.

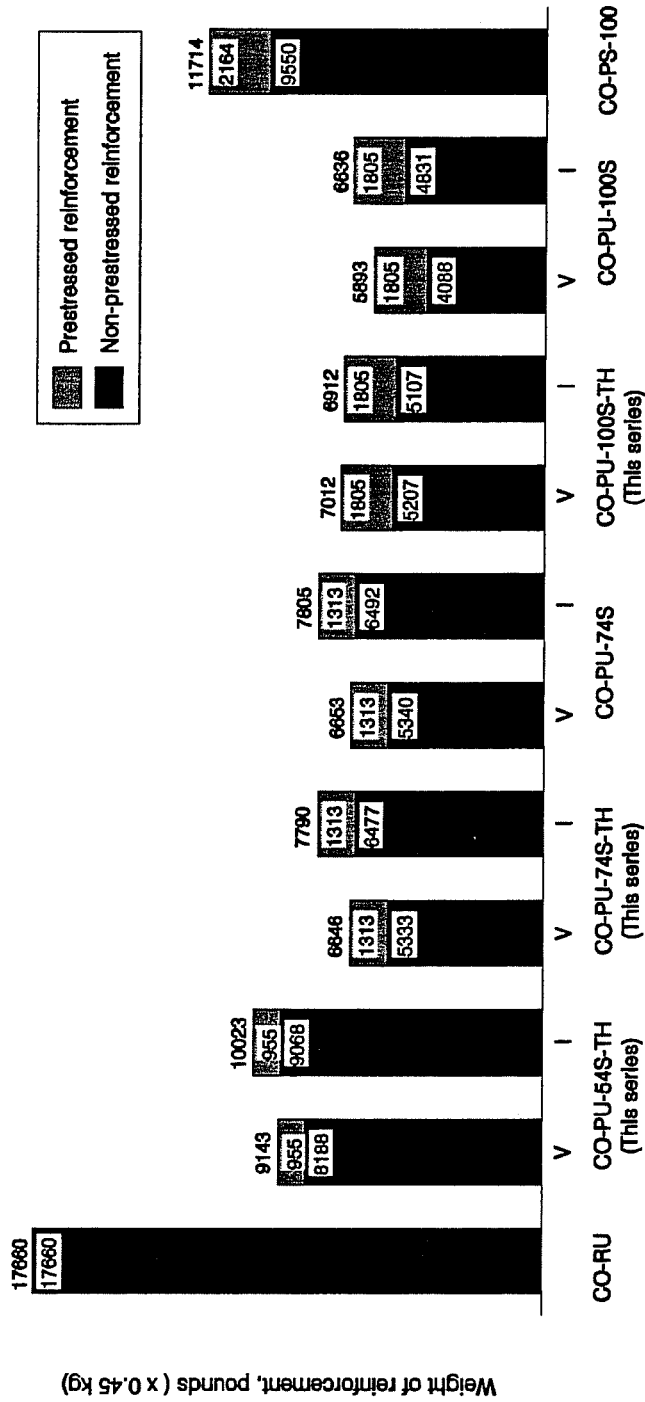


Figure 5.1 Comparison of Total Weight of Reinforcement for Prototype Overhangs

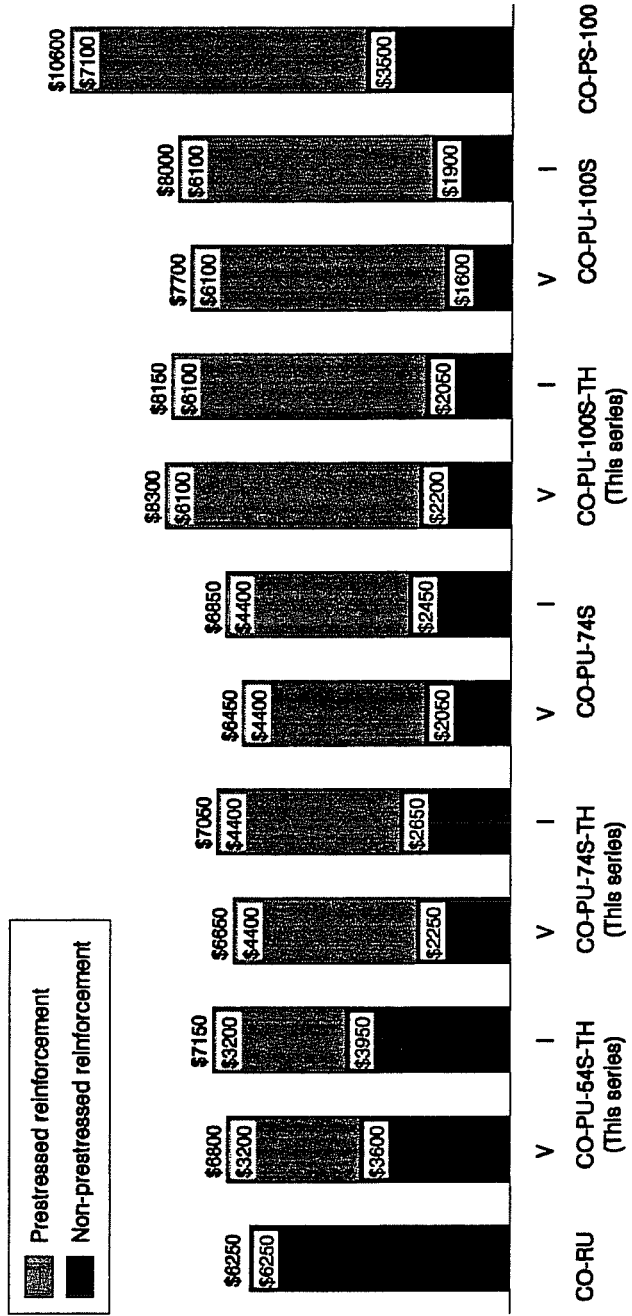


Figure 5.2 Comparison of Total Estimated Cost for the Reinforcement in Prototype Overhangs

Cost estimates obtained from Series 1364-1A correspond to the cost for the prestressed and non-prestressed reinforcement only. The Austin Bridge & Road, Inc. estimator concluded that the cost of forming, and, in spite of the fairly apparent differences in reinforcement congestion, the cost of supplying and placing concrete would be basically the same for all overhangs. This assumption was initially questioned by the author because the experience in the laboratory showed significant labor differences. It was certainly more difficult to place the concrete mix in the very congested models with higher percentages of reinforcing steel than in those with very light cages. However, a second opinion was sought from a senior engineer with Flatiron Construction. He confirmed that in spite of the obvious difference in degree of congestion, that while he would much rather build the less congested designs, the bid price for concrete including placement would probably be the same for all designs. Thus, the construction cost differences can be judged basically on the differences in cost of reinforcement including all prestressing operations.

T-headed reinforcement costs for all prototype overhangs from this series (Series 1364-1B) were obtained assuming that a project would consist of 25 overhangs with at least 625 T-headed #11 (35 mm diam.) reinforcing bars in total. Based on this information, the price for each 37.5 ft (11.5 m) long T-headed bar delivered to a jobsite in Austin, TX, was estimated as \$53.00 U.S.

Analyzing the graph, it can be observed that in general those overhangs designed with a mixture of prestressed and non-prestressed reinforcement are, as expected, below the cost of a prestressed concrete design with allowable stresses governing (overhang CO-PS-100S). Additionally, overhangs CO-PU-54S-TH (V&I) and CO-PU-74S-TH (V&I) are marginally above the cost for the CO-RU overhang. If some recognition was given to those structures with less congested cages, these designs could actually be even less expensive than the conventional reinforced concrete structure.

Particularly, there seems to be a trend of increasing price with increasing quantities of prestressed reinforcement. This conclusion was made even when it was realized that overhangs CO-PU-74S-TH-V and CO-PU-74S-TH-I were less expensive than overhangs CO-PU-54S-TH V and CO-PU-54S-TH-I, respectively. It is believed that the increased cost in the CO-PU-54S-TH overhangs is mainly due to the additional skin steel and the larger amount of T-headed reinforcement in the CO-PU-54S-TH overhangs. However, the use of T-headed reinforcement

would have less influence since it was found that the additional cost due to the use of this reinforcement never exceeded seven percent of the total reinforcing cost of any particular overhang in Series 1364-1B.

As a final observation, it is important to notice that if formwork, concrete material and concrete placement costs are included, the small differences in reinforcement cost between the non-prestressed and mixed prestressed designs would virtually disappear. Then overhangs CO-PU-74S-TH (V&I), and maybe even overhangs CO-PU-54S-TH (V&I), would be highly competitive with overhang CO-RU (conventionally reinforced concrete design).

CHAPTER 6

SUMMARY, CONCLUSIONS AND DESIGN RECOMMENDATIONS

6.1 SUMMARY

A number of difficulties were found by the Texas Department of Transportation, TxDOT, when using current AASHTO design specifications for the design of large cantilever bent caps to be used in the San Antonio Y project.

The problems arose when designers attempted to satisfy both serviceability and strength requirements which required the use of both reinforced concrete and prestressed concrete specifications found in completely separate chapters of the design standards. Additionally, problems were also found when designing overhangs with concentrated load span-to-depth (a/d) ratios near one. In these cases it was not clear whether corbel design or deep beam design should govern. Designers conservatively tried to satisfy both approaches. This resulted in highly congested reinforcing cages, poor constructability, and somewhat uneconomical designs.

To this end, with the main purpose of defining a more consistent design approach for structural concrete piers, and upon the request of TxDOT, an experimental program was initiated at the University of Texas at Austin, CTR Project No. 1364, with the general title of "Design of Large Structural Members Utilizing Partial Prestressing". This project was divided into three major series of tests. The first deals with the cantilever pier, the second with the design and behavior of two-span continuous pier caps, and the third with the overall structure including footing, pier and overhang.

This thesis was developed to report on the second part of the first series (Series 1364-1B). The objectives of this portion were to evaluate the behavior of post-tensioned cantilever piers designed with a mixture of prestressed and non-prestressed reinforcement with the ultimate strength approach governing, to evaluate the use of T-headed reinforcing bars in all flexural reinforcement, and to analyze the performance of different amounts of skin reinforcement in crack control at service levels.

Six concrete overhang structures with mixed reinforcement were tested under static loading. These included two overhangs with 54 percent of the main flexural reinforcement prestressed, two with 74 percent of the main flexural reinforcement prestressed and two with nearly 100 percent of the flexural reinforcement prestressed.

The particular characteristics of each model are described below:

a) Model CO-PU-54S-TH-V. Mixed reinforced concrete design (54 percent prestressed reinforcement) with the strength design approach governing for flexure, strut-and-tie modelling using vertical ties for shear, skin reinforcement as suggested by Frantz and Breen, and T-heads on all flexural non-prestressed reinforcement,

b) Model CO-PU-54S-TH-I. Mixed reinforced concrete design (54 percent prestressed reinforcement) with the strength design approach governing for flexure, strut-and-tie modelling using inclined ties for shear, minimum skin reinforcement, and T-heads on all flexural non-prestressed reinforcement,

c) Model CO-PU-74S-TH-V. Mixed reinforced concrete design (74 percent prestressed reinforcement) with the strength design approach governing for flexure, strut-and-tie modelling using vertical ties for shear, minimum skin reinforcement, and T-heads on all flexural non-prestressed reinforcement,

d) Model CO-PU-74S-TH-I. Mixed reinforced concrete design (74 percent prestressed reinforcement) with the strength design approach governing for flexure, strut-and-tie modelling using inclined ties for shear, minimum skin reinforcement, and T-heads on all flexural non-prestressed reinforcement,

e) Model CO-PU-100S-TH-V. Fully prestressed concrete design, with the strength design approach governing for flexure, strut-and-tie modelling using vertical ties for shear, skin reinforcement as suggested by Frantz and Breen, and T-heads on all #2 (horizontal) bars that were provided as part of the detailing process for construction purposes,

f) Model CO-PU-100S-TH-I. Fully prestressed concrete design with the strength design approach governing for flexure, strut-and-tie modelling using inclined ties for shear, minimum skin reinforcement, and T-heads on all #2 (horizontal) bars that were provided as part of the detailing process for construction purposes.

The performance of T-headed reinforcing bars was evaluated by comparing results from those models described above with models in Series 1364-1A (which used standard hooks in all flexural reinforcement).

Three models were tested to failure: CO-PU-54S-TH-V, CO-PU-74S-TH-V and CO-PU-100S-TH-I.

The analysis of test results included evaluation of deflections at service load levels, evaluation of moment-deflection responses, analysis of cracking moments, comparison of predicted maximum crack widths with test results, comparison of cracking patterns, and evaluation of ultimate capacities and behavior. Additionally, analyses based on constructability and economics associated with all the overhangs were also included.

6.2 CONCLUSIONS

The most important conclusions from the specimens in Series 1364-1B of this study are as follows:

1. All overhangs had deflections at service load levels well below the typical service flexure live load limit of $L/360$. Additionally, a clear trend was observed of decreased deflections with increased effective post-tensioning force in the structures.
2. Most probable maximum crack widths were predicted with very good accuracy using the modified Gergely and Lutz expressions presented in Section 4.4.2. In general, the maximum crack widths in the models decreased as the amount of post-tensioning force increased.
3. At higher post-tensioning forces, fewer cracks were observed, and as a result stiffer structures were attained.
4. Only flexural failures were observed. These consisted of the wide opening of one or two major cracks close to the face of the column at ultimate loads, followed by crushing in the compression zone.
5. Ultimate flexural capacities of all models were in excess of the required capacity at factored loads, by approximately 40 percent. This capacity could not be lowered in design because of the requirements for auxiliary reinforcement in terms of minimum skin reinforcement and fatigue related stress ranges in the post-tensioning steel. Stress ranges were found to control the design of the overhangs, especially in those models with low percentages of prestressed steel. Models CO-PU-74S-TH (V&I) were tested with somewhat higher stress ranges than allowed. This was properly documented and is not recommended.
6. For the prediction of ultimate flexural capacity, the current AASHTO expression which takes into account all non-prestressed reinforcement in tension, as documented in Section 4.8, gave excellent predictions when compared with test results.

7. Since no shear failures occurred, no difference was observed between the performance of the shear steel proportioned using an inclined tie or a vertical tie in the strut-and-tie modelling. The difference was more in terms of constructability and cost. Those overhangs designed with inclined ties required a higher percentage of steel which made the constructability of the reinforcing cages more difficult and somewhat more expensive. Based on the strain gage data, both shear designs proved to be very conservative. This was somewhat expected since no contribution from the concrete in shear was taken into account.

8. Skin reinforcement suggested by Frantz and Breen did not provide significant improvements in terms of crack width control at service load levels. The main reason was that maximum crack widths were always at the extreme top tension fibers in all specimens and not somewhere below in the side faces. Thus, both patterns worked successfully. Very good results, when using the Frantz and Breen skin reinforcement, were obtained at high loads (above factored flexure load level) where a good distribution of cracks was observed.

9. T-headed reinforcing bars showed to considerably improve the constructability of the cages. Placement and tying of bars was improved significantly. Congestion in anchorage areas was reduced by more than 50 percent. This improved the placement and consolidation of the concrete mix. No improvements were observed in terms of crack control at service load levels. Behavior of the specimens using either T-heads or standard hooks in the non-prestressed flexural reinforcement was basically the same over the entire range of loading.

10. Difficulty in constructing reinforcement cages was found to decrease with increased amounts of post-tensioning in the models. On the contrary, and as expected, post-tensioning operations were found to be less time consuming for those overhangs with a lesser amount of prestressed reinforcement.

In two areas, deflections and costs, comparisons were made of the specimens from both Series 1364-1A and Series 1364-1B. Based on these comparisons it was concluded:

1. Mixed reinforced concrete structures had in all cases smaller deflections than those in the reinforced concrete structure.

2. Mixed reinforced concrete structures designed with the ultimate strength approach governing for flexure and strut and tie modelling for shear had significantly less congested cages than overhangs designed according to current AASHTO standards for either reinforced concrete or fully-prestressed concrete with service load stresses governing.

3. Overall costs for the construction of the overhangs were found to increase with increasing quantities of post-tensioning reinforcement. Overhangs designed with 54 and 74 percent of the reinforcement prestressed had costs marginally above that of a conventional reinforced concrete design following the current AASHTO design specifications. If formwork, concrete material and concrete placement costs are included, the small differences in reinforcing cost between the mixed prestressed and non-prestressed designs would virtually disappear.

6.3 DESIGN RECOMMENDATIONS

Currently AASTHO design specifications do not explicitly allow the design of prestressed structures with a mixture of prestressed and non-prestressed reinforcement, using the ultimate strength philosophy for flexure. The purpose of this thesis was to study the behavior of intermediate length overhangs designed using that methodology, including strut-and-tie modelling for shear, various amounts of skin reinforcement, and including T-headed reinforcing bars as flexural reinforcement.

Based on the results from this study, some recommendations can be outlined for the design of similar structures. Before doing this, it has to be mentioned that this thesis is reporting on the second part of the first series of CTR Research Project No. 1364. A more comprehensive report will be presented in the near future including findings of the overall project, which is envisioned to include results on the overall performance of the structure including the overhang, column and footing. These results will be available for consideration by code and specification-writing bodies as soon as results of the complete research program are approved by TxDOT.

Concentrating on the design of intermediate length cantilever beams, some practical design recommendations are:

1. **Flexural Design:** This should be based on a mixed reinforced concrete ultimate strength design with approximately 75 percent of the main flexural reinforcement prestressed. Conventional AASHTO provisions for ultimate flexural capacity can be used to determine the post-tensioning steel required to achieve 100 percent of the capacity of the structure. Then

approximately 75 percent of this quantity of prestressing steel should be provided at its calculated ultimate tensile force. The proper amount of non-prestressed reinforcement should be determined to provide the balance of the required moment capacity. In addition, as given in step 6 for serviceability, the amount of non-prestressed reinforcement must be checked and increased if necessary for proper crack control and fatigue stress range control.

2. **Shear Design:** This should be based on a strut-and-tie model as shown in Figure 2.11. The vertical tie force should be provided by the use of vertical stirrups that should be distributed close to the location of the tie as shown in Figure 2.3. When doing this, observance of the minimum spacing limitations set in the AASHTO provisions for adequate placement of the concrete mix is necessary.

3. **Skin Reinforcement:** Minimum side face skin reinforcement should be proportioned based on recommendations by Frantz and Breen [6].

4. **T-headed reinforcement:** T-head anchorages on reinforcing bars should be used when reinforcement details indicate severe congestion or difficult bar development conditions. In these cases T-headed reinforcement will make the construction process of the reinforcing cages easier and will greatly assist in achieving good consolidation of the concrete mix in anchorage areas. No extra credit should be given to this system for controlling crack widths at service load levels.

5. **Post-tensioning Anchorage Zone Reinforcement:** This should be provided in accordance with the NCHRP Report No. 356 proposed provisions [9].

6. **Serviceability requirements:**

a) Flexural reinforcement should be checked to insure proper control of crack widths by meeting the reinforcement distribution provisions (z factor) of AASHTO. Prediction of the most probable maximum crack width on the tension face of the overhangs should be carried out using any of the Gergely and Lutz expressions discussed in Sections 4.4.1 and 4.4.2, but modifying them, as recommended in those sections, to account for prestressed reinforcement.

b) Stress ranges in all post-tensioning tendons should be evaluated at service load levels and compared against recommendations by Wollmann [10]. They may require supplementary non-prestressed reinforcement. For structures that have to be designed to withstand a fatigue life of two million cycles, Wollmann recommends a stress range limit of 14.5 ksi (96.5 MPa).

- c) Deflections should be calculated by common analytical methods and compared against acceptable values. A typical limit for concrete structures at service flexure live loads is $L/360$.
- d) Minimum area of reinforcement should be provided, where required as per AASHTO provisions, for shrinkage and temperature.

REFERENCES

- [1] American Association of State Highway and Transportation Officials (AASHTO) Standard Specifications for Highway Bridges, Thirteenth Edition, Washington D.C., 1983.
- [2] Schlaich, J., Shafer, K., and Jennewein, M., "Towards a Consistent Design of Structural Concrete," PCI Journal, May-June 1987, pp. 75-150.
- [3] "Structural Concrete." Summarizing Statement of the IABSE Colloquium on Structural Concrete, Stuttgart, April 10-12, 1991. Structural Engineering International. Vol. 1, No.3 Aug. 1991 , pp. 52-54.
- [4] Bergmeister, K., Breen, J.E., Jirsa, J.O., and Kreger, M.E., "Detailing for Structural Concrete", Research Report 1127-3F, Center for Transportation Research, The University of Texas at Austin, May 1993.
- [5] Armstrong, S.D., "Design and Behavior of Large Cantilever Overhangs with Combinations of Prestressed and Non-Prestressed Reinforcement," Unpublished Masters Thesis, The University of Texas at Austin, August 1992.
- [6] Frantz G.C., and Breen J.E., "Control of Cracking on the Side Faces of Large Reinforced Concrete Beams," Research Report 198-1F, Center for Transportation Research, The University of Texas at Austin, September 1978.
- [7] Billington, S., "Behavior of Two-Span Continuous Pier Caps with Varying Levels of Prestress," Unpublished Masters Thesis, The University of Texas at Austin, August 1992.
- [8] Leyendecker, E.V., "Behavior of Pan Formed Concrete Slab and Girder Bridges," PhD Dissertation, The University of Texas at Austin, June 1969.
- [9] Breen, J.E., Burdet, O., Roberts, C., Sanders, D., and Wollmann, G. "Anchorage Zone Reinforcement for Post-tensioned Concrete Girders," NCHRP, Report 356, Transportation Research Board, National Research Council, 1994.
- [10] Wollman, G.P., Yates, D.L., Breen, J.E., and Kreger, M.E., "Fretting Fatigue in Post-tensioned Concrete," Report 465-2F, Center for Transportation Research, The University of Texas at Austin, November 1988.
- [11] American Association of State Highway and Transportation Officials (AASHTO), Standard Specifications for Highway Bridges, Interim Specifications 1990-1991 to the Fourteenth Edition, Washington D.C., 1991.
- [12] Dyken, T., and Kepp B., "Properties of T-Headed Reinforcing Bars in High Strength Concrete," Norway (year not available).

- [13] Lyngaas Dahl, K., "The Development of Headed-Reinforcement Bar, System." Metalock, Norway (year not available).
- [14] Camping, M.J., "T-Headed Bars as Shear Reinforcement in High Strength Concrete," Metalock, Norway (year not available).
- [15] American Association of State Highway and Transportation Officials (AASHTO), Standard Specifications for Highway Bridges, Fourteenth Edition, Washington D.C., 1989.
- [16] American Concrete Institute, Building Code Requirements for Reinforced Concrete (ACI 318-89) and Commentary - 318-89, Detroit, 1989.
- [17] Gergely P., and Lutz L.A., "Maximum Crack Width in Reinforced Concrete Flexural Members," Causes, Mechanism and Control of Cracking in Concrete, ACI Publication SP-20, American Concrete Institute, Detroit, 1973, pp. 87-117.
- [18] Suri K.M. and Dilger W.H., "Crack Width of Partially Prestressed Concrete Members," ACI Journal, September-October, 1986.
- [19] MacGregor, J.G., Reinforced Concrete, Mechanics and Design, Prentice-Hall, Englewood Cliffs, 1992.
- [20] Borges, F. and Lima, A., "Crack and Deformation Similitude in Reinforced Concrete," RILEM, No. 7 June 1960.
- [21] Canadian Standards Association, Code for the Design of Concrete Structures for Buildings CAN-A23.3-M84, Ontario, 1984.
- [22] Comité Euro-International du Béton, CEB-FIP Model Code 1990 (Design Code), Thomas Telford, London, 1993.
- [23] Comité Euro-International du Béton, CEB-FIP Model Code for Concrete Structures 1978 (Design Code), London, 1978.
- [24] Collins, M.P., and Mitchell D., Prestressed Concrete Structures, Prentice-Hall, Englewood Cliffs, 1990.
- [25] Quotation for T-headed bar cost. David W. Mitchell, Production/Research Manager, Headed Reinforcement Canada, Inc., Mt. Pearl, Newfoundland, Canada, July 1994.

VITA

Rubén Mario Salas Pereira was born in San José, Costa Rica, on June 20, 1968, son of Rubén Salas Granados and María Teresa Pereira García. After graduating with honors from the Liceo Laboratorio (High School), San José, Costa Rica, in 1985, he entered the Universidad de Costa Rica in San José, Costa Rica, where he received the degree of Licenciado en Ingeniería Civil with high honors in April, 1991. During the summers of 1987 to 1989, and the year of 1990, he was employed as an Engineering Assistant at CARREZ S.A. Construction Company, San José, Costa Rica. In 1991, he worked part time in the Engineering Division of SALPER S.A. Construction Company, San José, Costa Rica. In the same year he joined the team that subsequently developed the "Great Metropolitan Area Transportation Master Plan" for the Ministry of Public Works and Transportation (Ministerio de Obras Públicas y Transportes). In June of 1991, he became a Professor in the Civil Engineering Department, Universidad de Costa Rica. In January of 1992, he was awarded a Professional Internship and travelled to the United States where he worked at the Pan American Institute of Highways, Turner- Fairbank Highway Research Center, Federal Highway Administration, McLean, Virginia. In January, 1993, he entered The Graduate School of Engineering of the University of Texas at Austin.

Permanent Address: Apartado 582-2070, Sabanilla
 San José, COSTA RICA

This thesis was typed by the author.